Investigation of the Nutrient Storage Pools in Microalgae by Raman Microscopy

Inaugural dissertation

for the attainment of the title of doctor
in the Faculty of Mathematics and Natural Sciences
at the Heinrich Heine University Düsseldorf

presented by

Lu Gao
from Beijing, China

Jülich, April 2021

from the institute for Quantitative and Theoretical Biology
at the Heinrich Heine University Düsseldorf

Published by permission of the
Faculty of Mathematics and Natural Sciences at
Heinrich Heine University Düsseldorf

Supervisor: Prof. Dr. Oliver Ebenhöh
Co-supervisor: Prof. Dr. Ilka Axmann

Date of the oral examination: 10.09.2021

Declaration of Honesty

I hereby declare that enclosed thesis was written completely by myself and that I have not used sources or means without declaring them in the text. Any thoughts or works by others are clearly marked as those. This work nor any similar version was not used to achieve an academic grading before nor is it being published elsewhere.

Lu Gao

Summary

Phosphorus, nitrogen, and other nutrients are discharged in waste streams, without being sequestered. The release of these nutrients leads to eutrophication of natural waters and, increases the likelyhood of algal blooms. The capacity of algal cells to accumulate reserves of nutrients can be used to complement conventional wastewater treatment. The resulting algal biomass can then be used to produce biofertilizers and soil conditioners for crop production.

The mechanisms of algal nutrient accumulation are still not adequately understood due to a lack of methods for rapidly identifying and quantifying relevant chemical forms in the compartments of algal cells *in situ*. Closing the nutrient cycle requires knowledge about the nature and dynamics of these reserve pools in algal cells, which can be obtained by using Raman microscopy. Until recently, the use of this highly potent technique to study nutrient storage pools in algal cells has been rare since the strong fluorescence emission from chlorophyll molecules obscues the Raman scattering signal. Photobleaching is an autofluorescence suppression approach that not only reduces the chlorophyll fluorescence emission but also enhances the signal-to-noise ratios of Raman spectra. This work provides experimental evidence that active photosynthesis and the release of reactive oxygen species in algae facilitates photobleaching with Raman microscopy. Based on this research, using formalin as a chemical fixation reagent for algae is proposed to improve the photobleaching protocol. This finding allows new opportunities for decoupling sampling and the Raman measurements.

The findings on the dynamics of polyphosphate formation and hydrolysis in algal cells analyzed by Raman spectroscopy are presented. Accumulation of polyphosphate occurs during the culture lag phase, within several hours after adding orthophosphate to the phosphorous-starved algae. As growth resumes, the polyphosphate reserves are being consumed. This transient accumulation of large amounts of polyphosphate reserves

presents an opportunity to produce algal biomass with elevated phosphorous contents as biofertilizers or soil conditioners.

Moreover, the presence of guanine crystals is widespread across microalgal species in taxonomically distant phyla and contrasting habitats, including free-living as well as endosymbiotic marine dinoflagellates, which are ecologically relevant. Guanine crystals accumulate after reintroducing nitrogen sources to the starved cells. Then, these intracellular guanine crystals are consumed for growth. This highly dynamic nature suggests that guanine crystals are an important N depot for life in highly dynamic environments. This is particularly important not only for water with fluctuating nutrient availability but also for fragile ecosystems, like coral reefs require low-nutrient environments and are severely threatened by anthropogenic eutrophication. These results may prompt new research that allows a deeper understanding of the mechanisms underlying nitrogen cycling and interactions within the holobiont.

Table of Contents

List of Figures

List of Tables

Chapter I. Introduction

I. A. Background

Phosphorus (P) and nitrogen (N) are essential elements for all organisms [1]. P- and N-fertilizers are two of the three most common agricultural fertilizers, along with potassium (K). Adequate fertilizer supply is crucial for global agricultural productivity to provide for an increasing population with rising food demands. However, fertilizers are inefficiently utilized by plants. Crops only convert and use ca. 20% of P [2] and 30% of N [3] from fertilizers. The remaining nutrients in the soil may be absorbed, continuously run off, or leached into water. Therefore, excess nutrients in the aquatic environment result in eutrophication with rapid, uncontrolled growth of phytoplankton [4] and reducing the water quality for other species that require dissolved oxygen [5, 6]. Figure I-1 demonstrates the nutrient-related relationships and problems among plant, soil and water.

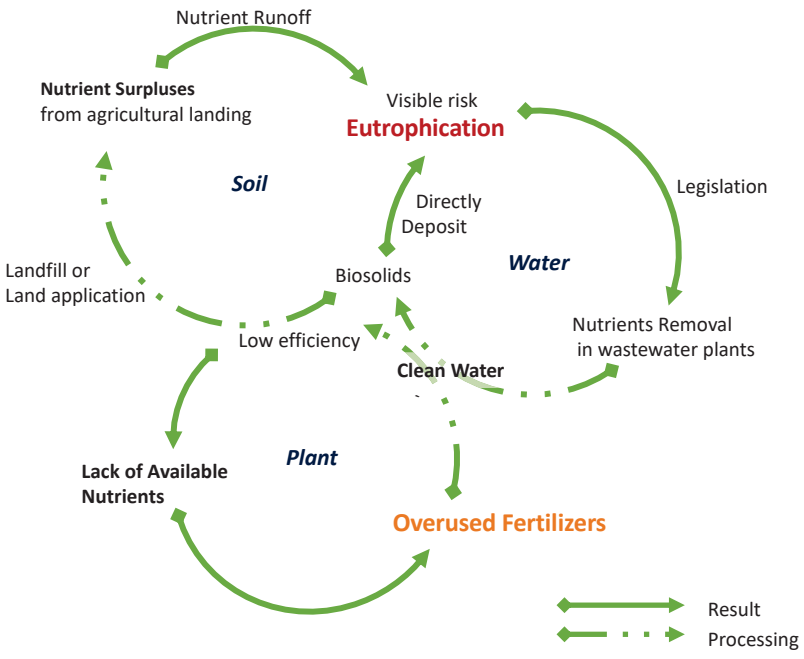

Figure I-1 A causal relationship diagram depicting the water-soil-plant systems showing the nutrient mobilizations. The overuse of P-fertilizer can result in excess nutrients flow into the watershed; this causes eutrophication of natural waters.

One possible solution is the creation of nutrient-rich products by recovering nutrients from waste streams to reduce the effluent to water and produce fertilizers for plants. The current biosolids from wastewater treatment facilities usually contain high contents of iron or aluminum. P in these biosoilds are insufficiently bioavailable for soil and plants due to low solubility. While the lack of nutrients in plants, low bioavailable nutrients accumulate in the soil and water. The use of these products may even accelerate an imbalance in the nutrient-cycle. Thus, it is necessary to convert nutrients in forms that are suitable for application as fertilizers or soil conditioners. This work focuses on the strategy of using microalgae to recover nutrients from waste streams and convert them into biofertilizers providing bioavailable nutrients to plants, as shown in Figure I-2.

In response to environmental circumstances, algae have evolved several strategies to scavenge nutrients from external sources, recycle and balance nutrient consumption within the cell, and manage cell growth and division with high or low nutrient supply [7]. For example, microalgae are able to acquire and accumulate large P-reserves [8]. Thus, we can utilize this capacity to sequester P from wastewater effluents for P-rich biomass [9]. In addition to algal biofertilizers, clean water and bioremediation are also algal biotechnological products that have great potential for a circular bioeconomy [9-11].

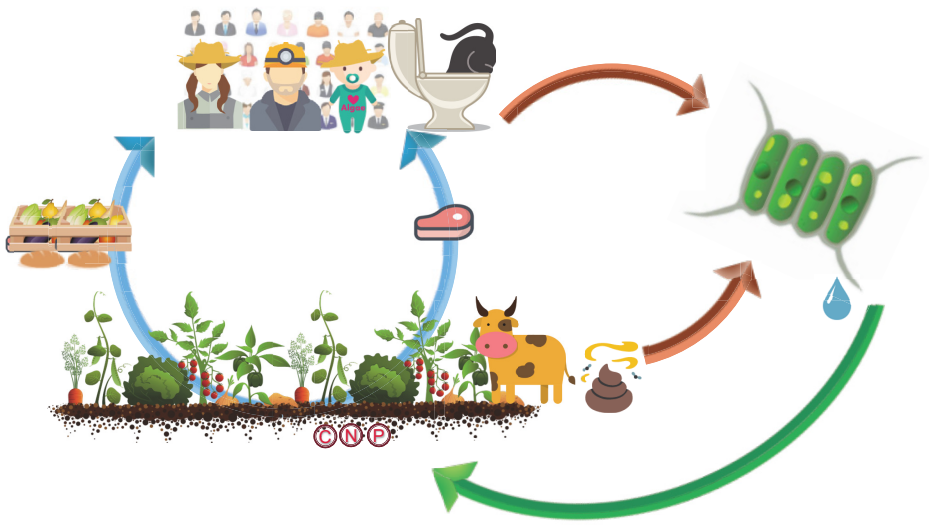

Figure I-2 A schematic of the future nutrient cycle of using microalgae.

I. B. Overview of the Dissertation

The two main objectives of this dissertation are to (*1*) review the literature on optical proxies for quantitation of algal biomass growth and composition; (*2*) demonstrate the dynamics of P and N reserves in nutrient deficiency, in nutrient surplus and in transitions between the respective forms of those two by Raman microscopy and by other techniques. This dissertation is organized into four chapters which are described in Figure I-3. The summary of each chapter and subsection is included in their introduction sections. This work approaches the problem of recovering nutrients from waste and producing algal biofertilizers from the following perspectives:

I. B. 1. Understanding Sensors to Investigate Microalgae

Earlier studies have reviewed the feasibility [9] and potential [12] for using algae as P-rich biofertilizers. In parallel, a protocol that includes a photobleaching pre-treatment was developed to characterize macromolecules *in situ* in living microalgae using Raman microscopy [13-17].

In Chapter II, the general background of using sensors for microalgae is given. The concept of using Raman microscopy for algal characterization is in focus (Section II.B.2.). In particular, the methods for determining polyphosphate (Section II.C.) and guanine crystals (Section II.D.) in cells are reviewed in order to utilize them for investigating nutrient storgae pools in algae (Section I.B.2. and Chapter III).

In the Section III.B., algal photobleaching with Raman microscopy was studied to confirm the contribution of photosynthesis and reactive oxygen species. A fixation reagent was proposed to decouple algal sampling and Raman measurement to improve the protocol. Usually, it is an advantage if no pretreatement is required for *in situ* or *in vivo* Raman analysis. However, rapid dynamic changes in algae may not be captured due to the time-consuming Raman mapping. Moreover, Raman microscopes are uncommon instrument in

most laboratories. Fixing algal cells and postponing Raman measurements may be practical for many situations.

I. B. 2. Revealing Dynamic Phosphorus and Nitrogen Storage Pools in Microalgae

The cultivation with P- or N-starvation and replenishment promotes dynamic changes during accumulating and consuming the corresponding pools in algae, polyphosphate or guanine crystals, respectively (Section III.A). Section III.C. and D. describes two related yet independent projects for these two main nutrient reserves in algae. The dynamic changes of polyphosphate in algae and the feasibility of phosphorous-rich algal biofertilizers are discussed (Section III.C.). The most significant contribution of this work is to study the presence of guanine crystals and their function as dynamic N storage pools in algae (Section III.D.). Due to their biophysiochemical properties, guanine crystal in algae may be multifunctional as nitrogen storage pools and light manipulators (Section II.D.4.).

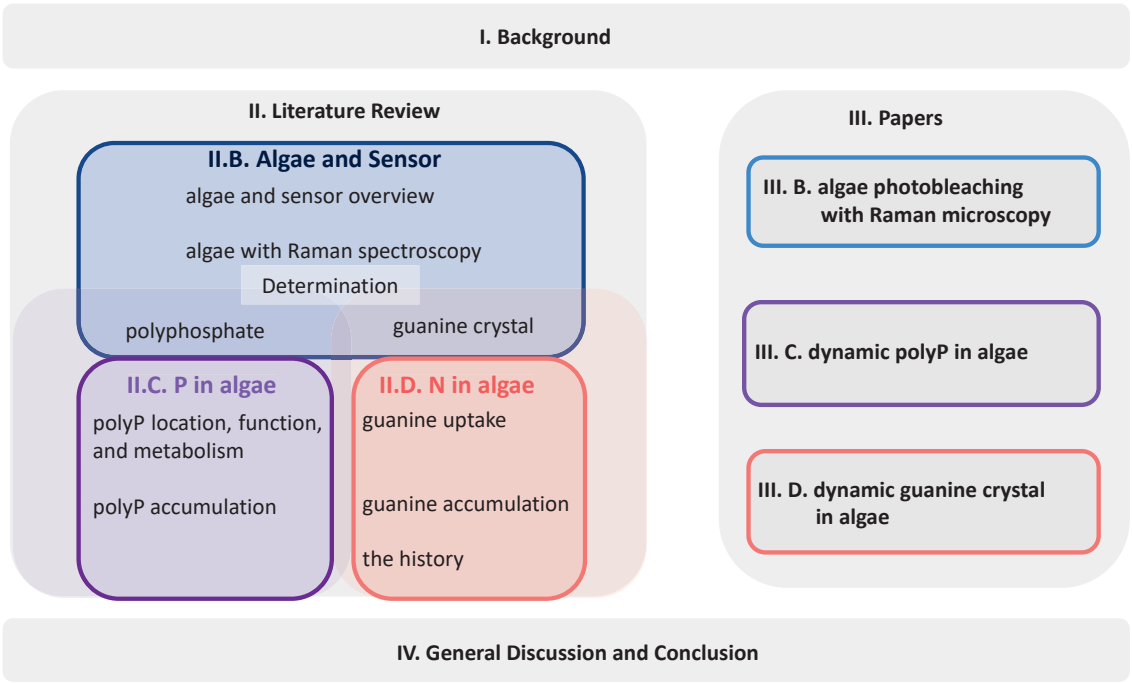

Figure I-3 Schematic layout of this thesis based on the chapter contents.

Chapter II. Literature Review

II. A. Introduction

This literature review is organized into three sections. The relationship between these sections is illustrated in Figure II-1. The objectives of this review are to (*1*) introduce optical sensors for studying microalgae, particularly focusing on Raman spectroscopic techniques which were used to investigate algal polyphosphate (inorganic polymers of (PO_3)—units, polyP) and guanine crystal in this work (Chapter III); (*2*) review studies focusing on algal polyphosphate and guanine crystals. This literature review also provides background information for Chapter III., where I introduce research on algal photobleaching with Raman microscopy (Chapter III.B.), polyphosphate as phosphorus (P) storage pools (Chapter III.C.), and guanine crystals as nitrogen (N) storage pools (Chapter III.D.).

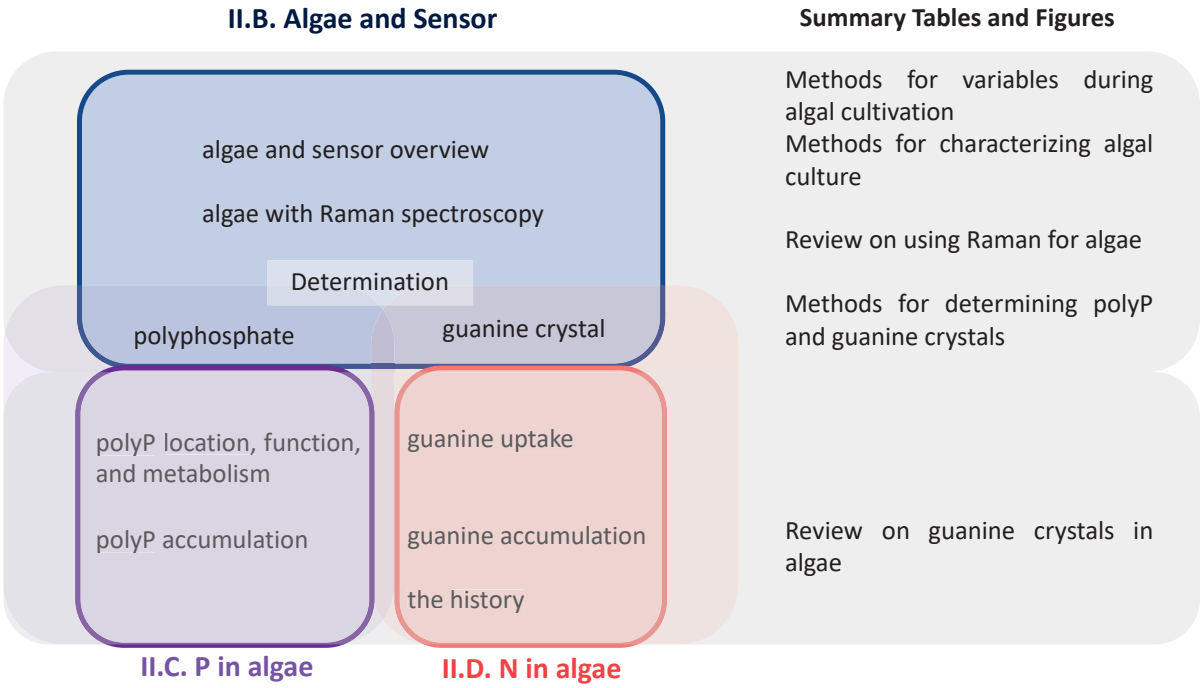

Figure II-1 Schematic layout of the literature review based on the contents.

II. B. Algae and Optical Sensors

II. B. 1. Algal Characterization with Optical Sensors

Microalgae compromise environments as a result of eutrophication and releasing of toxins [18-20] though many microalgae serve as primary producers, which are fundamental to the food chains of ecosystems [18, 21, 22]. To better understand algae, the techniques used to charaterize algae cultures and determine algal compositions are essential [23]. Figure II-1 and II-2 summarize the common optical determination methods used for algae cultivation and general characterization, respectively.

In recent years, the focus has shifted from characterizing algae cultures to monitoring algal production processes, which are crucial to produce the desired products of algal biotechnology. The common techniques have been reviewed in literature previously [23, 24], particularly high-throughput analysis techniques [25], spectroscopic techniques [26], microfluic techniques [27], microarray analysis techniques [28], and standard industrial offline techniques [29] for algal applications.

Vibrational spectroscopic methods, including Raman, near-infrared (NIR; 4000–14000 cm^{-1}, 2500–715 nm) and mid-infrared (MIR; wavenumber range at 600–4000 cm^{-1} or wavelength range at 17–2.5 μm) techniques, are gaining attention for studying algae [23, 30-34]. Raman spectroscopy, a technique that is sensitive, spatially resolved, non-contact, and nondestructive, is widely used to identify biomolecules, in particular, lipids and pigments in microalgae [14]. The application of Raman spectroscopy for identifying biomolecules is summarized in the next section (Section II.B.2). Although *in vitro* NIR can be used to identify many materials, including lipids, carbohydrates, proteins, and chlorophylls in algae, *in vivo* NIR has only been used to measure algal biomass, lipids, and carotenoids [30]. NIR-Raman spectrometry, which uses a combination of IR and Raman techniques, has been used to characterize organic phosphorus in freshwater sediments [35]. Yet, the complexity of NIR-Raman spectrometry limits its pratical application for characterizing algae. In addition, studies utilizing MIR spectroscopy for algal applications often focus on three aspects: characterizing algal macromolecular compositions, comparing phenotypic changes under

stresses, or identifying the compositions of mixed microalgal populations [36, 37]. The use of vibrational spectroscopic techniques for studying algae has been largely overlooked in comparision to other techniques. Their high sensitivity and the advantages of *in situ* analysis will contribute to future research on monitoring open and/or mixed microalgal systems and development of algal biotechnology, in particular for recovering of nutrients from wastewater.

Table II-1 Methods for determining physical, physicochemical, and biological variables during algal cultivation. *CO_2* carbon dioxide; *DO* dissolved oxygen; *IR* infrared; *ISFET* ion-specific field effect transistor; *PAR* photosynthetically active radiance; *PBR* photobioreactor; *pCO_2 or p02* partial pressure of carbon dioxide or oxygen; *PE* photosynthetic efficiency; *PQY* photosynthetic quantum yield; *UV* ultraviolet [23-26, 30-34].

Subject	Sensor	Range	Comment
Photon flux density **(single cell)**	Quantum sensor: flat cosine [38-41], fiber-optic spherical [39, 40, 42], PAR dosimeter [43], integration solarimeter/ pyranometer[42]	10-250 $pM \cdot m^{-2} \cdot s^{-1}$ (optimal); 0-2000 $pM \cdot m^{-2} \cdot s^{-1}$ (actual) [44]	**Low**: slow growth **High**: (*1*) PE sinks at PFD >250; (*2*) Photoinhibition at >1500 **Solution**: optimizing PBR design for low or reduce culture density or mixing for high [45, 46]
Temperature	Thermoelement (Pt-100)	15-35 °C	**Low**: slow growth **High**: a large drop in PQY [47], culture death **Solution**: water bath or spraying; heat exchanger or shading [48, 49]
pH	pH glass electrode or optical pH sensor [50] ISFET [51, 52]	7-10 [53]	Growth rates decrease and affects nutrient availability [54] **Solution**: CO_2 injection [55]
$C0_2$ (g)	IR analyzer (inlet gas [41, 56, 57]; outlet gas [41, 56-58]) Mass flow meter [39, 44, 57]	> 0.15% [58]	**Low**: growth rate decreases **Solution**: CO_2 injection

Subject	Sensor	Range	Comment
$pC0_2$ (l)	$pC0_2$ electrode (typical [57], dye fluorescence [59], pH-Severinghaus-based [60]) IR analyzer [58, 61] or flow meter [62] (measure $C0_2$ (g))	> 0.1-0.2 kPa [63]	**Low**: growth rate decreases below 0.1 kPa **High**: pH decrease, growth inhibition **Solution**: CO_2 injection (theoretically, at least supplied 1.65-2.93 g $C0_2$/g biomass [46])
0_2 (g)	Paramagnetic [64] or polarimetric [63] analyzer (in outlet gas) Mass spectrometry [65]	Depends on 0_2(l) and mixing intensity	**High**: growth rate decrease
$p0_2$ (l)	Optical sensor - Clark oxygen electrode [66] for rate of 02 evolution and a P/I curve [67] A dynamic luminescence quenching DO electrode [68] Oximeter	< 10-20 mg/L (< 120-200% of saturation) [46, 69]	**High**: growth rate decrease **Solution**: aeration
Inorganic nutrients	UV spectroscopy and colorimetric assays On-selective electrodes: ion chromatography [70-72]		**Low**: growth limitation; lipid or starch accumulation [73, 74] **High**: inhibitory or toxic effects by high ammonia [75]; intracellular accumulation by high P [76]

Table II-2 Methods for determining algal characteristic parameters [23-26, 30-34]

Subject	Sensor
Biomass	• OD sensor: optical density, reflectance [77-79] • Turbidity sensor using multichannel light scattering [80-82], NIR [83] • Color analysis-based by CCD/CMOS camera [84, 85] • Microscope + CCD/CMOS camera: *in situ* microscopy [86, 87] • Backscattered spectra by RGB camera [88] • Spectrophotometer: 2D fluorometry [89, 90] • Raman spectrometer: Raman spectroscopy [91] • Monitor by microfluidic arrays for OD [92, 93]; flow-through sensors [83, 94, 95]; IR sensor-integrated in photobioreactor [96] or visible light sensors combined with fluorescence
Cell counting	• Coulter [83] or optical particle [98] counters • Color analysis-based by CCD/CMOS camera (cell size) [84, 85] • Flow cytometry [78, 99-102]; Microfluidic cytometer [103] • Microscope with CCD/CMOS camera - *In situ* microscopy [104] (monitor cultivations by adding a flow-through cell [86])
Photosynthetic efficiency, Quantum yield, and RL curve	Chlorophyll-a fluorescence techniques [105-109]: • (*1*) The rapid fluorescence induction/relaxation kinetics (providing the Kautsky effect, dark-adapted) • (*2*) PAM fluorometer for photosynthetic activity *in situ* [39, 44, 57, 95, 97, 106, 110]; or a proxy for quantum yield [111]
Carbohydrates and proteins	• NIR spectrometer; ATR flow system (MIR) or fiber-optic probe: Infrared spectroscopy (MIR, NIR, FTIR) [112-114] • Raman spectrometer: Raman spectroscopy [14, 25, 33, 34] • Spectrophotometer: 2D fluorometry (proteins, glucose) [90]

Subject	Sensor
Lipids	• Spectrophotometer: absorbance spectra (fatty acids can be correlated with carotenoid-to-chlorophyll ratio [115, 116]) • Three color analysis-based by CCD/CMOS camera (estimating chlorophyll-a and lipid contents simultaneously [117]) • PAM fluorometry (by correlating neutral lipid yield and PE [74] • NIR spectrometer; ATR flow system (MIR) or fiber-optic probe: Infrared spectroscopy (MIR, NIR, FTIR) [113, 118-123] • NMR spectrometer: NMR spectroscopy [124, 125] • Raman spectrometer: Raman spectroscopy [14, 33, 34, 91, 126-128] • Vector network analyzer-dielectric spectroscopy [129-132] • Flow cytometry [99, 100, 133-137], microfluidic cytometer with Nile Red staining [138]
Pigments	• Color analysis by CCD/CMOS camera • Spectrophotometer: absorbance spectra [139, 140] • Pulse amplitude modulated fluorometer: chlorophyll fluorometry • Raman spectrometer: Raman spectroscopy [14, 25, 33, 34] • Microscope + CCD/CMOS camera: microscopy [87]
Substrates and metabolites	• Exopolysaccharides by spectrometer: Raman spectroscopy [34, 91, 141] • Ethanol and pyruvate by spectrophotometer: fluorometry [90] • Ethanol by standard ethanol oxidase-based analyzer [142] • Extracellular hydrogen by mass spectrometry [143] and a polymer electrolyte membrane (PEM) fuel cell [144]

II. B. 2. Raman Spectroscopy

Raman Spectroscopic Techniques

Raman spectroscopy utilizes the excited molecular vibrations of inelastic Raman scattering to identify the unique composition and structure of molecules [145, 146]. To date, Raman spectroscopic analysis techniques suitable for investigating biological materials and living cells are still in development [147], especially for investigating single cells [148]. The Raman signatures of common biomolecules in the cells have been summarized in several works [14, 34, 149-154]. The unique structures of each molecule dictates its Raman shift, which is not affected by the excitation wavelength. While the laser wavelength is usually reported in nanometer (nm) units, Raman spectral shifts ($\Delta\, \upsilon$) are commonly reported in wavenumbers (cm^{-1}) in biology and chemistry, and in wavelengths (nm) in physics. The reciprocal relationship between wavelength (λ, nm) and wavenumber ($\Delta\upsilon = \frac{1}{\lambda}$, cm^{-1}) is defined as

$$\text{Raman shift } \Delta\upsilon\ (\text{cm}^{-1}) = \frac{10^7(\text{nm})}{1(\text{cm})} \cdot \left[\frac{1}{\lambda_{laser}(\text{nm})} - \frac{1}{\lambda(\text{nm})}\right],$$

$$\text{or wavelength } \lambda\ (\text{nm}) = \frac{1}{\frac{1}{\lambda_{laser}(\text{nm})} - \frac{\Delta\upsilon\ (\text{cm}^{-1})}{\frac{10^7(\text{nm})}{1(\text{cm})}}}$$

Autofluorescence

In most microscopy studies on biological samples, it may seem as though there is no difference between background fluorescence and autofluorescence, since both are the result of the natural emission of light. However, background fluorescence is generated from at least two sources: 1) instruments, light sources or measuring parameters; 2) sample autofluorescence. The inherent noise from instruments is complicated. However, background arising from sample autofluorescence can be addressed more easily and remedied, for example by choosing proper solutions and sample containers.

Autofluorescence backgrounds, particularly chlorophyll fluorescence in photosynthetic organisms [33, 34], can obscure most Raman signals (e.g., as shown in Figure II-2). Thus, Raman studies of algae and higher plants are predominately focused on only a few components, such as carotenoids [155-158], lipids [159-162], or cell wall components [163, 164]. Apart from these, other intracellular components cannot be characterized until the fluorescence background is suppressed [14].

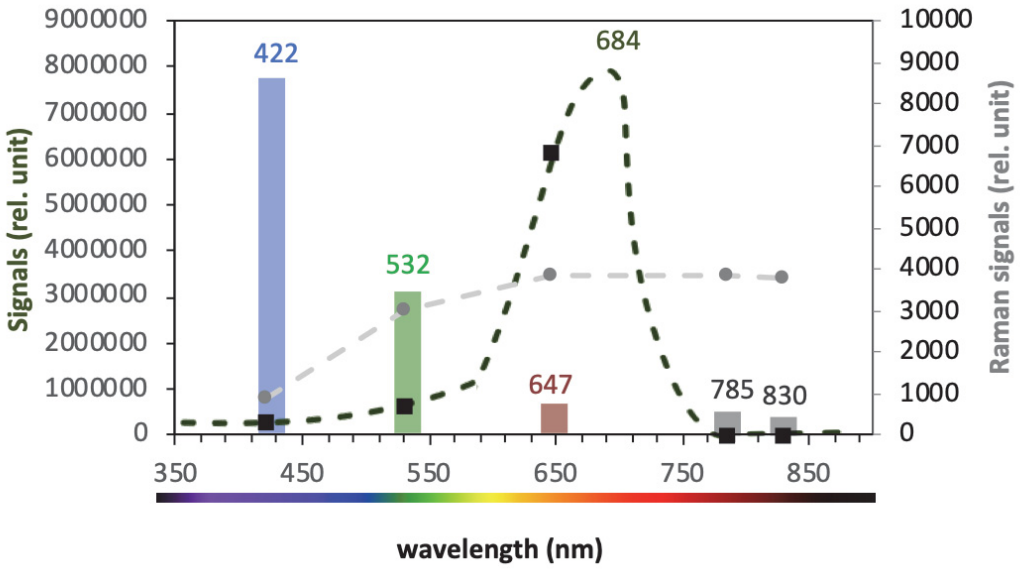

Figure II-2 A typical example of the fluorescence background of microalgae with the impact of excited laser wavelengths. The Raman signals of excited laser wavelengths (bars in colors: purple: high energy UV; green: 532-nm; red: low energy (near) IR of the corresponding algal chlorophyll signals (dark green dot line) and other Raman background signals (grey dot line) are shown.

Fluorescence background can be suppressed by several methods. Mathematical analysis is the most standard strategy and mainly involves correcting the spectra baseline [165-167]. However, this method usually is not able to subtract the inherent fluorescence from samples and does not consider the effect of impulsive photobleaching [168]. Enhancement of Raman signals can be achieved by choosing proper excitation laser(s) or by using advanced Raman systems. Visible (shorter) excitation laser wavelengths usually trigger stronger fluorescence [169].

The autofluorescence background might easily overlay the Raman spectral region created by the visible laser because of the stronger intensity. The trade-off for selecting a laser with a longer wavelength is a lower spatial resolution and lower Raman signal efficiency [170]. In addition, photobleaching [14] is particularly important for this study (Section III.B.).

II. B. 3. Raman Application for Algal Characterization

Recently, confocal Raman microscopy is used to detect and locate the fundamental constituents of photosynthetic energy biomolecules, such as reserves of polyP granules, pigments, lipids, and starch, in the green algae *Desmodesmus quadricauda* or *Chlorella vulgaris* [17]. Figure II-3 and Figure II-4 describe the Raman techniques used to measure components in algae and both include a brief history of Raman development for commemorating the 100th year after the discovery of Raman scattering. One of earliest use of Raman microscopy was to detect hydrocarbons in the green algal *Botryococcus braunii* [171] and carotenoids in the bioluminescent dinoflagellate *Pyrocystis lunula* [172]. These studies had been conducted soon after the invention of the first Raman microscope [173] which was used to detect polyphosphate in biological samples [174]. It is clear that science and technological developments have accelerated the use of Raman microscopy for algal study.

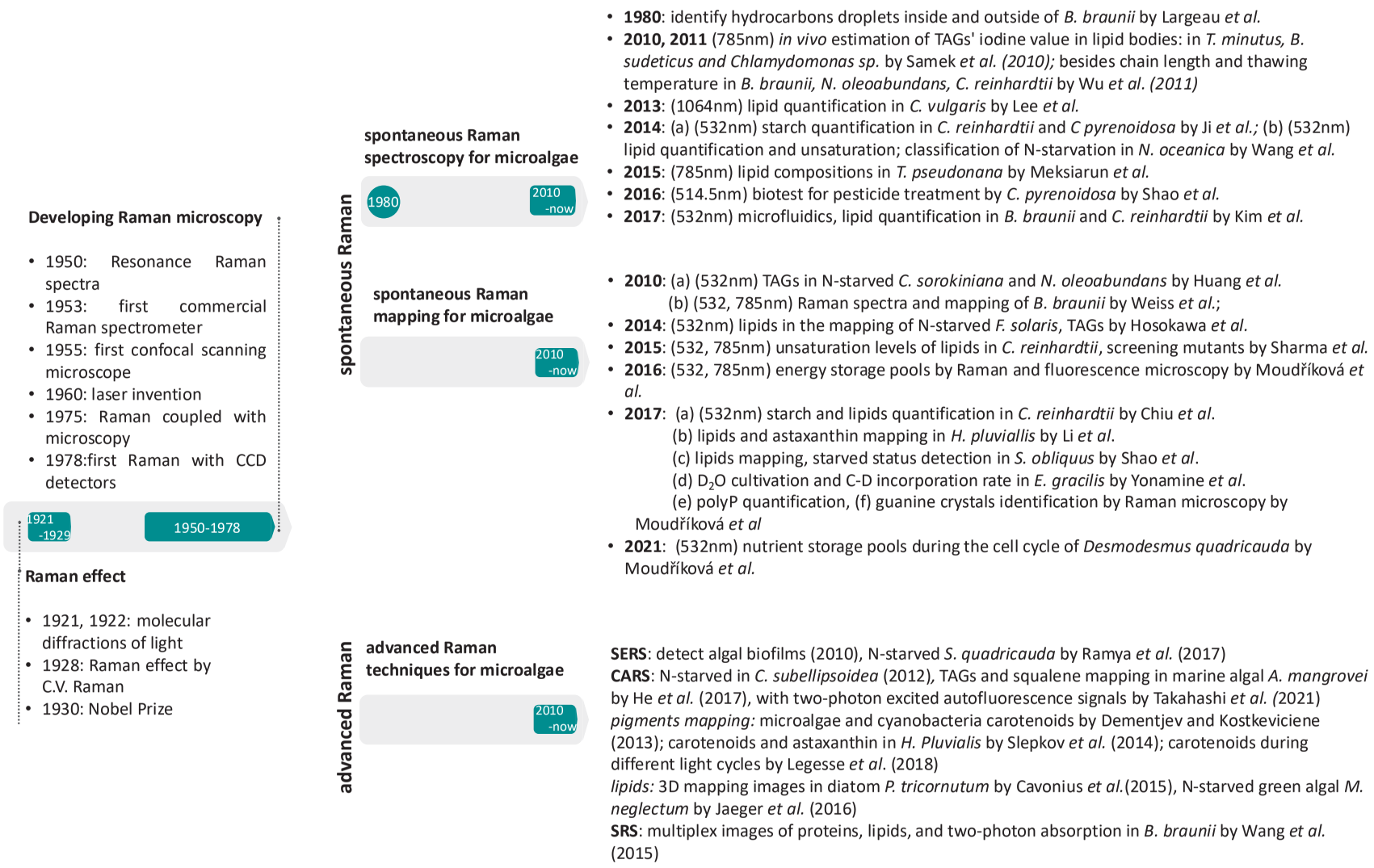

Figure II-3 Schematic of selected algal applications using Raman spectroscopic techniques [127, 159, 161, 162, 171, 172, 175-228].

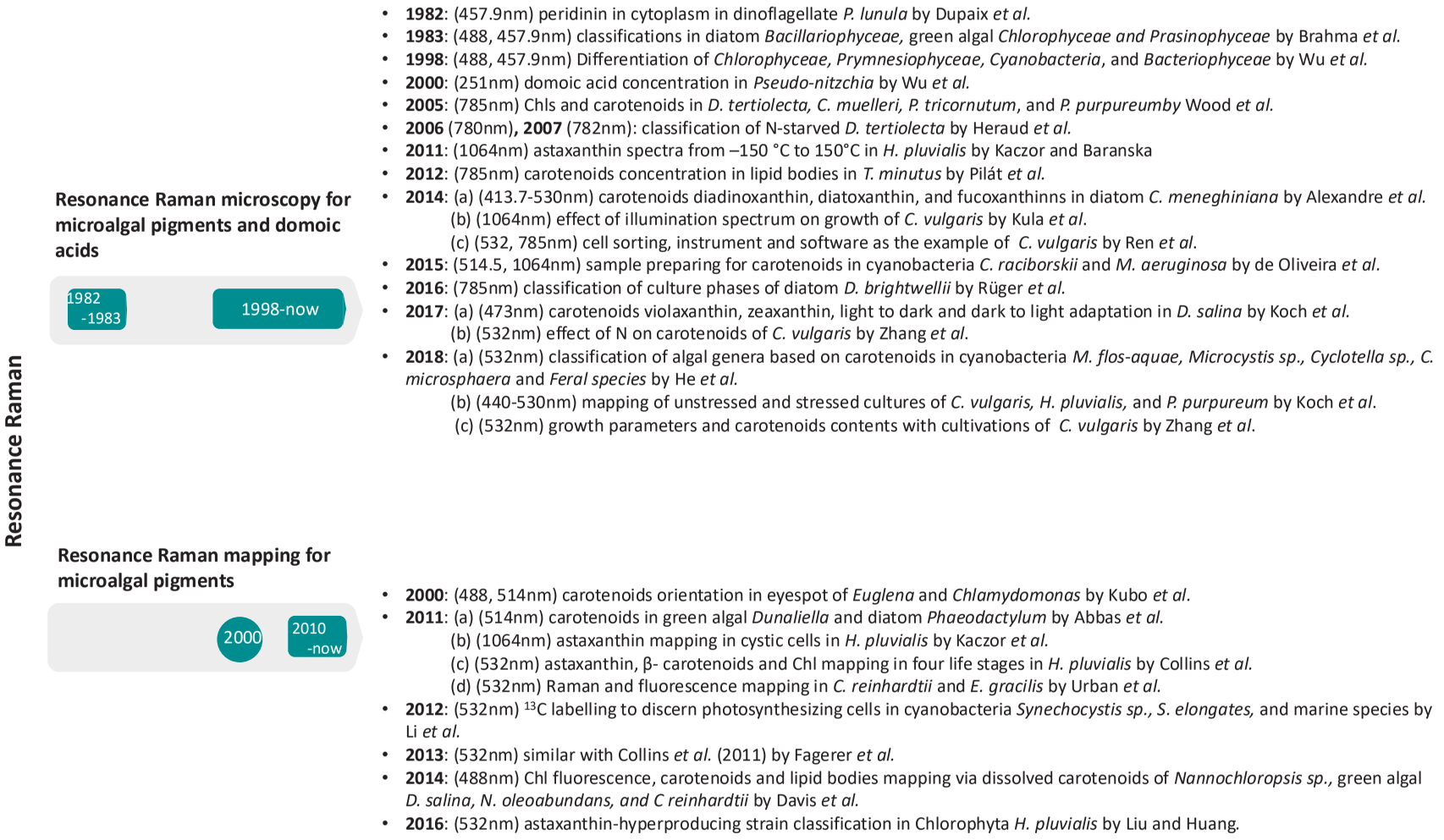

- **1982**: (457.9nm) peridinin in cytoplasm in dinoflagellate *P. lunula* by Dupaix *et al.*
- **1983**: (488, 457.9nm) classifications in diatom *Bacillariophyceae,* green algal *Chlorophyceae and Prasinophyceae* by Brahma *et al.*
- **1998**: (488, 457.9nm) Differentiation of *Chlorophyceae, Prymnesiophyceae, Cyanobacteria*, and *Bacteriophyceae* by Wu *et al.*
- **2000**: (251nm) domoic acid concentration in *Pseudo-nitzchia* by Wu *et al.*
- **2005**: (785nm) Chls and carotenoids in *D. tertiolecta, C. muelleri, P. tricornutum*, and *P. purpureumby* Wood *et al.*
- **2006** (780nm)**, 2007** (782nm): classification of N-starved *D. tertiolecta* by Heraud *et al.*
- **2011**: (1064nm) astaxanthin spectra from –150 °C to 150°C in *H. pluvialis* by Kaczor and Baranska
- **2012**: (785nm) carotenoids concentration in lipid bodies in *T. minutus* by Pilát *et al.*
- **2014**: (a) (413.7-530nm) carotenoids diadinoxanthin, diatoxanthin, and fucoxanthinns in diatom *C. meneghiniana* by Alexandre *et al.*
  (b) (1064nm) effect of illumination spectrum on growth of *C. vulgaris* by Kula *et al*.
  (c) (532, 785nm) cell sorting, instrument and software as the example of *C. vulgaris* by Ren *et al*.
- **2015**: (514.5, 1064nm) sample preparing for carotenoids in cyanobacteria *C. raciborskii* and *M. aeruginosa* by de Oliveira *et al*.
- **2016**: (785nm) classification of culture phases of diatom *D. brightwellii* by Rüger *et al.*
- **2017**: (a) (473nm) carotenoids violaxanthin, zeaxanthin, light to dark and dark to light adaptation in *D. salina* by Koch *et al.*
  (b) (532nm) effect of N on carotenoids of *C. vulgaris* by Zhang *et al*.
- **2018**: (a) (532nm) classification of algal genera based on carotenoids in cyanobacteria *M. flos-aquae, Microcystis sp., Cyclotella sp., C. microsphaera* and *Feral species* by He *et al.*
  (b) (440-530nm) mapping of unstressed and stressed cultures of *C. vulgaris, H. pluvialis,* and *P. purpureum* by Koch *et al*.
  (c) (532nm) growth parameters and carotenoids contents with cultivations of *C. vulgaris* by Zhang *et al*.

- **2000**: (488, 514nm) carotenoids orientation in eyespot of *Euglena* and *Chlamydomonas* by Kubo *et al.*
- **2011**: (a) (514nm) carotenoids in green algal *Dunaliella* and diatom *Phaeodactylum* by Abbas *et al.*
  (b) (1064nm) astaxanthin mapping in cystic cells in *H. pluvialis* by Kaczor *et al.*
  (c) (532nm) astaxanthin, β- carotenoids and Chl mapping in four life stages in *H. pluvialis* by Collins *et al.*
  (d) (532nm) Raman and fluorescence mapping in *C. reinhardtii* and *E. gracilis* by Urban *et al.*
- **2012**: (532nm) ^{13}C labelling to discern photosynthesizing cells in cyanobacteria *Synechocystis sp., S. elongates,* and marine species by Li *et al.*
- **2013**: (532nm) similar with Collins *et al.* (2011) by Fagerer *et al.*
- **2014**: (488nm) Chl fluorescence, carotenoids and lipid bodies mapping via dissolved carotenoids of *Nannochloropsis sp.,* green algal *D. salina, N. oleoabundans, and C reinhardtii* by Davis *et al.*
- **2016**: (532nm) astaxanthin-hyperproducing strain classification in Chlorophyta *H. pluvialis* by Liu and Huang.

Figure II-4 Schematic of selected applications using Resonance Raman spectroscopic techniques for algal pigments and domoic acids [127, 159, 161, 162, 171, 172, 175-228]

II. B. 4. Polyphosphate Determination

PolyP as an inorganic polymeric phosphate is considered as a crucial P component and the main P store pool in microalgae. PolyP is a molecule of interest in many fields, including the evolutional biology [229]. However, it is still challenging to identify and quantify polyP [8, 230-233]. The use of Raman spectroscopy to study polyP can reveal the utilization and capability of P to be taken up in algae [32], which will be applied to recover P from waste streams [9]. The strongest polyP Raman shift attributed to the stretch of P-O-P bond is expected in the 1145–1175 cm^{-1} region [234]. The shift range often results in interactions between polyP and other cations, such as calcium ions (Ca^{2+}) specifically at 1167, 1169 and 1172 cm^{-1} [14, 235] and sodium ions (Na^{+}) around 1158 cm^{-1} [14, 236-238]. The dissimilarity of the P-O bonds in polyP, phosphorous acid $P(OH)_3$ and (ortho-)phosphoric acid are assigned in the kinetic investigation by the hydrolyzing rate from polyP to Pi in the water with related the mathematical calculations with Raman spectroscopy [239, 240].

To investigate the feasibility of P-rich algal biofertilizers, the study of polyP with Raman microscopy is continued in this work (Chapter III-C). The identification and quantification of polyP in cells have been summarized in Table II-3. Previous works have summarized general P analytical techniques (e.g., [241]). One study provides a comprehensive summary table of the specificity of polyP identification in polyphosphate accumulation organisms (PAOs) [242]. Another report reviewed typical preservation methods for P determination in natural samples [42, 44]. Analytical methods [16] usually hydrolyze or extract polyP and measure the amount of degraded orthophosphate, which is measured with a colorimetric assay [243].

Table II-3 Summary of polyP identification techniques

Technique	Comment	Reference
Raman spectroscopy	Phytic acid but no polyP in higher plants [244]	microalgae [13, 15-17]; bacteria [237]; yeast [236, 245]; PAOs [235, 237, 241]
Nuclear Magnetic Resonance (NMR) spectroscopy	^{31}P NMR [232, 246, 247] only detects P-containing molecules on the basis of bond class, the presence of other molecules with phosphoanhydride bonds (e.g., of nucleotides) may cause inaccuracies. **Con**: limited sensitivity and resolution, however, hindering the detection of metabolites present at low concentrations [248]	[249, 250] microalgal [250-253]; negative in plant [254]
Transmission Electron Microscopy (TEM)	PolyP bodies appear as electron-dense granules Spatially resolved elemental analysis	microalgae [255, 256] and cyanobacteria [256, 257]; higher plant [258]
Energy-dispersive X-ray microanalysis	Determine the composition of these granules is by combining electron microscopy with energy-dispersive X-ray microanalysis	microalgae [259]; bacteria [260]; higher plant [261, 262].
Staining with basic dyes	Including toluidine blue [263, 264], methylene blue [265, 266], and neutral red by phase contrast or bright-field microscopy **Con**: all dyes can also bind nucleic acids and polyhydroxybutyrate in algae and cyanobacteria	[267, 268] microalgae [269, 270] and cyanobacteria [271]; fungi [272]; bacteria [267, 268] qualitatively for PAOs [232]

DAPI (nucleic acids, 4,-6-diamidino-2-phenylindole) staining	When bound to DNA, DAPI emits light at a wavelength of 461 nm. DAPI can also bind to RNA (emitting at appx. 500 nm) [273] and to Pi-rich compounds, including inositol polyphosphates and polyP (emitting at appx. 550 nm) **Con**: (*1*) also bind with inositol polyphosphate and nucleic acids [274]; (*2*) react with RNase and DNase [275, 276]; (3) necessary optimization for specific samples [230]	[274, 277, 278] microalgae [279]; yeast [280]
JC-D7 and JC-D8 staining	Bind polyP and heparin but do not bind to other Pi-containing molecules, such as nucleic acids, nucleotides, or sodium phosphate **Con**: lower affinities than DAPI, and binding to inositol polyphosphates was not assessed	[281] algae and higher plant [282]
High-affinity domain PPXc of PPX via immunofluorescence	polyP-binding domain (PPXc) of the E. coli polyphosphatase PPX via immunofluorescence a fluorescent protein fusion of PPXc [282] **Con**: low concentration of polyP might be detectable	yeast [283], human [284, 285] and trypanosomatids [286]
A fluorescent protein-tagged of protein RcCHAD	**Con**: to be substantiated [231]	higher plant [287]
Malachite green colorimetric assay	Involve polyP extraction and hydrolysis, e.g., by using yeast polyphosphatase PPX1 [230] **Con**: sensitive to contamination by free Pi or other Pi- containing metabolites	[288-290] yeast [291, 292]
Luciferase-based quantified assays	Reverse reaction of PPK1 causes conversion of ADP to ATP	bacteria [293]

II. B. 5. Guanine Crystal Determination

Figure II-5 displays the techniques used to identify or quantify guanine crystals in the cells. Crystal-like particles have been frequently seen in TEM images of dinoflagellates [294, 295] and symbiotic zooxanthellae over the last 50 years without being identified [296-298]. The N-rich compounds in microalgae can be detected and visualized at the ultrastructural level with advanced analytical TEM [255] or nanoscale secondary ion mass spectrometry (NanoSIMS) [299, 300]. Despite high resolution and sensitivity, these elemental imaging methods may not distinguish molecules such as uric acid and guanine, which consist of the same elements.

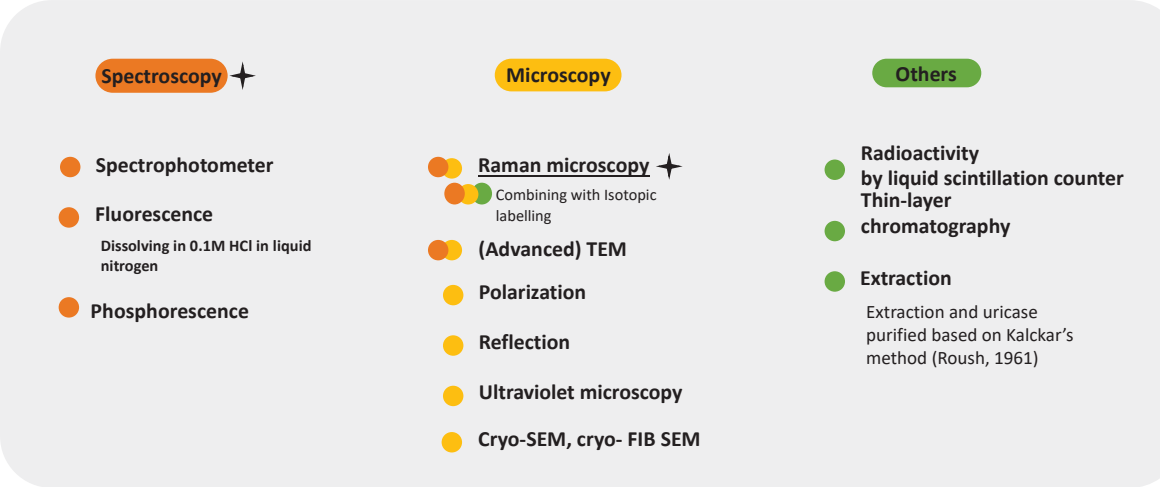

Figure II-5 Schematics of the techniques used for determining guanine crystals [301-306]. Stars (✦) label quantification methods. Note that after extraction, less stable β-guanine crystals from cells rapidly transform to stable α-guanine crystals when in the chamber [295].

Guanine crystals were first observed, extracted, and chemically identified in the free-living marine dinoflagellate *Gonyaulax polyedra* in the early 1960s [301]. This discovery was based on analogies of N storage in yeast, uptake of guanine as the N source by *Chlamydomonas roewusii,* and on a tentative interpretation of EM images of cellular inclusions that were difficult to chemically identify [307]. Guanine-liked particles in *G. polyedra* were studied further with TEM and absorption [308]. However, Clode *et al.* (2009) examined the dinoflagellate symbionts of the anemone *Aiptasia* sp. using the extracted fraction with mass spectrometry, adding an inhibitor, electron energy loss

spectroscopy (EELS), and TEM indentifing the intracellular crystalline particles as uric acid [309].

Until recently, the actual chemical natures of accumulated crystals in algae could not be analyzed *in situ* without utilizing Raman spectroscopy [17]. The difference between crystalline and amorphous solids with Raman spectroscopic analysis has been discussed by Tuschel [310]. Guanine crystals have been identified in two freshwater microalgae phylogenetically distant from dinoflagellates: the chlorophyte *D. quadricauda* [13] and the eustigmatophyte *Trachydiscus minutus* [15]. Later, the same approach was used by others to identify crystalline guanine in the marine dinoflagellate *Calciodinellum aff. operosum* [295].

II. C. Polyphosphate in Algae

II. C. 1. Background

The unusual high reactivity of P prevents it from being found in nature as a free element. [1] Historically, the identification of P was attributed to Hennig Brand, who reported distilling P from urine in 1669 [314, 315].The fertilizing effect of inorganic P and nitrogen salts on plant growth was discovered in 1840 [316]. Shortly after, guano and phosphate rock were in high demand in 1856 as external sources of fertilizers to increase crop yields [313]. Following World War II, the use of phosphate rock grew exponentially [313] even though P resources are scarce and limited. And phosphate rock takes ca. 10 to 15 million years to form naturally [317].

Under societal and commercial pressures for high agricultural output, an imbalance between depleted natural P mineral resources and excess P accumulation in the soil may be inevitable [318]. Excess phosphate and other nutrients from fertilizers applied to agricultural land leach from the soil into bodies of water, potentially causing harmful algal blooms. The capacity of microalgae to accumulate nutrients can be used to complement conventional wastewater treatment (reviewed in [9]).

[1] The flammable use of P was used for light sources originally. However, it was misused to cause many casualties since the first World War.

Reference:
311. Van Zee, R.J. and A.U. Khan, *Striking deuterium effect in phosphorus chemiluminescence. Identification of the emitting species.* Journal of the American Chemical Society, 1974. **96**(21): p. 6805-6806.
312. Nitschke, J.R., *The two faces of phosphorus.* Nature Chemistry, 2011. **3**(1): p. 90, 313. Ashley, K., D. Cordell, and D. Mavinic, *A brief history of phosphorus: from the philosopher's stone to nutrient recovery and reuse.* Chemosphere, 2011. **84**(6): p. 737-46.

Availability of biological avaliable P forms is crucial for microalgal utilization. P is mostly present in the form of orthophosphate (ortho-Pi or Pi), which is an essential nutrient for life. The speciation of inorganic phosphate as the mole fraction of total P is a function of the pH of the solution. Within the typical aquatic pH range, the dominant free Pi species range from $H_2PO_4^-$ at pH 5 to HPO_4^{2-} at pH 9 [319]. In addition to pH, Pi species are affected by cation species, other competitive complexing anion ligands, temperature, and pressure in the aquatic system [320].

Cation interactions are particularly crucial for P availability, especially in high algal cell densities. Precipitation and adsorption by Pi associated with Ca^{2+} reduce the availability of substantial Pi for algae. High photosynthetic activity may result in an increased pH [321] that can also facilitate P precipitation [322]. By contrast, free Pi leaching from apatite at environmental pH levels could also maintain the growth of mixed algal/bacterial cultures [323]. Similarly, because iron- or aluminum-Pi complexes are insoluble at neutral pH [322], they are usually biologically unavailable [324, 325]. Alternatively, exogenous organic P has been well demonstrated to be an important source of P for algal utilization [320]. The organic P may free the terminal Pi by enzymatic hydrolysis. For example, pyrophosphate supports the growth of the prymnesiophyte *Prymnesium parvum* [326] and freshwater chlorophytes *Chlorella* spp. [320].

II. C. 2. Polyphosphate

PolyP is composed of multiple Pi monomers linked with high-energy phosphoanhydride bonds [327], occurring as a linear or ring shape and having a variable degree of polymerization [328-330]. Evidence suggests that polyP may have appeared during volcanic and hydrothermal vent activities in the prebiotic Earth [229, 331]. PolyP was first described in the late 19th century in yeast and bacteria [231]. Historically, intracellular polyP was also known as "volutin" or "metachromatic" granules due to its discovery as "volutin" in *Spirillum volutans* [330, 332]. Although polyP is present in all kingdoms of life and affects many cellular functions, the importance of polyP was only discovered recently [245, 333-336]. Interestingly, no evidence to date has showed the presence of polyP in higher plants [231, 270, 337-339].

Microalgae can store a significant amount of polyP granules for diverse functions [7, 231, 340, 341], mainly in acidocalcisomes [341-345]. PolyP usually accumulates under stress conditions, though the numbers and sizes of polyP in algae might differ significantly [341, 346-348]. PolyP may play a role in forming a feedback loop in the P cycle to maintain bioavailable P in the ecosystem and primary production [349].

Polyphosphate Locations

Algae usually accumulate polyP in acidocalcisomes [341-345], as well as vacuoles and cell walls. Shortly after the discovery of polyP, acidocalcisomes were determined to be the main site of polyP synthesis and storage [350]. [2] A sophisticated TEM study identified

[2] PolyP accumulates in acidocalcisomes, nucleus, mitochondria, cytoplasm, cell wall, and endoplasmic reticulum in unicellular eukaryotes. Unlike algae, yeast accumulates polyP mainly in the vacuole and less than 10% in the mitochondria.

Reference:

351. Pestov, N.A., T.V. Kulakovskaya, and I.S. Kulaev, *Inorganic polyphosphate in mitochondria of Saccharomyces cerevisiae at phosphate limitation and phosphate excess.* Fems Yeast Research, 2004. **4**(6): p. 643-648, 352. Abramov, A.Y., et al., *Targeted polyphosphatase expression alters mitochondrial*

acidocalcisomes as *de novo* assembled vacuoles in trans-Golgi apparatus with several variations [345]. Acidocalcisomes are also calcium-rich acidic vacuoles which promote Ca^{2+} signaling and autophagy [353-356]. In addition, polyP granules can also accumulate in the cell wall of *C. reinhardtii, Volvox aureus,* and *Coleochaete scutata* [357]. However, polyP may not able to accumulate in the cell wall-deficient mutant *C. reinhardtii* CC503, which corresponds to my observation with Raman microscopy.

Polyphosphate Functions

Recently, the function and regulation of polyP in photosynthetic microorganisms was comprehensively reviewed [8, 231]. Briefly, the functions of polyP in microalgae include: (*1*) serving as the main Pi (Chapter II.C.) and energy reservoir [358]; (*2*) assisting with DNA and RNA synthesis [359-365]; (*3*) appearance in the stationary phase of algal growth; (*4*) P cycling in aquatic systems [288, 349, 366-369]; (*5*) acclimating to biotic and abiotic stresses, including nutrient deprivation, osmotic stress [370, 371], maintaining adenylate and metal cation homeostasis [372-374], and heat stress [375]; (*6*) acting as a structural or functional component for sequestering cations [376, 377] and assisting in detoxification [357]; (*7*) serving as a chaperone [378, 379]; (*8*) binding covalently to proteins to modify their activity [380]; (*9*) likely occurring in symbiotic or parasitic associations, such as in fungi [381]. Compared with the numbers and depths of polyP functions in bacteria and yeast, little is known about functions of polyP for microalgae, e.g. the functions of cell wall polyP in microalgae have not been studied yet. Cell wall polyP may serve to protect the cell from toxins and pathogens, which can be particularly crucial during cytokinesis [357, 382] in bacteria [383].

---

metabolism and inhibits calcium-dependent cell death. Proceedings of the National Academy of Sciences of the United States of America, 2007. **104**(46): p. 18091-6.

Polyphosphate Metabolisms – PolyP Kinases and Polyphosphatases

PolyP can be synthesized by polyP kinase (PPK) in prokaryotes and some eukaryotes [384-386]. The polyP polymerase activity of VTC4, as part of the vacuolar transporter chaperone (VTC) complex, in algae [341] and most other eukaryotes has gained some attention recently [387]. The synthesis reaction for polyP involves the transfer of the terminal PO_4^{3-} of ATP or 1,3-diphosphoglycerate from PPK to form a polyP chain [8]. PolyP also can degrade and releases Pi in the presence of specific enzymes, such as endo- and exo-polyphosphatases [8, 335, 388-391].

II. C. 3. Cellular Nutrient States and Polyphosphate Accumulation

Phosphate Starvation Effect and Luxury Phosphate Uptake

PolyP can serve as a dynamic Pi reservoir [332]. Hydrolyzed Pi from polyP, scavenged Pi from nucleic acids, phospholipids and other P-containing organic compounds, and spared Pi may redistribute and help algae survive during P-deprivation [320]. The indicators of P states in microalgae include the presence or absence of polyP granules [392, 393] in addition to high affinity Pi uptake, extracellular alkaline phosphatase activity, and the replacement of phospholipids with sulfolipids [358, 394-404].

PolyP accumulation significantly increases in acidocalcisomes as a result of luxury P uptake (so called “over-plus” or over-compensation responses), while algae replenish the Pi supply after being pre-cultivated in P-deficient conditions [268, 342, 343, 396, 405-411]. PolyP granules can accumulate within 3 minutes after luxury P uptake in cyanobacterium *Synechocystis sp.* PCC6803 [412]. The concentrations of total accumulated polyP vary between two *Chlamydomonas* species of *C. acidophila* KT-1 and *C. reinhardtii* C-9 during luxury P uptake [253]. The maximum accumulation in the green algae *Chlorella vulgaris* was demonstrated to occur after a minimum of eight hours of P deprivation and with 0.3 mM replenished Pi [408]. PolyP accumulation during luxury P uptake often increases under more extreme conditions, such as an extended P starvation period followed by the reintroduction of the same amount of Pi, the reintroduction of high concentration of Pi [413], or the presence of external metal ions [414, 415].

The common phenomenon of polyP accumulation and luxury P uptake has been suggested to be crucial for protecting algae from fluctuations of P availability in nature [246, 411, 416-418] and in preventing future P deficiency [246, 418]. Luxury P uptake is a special state that often causes polyP accumulation in algae [8, 419]. A better understanding and optimization of luxury P uptake and polyP accumulation will provide better strategies for recovering Pi from wastewater and producing P-rich algal biofertilizers.

Interaction with Other Factors

In addition to P deprivation, polyP accumulates significantly in algae in certain physiological states, or under stress conditions, such as during the stationary phase or with exposure to increasing temperature [375], light [412], sulfur [341, 420, 421], N deprivation [341, 345], or metal ion toxicity [332, 341, 345, 348, 414, 415, 422-427]. PolyP accumulation during the stationary phase may result in nutrient deficiency or other factors linked to cellular status. The polyP-rich acidocalcisomes have been visualized by TEM in *C. reinhardtii* during the stationary phase [345]. Similarly, *Chlorella vulgaris* accumulates more polyP when it approaches the stationary phase, in comparison with the exponential phase [408]. Interestingly, the polyP reserves in *Chlorella* strains, which accumulate during N starvation, are depleted after N reintroduction. However, the polyP reserves, which accumulate during both N and P starvation, remain in the cells after N and P repletion [428-430]. During stress from high ammonium levels, the degradation of polyP in the green algae *Dunaliella salina* maintains ATP levels and neutralizes cytosolic alkalinization [431]. Similarly, polyP degrades with sequestering metal ions in the presence of cadmium or mercury. Only the short chain polyP and Pi increase in the vacuoles of *C. reinhardtii* and and *C. acidophila* [259, 422, 423]. In addition, in green algae *D. salina* and diatom *P. tricornotum*, a hyperosmotic shock facilitates an increase in the chain length of polyP [370, 371].

II. D. Guanine in Microalgae

II. D. 1. Background

Nitrogen (N) is an essential element for all forms of life. For planktonic microalgae, N is also a key modulator for phytoplankton photosynthetic activity [432]. Primary productivity is limited by the N availability in many tropical and temperate seawaters [433]. In these N deficient waters, other essential nutrients like phosphorus [434] or iron [435] are usually limited, too. However, free-living and endosymbiotic microalgae thrive in N poor or N fluctuating environments, despite the dramatic consequences of N starvation. This finding raises questions about the long-term N reserves of microalgae.

N deficiency causes severe stress to algal cells. There are profound impacts of N deficiency on algal physiology and biochemistry [436-438], such as dramatically changing intracellular organization and rapidly rerouting metabolism. Evidence has shown that algae mobilize only intracellular inorganic N ions and low-molecular organic N compounds such as polyamines and amino acids. Furthermore, algae may obtain N from catabolizing proteins that are not essential for cell survival, followed by withdrawing from cell division or reducing the photosynthetic apparatus [439]. As a result, photosynthetic products may not be used for growth or division. However, the accumulation of energetic over-excitation and radicals have to be avoided by algae. The most well-known strategy is to generate intracellular energy carriers and carbon-rich reserves under N stress. This strategy is commonly used for neutral lipid production in algal biotechnology [436]. In addition to N deficiency, the anthropogenic efflux of N and other nutrients can produce the opposite extreme — eutrophication, which causes harmful microalgae blooms [440]. These aspects make N metabolism and storage in eukaryotic algae an ecologically, socially, and economically relevant subject in modern biology.

II. D. 2. Uptake of Guanine for Algal Utilization

The available N sources in nature usually are inorganic N, such as nitrate, ammonium or nitrite ions, and dissolved organic N [441-444] including purines [441], uric acid [442, 445-447], adenine [447], guanine [448], xanthine [449], and hypoxanthine [450]. Using purines often requires an enzymatic machinery to break down purines and utilize their N atoms. Several studies showed that guanine or adenine can serve as the only N source for algal growth, while adenine is less preferable [451, 452]. The rate of guanine uptake is also 1.6 times faster than adenine uptake [452]. Table II-4 summarizes the important studies of guanine uptake by algae. Notably, several nitrate-grown diatoms and chlorophytes can take up guanine as a N source, only after a period of N deprivation [451]. However, guanine's exocyclic nitrogenous group was thought to possibly make it difficult for guanine to be taken up by algae [450]. Thus, hypoxanthine, the prime purine, has been proposed to be a representative organic N source for marine microalgae [450]. In addition, uric acid is frequently thought to be a N source for algal growth (see review [441]). Guanine is often overlooked as a N source for algae.

Radiolabeling experiments demonstrate that *Chlorella fusca* possesses high-affinity, constitutive, active mechanisms for guanine uptake [448]. Once taken up by *C. fusca*, guanine neither leaks out of the cell nor exchanges with exogenous guanine [448]. Pettersen and Kuntsen (1974) further determines that active transport of guanine occurs in synchronized *C. fusca.* The intracellular guanine concentration is over 10-fold higher than the external guanine concentration. No guanine is observed after treatment with dinitrophenol [448], as this inhibitor disrupts the H^+ gradient, reducing ATP synthesis. There may not be sufficient evidence to demonstrate the active transport across the semipermeable plasmalemma. Future studies may focus on (*1*) if guanine transport requires the direct expenditure of algal metabolic energies and (*2*) if it is temperature sensitive or could be interrupted by metabolic inhibitors. An uptake model of the saturation kinetics of a typical enzymatic system as well as further electrochemical studies might also be considered for the future. This study should also aim to show a higher rate of transport than of permeability, the electrochemical gradient, or whether the steady-state electrochemical potential has attained equilibrium across membranes.

Table II-4 Key studies of uptake of guanine as N sources for algal growth

Strains	Reference
Six supralittoral *Haematococcus* relatives	[416]
Marine Cryptomonad *Heiniselmis virescens*	[449]
Prasinophycean flagellates	[453, 454]
Chlorella fusca and *Chlorella stigmatophora*	[448, 454]
Six marine chlorophytes	[454]
Diatoms, including *Phaeodactylum tricornutum*	[451, 455, 456]
Chlamydomonas reinhardtii	[452]
Tetraselmis subcordiformis	[454]
NEGATIVE: Two unicellular marine red algae, Porphyridium purpureum	[454]

II. D. 3. The Accumulation of Guanine Crystals

Before discovering the presence of guanine crystals in algae, in 1961, Roush has observed accumulated crystalline purine in the vacuoles of yeast *C. utilis* [304], which can actively take up guanine or other purines as their only N source [457]. The intracellular purine crystals were identified as *iso*guanine. Roush pioneered intracellular guanine studies. He utilized polarizing and ultraviolet microscopy. However, he did not explain his reasoning for identifying the crystalline structures as *iso*guanine, as the applied methods cannot distinguish between guanine and isoguanine. [3] Later, a purine metabolism study by Roush

[3] I suspect that his conclusion may relate to instability of the biogenically tautomeric structure of *iso*guanine, which may be easily mobilized and used as nutrients for yeast growth.

Reference:

and Shieh (1962) verified that (*1*) guanine, xanthine, and uric acid are catabolized; (*2*) demonstrated the presence of guanase and uricase; (*3*) showed that adenine, hypoxanthine, and several other purines are not actively accumulated in the yeast *Torulopsis candida* [459]. Unfortunately, this research was largely overlooked [460].

In algae, the accumulation of purine crystals was suspected by some without following up [307]. Pettersen thought that solid guanine accumulated in a "nonmetabolic compartment" (likely vacuoles) in *C. fusca* and metabolized only in response to the high metabolic demand of N after uptake and passing it through a "metabolic compartment" [461]. He attempted to explain the metabolic functions of guanine in *C. fusca* by his conclusion that the stored guanine is only metabolized for growth. He also concluded that the intracellular guanine is compartmentalized between a small cytoplasmic pool and a large vacuolar pool, which is consumed during N starvation [461]. The distributed location pattern of intracellular crystals was interpreted to be caused by metabolic waste or a N source [307]. The morphology of these crystals and the nutrient effects have been studied in dinoflagellates [462]. Little is known about the mechanisms of purine uptake in algae as only few studies have been conducted. These studies included investigation of guanine [463] and uric acid [441]. Lisa *et al.,* (1995) suggested the possibility that adenine and guanine are translocated into *C. reinhardtii* by a common system.

Figure II-6 summarizes that critical studies of guanine uptake by algae and algal intracellular guanine crystals in a timeline. This figure reveals the lack of studies regarding guanine in algae within the past decades. For at least a half century, the crystal-like particles have been frequently observed in dinoflagellates with TEM. The crystals also have been erroneously categorized as a part of a subcellular luminescent particle [301, 464] in the marine dinoflagellate *Gonyaulax polyedra* [307, 465]. Methodologies that allow simple but reliable

458. Jaworski, A., J.S. Kwiatkowski, and B. Lesyng, *Why isoguanine and isocytosine are not the components of the genetic code.* International Journal of Quantum Chemistry, 1985. **28**(S12): p. 209-216.

chemical identification of the cellular N reserves *in situ* are important for developing a deeper understanding of purine uptake, storage, and turnover in microalgae (Section II.B.4 and Chapter III. D.).

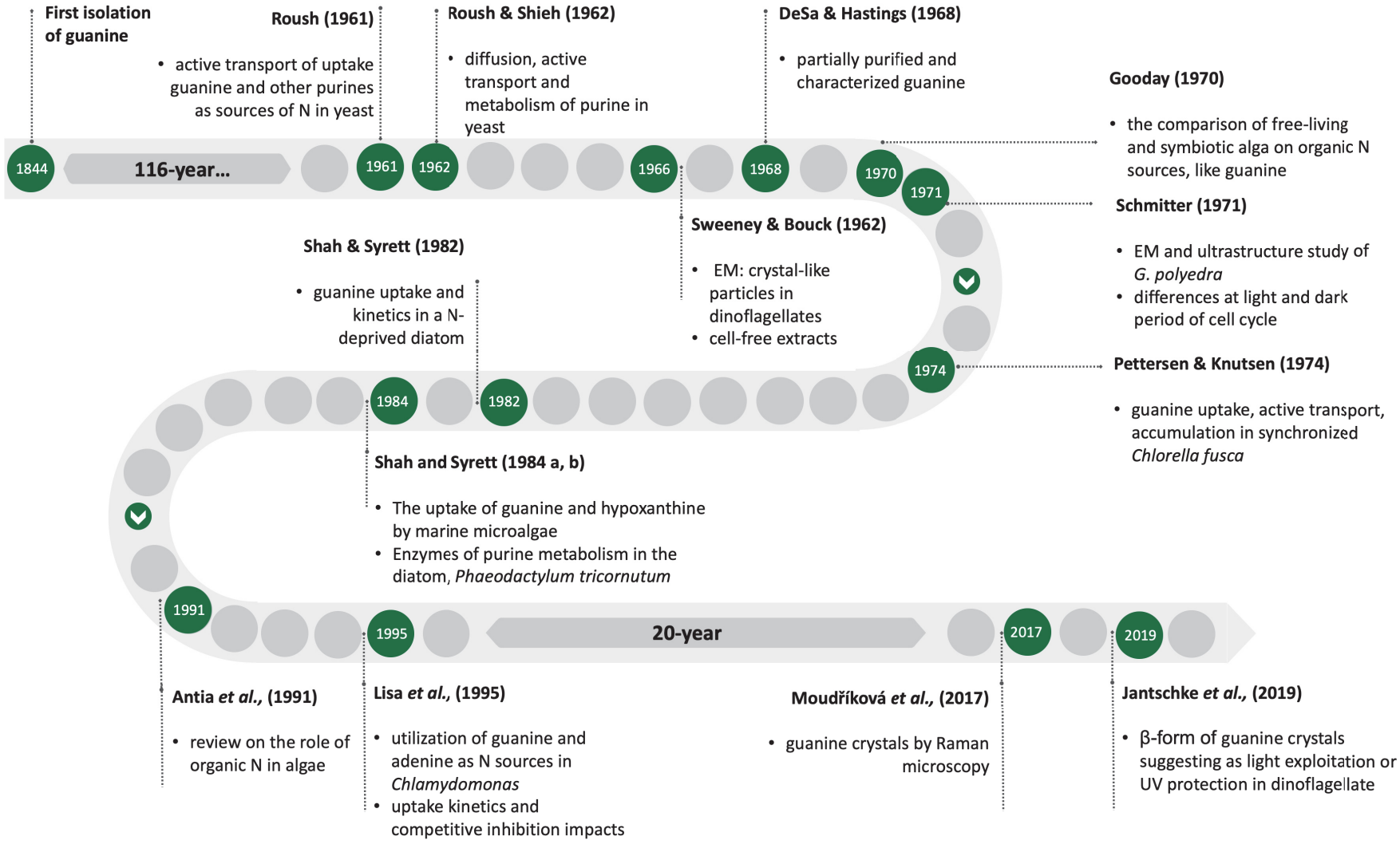

Figure II-6 Timeline of crucial guanine-related studies [13, 15, 294, 295, 301, 304, 307, 441, 448, 452-455, 457, 459, 461, 465-470]

II. D. 4. The Functions of Guanine Crystals

There is no consensus on the physiological role of guanine crystals. Biogenic guanine crystals are widespread in animals [471] but they seem to be restricted to marine dinoflagellates [294, 295, 301] and yeasts [304] in other kingdoms. Previously, the function of guanine in algae has been debated and suggested to be (*1*) an intracellular N depot [472], (*2*) photonic structures adjusting illumination of the environment [295], or (*3*) merely a metabolic waste product [295, 307, 308, 473]. At the time of this study, the possibility of multiple functions for guanine crystals has not been proposed in literature yet.

More indirect evidence suggests the function of light manipulators in marine algae [295]. The crystalline structures of guanine in algal cells might serve to modulate effective photosynthetically-active irradiance. Guanine crystals are optically active. Their high index of refraction plays an important role in reflecting or refracting light in many biological systems. The optical properties of guanine in animals are well established and have been studied by Addadi *et al.,* (e.g., [471, 474]). Interestingly, they strongly doubt that guanine can be a N source in microalgae [295].

Guanine crystals are well-known in the animal kingdom, where they mostly serve as diffusors, multi-layer mirrors, and photonic structures [471, 474, 475]. Biological control interacts with the crystal structure properties of guanine, which is speculated to be manipulated at the molecular level [475, 476]. Quenching of light scattering by biogenic guanine crystals from goldfish scales was observed [477]. The mechanism behind this observation of magnetic orientation of guanine crystals was further confirmed by diamagnetic anisotropy [478]. Guanine crystals from goldfish scale and from diatom cells were also studied for their magneto-optic properties in aqueous media [479]. Guanine crystals from goldfish scales were able to proportionally increase the fluorescence intensity at 600–700 nm of the photosynthetic activity by the marine algae *Pleurochrysis carterae* [477]. This increase may be caused by supplying light more effectively with a cooperative light reflection pattern of the magnetic field.

Chapter III. Studies

III. A. Overview

Phytoplankton thrives even in environments with fluctuating or scarce nutrients. However, the mechanisms of long-term nutrient reserves in microalgal cells remain unclear. Without chemical staining or other complex specimen preparations, Raman microscopy provides a sophisticated approach to identify, quantify, and localize crucial biomolecules, which are in particular involved in nutrient storage in microalgae.

This chapter contains three distinct manuscripts that are subsections of my thesis. Figure III-1 provides an overview of these studies. Section III.B. includes a systematical study of algal photobleaching by using inhibitors and other treatments. The study also proposes a practical solution to characterize fixated algae with Raman measurements. This solution provides the opportunity to study dynamic changes in algae at any timepoint throughout an experiment.

In the following Sections III.C. and D., it was demonstrated that dynamic changes occur in algal intracellular phosphorus (P) and nitrogen (N) storage pools, respectively. The experimental schematic in Figure III-2 shows how algae are first starved of the nutrient, then the nutrient supply is restored, to study nutrient accumulation. Following P reintroduction, the polyphosphate (polyP) pools were monitored while they accumulate for future growth (Section III.C.). During this stage, it can be harvested and processed as algal biofertilizers for crops. Section III.D. demonstrates that guanine crystals act as a dynamic N storage pool in various algae species. This work also suggests that guanine crystals may also be multifunctional, like polyP.

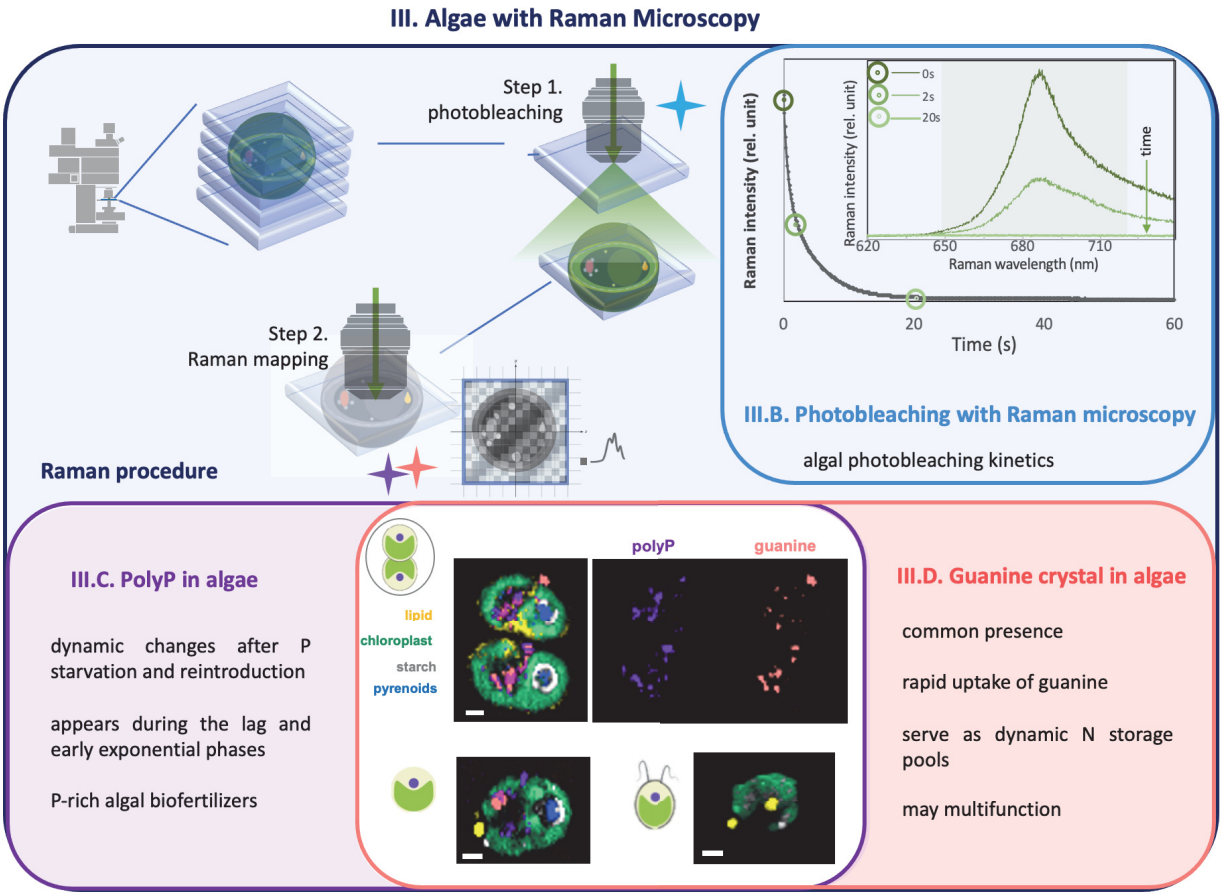

Figure III-1 A Venn diagram of the schematic layout of studies based on the chapter contents and their connections.

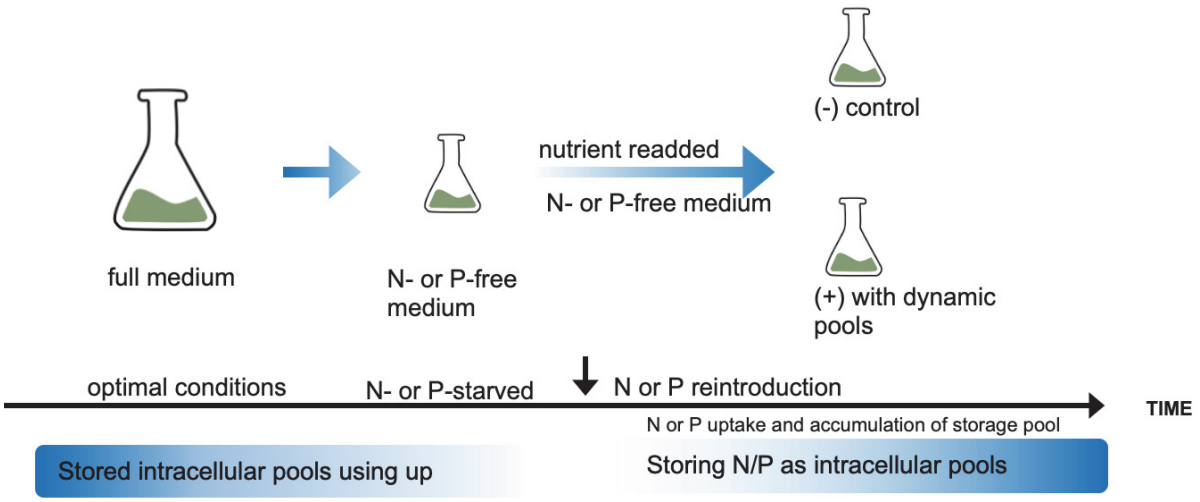

Figure III-2 Schematic of the process for studying the dynamic changes of algal nutrient storage pools.

III. B. Algal Photobleaching with Raman Microscopy

III. B. 1. Introduction

Photobleaching is a process that reduces algal fluorescence intensity due to the decomposition of luminescent materials by light. It can be used to suppress autofluorescence for easier Raman determination (Section II.B.), and is particularly important in Raman spectroscopy of highly fluorescent biological samples such as microalgae. Usually, the broad fluorescence peak of chlorophylls (Chls) is at least one hundred times higher than the strongest Raman signals in algae, such as these of carotenoids and lipids. Other biomolecules, which have weaker Raman signals, can only be detected after photobleaching. The photobleaching protocol has so far been reported only in photosynthetically competent algae [15-17, 303].

Here, it is aimed at extending the application range of photobleaching to photosynthetically impaired algae and, particularly, to algae that are chemically fixed, e.g., for storage. This study is expected to separate biological experiments and Raman measurements by allowing the sample to be stored. With this process, storage would not impair photobleaching efficiency. So far, this has not been possible. Thus, algae samples have had to be measured within a very short period after sampling. For example, Raman mapping of a typical algal cell of 5 μm diameter requires approxmately 20 minutes with a spatial resolution of 300 nm per pixel. This resolution is the minimum for identifying cell components such as starch, polyphosphate and guanine crystals. Despite the time constraint, to characterize a culture, minimum of four randomly selected cells need to be measured. Including sampling and sample preparation, characterzing a culture by Raman microscopy takes at least two hours. The comparable conventional analytical methods take significantly longer [15-17, 303]. The current way of Raman measurements limits the experimental time resolution that would be desirable for capturing the fast processes, such as the accumulation and mobilization of storage compounds. However, with a photobleaching protocol that would be applicable to chemically fixed samples, one could rapidly sample, fix, and store the samples and perform the photobleaching and Raman measurements at later time.

To achieve this, the kinetics of algal photobleaching was systematically studied, using the Raman microscope under different conditions. The central working hypothesis is that reactive oxygen species (ROS), byproducts of photosynthesis, are largely responsible for photobleaching during Raman microscopy for photosynthetically competent algal cells. This hypothesis is tested by applying chemical agents and treatments that reduce photosynthetic activity as well by agents that increase ROS generation or that directly increase ROS concentration. Further, the effects of two common chemical fixatives, formalin (typically used for histology) and glutaraldehyde (used for ultrastructural electron microscopy), were investigated on the kinetics of the photobleaching in Raman microscope.

A detailed report on this research has been submitted for publication to *Photochemistry and Photobiology*. My contribution to this study is the design and execution of the experiments, analysis of the data, writing of the manuscript, and organization of the submission.

III. B. 2. Result

Photobleaching significantly reduces autofluorescence of Chls in algae. A double exponential function simulates the kinetics of algal photobleaching well. ROS and active photosynthesis significantly support algal photobleaching. It is proposed that formalin-fixed cells and out-of-focus photobleaching should be used for Raman microscopy of algal cells. It requires quantification and localization of biomolecules, which have weak Raman signals. This approach will be particularly important for experiments where pools like polyphosphate or guanine occur transiently. Thus, rapid sampling is combined with fixation and storage for later Raman analysis.

Photochemistry and Photobiology

Photobleaching of algal cells for rapid chemical mapping by Raman microscopy

Lu Gao*[1, 2, 3], Peter Mojzeš [1, 2], Ladislav Nedbal[1]

[1]. Institute of Bio- and Geosciences/Plant Sciences (IBG-2), Forschungszentrum Jülich, Wilhelm-Johnen-Straße, D-52428 Jülich, Germany,
[2]. Institute of Physics, Faculty of Mathematics and Physics, Charles University, Ke Karlovu 5, CZ-12116 Prague 2, Czech Republic,
[3]. Faculty of Mathematics and Natural Sciences, Heinrich Heine University, Universitätsstraße 1, D-40225 Düsseldorf, Germany.

*Corresponding author e-mail: lugao100@uni-duesseldorf.de (Lu Gao)

Photochemistry AND Photobiology

Photobleaching of algal cells for rapid chemical mapping by Raman microscopy

Journal:	*Photochemistry and Photobiology*
Manuscript ID	Draft
Wiley - Manuscript type:	Research Note
Date Submitted by the Author:	n/a
Complete List of Authors:	Gao, Lu; Forschungszentrum Jülich Institut für Bio- und Geowissenschaften Bereich 2 Pflanzenwissenschaften; Charles University Faculty of Mathematics and Physics; Heinrich Heine University Dusseldorf Faculty of Mathematics and Natural Sciences Mojzeš, Peter; Forschungszentrum Julich Institut fur Bio und Geowissenschaften Bereich 2 Pflanzenwissenschaften; Charles University Faculty of Mathematics and Physics Nedbal, Ladislav; Forschungszentrum Julich Institut fur Bio und Geowissenschaften Bereich 2 Pflanzenwissenschaften
Keywords:	Photobleaching, Raman microscopy, Microalgae, Reactive oxygen species, Formalin

Photobleaching of algal cells for rapid chemical mapping by Raman microscopy

Lu Gao*[1,2,3], Peter Mojzeš[1,2], Ladislav Nedbal[1]

[1]. Institute of Bio- and Geosciences/Plant Sciences (IBG-2), Forschungszentrum Jülich, Wilhelm-Johnen-Straße, D-52428 Jülich, Germany, [2]. Institute of Physics, Faculty of Mathematics and Physics, Charles University, Ke Karlovu 5, CZ-12116 Prague 2, Czech Republic, [3]. Faculty of Mathematics and Natural Sciences, Heinrich Heine University, Universitätsstraße 1, D-40225 Düsseldorf, Germany

*Corresponding author e-mail: lugao100@uni-duesseldorf.de (Lu Gao)

ABSTRACT

Raman microscopy is an invaluable tool for *in situ* identification of molecular components in biological cells. However, the applicability of this method to photosynthetic organisms is reduced. The strong chlorophyll fluorescence may obscure relevant Raman signals. This fluorescence background can be eliminated by photobleaching, which is sometimes inefficient or too slow to be practical. To establish a reliable photobleaching protocol for algal cells, we studied their photobleaching kinetics by Raman microscopy, exploring how this process depends on the choice of the chemical pre-treatment of the cells. Particular attention was paid to identifying the roles of photosynthetic activity and reactive oxygen species in the photobleaching process. We also investigated whether photobleaching is pragmatic in cells that are chemically fixed by procedures, which are already routinely used in microscopic analysis. The main result of this study is the finding that fixation by formalin allows effective photobleaching of the algal cells. With this, one can collect samples during rapid biological processes, such as during accumulation or mobilization of storage reserves, or a cell cycle, fix the sampled cells by formalin and analyze the fixed cells later by Raman microscopy.

INTRODUCTION

Raman spectroscopy are increasingly used for chemical identification and quantification in a broad variety of biological samples in recent decades (1, 2). Interestingly, algal cells remained on the periphery of this interest. In spite of an early milestone of the Raman microscopic technique was used to identify *in situ* lipid droplets in the algae *Botryococcus braunii* (3) and a carotenoid peridinin in the light-harvesting complex of *Pyrocystis lunula* (4). Further expansion of Raman techniques in the research of algae and plants was limited because the relatively weak Raman signals were often overshadowed by strong fluorescence emissions from photosynthetic pigments (5). Only the strong Raman scattering of carotenoids (6-8), lipids (3, 9-12), or higher plant cell walls (13, 14) has been explored and exploited. Recently, the weaker Raman signals of other components in algae, such as starch and polyphosphate were unveiled only after photobleaching (15-19).

Photobleaching allowed for a substantial reduction of the fluorescence background from photosynthetic pigments and led to a higher signal-to-noise ratio in the Raman spectra (20-25). Photobleaching had earlier been applied to enable Raman analysis also of other samples, such as from plants (26), pollens (25), pigmented bacteria (27), waterborne pathogens (28), human tissues

(21-24, 26, 29-31), melanosomes (32), paints (20, 33), dyes (34, 35), as well as other materials (36-44). These earlier studies of photobleaching focused on the feasibility and the kinetics of autofluorescence suppression.

Here, we studied photobleaching specifically in microalgal cells, which contain high amounts of photosynthetic pigments that emit strong fluorescence with a quantum yield of several percent. The objective of this study was to develop rapid and robust photobleaching protocols suitable for specific requirements of Raman microscopy. Towards this goal, we first studied the wavelength dependence of photobleaching as well as the impact of various chemical interventions that limit photosynthetic reactions or influence the development of reactive oxygen species.

Based on this, we looked in detail at the well-established fixation agents, glutaraldehyde and formalin. The agents are known to preserve photosynthetic activity and they should not disrupt the photobleaching mechanisms that are needed for Raman analysis. While the application of glutaraldehyde had a detrimental effect on the Raman analysis, the fixation by formalin was found not to interfere with photobleaching and later Raman measurements. This capability is a key to separate sampling, storage, and Raman analysis of algal cell. Thus, it

allows investigation of dynamic cellular processes, such as those of carbon, phosphorus, nitrogen storage pool metabolism (16, 18, 19, 45-47) with a high time resolution.

MATERIALS AND METHODS

Strain, cultivation and chemicals: *Chlorella vulgaris* IPPAS C1 from K.A. Timiryazev Institute of Plant Physiology, Russian Academy of Sciences (IPPAS) (Moscow, Russia) and *Desmodesmus quadricauda* (Turpin) Brébisson strain Greifswald/15 from the Culture Collection of Autotrophic Microorganisms in the Institute of Botany (Třeboň, Czech Republic) were used. The cultures were cultivated and synchronized under alternating light and dark (14:10 h) conditions in lab-made 70 mL column photobioreactors sparged by air, illuminated by 200 μmol(photons)·m^{-2}·s^{-1} from warm-white light-emitting diodes at 25 °C. The algae grew in a rich cultivation medium (48). All chemicals used for media were purchased from Sigma-Aldrich (St. Louis, MO, USA). Chemical interventions with concentrations and application procedures are described in the Supplementary Material.

Raman microscopy, photobleaching, and data analysis: Raman scattering was measured with a WITec Alpha 300 RSA Raman microscope (WITec, Ulm, Germany) using an oil-immersion objective UPlanFLN 100×, NA 1.30 (Olympus, Tokyo, Japan) or with a LabRam

Evolution inverted Raman microscope (Horiba Scientific, Longjumeau, France) as described earlier (16-18). The time of integration of a single-pixel signal was always 0.1 s with a sampling frequency of 10 pixels per second. The software WITec Project Plus 5.1 (WITec, Ulm, Germany) and LabSpec 6 (Horiba Scientific, Longjumeau, France) were utilized to obtain and process the Raman spectra. Further details on the Raman microscopy methods were described earlier in (16-18).

RESULTS AND DISCUSSION

Detecting strong Raman signals in algal cells

To establish a reference for studying weak Raman signals, the first objective was to characterize the interfering fluorescence emission and compare it with a strong Raman signal of carotenoids, which can be detected even without photobleaching. In such a case, which illustrates the most common approach used for Raman imaging until recently, the algal cell is excited point-by-point using a high or moderate excitation power, without any preliminary photobleaching. The signal obtained with a 532 nm excitation laser on the cell of *Desmodesmus quadricauda* is dominated by the chlorophyll fluorescence (Chl-F) emission with a dominant peak at 684 nm, which corresponds in Fig. 1 (top panel) to ca. 4177 cm^{-1} of the Raman spectral shift relative to

the 532 nm excitation wavelength. At the strong fluorescence background, only the most intense Raman peaks of carotenoids at 1154 and 1518 cm^{-1} can be noticed (top panel of Fig. 1). However, carotenoids are often the only biomolecules that can be identified in unbleached cells using this direct approach. Such a direct Raman scanning results in the simultaneous in-focus photobleaching of the Chl-F as well as partial (or even full) photodegradation of carotenoids. If the cell does not burn during the first measurement and if such a point-by-point, in-focus pre-photobleached cell is scanned again, Raman features of other biomolecules are emerging at a substantially reduced background. The carotenoids were already largely photo-bleached after the first Raman scanning as can be seen in the bright field image in the middle panel of Fig. 1. The Chl-F peak at 684 nm in the second Raman scanning was already suppressed and replaced by a broad undifferentiated fluorescence background centered at ca. 1800 cm^{-1}, on top of which the Raman signal of carotenoids was well visible and could be effectively extracted by background subtraction. During a third scanning immediately following the second one, the fluorescence background was further reduced, so that even weaker Raman features of crystalline guanine became detectable (Fig. 1, bottom).

<Figure 1>

The cells in Fig. 1 were cultured under suboptimal nutritional conditions, which led, according to our experience with microalgae in various physiological states, to sluggish photobleaching regardless of stress mechanism and light-exposure history. This choice was made deliberately to illustrate the problems often encountered with stressed cultures that might be of great interest in biotechnology, aiming often at valuable compounds that are stress-induced or stress-enhanced (47, 49). The above examples show that, in principle, one can detect strong Raman signals such as those of carotenoids in spite of the fluorescence background already in the first scan. The weaker Raman signals, such as those of crystalline guanine, can be revealed after direct, in-focus photobleaching that may occur in multiple Raman laser scans. However, such a procedure is time-consuming, not reliable, and often ends in cell burning.

An additional argument against the point-by-point, in-focus photobleaching by direct Raman scanning is that the result depends on the scanning direction. The voxels close to the origin of the scanning are hit largely only by the focused laser beam while the voxels that are scanned later receive a large photon dose due to scattering prior to when the laser is aimed at them. This effect can cause asymmetry artifacts in the Raman maps showing the spatial distribution of photosensitive compounds, as

well as in the remaining fluorescence background and signal-to-noise ratio.

In addition to the point-by-point, in-focus photobleaching in the course of repeated Raman scanning, one can consider another possibility how to reduce interference of the strong autofluorescence. We could choose a laser wavelength that is not absorbed by photosynthetic pigments, and thus may be expected to excite little or no fluorescence emission. Excitation by 785 nm and 830 nm might be a good compromise as being far from the chlorophyll (around 430 nm and 662 nm) and carotenoid (400-500 nm) absorption bands. However, excitation by these commonly used laser wavelengths may suffer from being too far in the near-infrared range. The Raman signals of biomolecules are in general weak because of their fourth-power dependence on the excitation frequency, and because detection by silicon CCD detectors is ineffective (50). Moreover, Figure SM1 (see Supplementary Materials) demonstrates new challenges that occur with 785 nm excitation of photosynthetic microalgae. Namely, a non-specific background increases rather than decreases with prolonged laser exposure and the Raman signal of carotenoids progressively decreases, despite the fact that neither carotenoids nor chlorophyll absorbs at this wavelength. We do not have a mechanistic explanation for the observed phenomena. But we suspect the involvement of carotenoid triplet states (51)

resulting in photobleaching of carotenoid molecules when exposed by the intense near-infrared laser light needed for the excitation of Raman scattering.

Shifting the excitation further to 830 nm eliminates pigment photobleaching, as documented by the bright-field images of the exposed cell in Figure 2. Neither the comparison of the bright-field images taken before and after the laser scanning nor the time-evolution of the steep background show signs of significant photobleaching. The strong carotenoid signal was still visible in the background and it was not gradually photobleached as in the case at 785 nm as shown in Figure SM1 (see Supplementary Materials). This excitation may be advantageous for the non-destructive studies of the spatial distribution of carotenoids in living microalgae. However, the Raman signal of carotenoids was the only one that could be unambiguously identified in the 830 nm excited Raman spectra of microalgae. The long-wavelength excitation was thus confirmed to be effective for the detection of Raman signals of carotenoids that are strong enough for detection on the background of persistent fluorescence emission (Figure 2). This is, however, not a viable strategy for biomolecular compounds with weaker Raman signals.

<Figure 2>

Photobleaching for unveiling weak Raman signals

As demonstrated above, neither point-by-point, in-focus photobleaching, nor Raman excitation by wavelengths outside the absorption of the major photosynthetic pigments, leads to satisfactory results in terms of reliable detection of biomolecules other than carotenoids in algae. Nevertheless, for detecting weaker Raman signals in photosynthetic organisms, the correct photobleaching protocol remains a relevant choice but needs to be optimized. As already shown previously, the wide-field, low-power photobleaching allows practical Raman detection of starch, polyphosphate, lipids, and crystalline guanine (17).

The practical implementation of the wide-field, low-power photobleaching is described in Figure 3. First, the studied cell is placed in the focal plane of a microscopic objective. Then, the objective is displaced ca. 30 - 50 μm above the selected focal plane, and the specimen is exposed to the excitation laser beam for a selected period of time. This way, the entire cell is illuminated by a cone of the defocused beam instead of the beam focused on a selected point. In the course of illumination, the whole-cell fluorescence and the Raman signals detectable even in this out-of-focus position can be registered as time-series Raman spectra and used for monitoring the effectiveness of the photobleaching process. Finally, the objective is returned to

the initial focal plane, and scanning of the Raman spectra of the photobleached cell across the focal plane is executed.

<Figure 3>

This approach was successfully applied in several of our recent studies (16-19, 45). We proposed that photobleaching relying on oxidative destruction of the photosynthetic pigments as well as their transient photoproducts by the reactive oxygen species (ROS) produced by the photosynthetic apparatus itself often results in satisfactory suppression of the fluorescence background. Regardless of the detailed mechanism underlying the production of ROS by the self-degrading photosynthetic apparatus, the wide-field, low-power photobleaching has been found superior to the point-by-point, in-focus one. However, it should be openly noted that photobleaching of certain algal species or the cells in particular physiological states or in passing specific cell cycle phases was extremely difficult despite applying this approach. Those were typically algal cells with an impaired or reduced photosynthetic capacity such as those used in Figure 1.

Photobleaching of chemically-treated algal cells

To optimize the photobleaching protocol depicted in Figure 3, one needs first to quantify the photobleaching kinetics. In the earlier studies of non-photosynthetic systems, single, double, or stretched exponential functions were proposed to fit the

photobleaching kinetics in (32, 52-55), (21-23, 26, 29, 30, 35, 43), and (40), respectively. The kinetics of the photobleaching in photosynthetic organisms may differ from other organisms because ROS and singlet oxygen are the inherent by-products of the charge separation reactions, as described in (51). The photoinhibition, the loss of photosynthetic capacity under illumination (56), occurs even at moderate photon flux densities and is compensated for by a multitude of protection and repair mechanisms (57). Only when the light intensity is too strong and degradation of photosynthetic capacities too fast, does photoinhibition manifest, leading, in extreme cases, to photobleaching. The unregulated and uncompensated overproduction of the singlet oxygen and ROS, so undesirable for the proper functioning of the photosynthetic apparatus, is probably responsible for the photobleaching of microalgae enabling their Raman mapping. The photon flux density of the 532 nm laser beam, 10 mW power, in-point focused at the selected cell pixel, as used in the Raman mapping experiment shown in Figure 1, is ca. eight orders of magnitude higher than from the maximum sunshine possible in Nature. Therefore, it is not surprising that photo-destruction of the cell photosystem and the subsequent photobleaching of the illuminated pixel occurs even in a fraction of a second during the laser scanning. However, such high intensity often leads to local overheating and burning.

On the contrary, the photon flux densities in the wide-field, low-power, out-of-focus photobleaching configuration (Figure 3, Step 2) is around 4 - 5 orders of magnitude lower, achieving the levels of 10^6 - 10^7 $\mu mol(photons) \cdot m^{-2} \cdot s^{-1}$ and covering the areas of 10^3 – 10^4 μm^2, i.e., the entire cell or several cells at once. Those reduced photon flux densities are sufficient to achieve photobleaching within several seconds without any apparent heat damage to the large cellular structures. This process would be visible by bright-field imaging before and after the treatment (Figure 3).

The decay of the Chl-F during the photobleaching process can be monitored directly as a decrease of the 684 nm band shown in Fig. 1, top row. According to our experiments, the kinetics of this decrease can be well approximated as a sum of two exponentials with time constants τ_{fast} and τ_{slow}. The effects of various treatments on photobleaching kinetics can, thus, be quantified by determining the ratios $\frac{\tau_{fast}}{\tau_{fast}^{CONTROL}}$ and $\frac{\tau_{slow}}{\tau_{slow}^{CONTROL}}$ that are presented in Figure 4. Assuming that photosynthetically produced ROS, including singlet oxygen (see Supplementary Text in Supplementary Materials), are facilitating photobleaching under the wide-field, out-of-focus Raman illumination as they interfere with photoinhibition in plants and algae (51), several chemical agents were chosen to modulate the ROS formation.

First, the photosynthetic oxygen formation in the algal cell was impaired either by the herbicide DCMU (3-(3,4-dichlorophenyl)-1,1-dimethylurea) that blocks re-oxidation of the Photosystem II acceptor side or by a 60 ℃ heat treatment that destroys the oxygen-evolving complex on the Photosystem II donor side. With Photosystem II activity blocked, the photobleaching time constants τ_{fast} and τ_{slow} were more than 10-time slower than in the fully photosynthetically active control. This result independently confirms the earlier phenomenological observations, which photosynthetically incompetent cells are hard to photobleaching.

The involvement of molecular oxygen is supported by slow photobleaching rates that were measured when the concentration of dissolved oxygen was lowered by sodium dithionite or by glucose/glucose oxidase/catalase. Oxygen participates in the photobleaching process in the form of radicals so that superoxide dismutase (O_2^-) or catalase (H_2O_2) is slowing the process. Superoxide dismutase converts the superoxide radical into hydrogen peroxide also slowed the photobleaching considerably. This result indicated that hydrogen peroxide, which also occurs as an unwanted by-product of photosynthesis (58), contributes to the photobleaching less than superoxide. Indeed, catalase, which converts hydrogen peroxide to oxygen, influenced photobleaching only marginally. Production of hydrogen peroxide by reduction of

added methyl viologen on the reducing side of Photosystem I did not accelerate the photobleaching relative to the control. However, when hydrogen peroxide was added at a high concentration, the photobleaching became nearly 10-time faster than in the control without addition.

<Figure 4>

Of particular interest are chemical treatments that include cross-linking agents - glutaraldehyde and formalin (formaldehyde water solution). Both fixation agents are widely used for algal immobilization and do not necessarily lead to loss of photosynthetic oxygen evolution (59). This would make these agents optimal candidates for preserving the cells sampled during the biological experiment for later analysis by Raman microscopy. As Figure 4 shown, glutaraldehyde alone slows down the photobleaching, which would complicate the Raman experiment or at least make it longer. This deficit can be eliminated when a glutaraldehyde-fixed sample is treated with added hydrogen peroxide. The glutaraldehyde undergoes in water solution complex chemical transformation including generation of species that absorb visible light (60) (61). Empirically, as Table S2 summarized (see Supplementary Materials), we observed that glutaraldehyde-fixed cells, either treated with hydrogen peroxide or not, degraded quickly while Raman spectra were

359 measured. Most likely, the degradation was due to the sample
360 overheating by absorption of the strong laser light.

361 Most promising is, however, fixation by formalin alone, which
362 preserves photobleaching rates in stored samples at the level of
363 freshly sampled cells (Figure 4) and no enhanced burning of the
364 formalin-fixed cells by the laser was observed. The
365 photosynthetically fully competent *D. quadricauda* from
366 exponentially growing culture was sampled, fixed with formalin,
367 and stored for three days prior to the experiment presented in
368 Fig. 5. Before Raman mapping, the coenobium was photobleached
369 using the protocol used to produce Figure 3. The scanning of the
370 formalin-treated and photobleached cells revealed both the strong
371 spectral signatures of carotenoids as well as the weak Raman
372 scattering signal of guanine.

373 <Figure 5>

374 The wide-field, out-of-focus photobleaching suitable for Raman
375 microscopy of microalgae was shown to depend on the
376 photosynthetic activity of the investigated cells. However, even
377 in the case that the cell was photosynthetically incompetent,
378 the photobleaching after the addition of hydrogen peroxide was
379 shown to be effective. This is also the case when fixation by
380 glutaraldehyde or formalin was used to preserve the samples for
381 later Raman analysis. This is particularly important in

experiments when the analyzed molecules, e.g., starch, lipids, polyphosphate or crystalline guanine, occur transiently and rapid sampling is optimally combined with fixation and storage, followed by later Raman analysis.

ACKNOWLEDGMENTS: This work has been supported in part by Algnutrient-UrBioSol (Grant FKZ 031B0453A) of the Federal Ministry of Education and Research, Germany and GAČR grant (17-06264S). The advice from colleagues Dr. Silvia Schrey and Dr. Dean Calahan was greatly appreciated.

REFERENCE

1. H.J. Butler, L. Ashton, B. Bird, G. Cinque, K. Curtis, J. Dorney, K. Esmonde-White, N.J. Fullwood, B. Gardner, and P.L. Martin-Hirsch, *Using Raman spectroscopy to characterize biological materials.* Nature Protocols, 2016. **11**(4): p. 664.

2. J.R. Ferraro, *Introductory Raman spectroscopy*. 2003: Elsevier.

3. C. Largeau, E. Casadevall, C. Berkaloff, and P. Dhamelincourt, *Sites of accumulation and composition of hydrocarbons in Botryococcus braunii.* Phytochemistry, 1980. **19**(6): p. 1043-1051.

4. A. Dupaix, B. Arrio, B. Lecuyer, C. Fresneau, P. Volfin, J.C. Merlin, P. Dhamelincourt, and B. Debettignies, *Intracellular spectroscopic studies of a bioluminescent cell - Pyrocystis-lunula.* Biology of the Cell, 1982. **43**(3): p. 157-162.

5. G.C. Papageorgiou, *Chlorophyll a fluorescence: a signature of photosynthesis*. Vol. 19. 2007: Springer Science & Business Media.

6. V.E. de Oliveira, H.V. Castro, H.G. Edwards, and L.F.C. de Oliveira, *Carotenes and carotenoids in natural biological samples: a Raman spectroscopic analysis.* Journal of Raman Spectroscopy, 2010. **41**(6): p. 642-650.

7. H. Schulz, M. Baranska, and R. Baranski, *Potential of NIR-FT-Raman spectroscopy in natural carotenoid analysis.* Biopolymers, 2005. **77**(4): p. 212-21.

8. J. Jehlicka, H.G. Edwards, and A. Oren, *Raman spectroscopy of microbial pigments.* Applied and Environmental Microbiology, 2014. **80**(11): p. 3286-95.

9. L. Cavonius, H. Fink, J. Kiskis, E. Albers, I. Undeland, and A. Enejder, *Imaging of lipids in microalgae with coherent anti-stokes Raman scattering microscopy.* Plant Physiology, 2015. **167**(3): p. 603-16.

10. K. Czamara, K. Majzner, M.Z. Pacia, K. Kochan, A. Kaczor, and M. Baranska, *Raman spectroscopy of lipids: a review.* Journal of Raman Spectroscopy, 2015. **46**(1): p. 4-20.

11. O. Samek, A. Jonas, Z. Pilat, P. Zemanek, L. Nedbal, J. Triska, P. Kotas, and M. Trtilek, *Raman microspectroscopy of individual algal cells: sensing unsaturation of storage lipids in vivo.* Sensors (Basel), 2010. **10**(9): p. 8635-51.

12. Z. Pilát, S. Bernatová, J. Ježek, M. Šerý, O. Samek, P. Zemánek, L. Nedbal, and M. Trtílek, *Raman microspectroscopy of algal lipid bodies: β-carotene quantification.* Journal of Applied Phycology, 2012. **24**(3): p. 541-546.

13. N. Gierlinger, T. Keplinger, and M. Harrington, *Imaging of plant cell walls by confocal Raman microscopy.* Nature Protocols, 2012. **7**(9): p. 1694-708.

14. C.F. Sene, M.C. McCann, R.H. Wilson, and R. Grinter, *Fourier-transform Raman and Fourier-transform infrared spectroscopy (an investigation of five higher plant cell walls and their components).* Plant Physiology, 1994. **106**(4): p. 1623-1631.

15. D. Wei, S. Chen, and Q. Liu, *Review of fluorescence suppression techniques in Raman spectroscopy.* Applied Spectroscopy Reviews, 2015. **50**(5): p. 387-406.

16. S. Moudrikova, A. Sadowsky, S. Metzger, L. Nedbal, T. Mettler-Altmann, and P. Mojzes, *Quantification of Polyphosphate in Microalgae by Raman Microscopy and by a Reference Enzymatic Assay.* Anal Chem, 2017. **89**(22): p. 12006-12013.

17. Š. Moudříková, P. Mojzeš, V. Zachleder, C. Pfaff, D. Behrendt, and L. Nedbal, *Raman and fluorescence microscopy sensing energy-transducing and energy-storing structures in microalgae.* Algal research, 2016. **16**: p. 224-232.

18. Š. Moudříková, L. Nedbal, A. Solovchenko, and P. Mojzeš, *Raman microscopy shows that nitrogen-rich cellular inclusions in microalgae are microcrystalline guanine.* Algal Research, 2017. **23**: p. 216-222.

19. N. Siebers, D. Hofmann, H. Schiedung, A. Landsrath, B. Ackermann, L. Gao, P. Mojzeš, N.D. Jablonowski, L. Nedbal, and W. Amelung, *Towards phosphorus recycling for agriculture by algae: Soil incubation and rhizotron studies using 33P-labeled microalgal biomass.* Algal Research, 2019. **43**: p. 101634.

20. A. Macdonald and P. Wyeth, *On the use of photobleaching to reduce fluorescence background in Raman spectroscopy to improve the reliability of pigment identification on painted textiles.* Journal of Raman Spectroscopy, 2006. **37**(8): p. 830-835.

21. H. Wang, J. Zhao, A.M. Lee, H. Lui, and H. Zeng, *Improving skin Raman spectral quality by fluorescence photobleaching.* Photodiagnosis Photodyn Ther, 2012. **9**(4): p. 299-302.

22. J.S. Day, H.G. Edwards, S.A. Dobrowski, and A.M. Voice, *The detection of drugs of abuse in fingerprints using Raman spectroscopy I: latent fingerprints.* Spectrochimica Acta Part A: Molecular and Biomolecular Spectroscopy, 2004. **60**(3): p. 563-568.

23. J. Schleusener, J. Lademann, and M.E. Darvin, *Depth-dependent autofluorescence photobleaching using 325, 473, 633, and 785 nm of porcine ear skin ex vivo.* Journal of Biomedical Optics, 2017. **22**(9): p. 091503.

24. M. Tatarkovic, A. Synytsya, L. Stovickova, B. Bunganic, M. Miskovicova, L. Petruzelka, and V. Setnicka, *The minimizing of fluorescence background in Raman optical activity and Raman spectra of human blood plasma.* Anal Bioanal Chem, 2015. **407**(5): p. 1335-42.

25. N.P. Ivleva, R. Niessner, and U. Panne, *Characterization and discrimination of pollen by Raman microscopy.* Analytical and Bioanalytical Chemistry, 2005. **381**(1): p. 261-7.

26. N.N. Brandt, A.Y. Chikishev, M.G. Gangardt, and N.F. Karyakina. *Raman background photobleaching as a possible method of cancer diagnostics*. in *Optical Diagnostics and Sensing of Biological Fluids and Glucose and Cholesterol Monitoring*. 2001. International Society for Optics and Photonics.

27. V. Kumar, B. Kampe, P. Rosch, and J. Popp, *Classification and identification of pigmented cocci bacteria relevant to the soil environment via Raman spectroscopy.* Environmental Science and Pollution Research, 2015. **22**(24): p. 19317-25.

28. A. Tripathi, R.E. Jabbour, P.J. Treado, J.H. Neiss, M.P. Nelson, J.L. Jensen, and A.P. Snyder, *Waterborne pathogen detection using Raman spectroscopy.* Applied Spectroscopy, 2008. **62**(1): p. 1-9.

29. F. Bonnier, S.M. Ali, P. Knief, H. Lambkin, K. Flynn, V. McDonagh, C. Healy, T. Lee, F.M. Lyng, and H.J. Byrne, *Analysis of human skin tissue by Raman microspectroscopy: dealing with the background.* Vibrational Spectroscopy, 2012. **61**: p. 124-132.

30. M. Darvin, N. Brandt, and J. Lademann, *Photobleaching as a method of increasing the accuracy in measuring carotenoid concentration in human skin by Raman spectroscopy.* Optics and Spectroscopy, 2010. **109**(2): p. 205-210.

31. D. De Faria and M. De Souza, *Raman spectra of human skin and nail excited in the visible region.* Journal of Raman Spectroscopy, 1999. **30**(3): p. 169-171.

32. A. Saha, R. Arora, V.V. Yakovlev, and J.M. Burke, *Raman microspectroscopy of melanosomes: the effect of long term light irradiation.* J Biophotonics, 2011. **4**(11-12): p. 805-13.

33. J. Zięba-Palus and A. Michalska, *Photobleaching as a useful technique in reducing of fluorescence in Raman spectra of blue automobile paint samples.* Vibrational Spectroscopy, 2014. **74**: p. 6-12.

34. M. Pelletier and R. Altkorn, *Efficient elimination of fluorescence background from Raman spectra collected in a liquid core optical fiber.* Applied Spectroscopy, 2000. **54**(12): p. 1837-1841.

35. J. Weng, S. Zhao, Z. Li, K.B. Ricardo, F. Zhou, H. Kim, and H. Liu, *Raman Enhancement and Photo-Bleaching of Organic Dyes in the Presence of Chemical Vapor Deposition-Grown Graphene.* Nanomaterials (Basel), 2017. **7**(10): p. 337.

36. K. Golcuk, G.S. Mandair, A.F. Callender, N. Sahar, D.H. Kohn, and M.D. Morris, *Is photobleaching necessary for Raman imaging of bone tissue using a green laser?* Biochimica et Biophysica Acta (BBA)-Biomembranes, 2006. **1758**(7): p. 868-873.

37. D.A. Shea and M.D. Morris, *Bone tissue fluorescence reduction for visible laser Raman spectroscopy.* Applied spectroscopy, 2002. **56**(2): p. 182-186.

38. Y.C. Chiu, H.Y. Yang, S.H. Lu, and H.K. Chiang, *Micro - Raman spectroscopy identification of urinary stone composition from ureteroscopic lithotripsy urine powder.* Journal of Raman Spectroscopy, 2010. **41**(2): p. 136-141.

39. A.C. Stowe and N. Smyrl, *Raman spectroscopy of lithium hydride corrosion: Selection of appropriate excitation wavelength to minimize fluorescence.* Vibrational Spectroscopy, 2012. **60**: p. 133-136.

40. S. Bahrs, A. Goñi, C. Thomsen, B. Maiorov, G. Nieva, and A. Fainstein, *Light-induced oxygen-ordering dynamics in (Y, Pr) Ba 2 Cu 3 O 6.7: A Raman spectroscopy and Monte Carlo study.* Physical Review B, 2004. **70**(1): p. 014512.

41. S. Bahrs, S. Reich, A. Zwick, A. Goñi, W. Bacsa, G. Nieva, and C. Thomsen, *Raman spectroscopy with UV excitation on untwinned single crystals of YBa2Cu3O7–δ.* Physica Status Solidi (b), 2004. **241**(12): p. R63-R66.

42. J.S. Day, H.G. Edwards, S.A. Dobrowski, and A.M. Voice, *The detection of drugs of abuse in fingerprints using Raman spectroscopy II: cyanoacrylate-fumed fingerprints.* Spectrochimica Acta Part A: Molecular and Biomolecular Spectroscopy, 2004. **60**(8-9): p. 1725-1730.

43. K.Y. Noonan, M. Beshire, J. Darnell, and K.A. Frederick, *Qualitative and quantitative analysis of illicit drug mixtures on paper currency using Raman microspectroscopy.* Applied Spectroscopy, 2005. **59**(12): p. 1493-1497.

44. J.F. Kauffman, M. Dellibovi, and C.R. Cunningham, *Raman spectroscopy of coated pharmaceutical tablets and physical models for multivariate calibration to tablet coating thickness.* Journal of Pharmaceutical and Biomedical Analysis, 2007. **43**(1): p. 39-48.

45. P. Mojzes, L. Gao, T. Ismagulova, J. Pilatova, S. Moudrikova, O. Gorelova, A. Solovchenko, L. Nedbal, and A. Salih, *Guanine, a high-capacity and rapid-turnover nitrogen reserve in microalgal cells.* Proc Natl Acad Sci U S A, 2020. **117**(51): p. 32722-32730.

46. C. Schreiber, D. Behrendt, G. Huber, C. Pfaff, J. Widzgowski, B. Ackermann, A. Muller, V. Zachleder, S. Moudrikova, P. Mojzes, U. Schurr, J. Grobbelaar, and L. Nedbal, *Growth of algal biomass in laboratory and in large-scale algal photobioreactors in the temperate climate of western Germany.* Bioresour Technol, 2017. **234**: p. 140-149.

47. A. Solovchenko, A.M. Verschoor, N.D. Jablonowski, and L. Nedbal, *Phosphorus from wastewater to crops: An alternative path involving microalgae.* Biotechnol Adv, 2016. **34**(5): p. 550-564.

48. I. Gifuni, G. Olivieri, I.R. Krauss, G. D'Errico, A. Pollio, and A. Marzocchella, *Microalgae as new sources of starch: isolation and characterization of microalgal starch granules.* Chemical Engineering Transactions, 2017. **57**: p. 1423-1428.

49. E. Sanz-Luque, D. Bhaya, and A.R. Grossman, *Polyphosphate: A Multifunctional Metabolite in Cyanobacteria and Algae.* Frontiers in Plant Science, 2020. **11**: p. 938.

50. D. Tuschel, *Selecting an excitation wavelength for Raman spectroscopy.* 2016.

51. M. Lingvay, P. Akhtar, K. Sebok-Nagy, T. Pali, and P.H. Lambrev, *Photobleaching of Chlorophyll in Light-Harvesting Complex II Increases in Lipid Environment.* Front Plant Sci, 2020. **11**(849): p. 849.

52. D. Zhang, K. Vangala, D. Jiang, S. Zou, and T. Pechan, *Drop coating deposition Raman spectroscopy of fluorescein isothiocyanate labeled protein.* Appl Spectrosc, 2010. **64**(10): p. 1078-85.

53. K.A. Okotrub and N.V. Surovtsev, *Photobleaching of the resonance Raman lines of cytochromes in living yeast cells.* J Photochem Photobiol B, 2014. **141**: p. 269-74.

54. K.A. Okotrub and N.V. Surovtsev, *Redox State of Cytochromes in Frozen Yeast Cells Probed by Resonance Raman Spectroscopy.* Biophys J, 2015. **109**(11): p. 2227-34.

55. Y. Gu, Y. Zhang, Y. Li, X. Jin, C. Huang, S.A. Maier, and J. Ye, *Raman photostability of off-resonant gap-enhanced Raman tags.* RSC Advances, 2018. **8**(26): p. 14434-14444.

56. N. Murata, S. Takahashi, Y. Nishiyama, and S.I. Allakhverdiev, *Photoinhibition of photosystem II under environmental stress.* Biochim Biophys Acta, 2007. **1767**(6): p. 414-21.

550 57. B. Demmig-Adams and W. Adams III, *Photoinhibition.* 2017.

551 58. R.E. Blankenship and H. Hartman, *The origin and evolution of oxygenic photosynthesis.*
552 Trends in Biochemical Sciences, 1998. **23**(3): p. 94-7.

553 59. U.W. Hallier and R.B. Park, *Photosynthetic Light Reactions in Chemically Fixed*
554 *Anacystis nidulans, Chlorella pyrenoidosa, and Porphyridium cruentum.* Plant
555 Physiology, 1969. **44**(4): p. 535-9.

556 60. I. Migneault, C. Dartiguenave, M.J. Bertrand, and K.C. Waldron, *Glutaraldehyde:*
557 *behavior in aqueous solution, reaction with proteins, and application to enzyme*
558 *crosslinking.* Biotechniques, 2004. **37**(5): p. 790-6, 798-802.

559 61. T. Staughton, C. McGillicuddy, and P. Weinberg, *Techniques for reducing the*
560 *interfering effects of autofluorescence in fluorescence microscopy: improved detection*
561 *of sulphorhodamine B - labelled albumin in arterial tissue.* Journal of Microscopy,
562 2001. **201**(1): p. 70-76.

563

564

FIGURE CAPTIONS

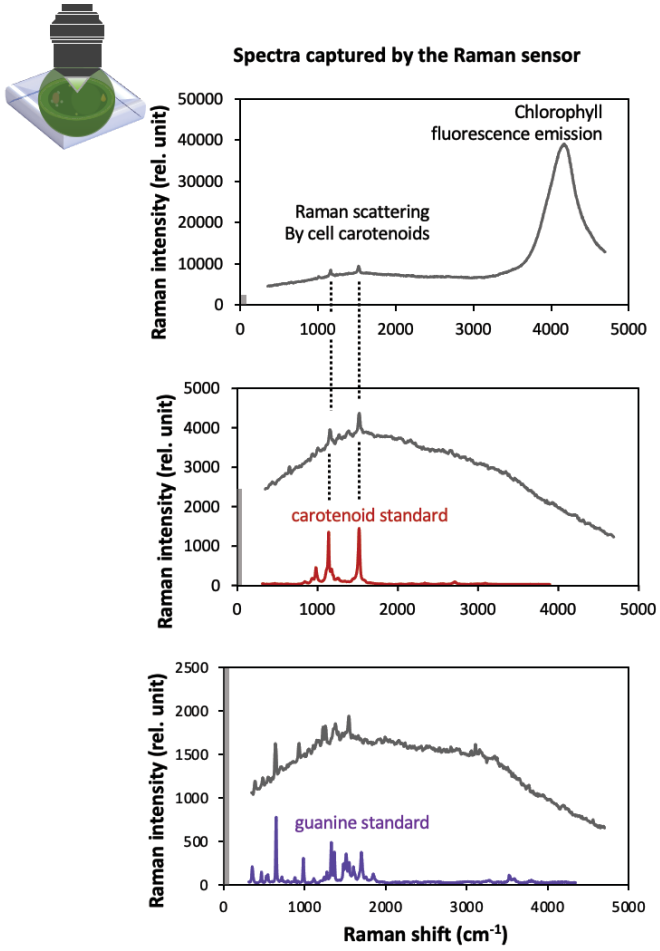

Figure 1. A bright field image of stressed *D. quadricauda* cells prior to the first Raman scanning is shown in the top panel at left. The cells were bleached by the first scanning to the level illustrated in the middle panel, and by the second scanning to the level shown in the bottom panel. The respective spectra captured by the Raman microscope at the selected locations inside the cell are indicated by the arrows. The mixed spectra detected at these locations inside the cells can be compared to reference spectra of pure carotenoids and crystalline guanine shown in the corresponding middle and bottom panels.

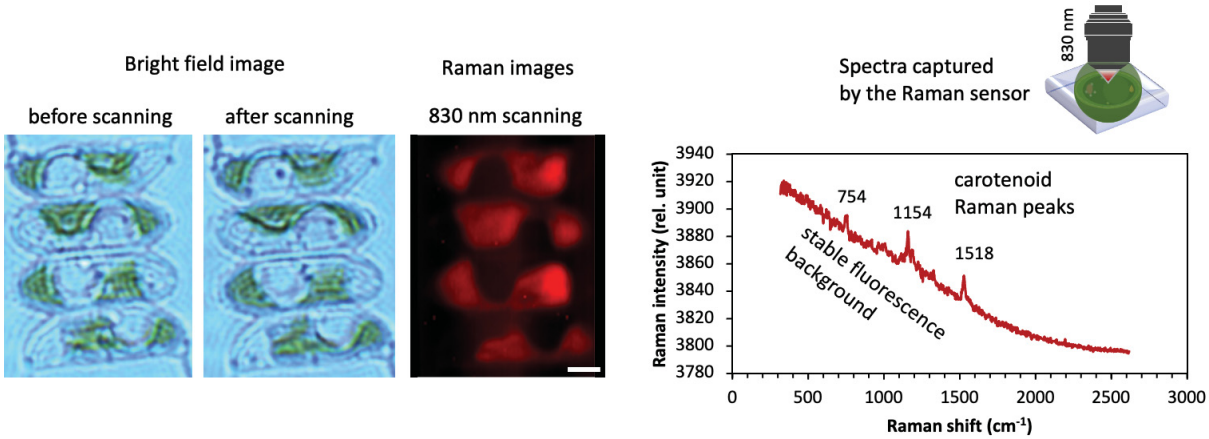

Figure 2. The characterization of *D. quadricauda* cell by Raman mapping by at 830 nm (power ca. 30 mW at the samples). The bright-field images of the same *D. quadricauda* cell were taken before and after Raman mapping. The Raman image (red) shows the spatial distribution of carotenoids based on intensity of their Raman signal. A typical raw Raman spectrum of carotenoids acquired with the 830 nm excitation is shown on the right panel. Scale bar: 2 µm.

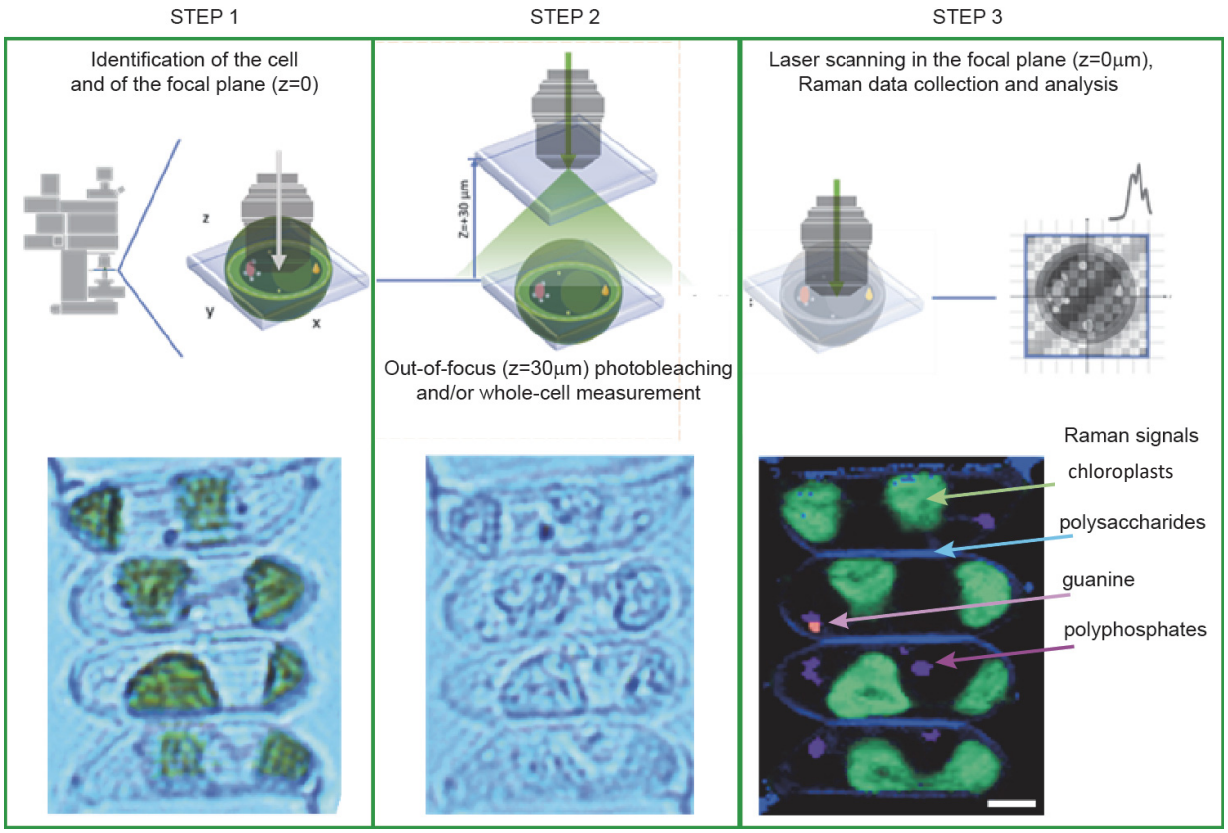

Figure 3. A schematic representation of the wide-field, low-power photobleaching and Raman measurement protocol. The characterization of algal cells by Raman mapping after photobleaching with a 532 nm laser. The bright-field images show the same *D. quadricauda* cell before and after photobleaching. The color legend in deconvoluted Raman images: crystalline guanine (pink), polyphosphate (purple), carotenoids (red), chlorophyll (green) and polysaccharides in the cell wall (blue). Scale bar: 2 µm.

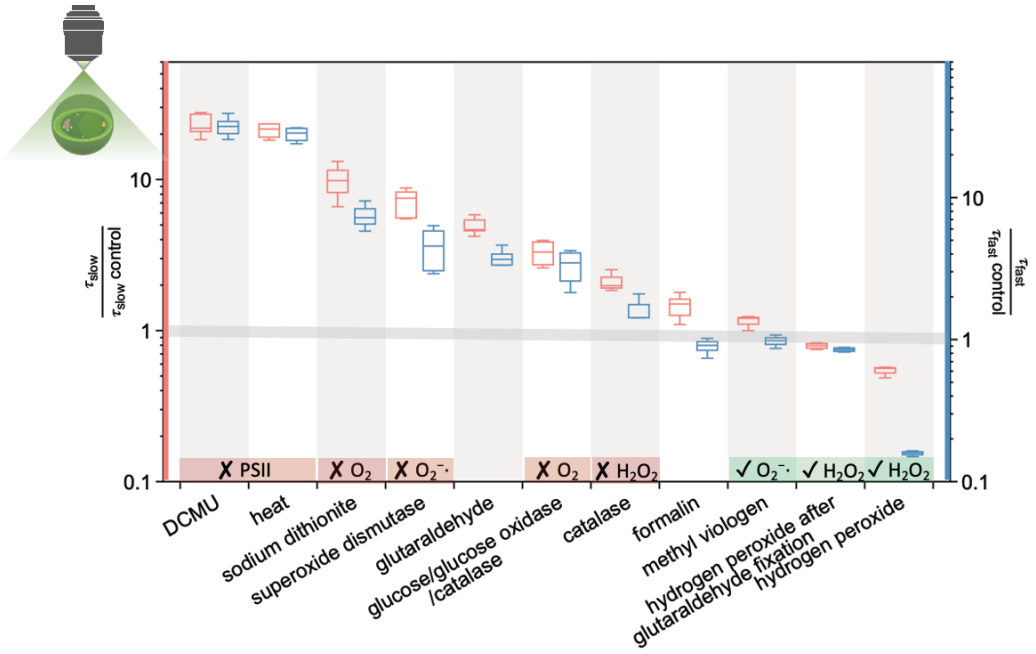

Figure 4. Photobleaching rates under various conditions. The kinetics of photobleaching in microalgae were evaluated by normalizing the two time-constants against the control, $\frac{\tau_i}{\tau_{i\ \mathrm{control}}}$. The photobleaching of the control was measured without any treatment. With the presence of H_2O_2, the absolute time constants τ_{slow} (average 1.76 ± 0.15 s, as mean ± SD) and τ_{fast} (average 1.62 ± 0.14 s) were not significantly different ($P = 9.3 \times 10^{-8} < 0.01$).

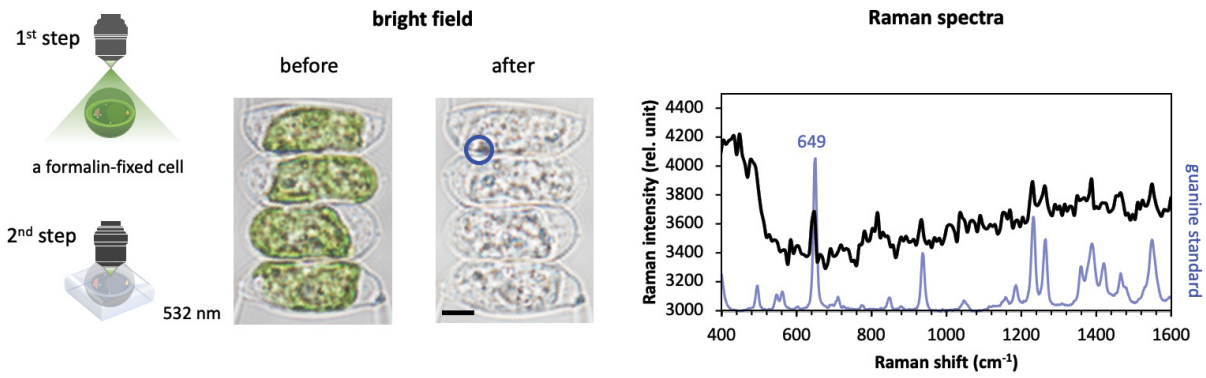

Figure 5. The characterization of a 4% formalin-fixed cell by Raman microscopy. The bright-field images show the formalin-fixed cell before and after the photobleaching by the wide-field, out-of-focus 532 nm excitation. The raw Raman spectrum (black line) of the area highlighted by the blue circle and the reference spectrum of the crystalline guanine (blue line) are shown on the right panel. Scale bar: 2 µm.

III. C. Dynamic Polyphosphate in Microalgae

III. C. 1. Introduction

Nutrients are crucial to life, soil, and water ecosystems, particularly influencing food demand and waste management. Unlike carbon (C) and N, P is commonly overlooked. As the most recognized P form [320], orthophosphate circulates in the aquatic and terrestrial ecosystems, particularly after being released from phosphate rock [480]. This P deposit is the only meaningful raw material that can produce P fertilizers suitable for securing agricultural demands. However, the public is largely unaware that a shortage of available phosphate rock will directly result in agricultural production capacity [481]. Phosphate rock is being depleted. The few countries that hold the significant phosphate rock resources have started reducing the exports [481, 482]. Some of the phosphate rock (<5% phosphorus pentoxide, P_2O_5) are insufficient for production of P fertilizers [483]. The inherent risks and hazards from mining phosphate rock and processing into P fertilizers are also scarcely discussed, including radioactivity and heavy metal contamination [484].

The P crisis is complex, long-term, and worldwide [485]. The total soil P can be very high in some regions due to overfertilization [486], including fertilizing with mineral fertilizers and manure. The problem of accumulation of P in soil and asscoiated reduction of P fertilizers should be mitigated through better P management [487, 488]. Furthermore, additional feedstocks for P fertilizer production should be estibilshed, such as recovering P from wastewater through microalgae cultivation [9].

In an earlier study, our group has demonstrated that algal biomass can serve as slow-release fertilizers and soil conditioners. The dry and wet biomass of the green algae *Chlorella vulgaris* both support the growth of wheat on nutrient-deficient soil substrates [12]. The dynamics of P storage pools in algae have not been adequately investigated. It had not been determined how to monitor the algal growth to harvest P-rich algal biomass. An advanced sample handling method using Raman microscopy [489] enabled us to detect a multitude of energy-transducing and energy-storing macromolecules *in situ*, including the main P storage pools, polyP, in a single algae [16, 17].

In this study, the previous work was continued by using the rapid and non-invasive Raman analysis method to identify the dynamic polyP pools in algae, particularly in the transitions following P starvation and P replenishment. My contribution to this study was the preparsion and cultivatation of algae cultures, and conducting of P starvation and replenishment experiments for Raman microscopic analysis, the writing of Material and methods, and together with the coauthors, the revision of the manuscript. The main results are shown in Figure 2.

III. C. 2. Result

In this work, Raman microscopy was used to investigate the dynamics of polyP formation and reuse in algae. The maximum polyP accumulation occurs in the P-replenished cells after starvation. This accumulation appears during the lag and early exponential phases, within a few hours after Pi is added to the medium for *Chlorella vulgaris* strain IPPAS C1. Later, the polyP reserves are consumed for growth. This transient accumulation of large amounts of polyP reserves represents an opportunity to produce algal biomass with high P content for agricultural applications.

In addition, this work also demonstrates that dry as well as wet biomasses of *Chlorella vulgaris* can support the growth of wheat on nutrient-deficient soil substrates. A rhizotron experiment visualized uptake of ^{33}P from algae through soil to the roots and shoots of wheat plants. In addition, algae increase labile P pools in the soil during the first two weeks of incubation. The effects of available P from mobile P pools are almost comparable to the effects of highly soluble and commercially available mineral P fertilizers. In conclusion, algal biomass could serve as slow-release biofertilizers, which can also improve soil quality.

Algal Research
Volume 43, November 2019, 101634

Towards phosphorus recycling for agriculture by algae: soil incubation and rhizotron studies using ^{33}P-labeled microalgal biomass

Nina Siebers[a*], Diana Hofmann[a**], Henning Schiedung[a.b**], Alexander Landsrath[b], Bärbel Ackermann[c], Lu Gao[c,e], Peter Mojzeš[c,d], Nicolai D. Jablonowski[c], Ladislav Nedbal[c], and W. Amelung[a.b]

[a] *Forschungszentrum Jülich GmbH, IBG-3: Agrosphere, 52428 Jülich, Germany*

[b] *Institute of Crop Science and Resource Conservation, Soil Science and Soil Ecology, Nussallee 13, University of Bonn, 53115 Bonn, Germany*

[c] *Forschungszentrum Jülich GmbH. IBG-2: Plant Sciences, 52428 Jülich, Germany*

[d] *Institute of Physics, Faculty of Mathematics and Physics, Charles University, CZ-12116 Prague 2, Czech Republic*

[e]. *Faculty of Mathematics and Natural Sciences, Heinrich Heine University, Universitätsstraße 1, D-40225 Düsseldorf, Germany.*

* Corresponding author: n.siebers@fz-juelich.de, Tel.: +49 (0)2461 61 96614

** Equal contributing authors

Algal Research 43 (2019) 101634

Contents lists available at ScienceDirect

Algal Research

journal homepage: www.elsevier.com/locate/algal

Towards phosphorus recycling for agriculture by algae: Soil incubation and rhizotron studies using ^{33}P-labeled microalgal biomass

Nina Siebers[a,*], Diana Hofmann[a,1], Henning Schiedung[a,b,1], Alexander Landsrath[b], Bärbel Ackermann[c], Lu Gao[c], Peter Mojzeš[c,d], Nicolai D. Jablonowski[c], Ladislav Nedbal[c], Wulf Amelung[a,b]

[a] Forschungszentrum Jülich GmbH, IBG-3: Agrosphere, 52428 Jülich, Germany
[b] Institute of Crop Science and Resource Conservation, Soil Science and Soil Ecology, University of Bonn, Nussallee 13, 53115 Bonn, Germany
[c] Forschungszentrum Jülich GmbH, IBG-2: Plant Sciences, 52428 Jülich, Germany
[d] Institute of Physics, Faculty of Mathematics and Physics, Charles University, CZ-12116 Prague 2, Czech Republic

ARTICLE INFO

Keywords:
Chlorella vulgaris
Sequential P fractionation
Autoradiography
Wheat
^{33}P labeling

ABSTRACT

Algae effectively accumulate phosphorus (P) from the environment, qualifying them as a promising novel P fertilizer. We hypothesized that P in algae can be rapidly transformed in soil and mobilized for plant growth. To determine the fate of algal fertilizer in soil and to trace its efficiency for plant uptake, we labeled the algae *Chlorella vulgaris* with the radioisotope ^{33}P. To optimize the labeling we studied P-uptake dynamics in detail using a pre-starved culture and additionally monitored polyphosphate (Poly-P) and organic carbon (C) reserve pools by Raman microscopy. Using an optimized labeling procedure, the concentrations and distribution of both algae-derived ^{33}P and mineral fertilizer ^{33}P (control) were characterized in incubation and rhizotron experiments. Soil incubation was performed with four major reference groups (Andosol, Alisol, Cambisol, and Vertisol). To assess ^{33}P plant uptake we grew wheat in rhizotrons on Cambisol. Soil analyses at different incubation times demonstrated sequential ^{33}P fractionation, while plant uptake of algae-derived ^{33}P was followed using sequential autoradiographic imaging. We found that the algae increased labile P pools comprising Resin- and $NaHCO_3$-extractable P in soils during the first 2 weeks of incubation, similar to the effects of NPK fertilizer. The soils with elevated concentrations of Fe- and Al-oxides (Andosol and Alisol) immediately bound 55 to 80% of the applied fertilizer ^{33}P into the moderately available NaOH-P fraction, whereas the soils with lower concentrations of Fe/Al-oxides (Cambisol, Vertisol) stored 35–71% of the algal-P in the labile fraction. The rhizotron experiments visually supported the release and plant-uptake of algal ^{33}P, thus verifying the suitability of algal-fertilizer for plant growth.

1. Introduction

Phosphorus (P) is an essential element for all organisms and plants. Besides nitrogen (N), P is the most important fertilizer in agriculture [1]. Rock phosphate – a non-renewable resource – is the major raw material for production of mineral P fertilizer. About 80% of the annual mined phosphate rock is used in agriculture [1], making it one of the key resources for maintaining food security for the continuously growing world population. There are considerable uncertainties on how long residual rock phosphate reserves may still support global requirements, with estimates ranging between 40 and 400 years [2]. In either scenario phosphate rock remains a limited, non-renewable resource. Additional concerns relate to contamination of rock phosphates with cadmium and uranium and to their occurrence in politically unstable regions [3,4]. Natural geochemical P cycling requires millions of years, so it is essential to capture P from waste streams close to their source and return this nutrient to agriculture in form of novel P fertilizers. Algae are promising in this regard, because they can rapidly acquire P from natural eutrophic water bodies [5,6] and from wastewater [7]. Optimizing algal P uptake from P rich waste and re-using the algal biomass as a fertilizer for agricultural production might thus help overcoming many of future limits in P fertilizer supply.

Microalgae are capable of accumulating P in reserves substantially larger than requirements for their immediate growth [8]. This capacity

* Corresponding author.
E-mail address: n.siebers@fz-juelich.de (N. Siebers).
[1] Equal contributing authors.

https://doi.org/10.1016/j.algal.2019.101634
Received 21 December 2018; Received in revised form 11 July 2019; Accepted 6 August 2019

evolved to cope with episodes of P starvation that frequently occur in nature. Often, P reserves in algal cells occur as Poly-P [9,10], which has already found use as industrial fertilizer [11]. Overall, microalgal biomass may contain up to several weight percent P [12–14]. In addition to P, algae accumulate reserves of other macronutrients such as N and K from waste streams [15].

To be used as a fertilizer for agricultural production, algal biomass must be transformed in soil to chemical forms that are available for uptake by plant roots. The polysaccharide and glycoprotein matrix of algal cell walls can provide a strong defense against the ambient environment, as reported, e.g., for the microalga *Chlorella emersonii* [16–18]. The *C. vulgaris* cell wall does not consist of a resistant, trilaminar outer cell wall of aliphatic, non-hydrolysable macromolecules [16] as does *Chlorella emersonii*, but is also an effective mechanically barrier. These properties may delay nutrient release, thus qualifying algal biomass as potential slow release fertilizer, with the additional benefit of limiting conversion of algal P into biologically inaccessible forms, a process occurring particularly in Al- or Fe-rich soils. However, mineralization of algal biomass should be fast enough to provide nutrients for plant growth. It is thus important to ask whether particularly biotechnologically relevant, fast growing microalgae, such as those of the genus *Chlorella,* can release sufficient P for plant nutrition when used as a fertilizer. This capability has been demonstrated in plant-growth experiments [19] but needs to be tested in broader spectrum of soil types.

To evaluate the degradation of algal biomass in soils and to study the bioavailability and uptake of this recycled P into plants, chemical differentiation between algae-derived P and P occurring in natural soil types is necessary. Here we used the radioisotope ^{33}P, to trace P from algal biomass into soil and finally into plants, visualized by autoradiographic imaging of plant roots and shoots in rhizotrons [20].

Raman microscopy is a convenient tool to monitor accumulation of Poly-P reserves in microalgal cells [21]. Poly-P can be clearly recognized by its unique Raman spectrum, and quantified in a label-free manner even in the presence of other biomolecules [22]. The Raman signal has been shown to be a good linear proxy for the much more time-demanding enzymatic assay [21]. Here, Raman microscopy was used to optimize the protocols for ^{33}P labeling of Poly-P in algal cells.

This study aimed at (i) characterizing P release from algae and its transformation into biologically accessible chemical forms in common agricultural soils, and (ii) at assessing the fertilizing effect of algal biomass for wheat growth. To accomplish these goals, we labeled *Chlorella vulgaris* with ^{33}P, studied the ^{33}P release from the algal biomass in four reference soil groups (Andosol, Alisol, Cambisol, Vertilsol) via an incubation experiment, and imaged the uptake of ^{33}P from algae in soil into wheat (*Triticum aestivum*) via a rhizotron experiment.

2. Material and methods

2.1. Algae cultivation and ^{33}P-labeling

Chlorella vulgaris IPPAS C1 was obtained from the culture collection of the K.A. Timiryazev Institute of Plant Physiology (IPPAS), Russian Academy of Science (courtesy of M. Sinetova). *Chlorella vulgaris* CCALA265 was purchased from the culture collection of the Botanical Institute, Trebon, Czech Republic. The growth medium was prepared as described in Brányiková et al. [23] and consisted of the following in mM: 18.32 $(NH_2)_2CO$, 1.74 KH_2PO_4, 0.83 $MgSO_4 \times 7H_2O$, 0.79 $CaCl_2$, 0.11 $FeNa\text{-}C_{10}H_{12}O_8N_2$, 0.017 $MnCl_2 \times 4H_2O$, 0.013 H_3BO_3, 0.009 $ZnSO_4 \times 7H_2O$, 0.004 $CuSO_4 \times 5H_2O$, 0.002 $CoSO_4 \times 7H_2O$, 0.0001 $(NH_4)_6Mo_7O_{24} \times 4H_2O$ and 0.0001 $(NH_4)VO_3$ made up in deionized water.

Cultivations for later radioactive labeling were done in the FMT150 photobioreactors (PSI, Brno, Czech Republic) as described in Nedbal et al. [24]. All experiments were done with five replicates (n = 5). The cultures were incubated at 35 °C, which was found to be the optimum temperature (data not shown), at pH 7–8, at saturating irradiance levels of 2200 µmol (photons)·m^{-2}·s^{-1} generated equally by sets of red and blue light emitting diodes. Cultures were first incubated for 3 days in a batch in complete medium to eliminate any influence of culture history and to standardize for reproducibility of initial culture properties. Subsequently, the algae were harvested by centrifugation and re-suspended in growth medium described above but without KH_2PO_4. Culture dynamics in P-free medium were determined by automated measurement of optical density in the photobioreactor until growth ceased. P-limitation was then confirmed by demonstrating that orthophosphate addition restores growth.

In preliminary experiments with two replicates, we found that efficient P-labeling requires at least a minimum P concentration; for this purpose we added 10 µL of a 680 µM ^{33}P solution to the algae cultures described above. To ensure that at the end the algae contain sufficient quantity of P for plant growth but to avoid that all of this P is radioactive and thus potentially toxic, we continued P uptake experiments by additionally adding 120 µL of non-radioactive P solution in the flask.

To prepare for ^{33}P labeling, algal growth dynamics after adding different concentrations of orthophosphate were either monitored to follow the uptake dynamics (Fig. 1) or to observe polyphosphate accumulation (Fig. 2). P-starved algae were labeled with ^{33}P by transferring the equivalent of 0.51 g algal biomass (dry weight) in 50 mL medium into Erlenmeyer flasks to which 870 kBq $^{33}PO_4^{3-}$ (Hartmann Analytic GmbH, Braunschweig) was added. These flasks were sealed with wadding plugs to prevent liquid from spilling out and to reduce evaporation, placed on an orbital shaker in a temperature-controlled growth chamber and exposed to a weak warm white light of 200 µmol (photons)·m^{-2}·s^{-1} to support photoautotrophic growth for up to 4 days. All treatments were conducted with two replicates. Preliminary experiments had shown that prolonging algal growth beyond 4 days did not improve ^{33}P uptake.

Radionucleotide uptake was monitored by taking aliquots of the culture and pelleting the algal cells by centrifugation at 12,500 ×*g* for 20 min. To determine $^{33}PO_4^{3-}$ activity in the supernatant we carefully removed the top half of it and measured it with a liquid scintillation counter (LSC) as described in Bauke et al. [20]. The pellets were washed several times using 50 mL deionized water in order to remove all ^{33}P that was not incorporated within the algal cells. The supernatant of each washing step was also analyzed by LSC. The final algae pellets were digested using 4 mL concentrated HNO_3 at 180 °C for 6 h prior to LSC analyses for which 10 mL aliquots were mixed with 10 mL LSC cocktail (ULTIMA Gold, PerkinElmer, Solingen, Germany) and subsequently measured by a Tri-Carb® 3110TR LSC counter (PerkinElmer, Solingen, Germany). These experiments showed that 66 and 99% of initially supplied ^{33}P was incorporated in algal cells in the two cultures, respectively. At the end of the cultivation period, labeled algae were then centrifuged at 12500 ×*g* for 20 min, and washed once using deionized water to remove ^{33}P that was not incorporated within the algae. Labeled biomass was dried at 40 °C for 48 h and ground in a mortar for soil incubation experiments and used in suspension for rhizotron experiments. The algae contained 47.6 ± 0.0% C; 9.6 ± 0.0% N, and 1.4 ± 0.1% P (n = 6).

Labeled mineral fertilizer was prepared in triplicate by mixing N (calcium ammonium nitrate), P (triple super phosphate; TSP), and K (potassium oxide) at the same proportions measured in the algal biomass. For the soil incubation experiment, prior to mixing the three single components we labeled the TSP with ^{33}P using 6.1 MBq $^{33}PO_4^{3-}$ added to 22 mg TSP that was dissolved in 300 mL deionized water. This labeled TSP solution was dried in an oven at 60 °C for 3 days, allowing the TSP to recrystallize. Finally, the crystals were ground for an evenly distribution of ^{33}P and applied to the soil as NPK fertilizer. The concentration measured by ^{33}P activity was 1736 ± 76 Bq g^{-1} soil.

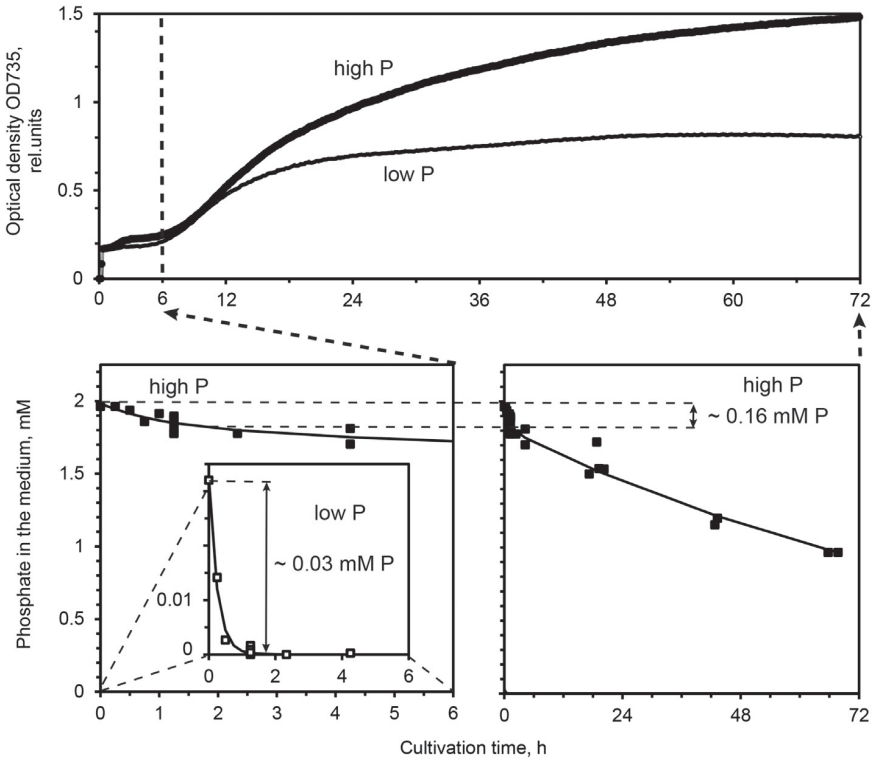

Fig. 1. The upper panel shows growth approximated by optical densities of *Chlorella vulgaris* C1 after P-starved cultures were added into a high-P medium with 2 mM KH_2PO_4 (thick line) and into low-P medium with 0.03 mM KH_2PO_4 (thin line). The maximal specific growth rate was 0.21 h^{-1} in the high-P medium and 0.14 h^{-1} in the low-P medium. The lower panels show dynamics of phosphate in the respective medium: 2 mM KH_2PO_4 (full squares) and 0.03 mM KH_2PO_4 (open squares). The curves approximate the uptake dynamics by numerical fits: 0.03 mM·exp(-time/0.25 h) for the low-P concentration and 0.16 mM·exp(-time/1.1 h) + 1.8 mM·exp(-time/110 h) for the high-P concentration. Only the results of one experiment (n = 1) are shown, as even though all five replicates yielded qualitatively identical results however variably long lag phases (between 4 and 8 h, data not shown). Therefore, calculating the mean of all replicates would mix statistical and systematic deviations and obscure the basic biphasic character.

2.2. Imaging polyphosphate reserves by Raman microscopy

Raman microscopy was used to identify the dynamics of Poly-P accumulation and to determine when to harvest cells having high Poly-P. Specimen preparation for Raman measurements, the experimental workflow, and the data analysis methodology are described in detail in Moudříková et al. [21]. Briefly, harvested algal cells were immobilized in 1% w/v solution of low-gelling agarose (T = 39 °C), spread between a quartz slide and coverslip, and sealed with a CoverGrip sealant (Biotium) to prevent cell movement and evaporation of water during the course of observations.

Raman maps were acquired using a confocal Raman microscope (WITec alpha300 RSA, WITec, Germany), an oil-immersion objective (UPlanFLN 100×, NA 1.30, Olympus, Japan), and 532 nm excitation (20 mW power at the objective focal plane). The scanning step in in the *x* and *y* directions was 220 nm, with an integration time of 0.1 s per pixel. Acquisition of a Raman map for a single cell of the size of *Chlorella vulgaris* CCALA256 requires about 150 s. To prevent chlorophyll autofluorescence, a wide-area, low-power photobleaching was applied prior to the mapping, as described previously [22].

For each sample, Raman maps of 30–50 randomly chosen cells were acquired to capture the natural heterogeneity of the cultures. Fig. 2 illustrates the transient Poly-P accumulation observed in four arbitrarily chosen pre-starved cells (blue) that occurred after addition of orthophosphate. Significant transient modulation of neutral lipids (red) and starch (green) accompanied the emergence of large Poly-P reserves. These observations demonstrated that 2 h after adding orthophosphate, cells with large Poly-P depots are available for harvest.

2.3. Soil sampling and general characteristics

The potential for using algae as an alternative fertilizer may be particularly relevant in the tropics or subtropics because uptake of P from wastewaters by algae is maximized with abundant solar radiation and stable temperatures throughout the year. Therefore, we used samples from the upper A horizon of a Vertisol (7.45°S, 111.61°E, 80 m a.s.l.), an Alisol (6.54°S, 106.52°E, 250 m a.s.l.), and an Andosol (6.88°S, 106.94E, 900 m a.s.l.) from the tropical island of Java, Indonesia, as described in Winkler et al. [25] and Lehndorff et al. [26]. All soils were obtained from lands managed with upland crops. For comparison to a widespread soil group typical of temperate climates, we additionally sampled the Ap horizon (0–10 cm) of a Cambisol [27] from Germany (6.45°S, 50.87°E, 108 m a.s.l.). General soil characteristics are shown in Table 1.

2.4. Soil incubation experiments and analyses

For incubation experiments, we used 15 g air-dried topsoil (0–30 cm) from each soil type, adjusted the soil moisture to 50% water holding capacity (WHC) and introduced it to the lower half of 250 mL Nalgene® vessels (Thermo Fisher Scientific, Waltham, Massachusetts, USA). The vessels were not completely filled in order to maintain a sufficient reservoir for soil aeration, and were opened twice a week for at least 1 h to compensate for oxygen consumption. Three replicates of each soil type were prepared. Samples were pre-incubated at 25 °C for one week prior to fertilizer addition. To ensure an equal distribution of the very small amount of ^{33}P-labeled fertilizer in the soil, we homogenized the amount of fertilizer needed (corresponding to an application rate of 35 kg P ha^{-1}) for each replicate in 1 g quartz sand and added this mixture to the soil sample with a vortex mixer. Samples were then further incubated at 25 °C for 10 weeks.

After one, two, three, five, seven, and ten weeks of incubation, 0.5 g of dry soil equivalent was sampled from each replicate (n = 3), added to 50 mL centrifugation tubes, and sequentially fractionated according to Hedley et al. [28]. Briefly, samples were serially treated with solutions of increasing extractant strength: Resin (Resin-P), 0.5 M $NaHCO_3$ ($NaHCO_3$-P), 0.1 M NaOH (NaOH-P), 1 M HCl (HCl-P), and Aqua regia (Residual-P). The ^{33}P activity of each fraction was analyzed by LSC.

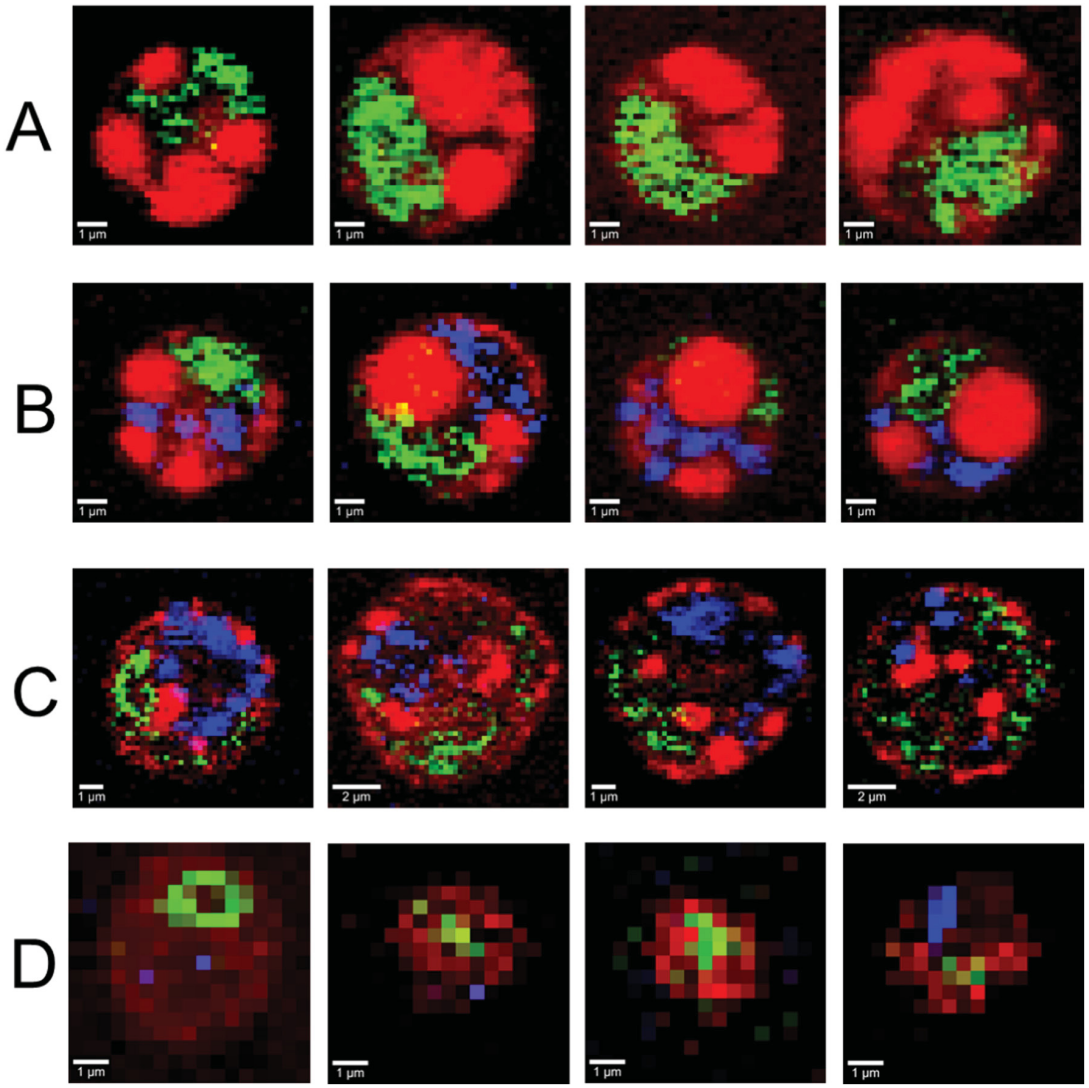

Fig. 2. Raman images of four (n = 4) cells *Chlorella vulgaris* CCALA256 representing the P-starved culture (row A), cells collected 2 h after adding 0.4 mM orthophosphate (row B), in early exponential phase (row C), and in rapidly growing and dividing cells (row D). The images represent Raman spectral signatures of neutral lipids (red) and of starch (green) that represent the major reserves of organic carbon while the blue color shows the Raman spectral signature of polyphosphates. (For interpretation of the references to color in this figure legend, the reader is referred to the web version of this article.)

2.5. Rhizotron experiments

To support the soil incubation data by visualizing P uptake from algal fertilizer, we compared the performance of ^{33}P-labeled algal fertilizer with ^{33}P-labeled conventional NPK fertilizer in a rhizotron study using spring wheat (*Triticum aestivum* cv, Cornetto, S.G.L GmbH, Erftstadt-Gymnich, Germany). For these experiments we used self-constructed rhizotrons, each built from a black polyvinyl chloride (PVC) frame supporting a 10 mm thick transparent polymethylmethacrylate (acrylic glass) plates, with a volume of 5.25 L (50 × 30 × 3.5 cm inner dimensions).

To simulate top- and subsoil, rhizotrons were filled with a 30 cm layer of sand (RBS GmbH, Inden, Germany; particle size: ≤1 mm) covered by a 10 cm layer of a 1:1 Sand:Cambisol [27] mixture, and finally a 5 cm layer of a 3:1 sand:Cambisol mixture. The Cambisol originates from a P-depleted plot (no P fertilization since 1942) of the long-term experiment at a former experimental research station of the University of Bonn at Dikopshof (50°48′27.8″N 6°57′10.8″E; as described in Mertens et al. [29]), and which was left over from a study by Bauke et al. [20]. Both soils were air-dried at 40 °C for 5 days and passed through a 2 mm sieve before introduction into the rhizotrons. After introduction into the rhizotrons each soil was re-compacted to a bulk density of 1.4 g cm^{-3} and separately moisture-adjusted to 50% water holding capacity and left for settlement for several days.

We performed four replicates of each treatment (algal and mineral fertilizer), applying the equivalent of 35 kg P ha^{-1}, thus utilizing 8 rhizotrons. In contrast to the incubation experiment, we added the mineral fertilizer as a solution and the algal fertilizer as a suspension in 150 mL H_2O, again adjusting the N-P-K ratio of the mineral fertilizer to match the nutrient content of the algal fertilizer. This allowed us to test whether fresh algal fertilizer (with intact cell walls) can quickly release P in a plant-available form. In these experiments, the elemental content of the algae was 9.2% N, 2.6% P, and 1.1% K (m/m dry weight) and thus the applied amount of added algae equaled 1.4 g dry weight (0.2 g ^{33}P-labeled and 1.2 g non-labeled algae) per rhizotron. The fertilizer solution/suspension was applied on the upper soil layer, incorporated with a fork, and covered with a 5 cm thick layer of the topsoil to prevent the release of radiolabeled material to the air. Spring wheat seeds were

Table 1
General soil characteristics of the soils used; Al_{ox}, Fe_t, $Fe_{DCB}/_{Fet}$, and Fe_{ox}/Fe_{DCB} data were obtained from Winkler et al. [25] for the Vertisol, Andosol, and Alisol being the same soil samples as used in this study. Phosphorus fractions determined using sequential fractionation for the different soils studied with proportions of total P (P_t) in parentheses. (Data are shown as mean ± standard deviation (SD), n = 3).

	Cambisol	Andosol	Alisol	Vertisol
Soil	Orthic Cambisol	Dystric silandic Andosol	Chromic abruptic Alisol	Pellic Vertisol
pH ($CaCl_2$)	5.9 ± 0.0	4.6 ± 0.0	4.9 ± 0.0	5.7 ± 0.0
Sand (%)	23.9 ± 0.9	76.3 ± 0.0	10.4 ± 0.0	5.6 ± 0.0
Silt (%)	58.1 ± 0.5	23.7 ± 0.6	19.6 ± 0.0	20.8 ± 0.2
Clay (%)	14.9 ± 0.3	3.9 ± 0.1	71.5 ± 0.4	77.3 ± 0.2
SOC (%)	1.90 ± 0.03	2.37 ± 0.01	1.62 ± 0.08	1.30 ± 0.07
N (%)	0.18 ± 0.00	0.27 ± 0.00	0.17 ± 0.01	0.1 ± 0.00
C/N	10.4	8.9	9.8	12.6
Al_{ox} (g kg^{-1})	< 0.4	2.9 ± 0.2	< 0.4	< 0.4
Fe_t (g kg^{-1})	19.0 ± 0.5	96.4 ± 1.4	85.8 ± 2.1	68.5 ± 1.3
Fe_{DCB}/Fe_t	0.41	0.44	0.67	0.09
Fe_{ox}/Fe_{DCB}	0.50	0.38	0.06	0.58
Resin-P	92 ± 1.9 (6)	3.0 ± 2.2 (0)	3.2 ± 0.3 (0)	19 ± 0.5 (5)
$NaHCO_3$-Pi (mg kg^{-1})	86 ± 0.8 (6)	30 ± 0.2 (1)	11 ± 1.0 (1)	11 ± 0.2 (3)
$NaHCO_3$-Po (mg kg^{-1})	245 ± 0.8 (16)	10 ± 2.6 (0)	11 ± 1.4 (1)	12 ± 0.5 (3)
NaOH-Pi (mg kg^{-1})	275 ± 14.9 (18)	803 ± 12 (32)	149 ± 46 (17)	35 ± 0.2 (9)
NaOH-Po (mg kg^{-1})	95 ± 24.5 (6)	499 ± 54 (20)	76 ± 2.5 (8)	6.9 ± 0.6 (2)
HCl-Pi (mg kg^{-1})	133 ± 2.0 (7)	44 ± 1.2 (2)	5.1 ± 1.1 (1)	23 ± 0.6 (5)
HCl-Po (mg kg^{-1})	11 ± 2.8 (1)	69 ± 0.0 (3)	8.8 ± 1.3 (1)	12 ± 1.0 (3)
Residual-P (mg kg^{-1})	603 ± 15.2 (39)	1070 ± 91 (42)	642 ± 8.0 (71)	286 ± 125 (70)
P_t (mg kg^{-1})	1540 ± 79	2528 ± 204	906 ± 77	405 ± 16

pre-germinated for 3 days and one healthy seedling with three roots was planted in each rhizotron after fertilizer addition, 1 cm deep in the upper soil layer. Rhizotrons were then placed at an angle of 45° in a climate chamber with a day-length of 16 h and a light intensity of 320 µmol m^{-2} s^{-1} PAR. Day and night temperatures were set to 20 °C and 12 °C, respectively, at a relative air humidity of 60%.

2.6. ^{33}P imaging

For weekly ^{33}P imaging, the front plate of one rhizotron per treatment was opened to ensure direct contact between roots, shoots, and soil with the image plates (IPs). All IPs were covered with a thin protective foil to prevent contamination or damage by water or soil. In the first three weeks we used one large IP (35 × 43 cm, DÜRR NDT GmbH & CO, KG. Bietigheim-Bissingen, Germany), later combining images from a large IP (roots) and a small IP (20 × 40 cm, DÜRR NDT GmbH & CO, KG, Bietigheim-Bissingen, Germany) (plant) for each rhizotron. To ensure close contact between IPs and rhizotrons/wheat plants, the imaging assemblies were compressed with small tungsten weights. The IPs on the soil surface and the shoots were exposed for 4 h. After exposure, the IPs were scanned in sensitive mode, with a resolution of 100 µm, using an Image Plate Scanner (CR35 Bio, Raytest, Germany).

No quantitative analysis of the ^{33}P activity was performed, nor was longer cultivation attempted because rhizotron cultivation was suboptimal and all treatments, including the control, developed fungal infestations with signs of the stem rust and reduced biomass productivity progressing with increasing time of growth.

2.7. Data treatment and statistical analyses

Statistical analyses were performed in SPSS (IBM SPSS Statistics, Version 22.0, Armonk, NY). We tested for normal distribution using the Shapiro-Wilk test ($P < 0.05$) and for homogeneity of variance using the Brown-Forsythe test ($P < 0.05$). To test for the effects of different fertilization treatments we performed one-way ANOVA. We considered the sampling times of the incubation study as paired samples. To account for this, we performed Repeated Measures ANOVA, with sampling times treated as repeated measures. If significant differences occurred we used the Tukey HSD test for post-hoc separation of means ($P < 0.05$). To test for the effect of fertilization within one sampling time, we performed a paired *t*-test separately ($P < 0.05$).

The evaluation software AIDA (AIDA Biopackage, Raytest, Germany), was used to convert the scans of the rhizotron images to rainbow-color images.

3. Results

3.1. Dynamics of growth, P-uptake, and ^{33}P labeling by starved algal culture

Addition of orthophosphate to the P-prestarved culture produced biphasic P uptake dynamics (Fig. 1). Here, the fast component was shorter than the lag phase observed in the culture growth. This fast uptake phase occurred during lag phase at both high and low orthophosphate concentrations; always leading to a rapid transient accumulation of large P-reserves because the cells were not growing during the lag phase.

In order to identify the chemical forms of the incorporated P, particularly Poly-P granules, We performed Raman microscopy. These experiments utilized *Chlorella vulgaris* CCALA265, whose cells are larger than the *C. vulgaris* IPPAS C1 cells used elsewhere in this study. These larger *C. vulgaris* CCALA265 cells were easier to image than *C. vulgaris* IPPAS C1 without having any effects on the dynamics of the Poly-P as confirmed by enzymatic analysis (Tabea Mettler-Altmann, unpublished). No Poly-P granules were detected in the initial P-starved culture (Fig. 2, row A). Substantial Poly-P reserves were detected 2 h after adding orthophosphate (Fig. 2, row B), and during early exponential growth phase (Fig. 2, row C). Rapidly growing cells (Fig. 2, row D) were typically somewhat smaller than lag phase cells and contained only traces of polyphosphate and small amounts of starch and neutral lipids representing organic C reserves. These experiments confirmed the effectiveness of our method for rapid labeling of P-starved culture with ^{33}P. Based on the results shown in Figs. 1 and 2 we expect that a large proportion of added ^{33}P will be incorporated into Poly-P granules during lag and early exponential phases, and that this P stored in form of Poly-P granules will subsequently be used for cell growth after conversion to other chemical forms during prolonged cultivation.

3.2. Sequentially extracted P fractions

The different soil groups contained different distributions of P: total P concentration (P_t) is described in Table 1 and was highest in the

Andosol, at 1.9 times higher than in the Cambisol, 2.8 times higher than in the Alisol, and 6.1 times higher than in the Vertisol (Table 1). The concentration of easily extractable P (Resin-P and $NaHCO_3$-P) was low in the Andosol, Alisol, and Vertisol, but 10 to 17 times larger in the Cambisol. This trend was reversed for the NaOH-P pool, especially for the Andosol; however, it was not as pronounced as for Resin-P and $NaHCO_3$-P pools. The Residual P fraction contributed most to P_t with proportions ranging between 42 and 70% (Table 1).

Due to the inhomogeneous distribution of the ^{33}P label within the TSP and the labeled algae, the replicates and variants exhibited different initial ^{33}P activities (Supplementary information, Table S1). Thus, a direct comparison of ^{33}P activities between replicates and variants was not possible. Therefore, we estimated the proportions of the ^{33}P activity in relation to the total ^{33}P activity applied (Supplementary information, Table S2). The typical ^{33}P distribution among the P fractions was similar, whether it was delivered as NPK fertilizer or as algal biomass. The HCl-P and Residual P pools received the lowest proportions of applied ^{33}P label (4 to 21% of the applied amount), whereas label was distributed variably into the other fractions, i.e., Resin-P, $NaHCO_3$-P, and NaOH-P (contributing between 12 and 82% of the applied ^{33}P) (Fig. 3, Supplementary information, Table S2). This large variation reflected the different ability of the soils to bind P to its constituents, whereas the fertilizer form affected this P pool distribution less drastically, and, intriguingly, not even consistently. Generally, the dissolution of NPK resulted in larger ^{33}P activities in the Resin- and $NaHCO_3$-extractable P pools, particularly in the Cambisol and Vertisol. In contrast, Algal fertilizer ^{33}P mainly accumulated in the NaOH-extractable P pool, commonly described as moderately labile P [30]. The lowest ^{33}P activities were found in the HCl-extractable P fraction ($< 6\%$ of applied ^{33}P), with comparable contributions from the algal and the NPK fertilizers (Fig. 3; Supplementary information, Table S2).

In respect to temporal trends, P release patterns were reflected in the changing proportions of ^{33}P activity of sequential fractionation P-pools over time of the incubation. The trends in NPK and algae treatments exhibited similar release patterns (Fig. 3). In the Cambisol and Vertisol, the proportions of the Resin-P and $NaHCO_3$-extractable P fractions ("labile" P according to Negassa and Leinweber [30]) increased rapidly, peaking after 2 weeks and then slowly decreasing. The proportions of the ^{33}P activity in the moderately labile, NaOH-extractable P pools showed the opposite trend: a slight decrease soon after fertilizer application with a minimum after two weeks of incubation, followed by a slight increase ($P < 0.05$). The stable fraction did not follow a pronounced temporal pattern (Fig. 3; Supplementary information, Table S1).

3.3. ^{33}P imaging

Autoradiographic imaging enabled qualitative tracing of ^{33}P released from the fertilizers within the Cambisol soil and plants (Fig. 4). Images on the left-hand side of Fig. 4 demonstrate that after one week of incubation a large proportion of the applied ^{33}P still occupied a layer at the soil surface where the NPK fertilizer and algal biomass were applied. This NPK fertilizer layer was slightly broader than that of the algal fertilizer treatment, indicating increased mobility, most likely due to the larger proportion of labile ^{33}P (the Resin-P pool) in the Cambisol also visible in Fig. 3. A slight infiltration of the fertilizers also occurred at the rhizotron sidewalls, revealed by vertical streaks of radioactivity (Fig. 4). However, there was no apparent leaching of ^{33}P through the soil matrix in the course of plant growth, from either the NPK or the algal fertilizer. A small amount of ^{33}P radioactivity was visible in the wheat shoots after the first week.

After three and six weeks of incubation, respectively, similar patterns were observed for both fertilizer forms (images on the right-hand site of Fig. 4): ^{33}P was clearly detectable in all above-ground wheat shoots. This finding suggests that comparable amounts of radioactivity were taken up by the wheat plants from both types of fertilizer. Radioactivity was evenly distributed within the shoots. This ^{33}P accumulation in leaves occurred at the expense of fertilizer layers at the soil surface that became much weaker compared to images that were taken after the first week of incubation. Remarkably, visible ^{33}P activity was also detected in the roots. Again, no visually noticeable differences in

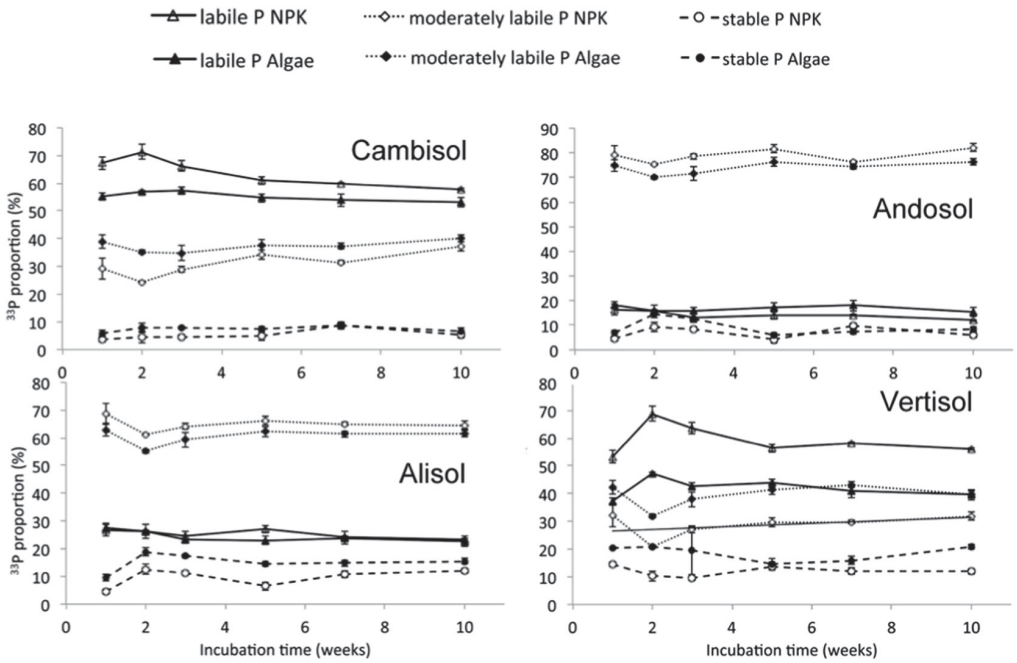

Fig. 3. Development of ^{33}P activity in different P fractions, i.e., labile P comprising Resin-P and $NaHCO_3$-P, moderately labile P comprising NaOH-P, and stable P comprising HCl-P and Residual-P, throughout 10 weeks of incubation after NPK and algae fertilizer application. (Data are shown as mean ± standard deviation (SD), n = 3).

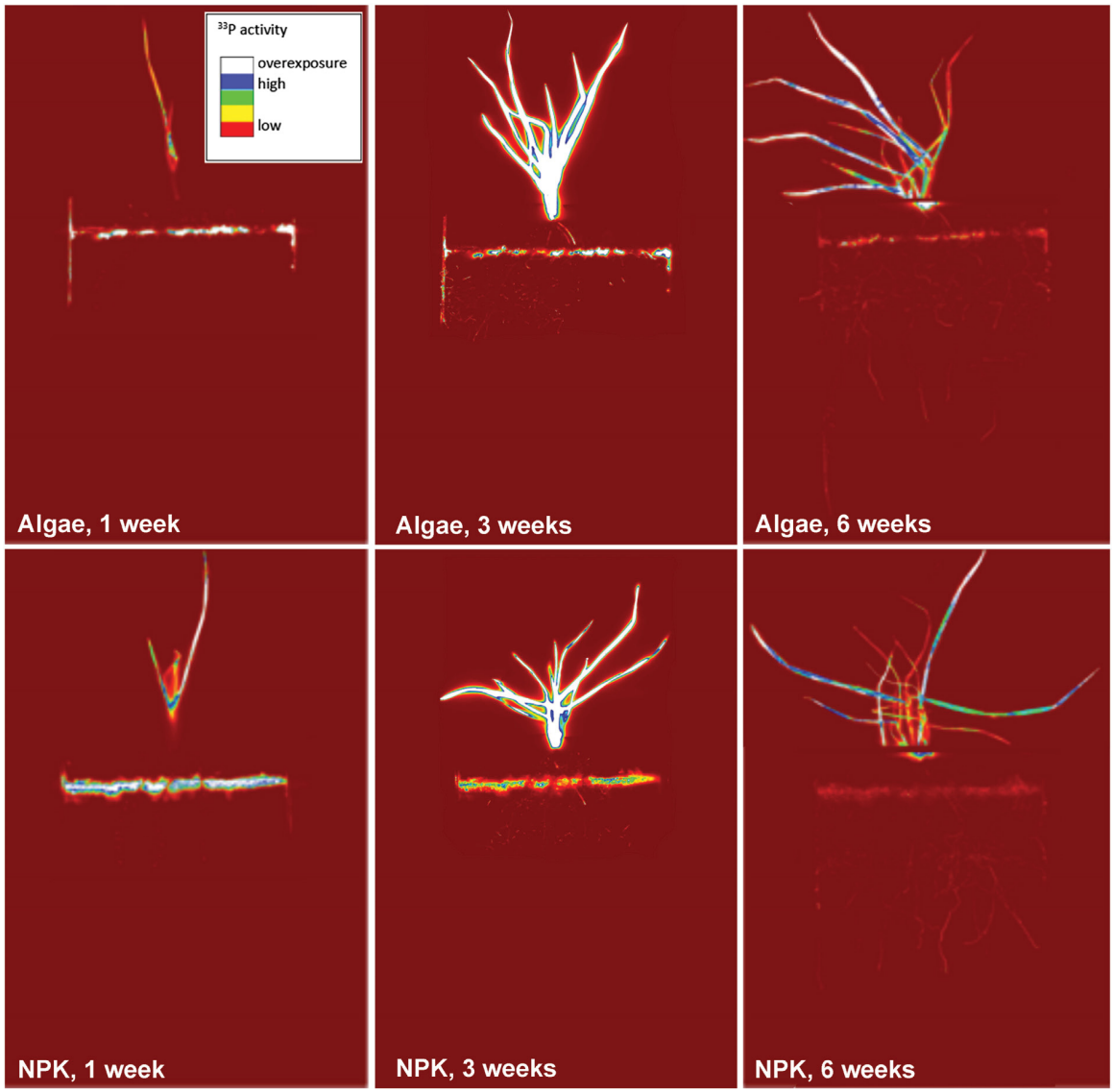

Fig. 4. ^{33}P-autoradiographic images of rhizotrons with wheat plants after fertilization using previously labeled ^{33}P-labeled algae and ^{33}P-labeled mineral NPK fertilizer after one, three, and six weeks of growth. The exposure time of the image plates was 4 h; n = 1.

the roots between NPK and algae fertilization could be observed.

4. Discussion

4.1. Algae P release kinetics affected by soil group

The higher ^{33}P activities in the labile P fraction of the Cambisol and Vertisol after mineral fertilizer dissolution are caused by the high solubility of TSP (e.g., [31,32]). The main component of TSP is Ca$(H_2PO_4)_2$, which has a high solubility [33]. This is different for the algae treatment, as *Chlorella vulgaris* stores P as complex compounds in cells as a P reservoir (e.g., [34,35]). The experiments depicted in Figs. 1 and 2 show that it is possible to prepare algal biomass in which P is incorporated largely in the form of Poly-P granules or, as done here for the soil incubation and rhizotron experiments, with Poly-P already largely converted to other biochemical compounds containing P. In any case, the organic P compounds have to be mineralized before being plant-available.

Due to their lower total Fe contents, the readily released P of the NPK fertilizer may remain in easily-extractable, i.e., bioavailable forms in the Cambisol and Vertisol. The situation is different in the Andosol and Alisol. As with other tropical and subtropical soils, these soils are highly weathered and exhibit elevated contents of Fe/Al-oxides combined with lower pH values (Table 1). While initial release of P from NPK and algae likely occurred at similar rates, the distribution of the released mineral P is thus increasingly superimposed by a contemporaneous sorption at and fixation of the dissolved P by the oxidic soil matrix [36–39]. In addition, the high Al_{ox} content and the low pH value of the Andosol favor the precipitation of P with Al^{3+}, resulting in mineral phases such as variscite [40], the formation of which additionally reduces P availability.

The high initial proportions of HCl- and aqua-regia extractable, i.e., stable P (Table 1; [30]) in these soils confirm these fixation processes and are in agreement with earlier findings stating that stable P generally comprises > 30% of the stable P fraction in moderately weathered soils and > 80% of the stable P fraction in soils that are strongly weathered or derived from volcanic parent material [41,42]. Nevertheless, we barely detected ^{33}P in these Residual-P pools (Fig. 3),

possibly reflecting limited transfer into these residual pools during the short incubation time of 10 weeks. Bauke et al. [43] argued that "although surplus P from fertilizers may remain available in the short to medium term, it will eventually be transformed to unavailable forms of P over a period of a few decades", which was also suggested by Koch et al. [44] detecting increased Residual-P concentrations after long-term compost fertilization.

By contrast to the stable P pools, P forms that are more easily extracted showed a temporal dynamics. Particularly the peak of labile P after 2 weeks of incubation is accompanied by a nadir of the proportions of moderately labile P fraction (Fig. 3) and thus also for the respective total ^{33}P activity (Table S1, Table S2) as well as for the proportions (Fig. 3). The moderately labile P fraction dynamics are fast and this fraction is still in equilibrium with the labile P fraction [30]. Thus, increasing moderately labile P observed after two weeks reflects the shift of the labile P fraction to more stable forms.

It is remarkable that 35–55% of algal-P can already be found in the labile P fraction after only one week of incubation in the Cambisol and Vertisol. This indicates that algal P is readily usable after microbial degradation of the cell wall of *Chlorella vulgaris*. The phospholipids present in cell membranes as well as sugar-phosphates are rapidly degraded within seconds to minutes after cell lysis [45,46]. This degradation likely involves phosphatases. According to Hui et al. [47], phosphatases operate at the scale of minutes to hours, similar to pyrophosphates, which also potentially release orthophosphate within several hours [48]. The remaining P that is released less rapidly likely originates from that stored in DNA/RNA, the degradation of which is further slowed when the DNA/RNA released after cell lysis is bound to the soil matrix [49].

4.2. Algae-P uptake by plants

The overexpression of ^{33}P activity observed in the imager during the first weeks of the experiment, using only 4 h of exposure, was caused by the high amount of ^{33}P initially applied to the rhizotrons, which was necessary to account for its half-life of 25.6 days, shorter than the growth period of the plants of 6 weeks. ^{33}P autoradiography demonstrated that algal P was being taken up by plants one week after fertilizer application at a rate visually comparable that of NPK fertilizer. Thus the results of our rhizotron experiments support the findings from our soil incubation experiments that algae decomposition was rapid and increased the labile P fraction in the Cambisol, if at a slightly lower rate than that provided by the NPK fertilizer. They also support the findings from a previous study showing that algal-P is available to plants [19].

In contrast to the incubation experiments the algal biomass in the fertilizer experiments was not dried but applied intact in order simulate practice-orientated conditions as a pre-treatment. The results nevertheless clearly showed that P from fresh, living algae (applied as a suspension in water) was quickly mineralized and taken up by wheat roots. We therefore conclude that in practice algal biomass does not need to be dried and granulated prior to application as a fertilizer, saving energy costs. Instead, application of algal biomass jointly with liquid manure or using a slurry applicator appears feasible at minimal extra costs. The combined application with a grubber should allow a direct incorporation into soil, which in turn minimizes wind erosion. If slower mineralization is desired (e.g., for perennial or more time-intensive cultures) granulation of algal biomass will likely delay mineralization.

5. Conclusion

In the soils under study, P release from algal biomass was rapid and increased the concentrations of labile and moderately labile P fractions in soil in a pattern comparable to that of mineral fertilizer, although at a rate 1–9% lower than P release from NPK. These findings thus support our two hypotheses that *Chlorella vulgaris* is capable of incorporating sufficient P into its biomass to act as P fertilizer, releasing P when incorporated into the soil to support or even sustain plant nutrition. Future work should now be performed to bring this fertilizer into the field under economically viable, practice-relevant conditions.

Acknowledgments

The authors thank Christina Schreiber for helpful hints to algae growth and labeling. In addition, we thank Meike Siebers and Peter Narf for valuable input regarding data interpretation. We also thank Andrea Ecker for helping with ^{33}P analyses. This research was financially supported by the Bioeconomy Science Center (BioSC) AlgalFertilizer and AlgalNutrient projects funded by the Ministry of Innovation, Science and Research of the German State of North Rhine-Westphalia (No. 313/323-400-002 13).

Declaration of competing interest

NS, DH, NDJ, LN, and WA inspired the project AlgalFertilizer that provided partial funding for this research. LN inspired the project AlgalNutrient that also provided partial funding for this research. BA and LN conducted the experiments and analyzed the data leading to Fig. 1. LG and PM conducted experiments involving Raman microscopy and analyzed the data leading to Fig. 2. NS, HS, AL, and WA designed and conducted the soil incubation experiment and analyzed the data leading to Table 1 and Fig. 3. NS, DH, HS, BA, and WA conducted the experiments for ^{33}P algae labeling and rhizotron experiments and analyzed the data leading to Fig. 4. NS, DH, HS, and WA wrote the paper. All authors contributed to the revision of the paper draft.

Statement of informed consent, human/animal rights

No conflicts, informed consent, human or animal rights applicable.

Appendix A. Supplementary data

Supplementary data to this article can be found online at https://doi.org/10.1016/j.algal.2019.101634.

References

[1] R.W. Scholz, A.E. Ulrich, M. Eilitta, A. Roy, Sustainable use of phosphorus: a finite resource, Sci. Total Environ. 461–462 (2013) 799–803.
[2] M. Obersteiner, J. Peñuelas, P. Ciais, M. van der Velde, I.A. Janssens, The phosphorus trilemma, Nat. Geosci. 6 (2013) 897–898.
[3] L. Reijnders, Phosphorus resources, their depletion and conservation, a review, Resour. Conserv. Recycl. 93 (2014) 32–49.
[4] D.A. Vaccari, Phosphorus: a looming crisis, Sci. Am. 300 (2009) 54–59.
[5] C.P. Mainstone, W. Parr, Phosphorus in rivers — ecology and management, Sci. Total Environ. 282–283 (2002) 25–47.
[6] K. Wallmann, Phosphorus imbalance in the global ocean? Global Biogeochemistry Cycles 24 (4) (2010).
[7] S. Aslan, K.K. Ilgi, Batch kinetics of nitrogen and phosphorus removal from synthetic wastewater by algae, Ecol. Eng. 28 (2006) 64–70.
[8] N. Brown, A. Shilton, Luxury uptake of phosphorus by microalgae in waste stabilisation ponds: current understanding and future direction, Rev. Environ. Sci. Biotechnol. 13 (3) (2014) 321–328.
[9] K. Nishikawa, H. Machida, Y. Yamakoshi, R. Ohtomo, K. Saito, M. Saito, N. Tominaga, Polyphosphate metabolism in an acidophilic alga Chlamydomonas acidophila KT-1 (Chlorophyta) under phosphate stress, Plant Sci. 170 (2006) 307–313.
[10] W.D. Stewart, Algal Physiology and Biochemistry. Botanical Monographs, 10 Univ. of California Press, Berkeley Calif, 1974 (u.a., XI, 989 S).
[11] T. McBeath, E. Lombi, M.J. McLaughlin, E.K. Bünemann, Polyphosphate-fertilizer solution stability with time, temperature, and pH, J. Plant Nutr. Soil Sci. 170 (2007) 387–391.
[12] N. Powell, A. Shilton, Y. Chisti, S. Pratt, Towards a luxury uptake process via microalgae—defining the polyphosphate dynamics, Water Res. 43 (2009) 4207–4213.
[13] A. Solovchenko, A.M. Verschoor, N.D. Jablonowski, L. Nedbal, Phosphorus from wastewater to crops: an alternative path involving microalgae, Biotechnol. Adv. 34 (2016) 550–564.
[14] R. Whitton, A. Le Mevel, M. Pidou, F. Ometto, R. Villa, B. Jefferson, Influence of microalgal N and P composition on wastewater nutrient remediation, Water Res. 91

(2016) 371–378.
[15] J. Ruiz, P. Alvarez, Z. Arbib, C. Garrido, J. Barragán, J.A. Perales, Effect of nitrogen and phosphorus concentration on their removal kinetic in treated urban wastewater by Chlorella vulgaris, International Journal of Phytoremediation 13 (2011) 884–896.
[16] L. Afi, P. Metzger, C. Largeau, J. Connan, C. Berkaloff, B. Rousseau, Bacterial degradation of green microalgae: incubation of Chlorella emersonii and Chlorella vulgaris with Pseudomonas oleovorans and Flavobacterium aquatile, Org. Geochem. 25 (1996) 117–130.
[17] J. Fleurence, The enzymatic degradation of algal cell walls: a useful approach for improving protein accessibility? J. Appl. Phycol. 11 (1999) 313–314.
[18] H.G. Gerken, B. Donohoe, E.P. Knoshaug, Enzymatic cell wall degradation of Chlorella vulgaris and other microalgae for biofuels production, Planta 237 (2013) 239–253.
[19] C. Schreiber, H. Schiedung, L. Harrison, C. Briese, B. Ackermann, J. Kant, S.D. Schrey, D. Hofmann, D. Singh, O. Ebenhöh, W. Amelung, U. Schurr, T. Mettler-Altmann, G. Huber, N.D. Jablonowski, L. Nedbal, Evaluating potential of green alga Chlorella vulgaris to accumulate phosphorus and to fertilize nutrient-poor soil substrates for crop plants, J. Appl. Phycol. 30 (2018) 2827–2836.
[20] S.L. Bauke, M. Landl, M. Koch, D. Hofmann, K.A. Nagel, N. Siebers, A. Schnepf, W. Amelung, Macropore effects on phosphorus acquisition by wheat roots – a rhizotron study, Plant Soil 416 (2017) 67–82.
[21] Š. Moudříková, A. Sadowsky, S. Metzger, L. Nedbal, T. Mettler-Altmann, P. Mojzeš, Quantification of polyphosphate in microalgae by Raman microscopy and by a reference enzymatic assay, Anal. Chem. 89 (2017) 12006–12013.
[22] Š. Moudříková, P. Mojzeš, V. Zachleder, C. Pfaff, D. Behrendt, L. Nedbal, Raman and fluorescence microscopy sensing energy-transducing and energy-storing structures in microalgae, Algal Res. 16 (2016) 224–232.
[23] I. Brányiková, B. Maršálková, J. Doucha, T. Brányik, K. Bišová, V. Zachleder, M. Vítová, Microalgae—novel highly efficient starch producers, Biotechnol. Bioeng. 108 (2011) 766–776.
[24] L. Nedbal, M. Trtílek, J. Červený, O. Komárek, H.B. Pakrasi, A photobioreactor system for precision cultivation of photoautotrophic microorganisms and for high content analysis of suspension dynamics, Biotechnol. Bioeng. 100 (2008) 902–910.
[25] P. Winkler, K. Kaiser, A. Kölbl, T. Kühn, P. Schad, L. Urbanski, S. Fiedler, E. Lehndorff, K. Kalbitz, S.R. Utami, Z. Cao, G. Zhang, R. Jahn, I. Kögel-Knabner, Response of vertisols, andosols, and alisols to paddy management, Geoderma 261 (2016) 23–35.
[26] E. Lehndorff, M. Houtermans, P. Winkler, K. Kaiser, A. Kölbl, M. Romani, D. Said-Pullicino, S.R. Utami, G.L. Zhang, Z.H. Cao, R. Mikutta, G. Guggenberger, W. Amelung, Black carbon and black nitrogen storage under long-term paddy and non-paddy management in major reference soil groups, Geoderma 284 (2016) 214–225.
[27] WRB, World Reference Base for Soil Resources 2014, Update 2015: International Soil Classification System for Naming Soils and Creating Legends for Soil Maps, (2015).
[28] M.J. Hedley, J.W.B. Stewart, B.S. Chauhan, Changes in inorganic and organic soil phosphorus fractions induced by cultivation practices and by laboratory incubations, Soil Sci. Soc. Am. J. 46 (1982) 970.
[29] M.F. Mertens, S. Pätzold, G. Welp, Spatial heterogeneity of soil properties and its mapping with apparent electrical conductivity, J. Plant Nutr. Soil Sci. 171 (2008) 146–154.
[30] W. Negassa, P. Leinweber, How does the Hedley sequential phosphorus fractionation reflect impacts of land use and management on soil phosphorus: a review, J. Plant Nutr. Soil Sci. 172 (2009) 305–325.
[31] N. Siebers, F. Godlinski, P. Leinweber, The phosphorus fertilizer value of bone char for potatoes, wheat, and onions: first results, Landbauforschung Volkenrode 62 (2012) 59–64.
[32] T. Vogel, J. Kruse, N. Siebers, M. Nelles, B. Eichler-Löbermann, Recycled products from municipal waste water: composition and effects on phosphorus mobility in a sandy soil, J. Environ. Qual. 46 (2017) 443–451.
[33] A.K. Kolay, Manures and Fertilizer, Atlantic Publ. Distrib, New Delhi, 2007.
[34] S. Eixler, U. Karsten, U. Selig, Phosphorus storage in Chlorella vulgaris (Trebouxiophyceae, Chlorophyta) cells and its dependence on phosphate supply, Phycologia 45 (2006) 53–60.
[35] N.N. Rao, M.R. Gómez-García, A. Kornberg, Inorganic polyphosphate: essential for growth and survival, Annu. Rev. Biochem. 78 (2009) 605–647.
[36] R.A. Dahlgren, M. Saigusa, F.C. Ugolini, The nature, properties and management of volcanic soils, Adv. Agron. 82 (2004) 113–182 Elsevier.
[37] J.R. Fink, A.V. Inda, T. Tiecher, V. Barrón, Iron oxides and organic matter on soil phosphorus availability, Ciênc. Agrotechnology. 40 (2016) 369–379.
[38] M.E. McGroddy, W.L. Silver, R.C. de Oliveira, W.Z. de Mello, M. Keller, Retention of phosphorus in highly weathered soils under a lowland Amazonian forest ecosystem, Journal Geophysical Research 113 (2008) 289–300.
[39] M. Takeda, T. Nakamoto, K. Miyazawa, T. Murayama, H. Okada, Phosphorus availability and soil biological activity in an andosol under compost application and winter cover cropping, Appl. Soil Ecol. 42 (2009) 86–95.
[40] J.A. Veith, G. Sposito, Reactions of aluminosilicates, aluminum hydrous oxides, and aluminum oxide with o-phosphate: the formation of X-ray amorphous analogs of variscite and montebrasite, Soil Sci. Soc. Am. J. 41 (1977) 870–876.
[41] L.M. Condron, S. Newman, Revisting the fundamentals of phosphorus fractionation of sediments and soils, Soils Sediments 11 (2011) 830–840.
[42] B.L. Turner, B.J. Cade-Menun, L.M. Condron, S. Newman, Extraction of soil organic phosphorus, Talanta 66 (2005) 294–306.
[43] S.L. Bauke, C. von Sperber, F. Tamburini, M.I. Gocke, B. Honermeier, K. Schweitzer, M. Baumecker, A. Don, A. Sandhage-Hofmann, W. Amelung, Subsoil phosphorus is affected by fertilization regime in long-term agricultural experimental trials, Eur. J. Soil Sci. 69 (2018) 103–112.
[44] M. Koch, J. Kruse, B. Eichler-Löbermann, D. Zimmer, S. Willbold, P. Leinweber, N. Siebers, Phosphorus stocks and speciation in a soil profile of a long-term fertilizer experiment: evidence from sequential fractionation, ^{31}P-NMR, and P K-edge XANES spectroscopy, Geoderma 316 (2018) 115–126.
[45] M. Siebers, P. Dörmann, G. Hölzl, Membrane remodelling in phosphorus-deficient plants, Annual Plant Reviews 48 (2015) 237–263.
[46] D.C. White, P. Meadows, G. Eglinton, M.L. Coleman, In situ measurement of microbial biomass, community structure and nutritional status [and discussion], Philos. Trans. R. Soc. A Math. Phys. Eng. Sci. 344 (1993) 59–67.
[47] D. Hui, M.A. Mayes, G. Wang, Kinetic parameters of phosphatase: a quantitative synthesis, Soil Biol. Biochem. 65 (2013) 105–113.
[48] C. von Sperber, H. Lewandowski, F. Tamburini, S.M. Bernasconi, W. Amelung, E. Frossard, Kinetics of pyrophosphatase catalyzed oxygen isotope exchange between phosphate and water revealed by Raman spectroscopy, Journal Raman Spectroscopy 48 (2016) 368–373.
[49] H. Keown, O.M. Callaghan, L.C. Greenfield, Decomposition of nucleic acids in soil, New Zealand Natural Sciences 29 (2004) 13.

III. D. Dynamic Guanine Crystals in Microalgae

III. D. 1. Introduction

In nature, microalgae thrive even during periods with nutrient fluctuations [490]. Unlike polyP, which provides the main P storage pools in algae (see Sections II.C. and III.C.), little is known about N storage pools in algae. While algae flourish under N deficient conditions, this is usually interpreted as a stop of growth and a transition into mobilizing intracellular inorganic or low-molecular-weight organic N compounds [436]. However, nutrient fluctuations in nature can occur periodically [491], regardless of the availability of mobilizable N compounds in algae. Without long-term N storage pools as a backup, algae might not spread under N deficienct conditions. With long-term N storage pools, algae are prepared for long-term survival. However, unlike cyanobacteria, eukaryotic microalgae do not possess N-rich cyanophycin to manage an N deficiency [492, 493].

In 2017, our group detected and identified the presence of crystalline guanine in the chlorophyte *Desmodesmus quadricauda* and the eustigmatophyte *Trachydiscus minutus* through the use of confocal Raman microscope [15]. Guanine functions universally in signaling molecules and in molecules providing free energetic potentials. However, these well-known functions cannot explain why algae contain abundant guanine as crystalline forms. The literature review for crystalline guanine in algae has been included in Chapter II. Briefly, there are two areas of focus in the history. The first examines algal ultrastructure, mainly by using transmission electron microscopy. Crystal-liked particles have been commonly demonstrated in marine dinoflagellates in the last six decades without proper identification. The second is focused on purine uptake by algae without proper investigation of potential algal N storage products. This work revealed the presence and a dynamic role of guanine crystals as a common long-term N source among microalgal species throughout the phylogenetic tree [303].

My contribution to this work is includes algal culturing, partially designing and conducting Raman measurements on *Amphidinium carterae* and for algae of the family

Symbiodiniaceae, preparing most of the graphics, and writing the manuscript and supplemental material.

III. D. 2. Method

The several biophysical approaches are combined, including confocal Raman microscopy, Raman with stable isotopic labeling (^{15}N and D), polarization/reflection microscopy, advanced electron microscopy, and absorption spectrophotometry studying guanine crystals in algae, as summarized in Figure III-3.

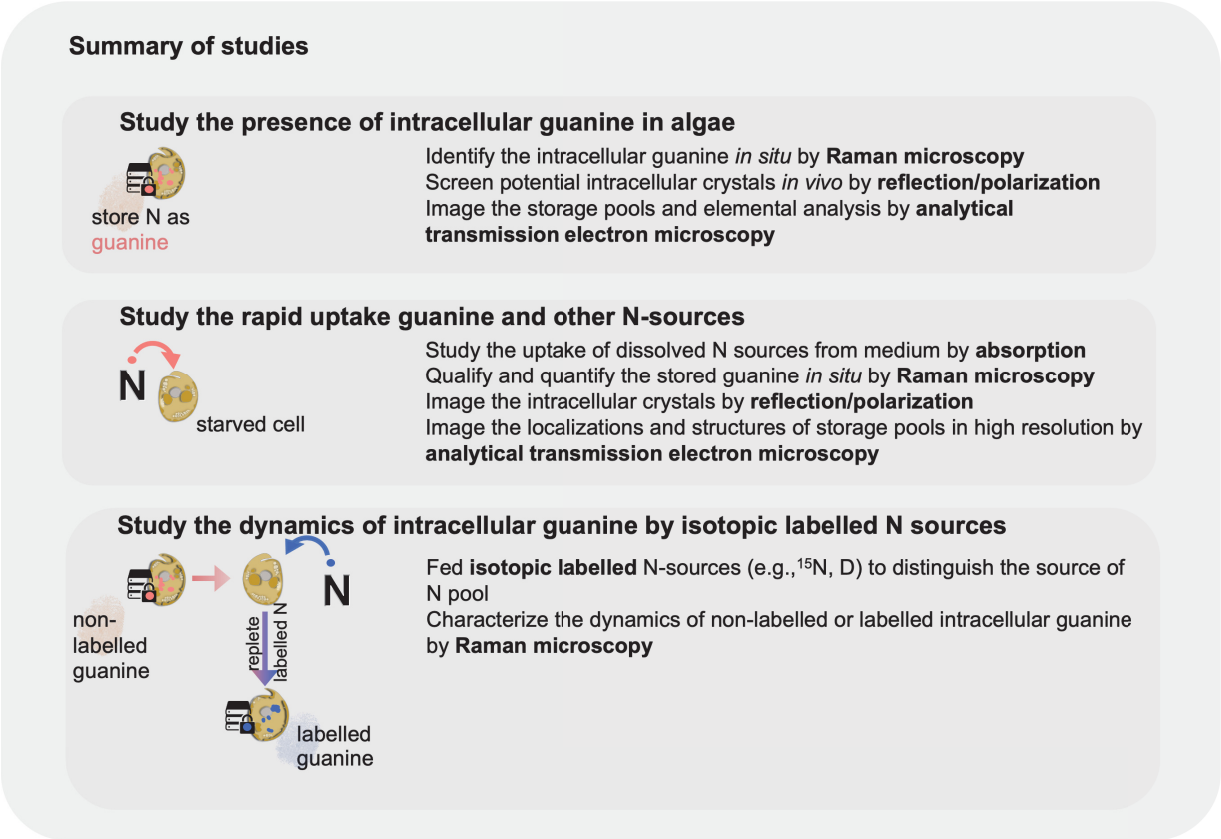

Figure III-3 Summary of methods for investigating guanine crystals in algae in this study

III. D. 3. Result

The main results are the following:

- Guanine crystals accumulate in various free-living and symbiotic algal species throughout the phylogenetic tree.

- Free-living and symbiotic N-starved marine dinoflagellates can rapidly take either dissolved guanine or solid guanine up as their sole N source. These N can also be stored as dynamic guanine pools in algae.

Algal guanine crystals accumulate during the lag phase, when N source is provided to N-starved algae, regardless of external nitrogen sources such as nitrate, ammonium, urea, or guanine. During the exponential phase, the previously stored guanine crystals are consumed for growth. N starved *A. carterae* requires about one hour to completely take up 30 mM guanine from suspension and store N as guanine in crystalline form. These accumulated guanine pools support the proliferation of several generations of cells without any additional nutrients. *A. carterae* stores guanine in at least two crystalline structures: large globules or small, flat crystals. The accumulation of guanine crystals in algae involves potential ion exchanges when extraneous guanine crystals are the sole N source.

III. D. 4. The publication

PNAS
www.pnas.org

Guanine, a high-capacity and rapid-turnover nitrogen reserve in microalgal cells

Peter Mojzeš[1,2], Lu Gao[2,3], Tatiana Ismagulova[4], Jana Pilátová[5], Šárka Moudříková[1], Olga Gorelova[4], Alexei Solovchenko[4,6], Ladislav Nedbal[2*], Anya Salih[7]

[1]Institute of Physics, Faculty of Mathematics and Physics, Charles University, Ke Karlovu 5, CZ-12116 Prague 2, Czech Republic

[2]Institute of Bio- and Geosciences/Plant Sciences (IBG-2), Forschungszentrum Jülich, Wilhelm-Johnen-Straße, D-52428 Jülich, Germany

[3]Faculty of Mathematics and Natural Sciences, Heinrich Heine University, Universitätstraße 1, D-40225 Düsseldorf, Germany

[4]Faculty of Biology, Moscow State University, Leninskie Gori 1/12, 119234, GSP-1, Moscow, Russia

[5]Department of Experimental Plant Biology, Faculty of Science, Charles University, Viničná 5, CZ-12844 Prague 2, Czech Republic

[6]Pskov State University, 2 Lenin Square, Pskov 180000, Russia

[7]Antares Fluoresci Research, Dangar Island, NSW 2083 and Confocal Bioimaging Facility, Western Sydney University, NSW 1797, Australia

* Corresponding author: Ladislav Nedbal (l.nedbal@fz-juelich.de)

PNAS December 22, 2020 117 (51) 32722-32730; first published December 8, 2020; https://doi.org/10.1073/pnas.2005460117

Edited by Donald R. Ort, University of Illinois at Urbana–Champaign, Urbana, IL, and approved November 4, 2020 (received for review May 3, 2020

Guanine, a high-capacity and rapid-turnover nitrogen reserve in microalgal cells

Peter Mojzeš[a,b], Lu Gao[b,c], Tatiana Ismagulova[d], Jana Pilátová[e], Šárka Moudříková[a], Olga Gorelova[d], Alexei Solovchenko[d,f], Ladislav Nedbal[b,1], and Anya Salih[g,h]

[a]Institute of Physics, Faculty of Mathematics and Physics, Charles University, CZ-12116 Prague 2, Czech Republic; [b]Institute of Bio- and Geosciences/Plant Sciences (IBG-2), Forschungszentrum Jülich, D-52428 Jülich, Germany; [c]Faculty of Mathematics and Natural Sciences, Heinrich Heine University, D-40225 Düsseldorf, Germany; [d]Faculty of Biology, Moscow State University, Leninskie Gori 1/12, 119234, GSP-1, Moscow, Russia; [e]Department of Experimental Plant Biology, Faculty of Science, Charles University, CZ-12844 Prague 2, Czech Republic; [f]Faculty of Geography and Natural Sciences, Pskov State University, 180000 Pskov, Russia; [g]Antares Fluoresci Research, Dangar Island, NSW 1797, Australia; and [h]Confocal Bioimaging Facility, Western Sydney University, NSW 1797, Australia

Edited by Donald R. Ort, University of Illinois at Urbana–Champaign, Urbana, IL, and approved November 4, 2020 (received for review May 3, 2020)

Nitrogen (N) is an essential macronutrient for microalgae, influencing their productivity, composition, and growth dynamics. Despite the dramatic consequences of N starvation, many free-living and endosymbiotic microalgae thrive in N-poor and N-fluctuating environments, giving rise to questions about the existence and nature of their long-term N reserves. Our understanding of these processes requires a unequivocal identification of the N reserves in microalgal cells as well as their turnover kinetics and subcellular localization. Herein, we identified crystalline guanine as the enigmatic large-capacity and rapid-turnover N reserve of microalgae. The identification was unambiguously supported by confocal Raman, fluorescence, and analytical transmission electron microscopies as well as stable isotope labeling. We discovered that the storing capacity for crystalline guanine by the marine dinoflagellate *Amphidinium carterae* was sufficient to support N requirements for several new generations. We determined that N reserves were rapidly accumulated from guanine available in the environment as well as biosynthesized from various N-containing nutrients. Storage of exogenic N in the form of crystalline guanine was found broadly distributed across taxonomically distant groups of microalgae from diverse habitats, from freshwater and marine free-living forms to endosymbiotic microalgae of reef-building corals (*Acropora millepora*, *Euphyllia paraancora*). We propose that crystalline guanine is the elusive N depot that mitigates the negative consequences of episodic N shortage. Guanine ($C_5H_5N_5O$) may act similarly to cyanophycin ($C_{10}H_{19}N_5O_5$) granules in cyanobacteria. Considering the phytoplankton nitrogen pool size and dynamics, guanine is proposed to be an important storage form participating in the global N cycle.

nitrogen cycle | nutrient storage | phytoplankton | guanine | coral

Planktonic algae represent an essential driver of the global carbon cycle, which may be constrained by low or fluctuating nitrogen (N) availability (1–3). At another extreme, high levels of bioavailable N, often from anthropogenic sources, may result in harmful algal blooms (4) or deterioration of coral reefs (5). The highly optimized nutrient interactions with symbiotic algae are also essential for reef corals that thrive in nutrient-poor waters and paradoxically form among the most productive and diverse ecosystems. Both high and low N availability may perturb the stability of individual organisms or entire ecosystems especially when not in proportion to other biogenic elements, such as phosphorus (6).

N shortages trigger extensive changes in algal metabolism (7), including cessation of cell division, reduction of photosynthesis, and accumulation of C- and energy-rich N-free compounds. Unlike cyanobacteria, eukaryotic microalgae do not possess N-rich cyanophycin to manage N deficiency (8, 9). N-deprived microalgae mobilize intracellular inorganic N; low-molecular organic N compounds, such as polyamines, amino acids, and chlorophyll (7); and polymeric N compounds, such as proteins and nucleic acids (10). However, none of these reserves may be sufficient to bridge long periods of N starvation. Thus, a pool capable of storing large amounts of N during periods of abundance and ensuring survival and growth of algae during deficiency remains to be identified.

Among candidate N storage pools in microalgae, crystalline inclusions were considered, although later, alternative roles, such as processing of metabolic wastes (11) and light modulation (12) were also suggested. The chemical identity of crystals from the free-living marine dinoflagellate *Gonyaulax polyedra* was proposed to be guanine (13). Other crystalline inclusions hypothesized of being guanine were also observed in symbiotic dinoflagellates of an anemone *Aiptasia* sp. (14), but their chemical nature was not experimentally confirmed (11, 14). Other earlier studies suggested the inclusions were calcium oxalate (15, 16) making the N-storage function of the inclusions unlikely. Subsequent analysis of symbiotic dinoflagellate extracts from *Aiptasia* sp. identified them as crystalline uric acid (17). This identification has since been adopted for microalgal inclusions in many recent publications (18–21).

In contrast with this proposed identity (17–21) and consistent with earlier studies (13, 14), recent direct in situ analyses identified inclusions as guanine in several marine dinoflagellates (12, 22), a freshwater chlorophyte and a eustigmatophyte (23). Guanine, similar to other purines, has the potential to serve as a large-capacity N pool, but this function has never been previously confirmed, nor was its in situ chemical identity explored in diverse algal species. Guanine is widespread and, thus, widely available in nature. It is an essential component of DNA and RNA, one of the end products of

Significance

Vast areas of the oceans are N limited, and how microalgae can flourish in these N-poor waters is still not known. Furthermore, mechanisms and sites of N uptake and storage have not been fully determined. We show that crystalline guanine ($C_5H_5N_5O$) is an important N storage form for phytoplankton and for symbiotic dinoflagellates of corals. The widespread occurrence of guanine reserves among taxonomically distant microalgal species suggests an early evolutionary origin of its function as N storage. Crystalline guanine appears to be a multifunctional biochemical with an important role in the N cycle that remains to be elucidated. In particular, a better knowledge of N-storage metabolism is necessary to understand the impact of eutrophication on coral-symbiont interaction.

Author contributions: P.M., A.So., and L.N. designed research; P.M., L.G., T.I., J.P., O.G., A.So., and A.Sa. performed research; P.M., L.G., T.I., O.G., A.So., L.N., and A.Sa. analyzed data; and P.M., L.G., A.So., L.N., and A.Sa. wrote the paper.

The authors declare no competing interest.

This article is a PNAS Direct Submission.

[1]To whom correspondence may be addressed. Email: l.nedbal@fz-juelich.de.

This article contains supporting information online at https://www.pnas.org/lookup/suppl/doi:10.1073/pnas.2005460117/-/DCSupplemental.

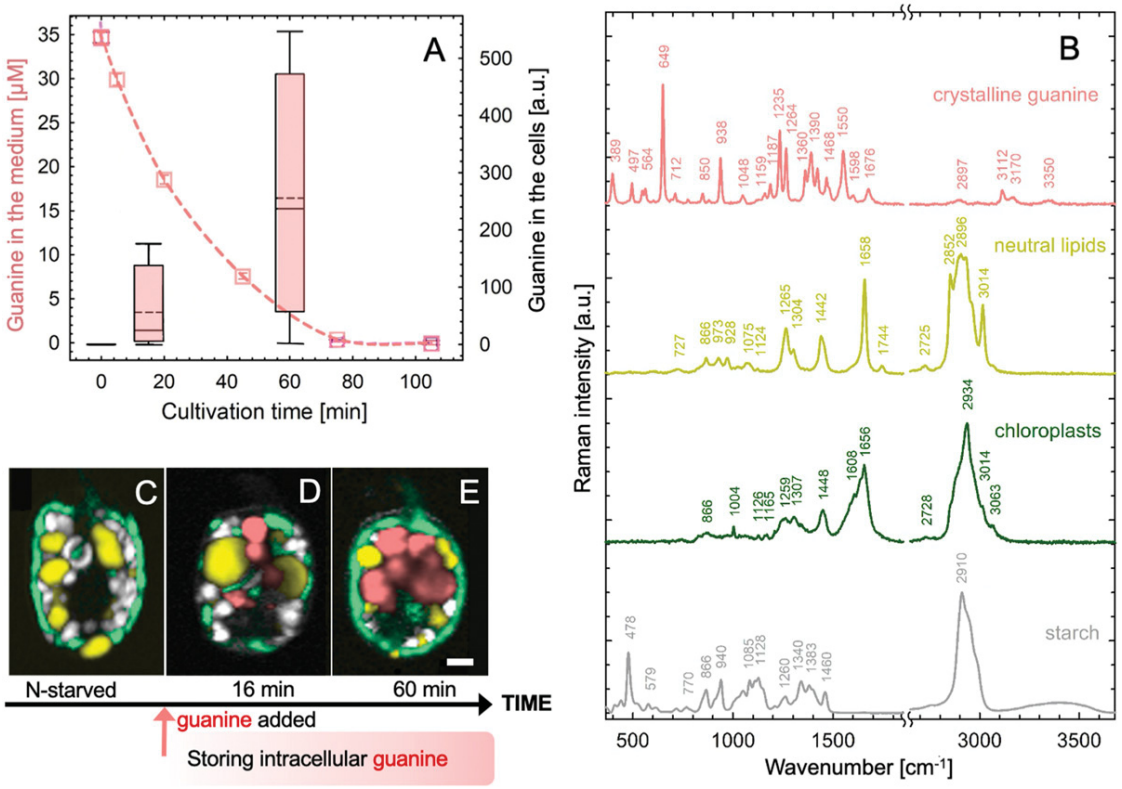

Fig. 1. Rapid uptake of guanine by N-starved *A. carterae* led to the accumulation of intracellular guanine inclusions. Cells were suspended in a saturated solution of guanine (~35 µM at 20 °C) in N-deficient f/2 medium at a density of 1.7 ± 0.3 × 10^5 cells·mL^{-1}. The dashed line in *A* shows the declining concentration of guanine in the medium as measured by ultraviolet absorption (*SI Appendix*, section II.1.B). The simultaneous accumulation of guanine in the cells was assessed using Raman microscopy (*SI Appendix*, section II.1.C) and is shown in the boxplot. Raman spectra in *B* were used to generate the Raman maps in *C–E* that represent: (*C*) a typical cell after 2 wk without a N source and (*D* and *E*) cells during progressive guanine accumulation. Color legend: guanine (pink), lipids (yellow), chloroplast (green), and starch (white/gray). (Scale bar, 2 µm.) Raman maps showing separate cellular constituents in *C–E* are constructed as described in *SI Appendix*, section I.1 and presented in *SI Appendix*, Fig. S1.

nucleic acid degradation in some organisms, and utilized by some for functional purposes, such as light scattering by silvery scales of fish and bio-optical systems of many invertebrates (reviewed in ref. 24). It is widely available from decomposing fish tissues and scales, from ciliates and some phytoplankton, barnacles, and other aquatic organisms and forms part of suspended and dissolved organic N pools in the ocean. Along with other purines, guanine can serve as a N source for algae (reviewed in ref. 1). We propose that crystalline guanine and other purines (17) play a more prominent role in the N cycle than recognized to date.

To test this hypothesis, we used the unique potential of Raman microscopy and analytical transmission electron microscopy (TEM) and identified the chemical nature and the dynamics of microalgal crystal inclusions. We confirm the occurrence of crystalline guanine in free-living and symbiotic dinoflagellates and other diverse microalgal species. Our research demonstrated widespread occurrence, large N-storage capacity, and prominent dynamics of guanine in the form of crystalline inclusions in microalgae.

Results

Fast Kinetics of Uptake and Large Storage Capacity of Intracellular Guanine Inclusions in *Amphidinium carterae*. We first characterized the uptake of guanine by the widespread potentially toxic marine dinoflagellate *A. carterae*. Details of cultivation are provided in *SI Appendix*, section II.1A. Cells were kept in N-free medium (*SI Appendix*, section II.1.Aa.) for approximately 2 wk before resuspension in a saturated solution of guanine (*SI Appendix*, section II.1.Ab.). We recorded a rapid uptake rate of dissolved guanine from the medium (dashed line, Fig. 1*A*) and its concurrent accumulation in cells (box plot, Fig. 1*A*). Dynamics and localization of guanine inclusions inside cells (in pink, Fig. 1 *C* and *D*) on the background of other cellular components was identified by the spectral signature of Raman confocal microscopy (Fig. 1*B*) (23). The rapid accumulation of the optically active guanine crystals was also documented via polarization microscopy (*SI Appendix*, section II.1.D. and Movie S1).

The dependence of uptake kinetics of dissolved guanine (Fig. 2 and *SI Appendix*, section I.2.) on cell density displayed an initial linear uptake phase (solid lines, the coefficient of determination RSQR ≥ 0.995) and its interpolation yielded an initial cellular uptake rate of 16 ± 4 fg (guanine)·s^{-1}·$cell^{-1}$, i.e., 6.3 ± 1.5 × 10^7 molecules·s^{-1}·$cell^{-1}$.* Uptake kinetics (Fig. 2) were used to quantify intracellular guanine accumulation inside cells (*SI Appendix*, Fig. S2*A*) resulting in a maximum storage capacity of 143 ± 37 pg of crystalline guanine $cell^{-1}$, that corresponded to 68 ± 17 pg (nitrogen)·$cell^{-1}$. Details of these calculations are provided in *SI Appendix*, section I.2. The N pool created by starvation and refeeding was significantly larger than 17–44 pg (nitrogen)·$cell^{-1}$ that was previously suggested to be the total N content in *A. carterae* under stationary conditions (25). Guanine storage pools may, thus, ameliorate N deficiency that occurs sporadically in a fluctuating environment.

*Numbers following the ± sign represent, in this work, standard deviation.

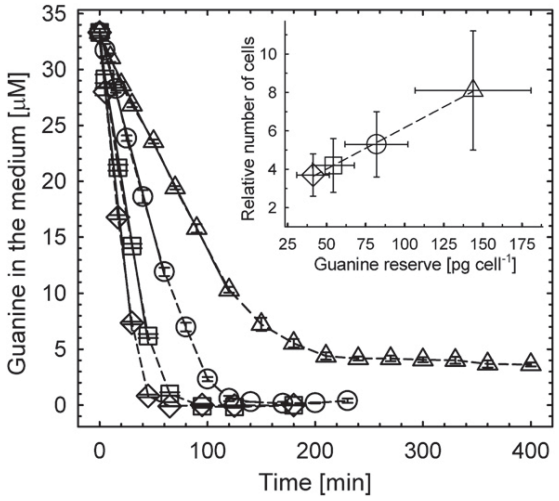

Fig. 2. Uptake of dissolved guanine from the medium by N-starved *A. carterae* and the number of generations supported by accumulated reserves (inset). The rate of guanine disappearance from the medium decreased with reduced cell density (±SD): from (122 ± 31) (◇) to (93 ± 23) (□), to (61 ± 15) (○), and to (31 ± 8) (△) × 10^3 cells·mL^{-1}. The most dilute culture (△) reduced guanine concentration in the medium from 35 to ∼4 μM, revealing the maximum storage capacity of cells of 143 ± 37 (SD) pg of crystalline guanine cell^{-1}. *Inset* shows the correlation between the number of cells grown on guanine reserve and the reserve size. Details of calculations for this figure are described in *SI Appendix*, section I.2 and Fig. S2.

Cells with new guanine reserves can, after a short lag period, resume normal cell division and growth. The exponential growth phase halted only after the reserves were once again exhausted (*SI Appendix*, Fig. S2*B*). The number of cells that grew on these reserves was a linear function of the initially available guanine (inset in Fig. 2). The number of cells that accumulated maximum N storage (△) increased 8.1 ± 3.1 times without N addition.

The resolution of the in situ localization of guanine crystals in *A. carterae* (Fig. 1) was increased via ultrastructural TEM imaging (Fig. 3 and *SI Appendix*, section II.1.E.) (26, 27). The solubility of guanine is known to be extremely low, and pieces of undissolved crystalline material (Fig. 3*A*, three white arrows) were confirmed via EDX (*SI Appendix*, section II.1.F.) to correspond to the elemental composition of a N-rich compound, likely to be guanine (Fig. 3*D*). *A. carterae* has a special organelle, the pusule, which is connected to the flagellar channel (28, 29). We found large globules in pusules (Fig. 3 *B* and *C*) and small crystals in vacuoles that consistently displayed typical EDX point spectra of guanine crystals (Fig. 3 *E* and *F*). Our results were inconclusive with respect to whether the guanine particles had been taken up into the pusules by phagocytosis (30) and/or via an active transport of guanine molecules dissolved in the medium from the added crystals. Guanine globules in pusules and vacuoles had irregular shapes, but the comparison of Raman spectra (Fig. 1*B*) with those in refs. 12, 31 confirmed that the molecules were organized in a regular anhydrous crystal structure. We hypothesized that algae may take up guanine microcrystals and, possibly, guanine-rich marine particulate fish debris via endocytosis or via the pusule (*SI Appendix*, sections I.3 and II.1.Ac and Fig. S3).

Uptake of Solid Guanine by *A. carterae* Involves Crystal Decomposition and Recrystallization. Guanine microparticles or guanine-rich debris might be taken up by dinoflagellates and directly deposited inside their cells without first dissolving or changing the original crystalline structure, similar to an engulfing mechanism proposed for algal feeding on bacteria (32). In an alternative scenario, the engulfed particles may be first dissolved within pusules or vacuoles into individual molecules. Globules of guanine may then be assembled at target intracellular locations by new crystallization (Figs. 1 and 3). Guanine crystals may also be dissolved extracellularly,

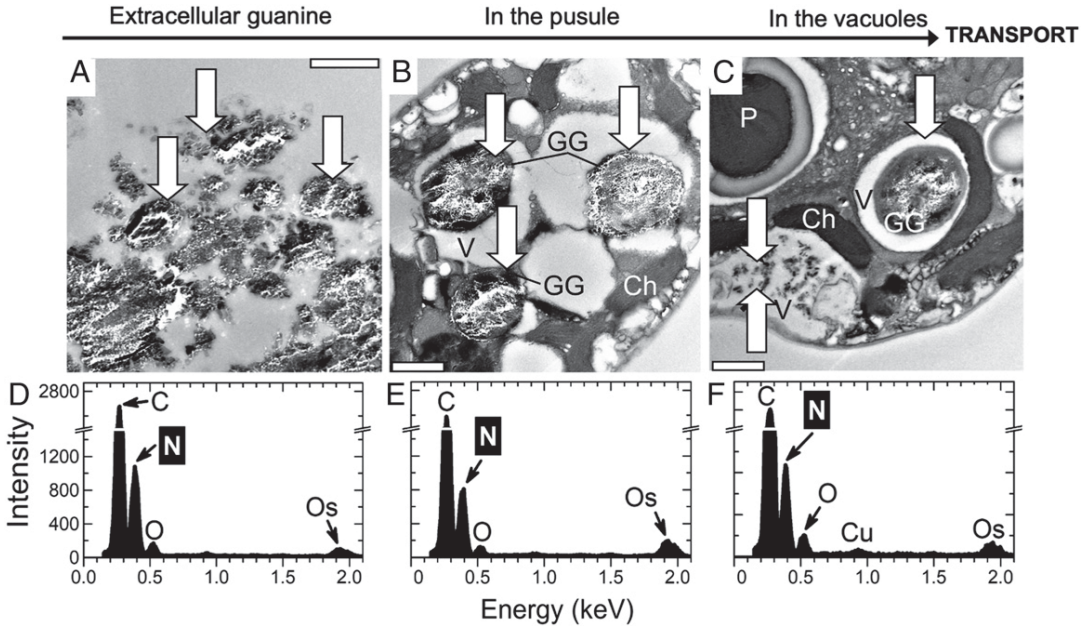

Fig. 3. TEM of semithin sections (*A–C*) and energy-dispersive X-ray spectroscopy (EDX) (*D–F*) analysis of *A. carterae* 6 h after refeeding N-starved cultures with guanine. Typical EDX point spectra of guanine crystals (*D–F*) indicating a high N content were obtained in the scanning TEM (STEM) mode from semithin cell sections. Arrows point to guanine particles outside (*A*) and inside cells (*B* and *C*). (Scale bars, 1 μm.) Ch, chloroplast; GG, globules with microcrystalline guanine; P, pyrenoid; V, vacuole.

subsequently taken up via active constitutive transport through their cell walls and reassembled into crystalline structures inside the cells.

Raman microscopy offers a unique opportunity to discriminate between the uptake mechanisms using the spectral contrast between fully (d_5) and partially (d_1) deuterated guanine (Fig. 4 and *SI Appendix*, sections I.3 and II.2.A and Fig. S7). The conversion of d_5-guanine to d_1-guanine requires that the molecules are directly exposed to an aqueous environment so that the four deuterium atoms bound to N can be exchanged by hydrogen from water, leaving only deuterium bound to C8 (33). Thus, if the guanine particle remained in its original crystalline form during the uptake by a cell, the N-D groups of d_5-guanine would have been protected from isotope exchange. Confirming this, a grain of guanine crystal outside of a cell (Fig. 4*B*) was found to remain in the d_5-guanine form (dark blue, white arrow).

The Raman spectra proved that the new reserves of intracellular guanine that appeared inside the N-starved *A. carterae* were in the d_1 form (Fig. 4, magenta). Only 30 min after the crystalline d_5-guanine was added to the cell suspension, both the d_5-guanine grain (dark blue, white arrow) outside the cell and the transformed d_1-guanine globules inside the cells (magenta) were captured simultaneously in Fig. 4 *A* and *B*. Crystalline d_1-guanine was also found in the cells 5–12 h after feeding (Fig. 4 *D* and *F*). The large guanine globules were preferentially located at the cell center 5 h after N feeding (Fig. 4 *C* and *D*), and, subsequently, some in the form of smaller particles moved toward the cell periphery (Figs. 4 *E* and *F* and 3*C*).

Our analyses suggest that the guanine microcrystals were dissolved outside cells and taken up as individual molecules. Alternately, if they were engulfed as intact microcrystals, they were then dissolved intracellularly before reassembling into new crystals. In either case, the original crystalline structure was released, deuterium atoms bound to N in the d_5-form were exchanged for hydrogen from water, and the d_1-guanine molecules were reassembled into much larger inclusions in the vacuoles and/or pusules (Figs. 3 and 4).

Guanine Crystals Are Biosynthesized in *A. carterae* de Novo from Diverse Exogenic N Sources. Raman spectroscopy can also easily distinguish between ^{14}N- and ^{15}N-guanine (*SI Appendix*, sections I.3 and II.2.B and Fig. S8), thus, making it useful for determining the source of N. Feeding N-starved *A. carterae* with ^{15}N-guanine, ^{15}N-nitrate, ^{15}N-ammonium (*Top* in Fig. 5), or ^{15}N-urea (*SI Appendix*, Fig. S10) restored the culture's growth and, regardless of the N source,

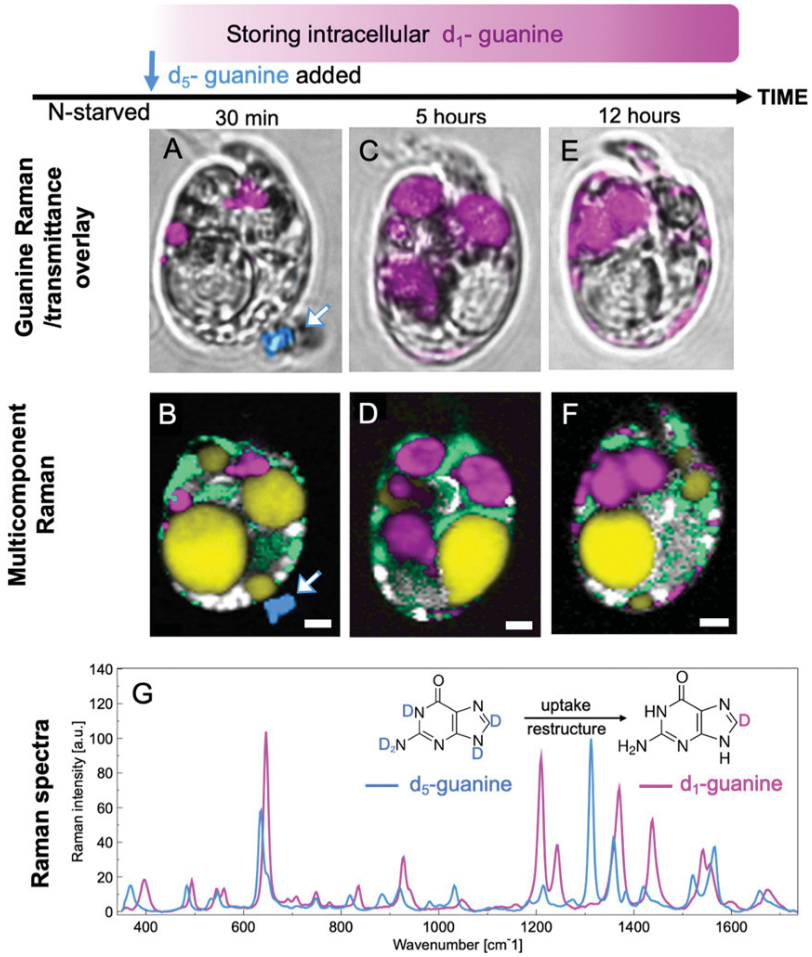

Fig. 4. Uptake of guanine includes exchange of deuterium for hydrogen atoms. Bright-field images overlaid by guanine (*A*, *C*, and *E*) and multicomponent Raman maps (*B*, *D*, and *F*) of N-starved *A. carterae* after the addition of solid crystalline fully deuterated d_5-guanine to N-depleted medium. Images collected 30 min (*A* and *B*), 5 h (*C* and *D*), and 12 h (*E* and *F*) after d_5-guanine addition. Data for d_5-guanine and partially deuterated d_1-guanine are presented in blue and magenta, respectively, in both the Raman spectrum and the images. *G* shows their respective Raman spectra. Other colors: yellow, neutral lipids; green, chloroplasts; white/gray, starch. (Scale bars [*A*–*F*], 2 μm.) More spectra of isotopically labeled guanine are shown in *SI Appendix*, Fig. S7. Raman maps showing separate components from data represented in *B*, *D*, and *F* are provided in *SI Appendix*, Fig. S9.

considerable amounts of crystalline ^{15}N-guanine appeared inside the cells during the *lag* phase that lasted ~24 h (Fig. 5, *Bottom*). On feeding *A. carterae* with nitrate, ammonium, or urea, no crystalline inclusions of other purines were observed. The accumulated or biosynthesized guanine crystals were later used to support growth until their complete disappearance in the new stationary phase. Regardless of the chemical identity of the N source, the total amount of N needed to produce a new *A. carterae* cell, estimated from the data in Fig. 5, was 14 ± 2 pg (N)·cell^{-1}. The calculation procedure was the same as in *SI Appendix*, section I.2. This amount corresponded theoretically to 30 ± 4 pg (guanine)·cell^{-1} of the presumed reserve, which was close to 23 ± 4 pg (guanine)·cell^{-1} obtained from the data presented in the graph inset in Fig. 2.

Interestingly, the intracellular guanine reserves generated by the assimilation of nitrate (middle graph in Fig. 5), ammonium, or urea were detected largely at the periphery of cells close to the chloroplasts (Fig. 6). This was in agreement with the earlier results obtained for nitrate (12). In contrast, the rapidly accumulated guanine was first located centrally in large globules (Fig. 4 *C* and *D* and *SI Appendix*, Fig. S11), which were later partially fragmented and moved to the cell periphery (Fig. 4*E*). This result obtained by Raman microscopy was confirmed with significantly higher spatial resolution by the combination of TEM and EDX methods (Figs. 3 and 6). We tentatively propose that the aforementioned differences in localization and storage dynamics indicate differences in transport and biochemical pathways following guanine biosynthesis from nitrate, ammonium, and urea compared with the direct uptake of guanine.

In Situ Chemical Identification of Inclusions in Algal Species of Diverse Taxonomical Classification and from Diverse Habitats. The chemical identity of inclusions in 14 microalgal species listed in Table 1 was examined by Raman microscopy as described in *SI Appendix*, section II.1.C. The selected species (*SI Appendix*, sections I.4. and II.3 for cultivation conditions) represent contrasting habitats, such as oligotrophic to mesotrophic marine species including both free-living (*A. carterae* and *Microchloropsis gaditana*) and coral endosymbiotic algae (*Chromera velia* and *Symbiodiniaceae*), oligotrophic to eutrophic freshwater (*Synura petersenii* and *Haematococcus pluvialis*, respectively), extremophilic/acidophilic (*Dunaliella acidophila*), terrestrial (*Lobosphaera incisa, Vischeria* sp., and *Klebsormidium flaccidum*), and algae from artificial anthropogenic environments (*Vacuoliviride crystalliferum* and *K. flaccidum*), their distribution ranging from tropical/subtropical regions (*A. carterae*, *C. velia*, and *Symbiodiniaceae*) and temperate zones (*Vischeria* sp.) to the cosmopolitan species extending to the Arctic (*K. flaccidum*). Some of the tested species were established model organisms (*Chlamydomonas reinhardtii* and *Microchloropsis gaditana*), others were important production species in algal biotechnology (*M. gaditana*, *D. acidophila*, *H. pluvialis*, and *L. incisa*). The diverse phylogeny among the selected species is shown in Table 1. Spectral signatures of inclusions found in the selected algal species were compared with the spectra of multiple purines (*SI Appendix*, Fig. S4) and with calcium oxalate and calcite (*SI Appendix*, Fig. S6). Guanine inclusions were found in 13 out of 14 tested species cultivated in commonly used media (*SI Appendix*, section II.3). Only one of the tested species *K. flaccidum* was found to contain uric acid in its inclusions. This identification was completed in situ, thus, eliminating the potential artifacts caused by extraction and chemical analyses. Differences between Raman spectral signatures of guanine and uric acid are large (*SI Appendix*, Fig. S4), enabling accurate discrimination needed in light of alternatives proposed in recent literature (12, 17, 23). We cannot rule out, however, that under specific cultivation conditions, stress factors, or feeding by other organic nutrients, crystalline inclusions of other purines may not be present. Furthermore, the abundance of guanine inclusions depended not only on the availability of N nutrients (Fig. 1 *C–E*), but also on cultivation factors, such as CO_2 availability for *Desmodesmus quadricauda* (23) or on the cell cycle phase in *C. reinhardtii* (*SI Appendix*, section I.4 and Fig. S12). We also cannot exclude possible transformation of different purine forms with some perhaps occurring transiently or even simultaneously. Nevertheless, our experiments reliably confirm that guanine is the dominant N-storage form in the investigated microalgal species, and uric acid is found only in *K. flaccidum*, a single representative of the Streptophyta lineage. However, many more species of this lineage must be tested in the future to conclude that the Streptophyta lineage deviates from other taxonomical groups.

Coral Symbiotic Microalgae Accumulate and Store Guanine. Of particular interest in relation to guanine cell storage are the photosynthetic *Symbiodiniaceae* dinoflagellates (zooxanthellae) that live in mutualistic symbiosis with reef-building corals. The finely tuned exchange of nutrients between the coral host and the symbionts forms the foundation of healthy coral reef ecosystems (5, 21, 34, 35). However, much remains poorly understood regarding the mechanisms of nutrient uptake and storage that allow corals to

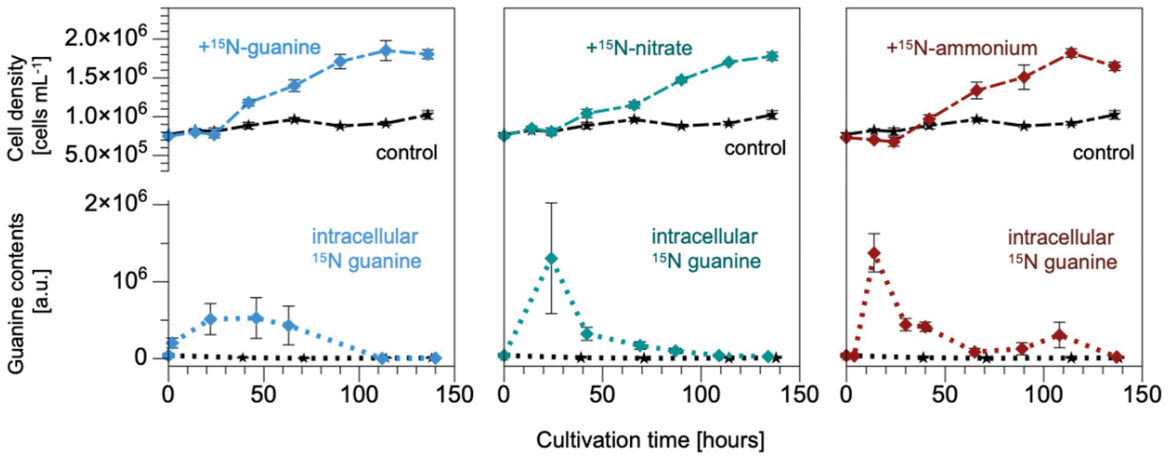

Fig. 5. N in guanine inclusions originated directly from the supplied guanine, nitrate, and ammonium. *A. carterae* cell density stagnated in controls without N feeding (black lines) and divided after addition of ^{15}N-labeled guanine, nitrate, and ammonium (all at 0.882-mM N). Intracellular crystalline guanine per cell is shown in the bottom graphs representing Raman measurements (n = 5–12 cells). The corresponding graph representing uptake of urea is shown in *SI Appendix*, Fig. S10.

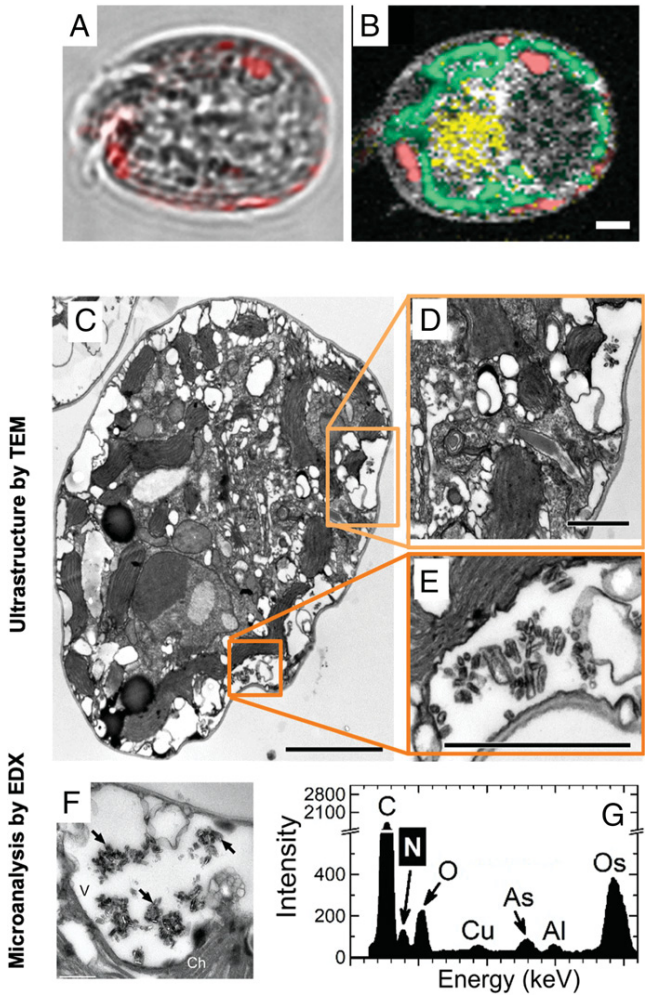

Fig. 6. Localization of guanine inclusions in *A. carterae* fed by nitrate by TEM. Bright-field images overlaid by guanine (pink) (*A*) and multicomponent Raman maps (*B*) of *A. carterae* cells 24 h after refeeding N-starved cells with nitrate. False color coding is the same as that in Fig. 1. (Scale bar, 2 μm.) TEM of ultrathin (*C*–*E*) and semithin (*F*) sections as well as EDX (*G*); (*F* and *G*) analysis of *A. carterae* cells and surrounding cells 26 h after refeeding N-starved cultures with nitrate. Typical EDX point spectra of guanine crystals (*G*) indicating high N content were obtained in the STEM mode from semithin cell sections. Arrows point to guanine crystals. (Scale bars, 2.5 [*C*], 1 [*D* and *E*], and 0.5 μm [*F*]. Ch, chloroplast; V, vacuole.)

survive in the N-poor waters of tropical seas or cope with pulses of excessive nutrients due to upwelling or rainfall (5, 34, 35).

We demonstrated in this study that the numerous crystalline inclusions of endosymbiotic *Symbiodiniaceae* consist of guanine and that the external guanine is rapidly assimilated into the symbionts (Fig. 7 and *SI Appendix*, section I.5.). According to Raman microscopy (*SI Appendix*, Fig. S14), *Symbiodiniaceae* cells in the tissue of the scleractinian coral *Euphyllia paraancora* (*SI Appendix*, sections I.5 and II.4.A) exhibited similar guanine pool dynamics (Fig. 7 *A*–*C*) as the free-living dinoflagellate *A. carterae* (Figs. 1–4). *Symbiodiniaceae* from corals grown under optimal conditions always contained large guanine reserves (Fig. 7*A*). After 4 mo of N starvation of corals, guanine reserves were found depleted (Fig. 7*B*), the polyps shrank and became partially bleached. Upon refeeding with ^{15}N-$NaNO_3$, the newly synthesized ^{15}N-guanine inclusions appeared within 24 h inside *Symbiodiniaceae* cells (Fig. 7*C* and *SI Appendix*, Fig. S14).

The dynamic uptake of guanine was further confirmed in the *Symbiodiniaceae*-hosting coral *Acropora millepora*, which is widespread on the GBR, Australia, by using a combination of confocal fluorescence and reflection imaging (Fig. 7 *D*–*F* and *SI Appendix*, sections I.6 and II.1.C). *A. millepora* that was freshly collected from the GBR (Marine Parks Authority Permit G17/39943.1 to A.Sa., method in *SI Appendix*, section II.4.B) contained varying quantities of guanine crystals scattered peripherally among chloroplast lobes (Fig. 7*D* and *SI Appendix*, Fig. S15). Prolonged N starvation resulted in complete depletion of the guanine reserves (Fig. 7*E*). When the N-starved *Symbiodiniaceae* cells isolated from *A. millepora* were fed by a small amount of guanine powder added directly to the medium, the highly reflective guanine particles that were first visualized outside *Symbiodiniaceae* cells, began to accumulate inside cells after ∼1 h (Fig. 7*F*). A similar direct uptake of guanine was observed in *Symbiodiniaceae* extracted from the zoanthid *Zoanthus* sp. (*SI Appendix*, Fig. S16, *Bottom*) and in free-living *A. carterae* (in *SI Appendix*, Fig. S16, *Top* and Movie S1).

The same dynamics of appearance and disappearance of guanine inclusions were observed for *Symbiodiniaceae* of four other cnidarian species—the anemone *Aiptasia* sp., corallimorpharian, *Rhodactis indosinensis*, leather soft coral, *Sinularia asterolobata*, and *Zoanthus* sp., cultivated in an experimental aquarium (method in *SI Appendix*, section II.4.A). This is an in situ identification of the crystalline guanine within the intact symbiotic zooxanthellae from multiple anthozoan species.

Discussion

Guanine ($C_5H_5N_5O$) holds 1.9-fold higher amounts of N per unit molecular weight than a monomer of N-storing cyanophycin ($C_{10}H_{19}N_5O_5$), known to be the long-term N reserve in cyanobacteria. The ratio is even higher when the hydration of cyanophycin is considered. As it is uncharged and almost insoluble at physiological pH, crystalline guanine is less metabolically active than various ionic N-containing compounds, enabling its accumulation in large quantities and its long-term storage inside cells without the risk of metabolic disorder. In comparison with other purines, guanine is one order of magnitude less soluble than uric acid or xanthine and two orders of magnitude less soluble than adenine or hypoxanthine. It is also more chemically stable than uric acid (1). Yet guanine can be easily mobilized from the solid state by changing pH of its aqueous environment. Although almost insoluble at neutral pH, its solubility in water increases greatly at acidic or basic pH (31). Algal metabolic activity is highly pH dependent: photosynthesis increases the pH during the day, respiration decreases it at night, and a variety of cellular pH controls alter it in response to environment and stress (36). Thus, it is possible that guanine's solubility is under cellular pH control, facilitating its transport and assimilation. In coral-algal symbiosis, pH influences the flow of N between the host and its symbionts (35) and guanine's pH solubility dependence may make it a perfect metabolic N-storage molecule. Importantly, our finding that the size of the guanine reserve in planktonic microalgae can be much higher than the N amount required for cell reproduction indicates that it is a major N pool of global importance, being proportional to the phytoplankton biomass and matching its contributions to global carbon and N cycles (2, 37).

Biogenic guanine forms a highly compact crystal structure, namely, the β-form of the anhydrous monoclinic polymorph, consisting of vertically stacked planes of hydrogen-bonded molecules (12, 38). This crystal structure explains its unique optical properties, including birefringence and an extremely high index of refraction, leading to high light scattering as recorded in our confocal reflective imaging analysis. Consequently, guanine's storage function does not exclude other possible functions, e.g., light scattering in microalgae to enhance the efficiency of photosynthesis, photoprotection from UV radiation, or the formation of photonic mirrors (12, 38).

Table 1. Microcrystalline purines identified by Raman microscopy in various algal strains

Species	Habitat	Phylogeny	Purine
Symbiodiniaceae	E-S	Alveolata–Dinoflagellata	Guanine
Amphidinium carterae	S	Alveolata–Dinoflagellata	Guanine
Chromera velia	S	Alveolata–Chromerida	Guanine
Microchloropsis gaditana	S	Stramenopiles–Eustigmatophyceae	Guanine
Vacuoliviridecrystalliferum	U	Stramenopiles–Eustigmatophyceae	Guanine
Vischeria sp.	T	Stramenopiles–Eustigmatophyceae	Guanine
Trachydiscus minutus	F	Stramenopiles–Eustigmatophyceae	Guanine
Synura petersenii	F	Stramenopiles–Chrysophyceae	Guanine
Lobosphaera incisa	F, T	Archaeplastida–Chlorophyta–Trebouxiophyceae	Guanine
Desmodesmus quadricauda	F	Archaeplastida–Chlorophyta–Chlorophyceae	Guanine
Chlamydomonas reinhardtii	F	Archaeplastida–Chlorophyta–Chlorophyceae	Guanine
Dunaliella acidophila	Acid	Archaeplastida–Chlorophyta–Chlorophyceae	Guanine
Haematococcus pluvialis	F	Archaeplastida–Chlorophyta–Chlorophyceae	Guanine
Klebsormidium flaccidum	T	Archaeplastida–Streptophyta–Klebsormidiophyceae	Uric acid

The screened species represent diverse habitats: Acid, acidophilic; E, endosymbiotic; F, freshwater; S, marine; T, terrestrial/aerophytic; U, unspecified. The origins of the examined species as well as cultivation approach are described in *SI Appendix*, sections I.4 and II.3.

N is limiting to phytoplankton primary productivity in many marine ecosystems and is often associated with sporadic or seasonal reintroduction from deeper waters by mixing via upwelling or storms, from organic matter remineralization and from land-based sources (1–3). N stimulates phytoplankton growth, and the connection of N metabolism to photosynthesis has long been recognized (1, 6). The ability to assimilate N from nitrate, ammonium, urea, or guanine dissolved in seawater, or, alternatively, from particulate N sources, and to rapidly sequester N as crystalline guanine for redeployment under conditions of N limitation has emerged as an important survival strategy of free-living phytoplankton algae. N storage is also a critical component of cnidarian-dinoflagellate symbiosis. Natural or anthropogenic N eutrophication is known to disrupt the N-limited state of coral symbionts, disturbing the host's control over them thereby exacerbating the damage following mass coral bleaching (5, 19). By locking excessive N in insoluble crystals and mobilizing them when required, symbiotic microalgae may effectively mitigate the negative effect of N excesses or deprivations and maintain stable nutrient stoichiometry (C:N and N:P ratios). Given the major nutritional role of the symbionts to corals and many other reef animals and the dependence of the reef ecosystem's health on efficient nutrient uptake and storage, our research addressed a critical knowledge gap regarding the mechanisms by which corals acquire and store inorganic nutrients. Such knowledge is increasingly important under escalating eutrophication and climate-induced warming of marine and freshwater ecosystems.

N storage and other diverse vital biological and biochemical functions underscore the versatility of crystalline guanine concerning symbiosis and phytoplankton dynamics. Its shared occurrence among microalgal species over the phylogenetic tree suggests the involvement of guanine in these roles early in evolution, a hypothesis consistent with the potential role of this purine close to the origins of life and its presumably prebiotic occurrence on early Earth (39). Analogous to polyphosphate, which was regarded as a molecular fossil (40) and was, subsequently, revealed to have a multitude of functions (41), the crystalline guanine can also be considered as an evolutionary old, overlooked, and forgotten multifunctional tool of nature popping up from oblivion.

Materials and Methods

Chemicals and Media. References for chemicals and protocols used for preparing cultivation media and stable isotope labeling are listed or described in detail in *SI Appendix*, section II.

Algal Strains, Corals, and Cultivation Protocols. The origins and cultivation conditions for the microalgal species in Table 1 are listed in *SI Appendix*, sections I.4. and II.3. Cnidarian species anemone, *Aiptasia* sp., corallimorpharian, *R. indosinensis*, scleractinian coral, *E. paraancora*, leather coral, *S. asterolobata*, and anthozoan *Zoanthus* sp., were purchased from a local marine aquarium shop. *A. millepora* was collected from the GBR, Australia, and studied immediately after collection or as explants cultivated in experimental aquaria. Details of the laboratory cultivation and methods to study the kinetics of guanine assimilation and turnover are provided in *SI Appendix*, sections I, II.1.A, II.3, and II.4.

Confocal Raman Microscopy. The samples for Raman measurements were prepared and treated according to the methodology described in detail elsewhere (23, 42, 43) and summarized in *SI Appendix*, section II.1.C. The inverted Raman microscope LabRam Evolution (Horiba Scientific, Longjumeau, France) and upright Raman microscope WITec alpha 300 RSA (WITec, Ulm, Germany) were used with laser excitation at 532 nm in the study. To remove interference by autofluorescence of chlorophyll, wide-area low-power photobleaching of entire cells using a defocused 532-nm laser beam was employed before mapping. No differences that would affect data interpretation were observed between measurements on the Horiba and WITec systems.

Confocal Reflection Microscopy. *Symbiodiniaceae* cells of *A. carterae* and *Zoanthus* sp. confirmed by Raman microscopy to include guanine crystals were concurrently imaged using a confocal fluorescence microscope Leica TCS SP8 (Leica Microsystems, Germany) in the reflection mode using laser excitation at 488 nm. The guanine inclusions were seen in the reflection as crystal-like highly light-scattering objects. Further details are provided in *SI Appendix*, sections I.6, II.1.C, and II.4.

Analytical Electron Microscopy. The protocol of specimen preparation for TEM is described in *SI Appendix*, section II.1.E. Ultrathin sections were cut with a LKB-8800 (LKB, Sweden) ultratome, stained with lead citrate according to the method described by Reynolds (44) and examined under a JEM-1011 (JEOL, Tokyo, Japan) electron microscope. Samples for nanoscale elemental analysis using analytical TEM with EDX were fixed, dehydrated, and embedded as above, except that sections were stained with uranyl acetate and lead citrate. Semithin sections were examined under a JEM-2100 (JEOL, Japan) electron microscope. Point EDX spectra were recorded using a JEOL bright-field STEM module and an X-Max X-ray detector system (Oxford Instruments, United Kingdom). Further details are provided in *SI Appendix*, sections II.1.E and II.1.F.

Data Availability. All study data are included in the article and supporting information.

ACKNOWLEDGMENTS. This study received financial support from the Czech Science Foundation (Grant 17-06264S), Russian Science Foundation

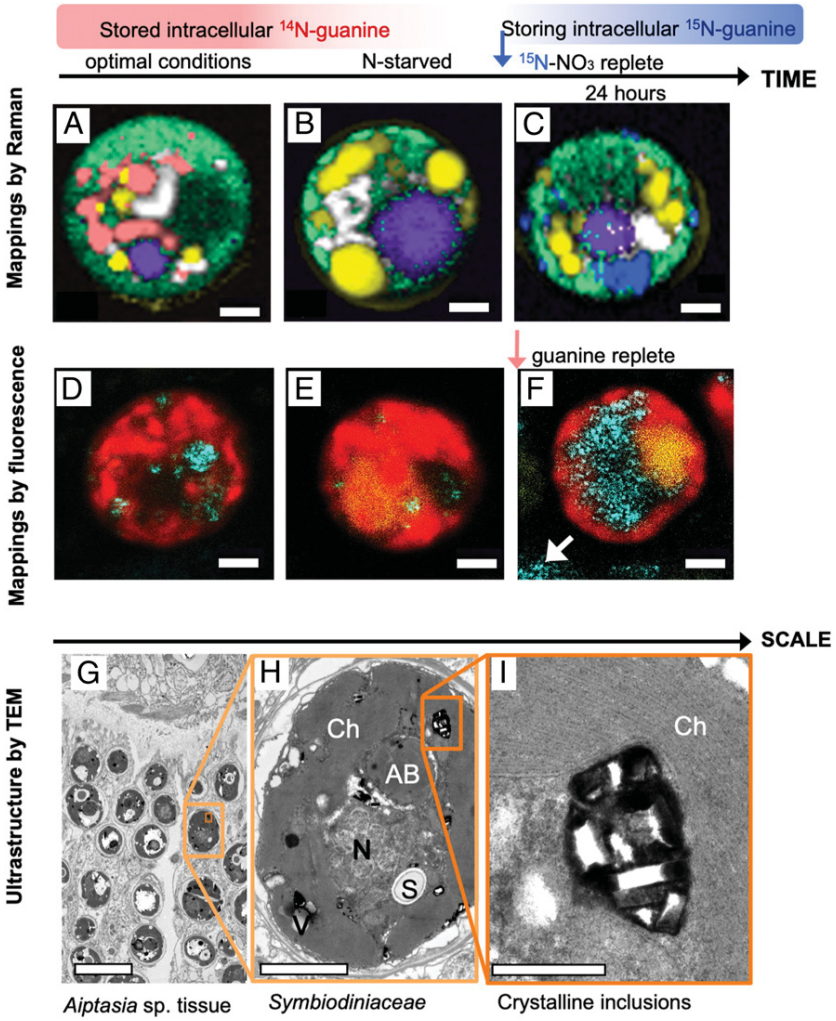

Fig. 7. Guanine in the endosymbiotic *Symbiodiniaceae* cells in corals. Raman maps of cells from tissue of the coral *E. paraancora* (*A*–*C*). The spectra used to construct these maps are shown in *SI Appendix*, Fig. S13. Symbionts in corals maintained under optimal nutrient conditions contained guanine crystals (*A*). Cells from corals that were kept in N-depleted seawater for 4 mo contained very few guanine crystals (*B*). Twenty-four hours after feeding the starved coral 0.3-mM ^{15}N-$NaNO_3$, cells showed large ^{15}N-guanine depots (*C*). The false color coding is the same as that in Figs. 1 and 4 with magenta added to represent accumulation bodies. (Scale bar, 2 μm.) *Symbiodiniaceae* cells isolated from the Great Barrier Reef (GBR) coral, *A. millepora* (*D*–*F*). Cell from freshly collected coral (*D*), N-depleted coral (*E*), and from one day after feeding with medium containing traces of undissolved guanine grains (*F*). Cyan, 488-nm laser reflection of guanine grains outside (white arrow) and inside the cells; red, chlorophyll autofluorescence at 670–700 nm; yellow, fluorescence in accumulation bodies at 500–560 nm; white arrow, remains of undissolved crystalline guanine in medium. (Scale bar, 2 μm.) Ultrastructure of *Symbiodiniaceae* cells in *Aiptasia sp.* shown at increasing magnification (*G*–*I*). AB, accumulation body; Ch, chloroplast; N, nucleus; S, floridean starch; V, vacuole. (Scale bars, 10 [*G*], 2 [*H*], and 0.5 μm [*I*].)

(Grant 20-64-46018), Grant Agency of Charles University (Grant 796217), and the project Algnutrient-UrBioSol (Grant FKZ 031B0453A) of the Federal Ministry of Education and Research, Germany. Electron microscopy was supported by the User Facilities Center of M. V. Lomonosov Moscow State University. Confocal imaging was supported by Western Sydney University.

1. N. J. Antia, P. J. Harrison, L. Oliveira, The role of dissolved organic nitrogen in phytoplankton nutrition, cell biology and ecology. *Phycologia* **30**, 1–89 (1991).
2. P. G. Falkowski, Evolution of the nitrogen cycle and its influence on the biological sequestration of CO_2 in the ocean. *Nature* **387**, 272–275 (1997).
3. P. G. Falkowski, R. T. Barber, V. Smetacek, Biogeochemical controls and feedbacks on ocean primary production. *Science* **281**, 200–207 (1998).
4. D. M. Anderson, P. M. Glibert, J. M. Burkholder, Harmful algal blooms and eutrophication: Nutrient sources, composition, and consequences. *Estuaries* **25**, 704–726 (2002).
5. N. Rädecker, C. Pogoreutz, C. R. Voolstra, J. Wiedenmann, C. Wild, Nitrogen cycling in corals: The key to understanding holobiont functioning? *Trends Microbiol.* **23**, 490–497 (2015).
6. T. Tyrrell, The relative influences of nitrogen and phosphorus on oceanic primary production. *Nature* **400**, 525–531 (1999).
7. S. Schmollinger *et al.*, Nitrogen-sparing mechanisms in *Chlamydomonas* affect the transcriptome, the proteome, and photosynthetic metabolism. *Plant Cell* **26**, 1410–1435 (2014).
8. K. Forchhammer, R. Schwarz, Nitrogen chlorosis in unicellular cyanobacteria–A developmental program for surviving nitrogen deprivation. *Environ. Microbiol.* **21**, 1173–1184 (2019).
9. B. Watzer, K. Forchhammer, Cyanophycin synthesis optimizes nitrogen utilization in the unicellular cyanobacterium *Synechocystis* sp strain PCC 6803. *Appl. Environ. Microbiol.* **84**, e01298-18 (2018).
10. O. Baulina *et al.*, Diversity of the nitrogen starvation responses in subarctic *Desmodesmus* sp. (Chlorophyceae) strains isolated from symbioses with invertebrates. *FEMS Microbiol. Ecol.* **92**, fiw031 (2016).
11. J. Lewis, P. Burton, A study of newly excysted cells of *Gonyaulax polyedra* (Dinophyceae) by electron microscopy. *Br. Phycol. J.* **23**, 49–60 (1988).
12. A. Jantschke *et al.*, Anhydrous β-guanine crystals in a marine dinoflagellate: Structure and suggested function. *J. Struct. Biol.* **207**, 12–20 (2019).
13. R. DeSa, J. W. Hastings, The characterization of scintillons. Bioluminescent particles from the marine dinoflagellate, *Gonyaulax polyedra*. *J. Gen. Physiol.* **51**, 105–122 (1968).

14. K. B. Strychar, P. W. Sammarco, T. J. Piva, Apoptotic and necrotic stages of *Symbiodinium* (Dinophyceae) cell death activity: Bleaching of soft and scleractinian corals. *Phycologia* **43**, 768–777 (2004).
15. D. L. Taylor, *In situ* studies on cytochemistry and ultrastructure of a symbiotic marine dinoflagellate. *J. Mar. Biol. Assoc. U. K.* **48**, 349–366 (1968).
16. M. J. Kevin, W. T. Hall, J. J. McLaughlin, P. A. Zahl, *Symbiodinium microadriaticum* Freudenthal, a revised taxonomic description, ultrastructure. *J. Phycol.* **5**, 341–350 (1969).
17. P. L. Clode, M. Saunders, G. Maker, M. Ludwig, C. A. Atkins, Uric acid deposits in symbiotic marine algae. *Plant Cell Environ.* **32**, 170–177 (2009).
18. T. Krueger *et al*., Temperature and feeding induce tissue level changes in autotrophic and heterotrophic nutrient allocation in the coral symbiosis–A NanoSIMS study. *Sci. Rep.* **8**, 12710 (2018).
19. S. Rosset, J. Wiedenmann, A. J. Reed, C. D'Angelo, Phosphate deficiency promotes coral bleaching and is reflected by the ultrastructure of symbiotic dinoflagellates. *Mar. Pollut. Bull.* **118**, 180–187 (2017).
20. H. Yamashita, A. Kobiyama, K. Koike, Do uric acid deposits in *zooxanthellae* function as eye-spots? *PLoS One* **4**, e6303 (2009).
21. C. Kopp *et al*., Highly dynamic cellular-level response of symbiotic coral to a sudden increase in environmental nitrogen. *MBio* **4**, e00052–e13 (2013).
22. A. Jantschke, I. Pinkas, A. Schertel, L. Addadi, S. Weiner, Biomineralization pathways in calcifying dinoflagellates: Uptake, storage in MgCaP-rich bodies and formation of the shell. *Acta Biomater.* **102**, 427–439 (2020).
23. Š. Moudříková, L. Nedbal, A. Solovchenko, P. Mojzeš, Raman microscopy shows that nitrogen-rich cellular inclusions in microalgae are microcrystalline guanine. *Algal Res.* **23**, 216–222 (2017).
24. D. Gur, B. A. Palmer, S. Weiner, L. Addadi, Light manipulation by guanine crystals in organisms: Biogenic scatterers, mirrors, multilayer reflectors and photonic crystals. *Adv. Funct. Mater.* **27**, 1603514 (2017).
25. S. Menden-Deuer, E. J. Lessard, Carbon to volume relationships for dinoflagellates, diatoms, and other protist plankton. *Limnol. Oceanogr.* **45**, 569–579 (2000).
26. A. Shebanova *et al*., Versatility of the green microalga cell vacuole function as revealed by analytical transmission electron microscopy. *Protoplasma* **254**, 1323–1340 (2017).
27. T. Ismagulova, A. Shebanova, O. Gorelova, O. Baulina, A. Solovchenko, A new simple method for quantification and locating P and N reserves in microalgal cells based on energy-filtered transmission electron microscopy (EFTEM) elemental maps. *PLoS One* **13**, e0208830 (2018).
28. R. E. Schmitter, The fine structure of *Gonyaulax polyedra*, a bioluminescent marine dinoflagellate. *J. Cell Sci.* **9**, 147–173 (1971).
29. J. D. Dodge, Ultrastructure of dinoflagellate pusule - unique osmo-regulatory organelle. *Protoplasma* **75**, 285–302 (1972).
30. R. Onuma, T. Horiguchi, Morphological transition in kleptochloroplasts after ingestion in the dinoflagellates *Amphidinium poecilochroum* and *Gymnodinium aeruginosum* (Dinophyceae). *Protist* **164**, 622–642 (2013).
31. D. Gur *et al*., Guanine crystallization in aqueous solutions enables control over crystal size and polymorphism. *Cryst. Growth Des.* **16**, 4975–4980 (2016).
32. H. J. Jeong *et al*., Heterotrophic feeding as a newly identified survival strategy of the dinoflagellate *Symbiodinium*. *Proc. Natl. Acad. Sci. U.S.A.* **109**, 12604–12609 (2012).
33. J. M. Delabar, M. Majoube, Infrared and Raman-spectroscopic study of N-15 and D-substituted guanines. *Spectrochim. Acta A* **34**, 129–140 (1978).
34. L. Muscatine, J. W. Porter, Reef corals: Mutualistic symbioses adapted to nutrient-poor environments. *BioSci.* **27**, 454–460 (1977).
35. D. Yellowlees, T. A. V. Rees, W. Leggat, Metabolic interactions between algal symbionts and invertebrate hosts. *Plant Cell Environ.* **31**, 679–694 (2008).
36. K. L. Barott, A. A. Venn, S. O. Perez, S. Tambutté, M. Tresguerres, Coral host cells acidify symbiotic algal microenvironment to promote photosynthesis. *Proc. Natl. Acad. Sci. U.S.A.* **112**, 607–612 (2015).
37. P. G. Falkowski, The role of phytoplankton photosynthesis in global biogeochemical cycles. *Photosynth. Res.* **39**, 235–258 (1994).
38. A. Hirsch *et al*., "Guanigma": The revised structure of biogenic anhydrous guanine. *Chem. Mater.* **27**, 8289–8297 (2015).
39. N. Kitadai, S. Maruyama, Origins of building blocks of life: A review. *Geoscience Frontiers* **9**, 1117–1153 (2018).
40. A. Kornberg, N. N. Rao, D. Ault-Riché, Inorganic polyphosphate: A molecule of many functions. *Annu. Rev. Biochem.* **68**, 89–125 (1999).
41. L. Xie, U. Jakob, Inorganic polyphosphate, a multifunctional polyanionic protein scaffold. *J. Biol. Chem.* **294**, 2180–2190 (2019).
42. Š. Moudříková *et al*., Raman and fluorescence microscopy sensing energy-transducing and energy-storing structures in microalgae. *Algal Res.* **16**, 224–232 (2016).
43. Š. Moudříková *et al*., Quantification of polyphosphate in microalgae by Raman microscopy and by a reference enzymatic assay. *Anal. Chem.* **89**, 12006–12013 (2017).
44. E. S. Reynolds, The use of lead citrate at high pH as an electron-opaque stain in electron microscopy. *J. Cell Biol.* **17**, 208–212 (1963).

Chapter IV. General Discussion and Conclusion

IV. A. Overall Conclusion and Perspective

The main objective of this thesis was to investigate algal photobleaching, dynamic phosphorus (P) and nitrogen (N) storage pools in algae using Raman microscopy. This work accomplished by the following:

- Algal photosynthesis and reactive oxygen species facilate algal photobleaching with Raman microscopy. In comparsion with glutaraldehyde, formalin is recommended to fix algal cells for desampling and using Raman microscopic analysis.

- Raman microscopy enables to monitor the dynamic changes of polyphosphate (polyP) as the main P storage pool in algae to harvest the P-rich algal biomass. These P-rich algal biomass is efficient as a slow-release biofertilizer for crops.

- The common presence, the rapid uptake, and the role as a dynamic N storage pool were discoveryed for guanine crystals in algae.

The use of Raman microscopy led to concerns of algal photobleaching and subsequent discussion about its mechanisms and the possible improvements (Section IV.B.1.). Moreover, the aspects on the P-rich biomass be produced as a slow-release biofertilizer are discussed (Section IV.C.1.). The work also opens up major questions in the fields of algal N storge pools to reveal the unique nature of guanine crystals (Section IV.D.2.) as this study is the first known attempt to understand the function of guanine crystal in algae.

Since the mechanisms of algal photobleaching are not clear yet, practical improvement of photobleaching remains an open area of scientific inquiry. Further work will also investigate the mechanisms of how algae accumulate and consume guanine crystals as well as examine the functions of guanine crystals in microalgae and its environment. In addition, potential relationships among polyphosphate, guanine crystals and carbon reserves in algae should be investigated. In the long-term, closing the nutrient loop is a key focus for recycling and sustainable nutrient development. Two main perspectives for furthering nutrient

sustainability should be studied in the future: (*1*) how to apply algal biomass as a biofertilizer to reduce nutrient loss from excessive agricultural applications, and (*2*) how to improve algal biotechnologies to increase nutrient recovery from nutrient-rich waste streams.

IV. B. Algae with Raman Microscopy

IV. A. 1. Raman Microscopy

Raman microscopy is developed for identifying chemical species within a specific location [146]. In this work, Raman microscopy is used as a powerful tool for investigating algae applications. In future studies, Raman microscopy can be used to monitor algal cultivation online, including investigating the culture *in vivo* and analyzing algal cell metabolism in real time. Combining Raman spectroscopy with other techniques, such as fluorometry, stable isotopic labelling [494], or microfluidics [27], can facilitate the assessment of algal cells with high spatial resolution and accuracy. Characterization with Raman spectroscopy is likely to be extended from examining algae and plant cell walls to include other targets, such as shoot, root, fungus, or mycorrhiza. [4]

IV. A. 2. Algal Photobleaching with Raman Microscopy

Photobleaching as a pretreatment significantly reduces autofluorescence of chlorophylls in algae. Photobleaching also can destroy algal carotenoids when the excitation wavelengths are between visible and near infrared. In this work, the investigation of algal photobleaching revealed how the photobleaching kinetics change, while reactive oxygen species in algae are either suppressed or stimulated, or photosynthetic reactions are inhibited. A double exponential function simulates the kinetics of algal photobleaching well. Unlike sampling with glutaraldehyde, sampling with formalin fixation ensures effective photobleaching and Raman measurements for microalgae.

[4] Barley leaf by portable Raman and leek mycorrhiza by Raman microscopy were measured. These tangents were not followed up due to time constraints.

A concern of photobleaching is if samples are damaged [495, 496]. However, no evidence suggests it yet [497, 498]. Photodecomposition usually is caused by inherent properties of samples [499]. Bovine bone, for example, is unharmed by a 40-minute period of photobleaching (by in-focus illumination) with a 532nm laser [500]. Similarly, carotenes in human skin are also unchanged by photobleaching with a 488-nm laser [501]. However, carotenoids in algae are considerably reduced by photobleaching. This difference shows that photosynthesis significantly affects algal photobleaching. In general, an experimental confirmation may be needed based on the specific measured samples.

Multiple mechanisms likely contribute to photobleaching, which may involve both photosynthetic and non-photosynthetic pathways. The triplet-states [498, 502, 503] and modifications of covalent and double- or multi-photon excitations [500, 504, 505] as potential mechanisms have not been studied yet. Photobleaching in algae might be caused by singlet oxygen, which can be produced by the interaction of molecular oxygen with triplet chlorophyll states. These triplet states can be effectively quenched by carotenoids and generated by the intersystem crossing from singlet excitons in photosystem II antennae or by charge recombination in the photosystem II reaction center [506]. This currently experimentally unconfirmed mechanism may explain why algal carotenoids can be reduced by a near-infrared excitation laser of 785 nm.

Usually, effective photobleaching is independent of excitation wavelengths. Longer excitation wavelengths and lower temperatures might reduce the effectiveness of photobleaching. In future study, it opens up the opportunity to replace the common green excitation laser with a shorter wavelength blue laser. This could be used to conduct photobleaching for autofluorescence-resistant samples, such as photosynthetically impaired algae or higher plants. The efficiency of photobleaching is also severely affected by the reservoir sizes of autofluorescence sources and sample environments. Based on this work, hydrogen peroxide can be useful for inducing photobleaching to one or few gathering cells each time. A feasible approach for using non-image portable Raman devices should remove massive amont of chlorophylls in algal biomass. However, in a preliminary experiment for characterizing mass algal culture by such a portable Raman device, neither adding hydrogen peroxide nor UV-illumination could reliably replace photobleaching.

IV. B. 1. Polyphosphate in Algae

In typical algae cells, P constitutes 0.5 to 7% of their dry weight. The transient accumulation during the lag and early exponential phases for large amounts of polyP reserves represents an opportunity to produce algal biomass as slow-release biofertilizers. A core question that remains to be resolved in the future is how algae can effectively contribute to closing the nutrient loops. For example, it will be important to investigate how polyP storage pools in algal biofertilizers affect both microbial interactions and the release of plant-available P in soil. The capacity of algae for removing toxic metals and other materials to clean waste streams is another perspective for the future. However, one should be worried to extrapolate from the experimental results onto natural conditions. Algae can easily adapt to controlled laboratory conditions [507, 508]. In addition to microalgae, bacteria and fungi also can accumulate polyP, these are known as polyP-accumulating organisms [509-512]. As consortia, they may utilize nutrients more effectively under natural conditions than they do under laboratory conditions. Low-cost, algae-based technologies like algae turf scrubbers shoud therefore be examined for their potential to grow such P-rich mixed biomass for production of biofertilizers. Examining multiple stress factors may help to select strains suitable for treatment of wastewater with specific features, such as low nutrient concentrations, high or low pH, high iron concentrations, etc.

IV. B. 2. Guanine Crystals in Algae

Guanine is common in nature, as demonstrated in Figure IV-1. It is known that bacteria take up purine as an alternative N source [508, 513]. Evidence suggests that even higher organism, like barnacles might take up guanine as an original dietary resource [302]. In this work, the feasibility of algae using natural guanine resources was verified by feeding ground up fish scales to N-starved *A. carterae* [303]. Guanine may be released through excretion, or death and decompositions of guanine-rich organisms [514]. Fish scales and the skin of

fish [515] and amphibians [516], for example, leach out guanine (and hypoxanthine) during degradation. Also, guanine can be released during DNA hydrolysis from marine bacteria [517].

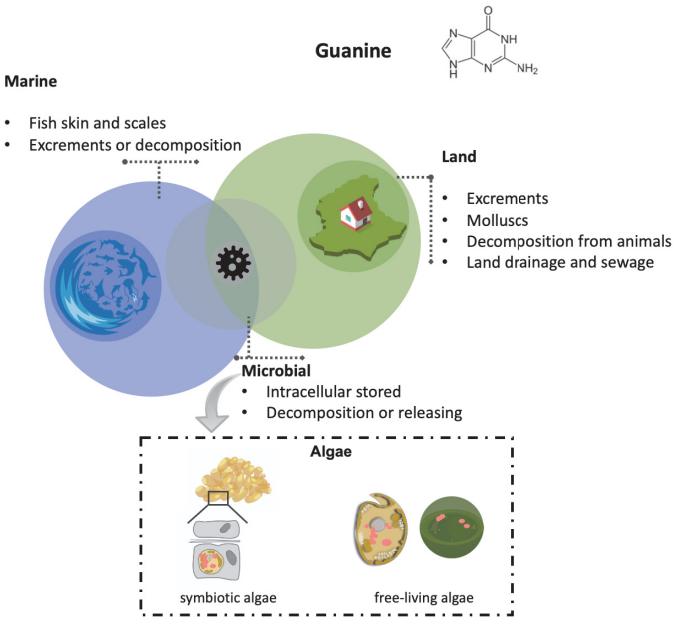

Figure IV-1 The common presence of guanine.

Following the common patterns of evolution, algae should require less effort to repurpose guanine for other tasks than to use a separate molecule. The physicochemical properties of guanine make it uniquely suited for algae compared to other purines for several reasons, as listed in Table IV-1. Guanine has 5 N atoms, instead of 4 N atoms among purines, besides adenine and isoguanine [518]. Guanine is insoluble at neutral pH and stable [441]. Compared to guanine [519], adenine is soluble in water but less stable than guanine [520]. Uric acid is less soluble than guanine but it is not stable [441]. Thus, a crystalline form of guanine can ensure that N is stored in a safe, compact, easily mobilized [521], and effective manner in algae.

In addition to providing N storage pools in algae, the specific plate-like crystal features of guanine also benefit algae for other proposes. Biogenic guanine crystals have also been observed in the animal kingdom [471]. Guanine crystals have unique optical properties,

including a remarkeably high index of refraction (n = 1.85) and birefringence [5], which induces high light scattering. Due to inconsistencies of the crystalline guanine structures, *A. carterae* and other microalgae might be able to control the crystal morphology of guanine to optimize their reflectivity [295, 303]. Thus, guanine crystals may modulate photon flux density in algae and other cells in their vicinity to enhance the efficiency of algal photosynthesis and protect them against UV radiation [295, 303, 522]. These optical functions may be particularly important in environments with a high degree of light fluctuation, such as corals in (sub)tropical oceans, in which corals depend on their symbiotic algae.

Table IV-1 Summary of purine properties

Purine	# N	Solubility (per 100 mL)	Stability	Reference
Guanine	5	0.45 mg at 20 °C	stable in darkness; in sterile seawater with continuous low white-light photon	[441, 451, 519]
Adenine	5	103 mg at 20 °C	stable in darkness; less stable than guanine	[520, 523]
Hypoxanthine	4	70 mg at 23 °C	stable in darkness	[441, 469, 523]
Xanthine	4	6.90 mg at 16 °C	stable in darkness but significant decomposition in light	[441, 523]
Uric acid	4	6 mg at 20 °C	unstable over time, largely due to the trace-metal ions in seawater, light facilitates degradation	[441, 463, 469]

[5] Refractive index that depends on a changes with the polarization and propagation direction of light.

Coral reefs owe their success to the symbiosis with the family *Symbiodiniaceae*, commonly known as zooxanthellae. When corals are stressed, the symbiosis can break-down, leading to the loss of microalgae, known as coral bleaching [524]. Severe cases of coral bleaching can be fatal to the coral host [525]. In recent years, anthropogenic ocean warming has caused global mass coral bleaching events that are increasing in frequency and extent, threatening the survival of coral reefs worldwide [526]. Anthropogenic eutrophication has been linked to a reduction of the temperature threshold of coral bleaching due to intracellular nutrient imbalances in the algal symbiont [527], especially in the ratios of N to P [527, 528]. Consequently, it is crucial to gain an improved understanding of the underlying cellular and physiological processes of algal symbiont nutrient metabolism for elucidating the resilience and adaptability of coral reefs to climate change. Having microstructural biomarkers of algal symbiont nutrient health will aid in reef management of nutrients and predictions of reef resilience to climate change.

Chapter V. Bibliography

1. Penuelas, J., et al., *Human-induced nitrogen-phosphorus imbalances alter natural and managed ecosystems across the globe.* Nature Communications, 2013. **4**(1): p. 2934.

2. Simpson, R.J., et al., *Strategies and agronomic interventions to improve the phosphorus-use efficiency of farming systems.* Plant and Soil, 2011. **349**(1-2): p. 89-120.

3. Sharma, L.K. and S.K. Bali, *A review of methods to improve nitrogen use efficiency in agriculture.* Sustainability, 2017. **10**(1): p. 1-23.

4. Smith, V.H., *Cultural eutrophication of inland, estuarine, and coastal waters*, in *Successes, Limitations, and Frontiers in Ecosystem Science*. 1998, Springer. p. 7-49.

5. Anderson, D.M., *Red tides.* Scientific American, 1994. **271**(2): p. 62-8.

6. Anderson, D.M., *The ecology and oceanography of harmful algal blooms: multidisciplinary approaches to research and management*. UNESCO IOC Technical Series. 2007: UNESCO IOC Technical Series.

7. Grossman, A.R. and M. Aksoy, *Algae in a phosphorus-limited landscape.* Annual Plant Reviews, 2018: p. 337-374.

8. Sanz-Luque, E., D. Bhaya, and A.R. Grossman, *Polyphosphate: a multifunctional metabolite in cyanobacteria and algae.* Frontiers in Plant Science, 2020. **11**: p. 938.

9. Solovchenko, A., et al., *Phosphorus from wastewater to crops: An alternative path involving microalgae.* Biotechnol Adv, 2016. **34**(5): p. 550-564.

10. Kulakovskaya, T.V., V.M. Vagabov, and I.S. Kulaev, *Inorganic polyphosphate in industry, agriculture and medicine: Modern state and outlook.* Process Biochemistry, 2012. **47**(1): p. 1-10.

11. Mukherjee, C., R. Chowdhury, and K. Ray, *Phosphorus recycling from an unexplored source by polyphosphate accumulating microalgae and cyanobacteria-A step to phosphorus security in agriculture.* Frontiers in Microbiology, 2015. **6**: p. 1421.

12. Schreiber, C., et al., *Evaluating potential of green alga Chlorella vulgaris to accumulate phosphorus and to fertilize nutrient-poor soil substrates for crop plants.* Journal of Applied Phycology, 2018. **30**(5): p. 2827-2836.

13. Moudrikova, S., et al., *Comparing biochemical and Raman microscopy analyses of starch, lipids, polyphosphate, and guanine pools during the cell cycle of Desmodesmus quadricauda.* Cells, 2021. **10**(1): p. 62.

14. Moudříková, Š., *Raman microspectroscopy of living cells and biological tissues*, in *Institute of Physics of Charles University*. 2019, Charles University: Univerzita Karlova, Matematicko-fyzikální fakulta.

15. Moudříková, Š., et al., *Raman microscopy shows that nitrogen-rich cellular inclusions in microalgae are microcrystalline guanine.* Algal Research, 2017. **23**: p. 216-222.

16. Moudříková, Š., et al., *Quantification of polyphosphate in microalgae by Raman microscopy and by a reference enzymatic assay.* Analytical Chemistry, 2017. **89**(22): p. 12006-12013.

17. Moudříková, Š., et al., *Raman and fluorescence microscopy sensing energy-transducing and energy-storing structures in microalgae.* Algal Research, 2016. **16**: p. 224-232.

18. Sliwinska-Wilczewska, S., et al., *Allelopathic and bloom-forming picocyanobacteria in a changing world.* Toxins (Basel), 2018. **10**(1).

19. Wang, D.Z., *Neurotoxins from marine dinoflagellates: a brief review.* Marine Drugs, 2008. **6**(2): p. 349-71.

20. Anderson, D.M., A.D. Cembella, and G.M. Hallegraeff, *Progress in understanding harmful algal blooms: paradigm shifts and new technologies for research, monitoring, and management.* Annual Review of Marine Science, 2012. **4**: p. 143-176.

21. Waterbury, J.B., et al., *Widespread occurrence of a unicellular, marine, planktonic, cyanobacterium.* Nature, 1979. **277**(5694): p. 293-294.

22. Weisse, T., *Dynamics of autotrophic picoplankton in marine and freshwater ecosystems.* Advances in Microbial Ecology, 1993. **13**: p. 327-370.

23. Havlik, I., T. Scheper, and K.F. Reardon, *Monitoring of microalgal processes.* Microalgae Biotechnology, 2015: p. 89-142.

24. Han, Y., et al., *Review of methods used for microalgal lipid-content analysis.* Energy Procedia, 2011. **12**: p. 944-950.

25. Lee, T.H., J.S. Chang, and H.Y. Wang, *Current developments in high-throughput analysis for microalgae cellular contents.* Biotechnology Journal, 2013. **8**(11): p. 1301-1314.

26. Liu, J.-Y., L.-H. Zeng, and Z.-H. Ren, *Recent application of spectroscopy for the detection of microalgae life information: A review.* Applied Spectroscopy Reviews, 2020. **55**(1): p. 26-59.

27. Kim, H.S., T.P. Devarenne, and A. Han, *Microfluidic systems for microalgal biotechnology: a review.* Algal Research, 2018. **30**: p. 149-161.

28. Haisch, C., *Raman-based microarray readout: a review.* Analytical and Bioanalytical Chemistry, 2016. **408**(17): p. 4535-45.

29. Committee, A.T.S., *Industrial algae measurements, Version 8.0* 2017.

30. Podevin, M., I.A. Fotidis, and I. Angelidaki, *Microalgal process-monitoring based on high-selectivity spectroscopy tools: status and future perspectives.* Crit Rev Biotechnol, 2018. **38**(5): p. 704-718.

31. Wagner, H., et al., *Surveillance of C-allocation in microalgal cells.* Metabolites, 2014. **4**(2): p. 453-64.

32. Porizka, P., et al., *Algal biomass analysis by laser-based analytical techniques--a review.* Sensors (Basel), 2014. **14**(9): p. 17725-52.

33. Wei, X., et al., *Microalgal detection by Raman microspectroscopy.* TrAC Trends in Analytical Chemistry, 2014. **53**: p. 33-40.

34. Parab, N. and V. Tomar, *Raman spectroscopy of algae: a review.* Journal of Nanomedicine and Nanotechnology, 2012. **3**(131137): p. 24.

35. Malley, D.F., et al., *Determination of carbon, carbonate, nitrogen, and phosphorus in freshwater sediments by near-infrared reflectance spectroscopy: Rapid analysis and a check on conventional analytical methods.* Journal of Paleolimnology, 2000. **24**(4): p. 415-425.

36. Roychoudhury, P., L.M. Harvey, and B. McNeil, *The potential of mid infrared spectroscopy (MIRS) for real time bioprocess monitoring.* Analytica Chimica Acta, 2006. **571**(2): p. 159-66.

37. Vogel, M., et al., *Biosorption of U(VI) by the green algae Chlorella vulgaris in dependence of pH value and cell activity.* Science of the Total Environment, 2010. **409**(2): p. 384-95.

38. Lopez, M.C., et al., *Comparative analysis of the outdoor culture of Haematococcus pluvialis in tubular and bubble column photobioreactors.* Journal of Biotechnology, 2006. **123**(3): p. 329-42.

39. Masojídek, J., et al., *A two-stage solar photobioreactor for cultivation of microalgae based on solar concentrators.* Journal of Applied Phycology, 2008. **21**(1): p. 55-63.

40. Kliphuis, A.M., et al., *Light respiration in Chlorella sorokiniana.* Journal of Applied Phycology, 2011. **23**(6): p. 935-947.

41. Bosma, R., et al., *Design and construction of the microalgal pilot facility AlgaePARC.* Algal Research, 2014. **6**: p. 160-169.

42. Obata, M., T. Toda, and S. Taguchi, *Using chlorophyll fluorescence to monitor yields of microalgal production.* Journal of Applied Phycology, 2008. **21**(3): p. 315-319.

43. Jimenez, C., *Relationship between physicochemical variables and productivity in open ponds for the production of Spirulina: a predictive model of algal yield.* Aquaculture, 2003. **221**(1-4): p. 331-345.

44. Kromkamp, J.C., et al., *Short-term variations in photosynthetic parameters of Nannochloropsis cultures grown in two types of outdoor mass cultivation systems.* Aquatic Microbial Ecology, 2009. **56**(2-3): p. 309-322.

45. Quinn, J.C., C.W. Turner, and T.H. Bradley, *Scale-Up of flat plate photobioreactors considering diffuse and direct light characteristics.* Biotechnol Bioeng, 2012. **109**(2): p. 363-70.

46. Posten, C., *Design principles of photo-bioreactors for cultivation of microalgae.* Engineering in Life Sciences, 2009. **9**(3): p. 165-177.

47. Sukenik, A., et al., *Photosynthetic performance of outdoor Nannochloropsis mass cultures under a wide range of environmental conditions.* Aquatic Microbial Ecology, 2009. **56**(2-3): p. 297-308.

48. Torzillo, G., et al., *Biological constraints in algal biotechnology.* Biotechnology And Bioprocess Engineering, 2003. **8**(6): p. 338-348.

49. Ugwu, C.U. and H. Aoyagi, *Influence of shading inclined tubular photobioreactor surfaces on biomass productivity of C. sorokiniana.* Photosynthetica, 2008. **46**(2): p. 283-285.

50. Orellana, G. and D. Haigh, *New trends in fiber-optic chemical and biological sensors.* Current Analytical Chemistry, 2008. **4**(4): p. 273-295.

51. Llovet, X., E. Valovirta, and E. Heikinheimo, *Monte Carlo simulation of secondary fluorescence in small particles and at phase boundaries.* Microchimica Acta, 2000. **132**(2-4): p. 205-212.

52. Malinowski, J. and E.J. Geiger, *Development of a wireless sensor network for algae cultivation using ISFET pH probes.* Algal Research, 2014. **4**: p. 19-22.

53. Barsanti, L. and P. Gualtieri, *Algae: anatomy, biochemistry, and biotechnology*. 2014: CRC press.

54. Suh, I.S. and C.-G. Lee, *Photobioreactor engineering: design and performance.* Biotechnology And Bioprocess Engineering, 2003. **8**(6): p. 313-321.

55. De Swaaf, M.E., L. Sijtsma, and J.T. Pronk, *High-cell-density fed-batch cultivation of the docosahexaenoic acid producing marine alga Crypthecodinium cohnii.* Biotechnol Bioeng, 2003. **81**(6): p. 666-72.

56. Nedbal, L., et al., *Experimental validation of a nonequilibrium model of CO(2) fluxes between gas, liquid medium, and algae in a flat-panel photobioreactor.* Journal of Industrial Microbiology & Biotechnology, 2010. **37**(12): p. 1319-26.

57. Červený, J., et al., *Photobioreactor for cultivation and real-time,in-situmeasurement of O2and CO2exchange rates, growth dynamics, and of chlorophyll fluorescence emission of photoautotrophic microorganisms.* Engineering in Life Sciences, 2009. **9**(3): p. 247-253.

58. Doucha, J. and K. Lívanský, *Productivity, CO 2/O 2 exchange and hydraulics in outdoor open high density microalgal (Chlorella sp.) photobioreactors operated in a Middle and Southern European climate.* Journal Of Applied Phycology, 2006. **18**(6): p. 811-826.

59. Tebbani, S., et al., *Nonlinear predictive control for maximization of CO(2) bio-fixation by microalgae in a photobioreactor.* Bioprocess and Biosystems Engineering, 2014. **37**(1): p. 83-97.

60. Janata, J. and J. Janata, *Introduction to Sensors*. Principles Of Chemical Sensors, Second Edition. 2009, New York: Springer. 1-11.

61. Borges, M.-T., et al., *Direct and continuous dissolved CO2 monitoring in shallow raceway systems: From laboratory to commercial-scale applications.* Aquacultural Engineering, 2012. **49**: p. 10-17.

62. Moran, D., B. Tirsgård, and J.F. Steffensen, *The accuracy and limitations of a new meter used to measure aqueous carbon dioxide.* Aquacultural Engineering, 2010. **43**(3): p. 101-107.

63. Doucha, J., F. Straka, and K. Lívanský, *Utilization of flue gas for cultivation of microalgae Chlorella sp.) in an outdoor open thin-layer photobioreactor.* Journal of Applied Phycology, 2005. **17**(5): p. 403-412.

64. Cuaresma, M., et al., *Horizontal or vertical photobioreactors? How to improve microalgae photosynthetic efficiency.* Bioresource Technology, 2011. **102**(8): p. 5129-37.

65. Melnicki, M.R., et al., *Feedback-controlled LED photobioreactor for photophysiological studies of cyanobacteria.* Bioresource Technology, 2013. **134**: p. 127-33.

66. Lindner, P., et al., *Disposable sensor systems*, in *Single-Use Technology in Biopharmaceutical Manufacture*. 2010. p. 67-81.

67. Vonshak, A., et al., *The effect of light availability on the photosynthetic activity and productivity of outdoor cultures of Arthrospira platensis (Spirulina).* Journal of Applied Phycology, 2013. **26**(3): p. 1309-1315.

68. Brindley, C., F.G. Acien, and J.M. Fernandez-Sevilla, *The oxygen evolution methodology affects photosynthetic rate measurements of microalgae in well-defined light regimes.* Biotechnol Bioeng, 2010. **106**(2): p. 228-37.

69. Lívanský, K., *Effect of O2, CO2 and temperature on the light saturated growth of Scenedesmus obliquus*, in *Algological Studies/Archiv Für Hydrobiologie*. 1996. p. 69-82.

70. Gutierrez, M., et al., *Nutrient solution monitoring in greenhouse cultivation employing a potentiometric electronic tongue.* Journal of Agricultural and Food Chemistry, 2008. **56**(6): p. 1810-7.

71. Radomska, A., et al., *Biocompatible ion selective electrode for monitoring metabolic activity during the growth and cultivation of human cells.* Biosensors and Bioelectronics, 2008. **24**(3): p. 435-41.

72. Mueller, A.V. and H.F. Hemond, *Extended artificial neural networks: incorporation of a priori chemical knowledge enables use of ion selective electrodes for in-situ measurement of ions at environmentally relevant levels.* Talanta, 2013. **117**: p. 112-8.

73. Rodolfi, L., et al., *Microalgae for oil: strain selection, induction of lipid synthesis and outdoor mass cultivation in a low-cost photobioreactor.* Biotechnol Bioeng, 2009. **102**(1): p. 100-12.

74. White, S., A. Anandraj, and F. Bux, *PAM fluorometry as a tool to assess microalgal nutrient stress and monitor cellular neutral lipids.* Bioresource Technology, 2011. **102**(2): p. 1675-82.

75. Collos, Y. and P.J. Harrison, *Acclimation and toxicity of high ammonium concentrations to unicellular algae.* Marine Pollution Bulletin, 2014. **80**(1-2): p. 8-23.

76. Powell, N., et al., *Factors influencing luxury uptake of phosphorus by microalgae in waste stabilization ponds.* Environmental Science & Technology, 2008. **42**(16): p. 5958-62.

77. Jiménez, C., et al., *The Feasibility of industrial production of Spirulina (Arthrospira) in Southern Spain.* Aquaculture, 2003. **217**(1-4): p. 179-190.

78. Chioccioli, M., B. Hankamer, and I.L. Ross, *Flow cytometry pulse width data enables rapid and sensitive estimation of biomass dry weight in the microalgae Chlamydomonas reinhardtii and Chlorella vulgaris.* Plos One, 2014. **9**(5): p. e97269.

79. Gitelson, A.A., et al., *Optical properties ofNannochloropsis sp and their application to remote estimation of cell mass.* Biotechnology And Bioengineering, 2000. **69**(5): p. 516-525.

80. Bosma, R., et al., *Prediction of volumetric productivity of an outdoor photobioreactor.* Biotechnol Bioeng, 2007. **97**(5): p. 1108-20.

81. Quinn, J., L. de Winter, and T. Bradley, *Microalgae bulk growth model with application to industrial scale systems.* Bioresource Technology, 2011. **102**(8): p. 5083-92.

82. Schmidt-Hager, J., et al., *Noninvasive online biomass detector system for cultivation in shake flasks.* Engineering in Life Sciences, 2014. **14**(5): p. 467-476.

83. Sandnes, J.M., et al., *Real-time monitoring and automatic density control of large-scale microalgal cultures using near infrared (NIR) optical density sensors.* Journal of Biotechnology, 2006. **122**(2): p. 209-15.

84. Córdoba-Matson, M.V., J. Gutiérrez, and M.Á. Porta-Gándara, *Evaluation of Isochrysis galbana (clone T-ISO) cell numbers by digital image analysis of color intensity.* Journal of Applied Phycology, 2009. **22**(4): p. 427-434.

85. Uyar, B., *A novel non-invasive digital imaging method for continuous biomass monitoring and cell distribution mapping in photobioreactors.* Journal of Chemical Technology & Biotechnology, 2013. **88**(6): p. 1144-1149.

86. Havlik, I., et al., *Monitoring of microalgal cultivations with on-line, flow-through microscopy.* Algal Research, 2013. **2**(3): p. 253-257.

87. Ohnuki, S., et al., *Image-based monitoring system for green algal Haematococcus pluvialis (Chlorophyceae) cells during culture.* Plant and Cell Physiology, 2013. **54**(11): p. 1917-29.

88. Murphy, T.E., K. Macon, and H. Berberoglu, *Multispectral image analysis for algal biomass quantification.* Biotechnology Progress, 2013. **29**(3): p. 808-16.

89. Olaizola, M., *Microalgal removal of CO2 from flue gases: Changes in medium pH and flue gas composition do not appear to affect the photochemical yield of microalgal cultures.* Biotechnology And Bioprocess Engineering, 2003. **8**(6): p. 360-367.

90. Glindkamp, A., et al., *Sensors in disposable bioreactors status and trends*, in *Disposable Bioreactors*, R. Eibl and D. Eibl, Editors. 2009, Springer-Verlag Berlin: Berlin. p. 145-+.

91. Nadadoor, V.R., et al., *Online sensor for monitoring a microalgal bioreactor system using support vector regression.* Chemometrics and Intelligent Laboratory Systems, 2012. **110**(1): p. 38-48.

92. Szita, N., et al., *Development of a multiplexed microbioreactor system for high-throughput bioprocessing.* Lab on a Chip, 2005. **5**(8): p. 819-26.

93. Han, A., et al., *Microfabricated devices in microbial bioenergy sciences.* Trends in Biotechnology, 2013. **31**(4): p. 225-32.

94. Briassoulis, D., et al., *An experimental helical-tubular photobioreactor for continuous production of Nannochloropsis sp.* Bioresource Technology, 2010. **101**(17): p. 6768-77.

95. Marxen, K., et al., *A photobioreactor system for computer controlled cultivation of microalgae.* Journal of Applied Phycology, 2006. **17**(6): p. 535-549.

96. Lucker, B.F., et al., *The environmental photobioreactor (ePBR): An algal culturing platform for simulating dynamic natural environments.* Algal Research, 2014. **6**: p. 242-249.

97. Nedbal, L., et al., *A photobioreactor system for precision cultivation of photoautotrophic microorganisms and for high-content analysis of suspension dynamics.* Biotechnol Bioeng, 2008. **100**(5): p. 902-10.

98. Mairet, F., et al., *Modelling neutral lipid production by the microalga Isochrysis aff. galbana under nitrogen limitation.* Bioresource Technology, 2011. **102**(1): p. 142-9.

99. Hyka, P., et al., *Flow cytometry for the development of biotechnological processes with microalgae.* Biotechnol Adv, 2013. **31**(1): p. 2-16.

100. da Silva, T.L., J.C. Roseiro, and A. Reis, *Applications and perspectives of multi-parameter flow cytometry to microbial biofuels production processes.* Trends in Biotechnology, 2012. **30**(4): p. 225-32.

101. Davis, R.W., et al., *Multiplex fluorometric assessment of nutrient limitation as a strategy for enhanced lipid enrichment and harvesting of Neochloris oleoabundans.* Biotechnol Bioeng, 2012. **109**(10): p. 2503-12.

102. Broger, T., et al., *Real-time on-line flow cytometry for bioprocess monitoring.* Journal of Biotechnology, 2011. **154**(4): p. 240-7.

103. Song, Y., et al., *Capacitive detection of living microalgae in a microfluidic chip.* Sensors and Actuators B: Chemical, 2014. **194**: p. 164-172.

104. Gray, A.J., et al., *Cell identification and sizing using digital image analysis for estimation of cell biomass in High Rate Algal Ponds.* Journal of Applied Phycology, 2002. **14**(3): p. 193-204.

105. Masojídek, J., A. Vonshak, and G. Torzillo, *Chlorophyll fluorescence applications in microalgal mass cultures*, in *Chlorophyll a Fluorescence in Aquatic Sciences: Methods and Applications*. 2010, Springer. p. 277-292.

106. Malapascua, J.R.F., et al., *Photosynthesis monitoring to optimize growth of microalgal mass cultures: application of chlorophyll fluorescence techniques.* Aquatic Biology, 2014. **22**: p. 123-140.

107. Baker, N.R. and K. Oxborough, *Chlorophyll fluorescence as a probe of photosynthetic productivity*, in *Chlorophyll a Fluorescence*. 2004, Springer. p. 65-82.

108. Maxwell, K. and G.N. Johnson, *Chlorophyll fluorescence--a practical guide.* Journal of Experimental Botany, 2000. **51**(345): p. 659-68.

109. Schreiber, U., *Pulse-amplitude-modulation (PAM) fluorometry and saturation pulse method: an overview.* Chlorophyll a Fluorescence, 2004: p. 279-319.

110. Masojidek, J., et al., *Productivity correlated to photobiochemical performance of Chlorella mass cultures grown outdoors in thin-layer cascades.* Journal of Industrial Microbiology & Biotechnology, 2011. **38**(2): p. 307-17.

111. Hulatt, C.J. and D.N. Thomas, *Productivity, carbon dioxide uptake and net energy return of microalgal bubble column photobioreactors.* Bioresource Technology, 2011. **102**(10): p. 5775-87.

112. Tan, S.T., et al., *Application of mid-infrared chemical imaging and multivariate chemometrics analyses to characterise a population of microalgae cells.* Bioresource Technology, 2013. **134**: p. 316-23.

113. Mayers, J.J., K.J. Flynn, and R.J. Shields, *Rapid determination of bulk microalgal biochemical composition by Fourier-Transform Infrared spectroscopy.* Bioresource Technology, 2013. **148**: p. 215-20.

114. Schenk, J., I.W. Marison, and U. von Stockar, *A simple method to monitor and control methanol feeding of Pichia pastoris fermentations using mid-IR spectroscopy.* Journal of Biotechnology, 2007. **128**(2): p. 344-53.

115. Solovchenko, A.E., et al., *Carotenoid-to-chlorophyll ratio as a proxy for assay of total fatty acids and arachidonic acid content in the green microalga Parietochloris incisa.* Journal of Applied Phycology, 2008. **21**(3): p. 361-366.

116. Solovchenko, A., et al., *Stress-induced changes in optical properties, pigment and fatty acid content of Nannochloropsis sp.: implications for non-destructive assay of total fatty acids.* Marine Biotechnology, 2011. **13**(3): p. 527-35.

117. Su, C.H., et al., *Simultaneous estimation of chlorophyll a and lipid contents in microalgae by three-color analysis.* Biotechnol Bioeng, 2008. **99**(4): p. 1034-9.

118. Riley, M.R., et al., *Simultaneous measurement of 19 components in serum-containing animal cell culture media by fourier transform near-infrared spectroscopy.* Biotechnology Progress, 2001. **17**(2): p. 376-8.

119. Laurens, L.M.L. and E.J. Wolfrum, *Feasibility of Spectroscopic Characterization of Algal Lipids: Chemometric Correlation of NIR and FTIR Spectra with Exogenous Lipids in Algal Biomass.* Bioenergy Research, 2010. **4**(1): p. 22-35.

120. Brown, M.R., et al., *Assessing near-infrared reflectance spectroscopy for the rapid detection of lipid and biomass in microalgae cultures.* Journal of Applied Phycology, 2013. **26**(1): p. 191-198.

121. Laurens, L.M. and E.J. Wolfrum, *High-throughput quantitative biochemical characterization of algal biomass by NIR spectroscopy; multiple linear regression and multivariate linear regression analysis.* Journal of Agricultural and Food Chemistry, 2013. **61**(50): p. 12307-14.

122. Challagulla, V., K.B. Walsh, and P. Subedi, *Biomass and total lipid content assessment of microalgal cultures using near and short wave infrared spectroscopy.* Bioenergy Research, 2013. **7**(1): p. 306-318.

123. Coat, R., et al., *Unravelling the matrix effect of fresh sampled cells for in vivo unbiased FTIR determination of the absolute concentration of total lipid content of microalgae.* Bioprocess and Biosystems Engineering, 2014. **37**(11): p. 2175-87.

124. Gao, C., et al., *Rapid quantitation of lipid in microalgae by time-domain nuclear magnetic resonance.* Journal of Microbiological Methods, 2008. **75**(3): p. 437-40.

125. Beal, C.M., et al., *Lipid analysis of Neochloris oleoabundans by liquid state NMR.* Biotechnol Bioeng, 2010. **106**(4): p. 573-83.

126. Lee, T.H., J.S. Chang, and H.Y. Wang, *Current developments in high-throughput analysis for microalgae cellular contents.* Biotechnology Journal, 2013. **8**(11): p. 1301-14.

127. Lee, T.H., J.S. Chang, and H.Y. Wang, *Rapid and in vivo quantification of cellular lipids in Chlorella vulgaris using near-infrared Raman spectrometry.* Analytical Chemistry, 2013. **85**(4): p. 2155-60.

128. Davis, R.W., H.W. Wu, and S. Singh, *Multispectral sorter for rapid, nondestructive optical bioprospecting for algae biofuels*, in *Imaging, Manipulation, And Analysis Of Biomolecules, Cells, And Tissues Xii*, D.L. Farkas, D.V. Nicolau, and R.C. Leif, Editors. 2014, Spie-Int Soc Optical Engineering: Bellingham.

129. Schor, A.R., C.R. Buie, and Asme. *Non-invasive sorting of lipid producing microalgae with dielectrophoresis using microelectrodes*. in *ASME 2012 International Mechanical Engineering Congress and Exposition*. 2012. Houston, Texas, USA: American Society of Mechanical Engineers.

130. Deng, Y.L., J.S. Chang, and Y.J. Juang, *Separation of microalgae with different lipid contents by dielectrophoresis.* Bioresource Technology, 2013. **135**: p. 137-41.

131. Bono, M.S., Jr., B.A. Ahner, and B.J. Kirby, *Detection of algal lipid accumulation due to nitrogen limitation via dielectric spectroscopy of Chlamydomonas reinhardtii suspensions in a coaxial transmission line sample cell.* Bioresource Technology, 2013. **143**: p. 623-31.

132. Michael, K.A., S.R. Hiibel, and E.J. Geiger, *Dependence of the dielectrophoretic upper crossover frequency on the lipid content of microalgal cells.* Algal Research, 2014. **6**: p. 17-21.

133. Brennan, L., et al., *Enhancement of BODIPY505/515 lipid fluorescence method for applications in biofuel-directed microalgae production.* Journal of Microbiological Methods, 2012. **90**(2): p. 137-43.

134. Brennan, L. and P. Owende, *Biofuels from microalgae—A review of technologies for production, processing, and extractions of biofuels and co-products.* Renewable and Sustainable Energy Reviews, 2010. **14**(2): p. 557-577.

135. Gouveia, L., et al., *Neochloris oleabundans UTEX #1185: a suitable renewable lipid source for biofuel production.* Journal of Industrial Microbiology & Biotechnology, 2009. **36**(6): p. 821-6.

136. da Silva, T.L., et al., *Oil production towards biofuel from autotrophic microalgae semicontinuous cultivations monitorized by flow cytometry.* Biotechnology and Applied Biochemistry, 2009. **159**(2): p. 568-78.

137. Mendoza Guzmán, H., et al., *Analysis of interspecific variation in relative fatty acid composition: use of flow cytometry to estimate unsaturation index and relative polyunsaturated fatty acid content in microalgae.* Journal of Applied Phycology, 2010. **23**(1): p. 7-15.

138. Erickson, R.A. and R. Jimenez, *Microfluidic cytometer for high-throughput measurement of photosynthetic characteristics and lipid accumulation in individual algal cells.* Lab on a Chip, 2013. **13**(15): p. 2893-901.

139. Eriksen, N.T. and J.J.r.L.n. Iversen, *On-line determination of pigment composition and biomass in cultures of microalgae.* Biotechnology Techniques, 1995. **9**(1): p. 49-54.

140. Eriksen, N.T., T. Geest, and J.J.L. Iversen, *Phototrophic growth in the lumostat: a photo-bioreactor with on-line optimization of light intensity.* Journal of Applied Phycology, 1996. **8**(4-5): p. 345-352.

141. Noack, K., et al., *Combined shifted-excitation Raman difference spectroscopy and support vector regression for monitoring the algal production of complex polysaccharides.* Analyst, 2013. **138**(19): p. 5639-46.

142. Gao, Z., et al., *Photosynthetic production of ethanol from carbon dioxide in genetically engineered cyanobacteria.* Energy & Environmental Science, 2012. **5**(12): p. 9857-9865.

143. Tamburic, B., et al., *Design of a novel flat-plate photobioreactor system for green algal hydrogen production.* International Journal of Hydrogen Energy, 2011. **36**(11): p. 6578-6591.

144. Oncel, S. and A. Kose, *Comparison of tubular and panel type photobioreactors for biohydrogen production utilizing Chlamydomonas reinhardtii considering mixing time and light intensity.* Bioresource Technology, 2014. **151**: p. 265-70.

145. Schuster, K.C., E. Urlaub, and J.R. Gapes, *Single-cell analysis of bacteria by Raman microscopy: spectral information on the chemical composition of cells and on the heterogeneity in a culture.* Journal of Microbiological Methods, 2000. **42**(1): p. 29-38.

146. Puppels, G.J., et al., *Studying single living cells and chromosomes by confocal Raman microspectroscopy.* Nature, 1990. **347**(6290): p. 301-3.

147. Smith, R., K.L. Wright, and L. Ashton, *Raman spectroscopy: an evolving technique for live cell studies.* Analyst, 2016. **141**(12): p. 3590-600.

148. Krafft, C. and J. Popp, *The many facets of Raman spectroscopy for biomedical analysis.* Analytical and Bioanalytical Chemistry, 2015. **407**(3): p. 699-717.

149. Shen, Y., F. Hu, and W. Min, *Raman Imaging of Small Biomolecules.* Annual Review of Biophysics, 2019. **48**: p. 347-369.

150. De Gelder, J., et al., *Reference database of Raman spectra of biological molecules.* Journal of Raman Spectroscopy, 2007. **38**(9): p. 1133-1147.

151. Pappas, D., B.W. Smith, and J.D. Winefordner, *Raman spectroscopy in bioanalysis.* Talanta, 2000. **51**(1): p. 131-44.

152. Baena, J.R. and B. Lendl, *Raman spectroscopy in chemical bioanalysis.* Current Opinion in Chemical Biology, 2004. **8**(5): p. 534-9.

153. Fabian, H. and P. Anzenbacher, *New developments in Raman spectroscopy of biological systems.* Vibrational Spectroscopy, 1993. **4**(2): p. 125-148.

154. Wang, W., et al., *Photobleaching and stabilization of carbon nanodots produced by solvothermal synthesis.* Physical Chemistry Chemical Physics, 2016. **18**(1): p. 466-75.

155. de Oliveira, V.E., et al., *Carotenes and carotenoids in natural biological samples: a Raman spectroscopic analysis.* Journal of Raman Spectroscopy, 2010. **41**(6): p. 642-650.

156. Schulz, H., M. Baranska, and R. Baranski, *Potential of NIR-FT-Raman spectroscopy in natural carotenoid analysis.* Biopolymers, 2005. **77**(4): p. 212-21.

157. Jehlicka, J., et al., *Potential and limits of Raman spectroscopy for carotenoid detection in microorganisms: implications for astrobiology.* Philosophical Transactions of The Royal Society A Mathematical Physical and Engineering Sciences, 2014. **372**(2030): p. 20140199.

158. Jehlicka, J., H.G. Edwards, and A. Oren, *Raman spectroscopy of microbial pigments.* Applied and Environmental Microbiology, 2014. **80**(11): p. 3286-95.

159. Cavonius, L., et al., *Imaging of lipids in microalgae with coherent anti-stokes Raman scattering microscopy.* Plant Physiol, 2015. **167**(3): p. 603-16.

160. Czamara, K., et al., *Raman spectroscopy of lipids: a review.* Journal of Raman Spectroscopy, 2015. **46**(1): p. 4-20.

161. Samek, O., et al., *Raman microspectroscopy of individual algal cells: sensing unsaturation of storage lipids in vivo.* Sensors (Basel), 2010. **10**(9): p. 8635-51.

162. Pilát, Z., et al., *Raman microspectroscopy of algal lipid bodies: β-carotene quantification.* Journal of Applied Phycology, 2012. **24**(3): p. 541-546.

163. Gierlinger, N., T. Keplinger, and M. Harrington, *Imaging of plant cell walls by confocal Raman microscopy.* Nature Protocols, 2012. **7**(9): p. 1694-708.

164. Sene, C.F., et al., *Fourier-transform Raman and Fourier-transform infrared spectroscopy (an investigation of five higher plant cell walls and their components).* Plant Physiology, 1994. **106**(4): p. 1623-1631.

165. Liu, J., et al., *Deep convolutional neural networks for Raman spectrum recognition: a unified solution.* Analyst, 2017. **142**(21): p. 4067-4074.

166. Gautam, R., et al., *Review of multidimensional data processing approaches for Raman and infrared spectroscopy.* EPJ Techniques and Instrumentation, 2015. **2**(1): p. 1-38.

167. Palacký, J., P. Mojzeš, and J. Bok, *SVD-based method for intensity normalization, background correction and solvent subtraction in Raman spectroscopy exploiting the properties of water stretching vibrations.* Journal of Raman Spectroscopy, 2011. **42**(7): p. 1528-1539.

168. Barman, I., et al., *Effect of photobleaching on calibration model development in biological Raman spectroscopy.* Journal of Biomedical Optics, 2011. **16**(1): p. 011004.

169. Dieing, T., O. Hollricher, and J. Toporski, *Confocal raman microscopy*. Vol. 158. 2011: Springer.

170. Tuschel, D., *Selecting an excitation wavelength for Raman spectroscopy.* Spectroscopy, 2016. **31**(3): p. 14-23.

171. Largeau, C., et al., *Sites of accumulation and composition of hydrocarbons in Botryococcus braunii.* Phytochemistry, 1980. **19**(6): p. 1043-1051.

172. Dupaix, A., et al., *Intracellular spectroscopic studies of a bioluminescent cell: Pyrocystis lunula.* Biology of the Cell, 1982. **43**(3): p. 157-&.

173. Delhaye, M. and P. Dhamelincourt, *Raman microprobe and microscope with laser excitation.* Journal of Raman Spectroscopy, 1975. **3**(1): p. 33-43.

174. Steger, E. and A. Simon, *Raman-spektroskopische Untersuchungen an kondensierten Phosphaten und Phosphorsäuren. Raman-Spektrum und Struktur des Tetrametaphosphat-Ions.* Zeitschrift für anorganische und allgemeine Chemie, 1957. **291**(1-4): p. 76-88.

175. Brahma, S., et al., *A resonance Raman method for the rapid detection and identification of algae in water.* Applied Spectroscopy, 1983. **37**(1): p. 55-58.

176. Heraud, P., et al., *Effects of pre-processing of Raman spectra on in vivo classification of nutrient status of microalgal cells.* Journal of Chemometrics, 2006. **20**(5): p. 193-197.

177. Heraud, P., et al., *In vivo prediction of the nutrient status of individual microalgal cells using Raman microspectroscopy.* FEMS Microbiology Letters, 2007. **275**(1): p. 24-30.

178. Huang, Y.Y., et al., *Micro-Raman spectroscopy of algae: composition analysis and fluorescence background behavior.* Biotechnol Bioeng, 2010. **105**(5): p. 889-98.

179. Weiss, T.L., et al., *Raman spectroscopy analysis of botryococcene hydrocarbons from the green microalga Botryococcus braunii.* Journal of Biological Chemistry, 2010. **285**(42): p. 32458-66.

180. Samek, O., et al., *Characterization of oil-producing microalgae using Raman spectroscopy.* Laser Physics Letters, 2011. **8**(10): p. 701-709.

181. Wu, H., et al., *In vivo lipidomics using single-cell Raman spectroscopy.* Proceedings of the National Academy of Sciences of the United States of America, 2011. **108**(9): p. 3809-14.

182. Ji, Y., et al., *Raman spectroscopy provides a rapid, non-invasive method for quantitation of starch in live, unicellular microalgae.* Biotechnology Journal, 2014. **9**(12): p. 1512-8.

183. Wang, T., et al., *Quantitative dynamics of triacylglycerol accumulation in microalgae populations at single-cell resolution revealed by Raman microspectroscopy.* Biotechnol Biofuels, 2014. **7**(1): p. 58.

184. Meksiarun, P., et al., *Analysis of the effects of dietary fat on body and skin lipids of hamsters by Raman spectroscopy.* Analyst, 2015. **140**(12): p. 4238-44.

185. Meksiarun, P., et al., *In vivo study of lipid accumulation in the microalgae marine diatom Thalassiosira pseudonana using Raman spectroscopy.* Applied Spectroscopy, 2015. **69**(1): p. 45-51.

186. Shao, Y., et al., *Identification of pesticide varieties by detecting characteristics of Chlorella pyrenoidosa using Visible/Near infrared hyperspectral imaging and Raman microspectroscopy technology.* Water Research, 2016. **104**: p. 432-440.

187. Kim, H.S., et al., *Raman spectroscopy compatible PDMS droplet microfluidic culture and analysis platform towards on-chip lipidomics.* Analyst, 2017. **142**(7): p. 1054-1060.

188. Hosokawa, M., et al., *In vivo live cell imaging for the quantitative monitoring of lipids by using Raman microspectroscopy.* Analytical Chemistry, 2014. **86**(16): p. 8224-30.

189. Sharma, S.K., et al., *An integrative Raman microscopy-based workflow for rapid in situ analysis of microalgal lipid bodies.* Biotechnol Biofuels, 2015. **8**(1): p. 164.

190. Chiu, L.D., et al., *Rapid in vivo lipid/carbohydrate quantification of single microalgal cell by Raman spectral imaging to reveal salinity-induced starch-to-lipid shift.* Biotechnol Biofuels, 2017. **10**(1): p. 9.

191. Li, K., et al., *In vivo kinetics of lipids and astaxanthin evolution in Haematococcus pluvialis mutant under 15% CO2 using Raman microspectroscopy.* Bioresource Technology, 2017. **244**(Pt 2): p. 1439-1444.

192. Yonamine, Y., et al., *Monitoring photosynthetic activity in microalgal cells by Raman spectroscopy with deuterium oxide as a tracking probe.* ChemBioChem, 2017. **18**(20): p. 2063-2068.

193. Shao, F., et al., *Nanoscale chemical imaging of interfacial monolayers by tip-enhanced Raman spectroscopy.* Angewandte Chemie International Edition in English, 2017. **56**(32): p. 9361-9366.

194. Wu, Q., et al., *Differentiation of algae clones on the basis of resonance Raman spectra excited by visible light.* Analytical Chemistry, 1998. **70**(9): p. 1782-7.

195. Wu, Q., et al., *UV resonance Raman detection and quantitation of domoic acid in phytoplankton.* Analytical Chemistry, 2000. **72**(7): p. 1666-71.

196. Wood, B.R., et al., *A portable Raman acoustic levitation spectroscopic system for the identification and environmental monitoring of algal cells.* Analytical Chemistry, 2005. **77**(15): p. 4955-61.

197. Kaczor, A., K. Turnau, and M. Baranska, *In situ Raman imaging of astaxanthin in a single microalgal cell.* Analyst, 2011. **136**(6): p. 1109-12.

198. Kaczor, A. and M. Baranska, *Structural changes of carotenoid astaxanthin in a single algal cell monitored in situ by Raman spectroscopy.* Analytical Chemistry, 2011. **83**(20): p. 7763-70.

199. Alexandre, M.T., et al., *Probing the carotenoid content of intact Cyclotella cells by resonance Raman spectroscopy.* Photosynthesis Research, 2014. **119**(3): p. 273-81.

200. Kula, M., et al., *Metabolic activity, the chemical composition of biomass and photosynthetic activity ofChlorella vulgarisunder different light spectra in photobioreactors.* Engineering in Life Sciences, 2014. **14**(1): p. 57-67.

201. Ho, S.-H., et al., *Rapid in vivo lipid/carbohydrate quantification of single microalgal cell by Raman spectral imaging to reveal salinity-induced starch-to-lipid shift.* Biotechnology for Biofuels, 2017. **10**(1): p. 1-9.

202. Lieutaud, C., et al., *Fast non-invasive monitoring of microalgal physiological stage in photobioreactors through Raman spectroscopy.* Algal Research, 2019. **42**: p. 101595.

203. Ren, J., et al., *Fouling-resistant behavior of silver nanoparticle-modified surfaces against the bioadhesion of microalgae.* ACS Applied Materials & Interfaces, 2014. **6**(6): p. 3829-38.

204. de Oliveira, V.E., et al., *Study of carotenoids in cyanobacteria by Raman spectroscopy.* Spectrochimica Acta Part A: Molecular Spectroscopy; Spectrochimica Acta, Part A: Molecular and Biomolecular Spectroscopy, 2015. **150**: p. 373-80.

205. Rüger, J., et al., *Assessment of growth phases of the diatom Ditylum brightwellii by FT-IR and Raman spectroscopy.* Algal Research, 2016. **19**: p. 246-252.

206. Koch, M., et al., *Iterative morphological and mollifier-based baseline correction for Raman spectra.* Journal of Raman Spectroscopy, 2017. **48**(2): p. 336-342.

207. Koch, M., et al., *Violaxanthin cycle kinetics analysedin vivowith resonance Raman spectroscopy.* Journal of Raman Spectroscopy, 2017. **48**(5): p. 686-691.

208. Zhang, P., et al., *Effects of stepwise nitrogen depletion on carotenoid content, fluorescence parameters and the cellular stoichiometry of Chlorella vulgaris.* Spectrochimica Acta Part A: Molecular Spectroscopy; Spectrochimica Acta, Part A: Molecular and Biomolecular Spectroscopy, 2017. **181**: p. 30-38.

209. He, S., et al., *Preliminary identification of unicellular algal genus by using combined confocal resonance Raman spectroscopy with PCA and DPLS analysis.* Spectrochimica Acta Part A: Molecular Spectroscopy; Spectrochimica Acta, Part A: Molecular and Biomolecular Spectroscopy, 2018. **190**: p. 417-422.

210. Zhang, Y., et al., *Development of a method to evaluate the tenderness of fresh tea leaves based on rapid, in-situ Raman spectroscopy scanning for carotenoids.* Food Chemistry, 2020. **308**: p. 125648.

211. Kubo, Y., et al., *Orientation of Carotenoid Molecules in the Eyespot of Alga: In Situ Polarized Resonance Raman Spectroscopy.* Applied Spectroscopy, 2016. **54**(8): p. 1114-1119.

212. Qi, J. and W.C. Shih, *Performance of line-scan Raman microscopy for high-throughput chemical imaging of cell population.* Applied Optics, 2014. **53**(13): p. 2881-5.

213. Urban, P.L., et al., *Multidimensional analysis of single algal cells by integrating microspectroscopy with mass spectrometry.* Analytical Chemistry, 2011. **83**(5): p. 1843-9.

214. Abbas, A., M. Josefson, and K. Abrahamsson, *Characterization and mapping of carotenoids in the algae Dunaliella and Phaeodactylum using Raman and target orthogonal partial least squares.* Chemometrics and Intelligent Laboratory Systems, 2011. **107**(1): p. 174-177.

215. Abbas, A., et al., *Chemical images of marine bio-active compounds by surface enhanced Raman spectroscopy and transposed orthogonal partial least squares (T-OPLS).* Analytica Chimica Acta, 2012. **737**: p. 37-44.

216. Collins, A.M., et al., *Resolving carotenoid distribution in living cells of Haematococcus pluvialis with hyperspectral confocal Raman microscopy*. 2011, Sandia National Laboratories (SNL-NM), Albuquerque, NM (United States).

217. Li, M., et al., *Rapid resonance Raman microspectroscopy to probe carbon dioxide fixation by single cells in microbial communities.* The ISME Journal, 2012. **6**(4): p. 875-85.

218. Fagerer, S.R., et al., *Analysis of single algal cells by combining mass spectrometry with Raman and fluorescence mapping.* Analyst, 2013. **138**(22): p. 6732-6.

219. Davis, R.W., et al., *Label-free measurement of algal triacylglyceride production using fluorescence hyperspectral imaging.* Algal Research, 2014. **5**: p. 181-189.

220. Liu, J. and Q. Huang, *Screening of Astaxanthin-Hyperproducing Haematococcus pluvialis Using Fourier Transform Infrared (FT-IR) and Raman Microspectroscopy.* Applied Spectroscopy, 2016. **70**(10): p. 1639-1648.

221. Ramya, A.N., et al., *Single cell lipid profiling of Scenedesmus quadricauda CASA-CC202 under nitrogen starved condition by surface enhanced Raman scattering (SERS) fingerprinting.* Algal Research, 2017. **25**: p. 200-206.

222. He, X.N., et al., *Coherent anti-Stokes Raman scattering and spontaneous Raman spectroscopy and microscopy of microalgae with nitrogen depletion.* Biomedical Optics Express, 2012. **3**(11): p. 2896-906.

223. Dementjev, A. and J. Kostkevičiene, *Applying the method of Coherent Anti-stokes Raman microscopy for imaging of carotenoids in microalgae and cyanobacteria.* Journal of Raman Spectroscopy, 2013. **44**(7): p. 973-979.

224. Slepkov, A.D., et al., *In vivo hyperspectral CARS and FWM microscopy of carotenoid accumulation in H. Pluvialis*, in *Proceedings of SPIE*. 2014. p. 893709.

225. Takahashi, T., et al., *Selective imaging of microplastic and organic particles in flow by multimodal coherent anti-stokes Raman scattering and two-photon excited autofluorescence analysis.* Analytical Chemistry, 2021. **93**(12): p. 5234-5240.

226. Legesse, F.B., et al., *Investigation of microalgal carotenoid content using coherent anti-Stokes Raman scattering (CARS) microscopy and spontaneous Raman spectroscopy.* ChemPhysChem, 2018. **19**(9): p. 1048-1055.

227. Jaeger, D., et al., *Label-free in vivo analysis of intracellular lipid droplets in the oleaginous microalga Monoraphidium neglectum by coherent Raman scattering microscopy.* Scientific Reports, 2016. **6**: p. 35340.

228. Wang, C.-C., et al. *Monitoring lipid accumulation in the green microalga Botryococcus braunii with frequency-modulated stimulated Raman scattering*. in *Multiphoton Microscopy in the Biomedical Sciences XV*. 2015. International Society for Optics and Photonics.

229. Achbergerová, L. and J. Nahálka, *Polyphosphate-an ancient energy source and active metabolic regulator.* Microbial Cell Factories, 2011. **10**(1): p. 1-14.

230. Bru, S., et al., *Improvement of biochemical methods of polyP quantification.* Microbial Cell Factories, 2016. **4**(1): p. 6-15.

231. Lorenzo-Orts, L., D. Couto, and M. Hothorn, *Identity and functions of inorganic and inositol polyphosphates in plants.* New Phytologist, 2020. **225**(2): p. 637-652.

232. Hupfer, M., et al., *Methods for Detection and Quantification of Polyphosphate and Polyphosphate Accumulating Microorganisms in Aquatic Sediments.* International Review of Hydrobiology, 2008. **93**(1): p. 1-30.

233. Majed, N., Y. Li, and A.Z. Gu, *Advances in techniques for phosphorus analysis in biological sources.* Curr Opin Biotechnol, 2012. **23**(6): p. 852-9.

234. Omelon, S., et al., *Colocation and role of polyphosphates and alkaline phosphatase in apatite biomineralization of elasmobranch tesserae.* Acta Biomaterialia, 2014. **10**(9): p. 3899-910.

235. Majed, N. and A.Z. Gu, *Application of Raman microscopy for simultaneous and quantitative evaluation of multiple intracellular polymers dynamics functionally relevant to enhanced biological phosphorus removal processes.* Environmental Science & Technology, 2010. **44**(22): p. 8601-8.

236. Bednárová, L., et al., *Raman microspectroscopy of the yeast vacuoles.* Spectroscopy: An International Journal, 2012. **27**(5-6): p. 503-507.

237. Majed, N., et al., *Evaluation of intracellular polyphosphate dynamics in enhanced biological phosphorus removal process using Raman microscopy.* Environmental Science & Technology, 2009. **43**(14): p. 5436-42.

238. Koda, S., T. Kawakami, and H. Nomura, *Raman spectroscopic studies on the interaction between counterions and polyphosphate ion.* Polymer Journal, 1994. **26**(4): p. 473-477.

239. de Jager, H.J. and A.M. Heyns, *Kinetics of acid-catalyzed hydrolysis of a polyphosphate in water.* The Journal of Physical Chemistry A, 1998. **102**(17): p. 2838-2841.

240. de Jager, H.J. and A.M. Heyns, *Study of the hydrolysis of sodium polyphosphate in water using Raman spectroscopy.* Applied Spectroscopy, 1998. **52**(6): p. 808-814.

241. Majed, N., et al., *Identification of functionally relevant populations in enhanced biological phosphorus removal processes based on intracellular polymers profiles and insights into the metabolic diversity and heterogeneity.* Environmental Science & Technology, 2012. **46**(9): p. 5010-7.

242. Tarayre, C., et al., *Characterisation of phosphate accumulating organisms and techniques for polyphosphate detection: A review.* Sensors (Basel), 2016. **16**(6): p. 797-14.

243. Association, A.P.H., A.W.W. Association, and W.P.C. Federation, *Standard methods for the examination of water and wastewater. 17th edition.* 1989, American Public Health Association.

244. Kolozsvari, B., S. Firth, and A. Saiardi, *Raman spectroscopy detection of phytic acid in plant seeds reveals the absence of inorganic polyphosphate.* Mol Plant, 2015. **8**(5): p. 826-8.

245. Rao, N.N., M.R. Gomez-Garcia, and A. Kornberg, *Inorganic polyphosphate: essential for growth and survival.* Annual Review of Biochemistry, 2009. **78**(1): p. 605-47.

246. Hupfer, M., B. Ruübe, and P. Schmieder, *Origin and diagenesis of polyphosphate in lake sediments: A 31P‐NMR study.* Limnology and Oceanography, 2004. **49**(1): p. 1-10.

247. Kizewski, F., et al., *Spectroscopic approaches for phosphorus speciation in soils and other environmental systems.* Journal of Environmental Quality, 2011. **40**(3): p. 751-66.

248. Gowda, G.N. and D. Raftery, *Can NMR solve some significant challenges in metabolomics?* Journal of Magnetic Resonance, 2015. **260**: p. 144-160.

249. Klein, G., et al., *Germination of Dictyostelium discoideum spores. A phosphorus-31 NMR analysis.* Biochemistry, 1988. **27**(21): p. 8199-8203.

250. Bental, M., et al., *Polyphosphate metabolism in the alga Dunaliella salina studied by 31P-NMR.* Biochimica et Biophysica Acta, 1991. **1092**(1): p. 21-8.

251. Wang, L., C. Kuchendorf, and S. Willbold, *Determination of individual chain length and chain-length distribution of polyphosphates in microalgae by 31P-DOSY-NMR.* Algal Research, 2019. **43**: p. 101631.

252. Pick, U. and M. Weiss, *Polyphosphate hydrolysis within acidic vacuoles in response to amine-induced alkaline stress in the halotolerant alga Dunaliella salina.* Plant Physiology, 1991. **97**(3): p. 1234-1240.

253. Nishikawa, K., et al., *Polyphosphate metabolism in an acidophilic alga Chlamydomonas acidophila KT-1 (Chlorophyta) under phosphate stress.* Plant Science, 2006. **170**(2): p. 307-313.

254. Pratt, J., et al., *Phosphate (Pi) starvation effect on the cytosolic Pi concentration and Pi exchanges across the tonoplast in plant cells: an in vivo 31P-nuclear magnetic resonance study using methylphosphonate as a Pi analog.* Plant Physiology, 2009. **151**(3): p. 1646-1657.

255. Shebanova, A., et al., *Versatility of the green microalga cell vacuole function as revealed by analytical transmission electron microscopy.* Protoplasma, 2017. **254**(3): p. 1323-1340.

256. Eixler, S., U. Selig, and U. Karsten, *Extraction and detection methods for polyphosphate storage in autotrophic planktonic organisms.* Hydrobiologia, 2005. **533**(1-3): p. 135-143.

257. Jensen, T.E., *Electron microscopy of polyphosphate bodies in a blue-green alga, Nostoc pruniforme.* Archiv für Mikrobiologie, 1968. **62**(2): p. 144-152.

258. Mamun, E.A., et al., *Cellular organisation and differentiation of organelles in pre-meiotic rice anthers.* Cell Biology International, 2005. **29**(9): p. 792-802.

259. Nishikawa, K., et al., *Ultrastructural changes in Chlamydomonas acidophila (Chlorophyta) induced by heavy metals and polyphosphate metabolism.* FEMS Microbiology Ecology, 2003. **44**(2): p. 253-9.

260. Alvarez, S. and C.A. Jerez, *Copper ions stimulate polyphosphate degradation and phosphate efflux in Acidithiobacillus ferrooxidans.* Applied and Environmental Microbiology, 2004. **70**(9): p. 5177-82.

261. Demason, D.A. and J.I. Stillman, *Identification of phosphate granules occurring in seedling tissue of two palm species (Phoenix dactylifera and Washingtonia filifera).* Planta, 1986. **167**(3): p. 321-9.

262. Otegui, M.S., R. Capp, and L.A. Staehelin, *Developing seeds of Arabidopsis store different minerals in two types of vacuoles and in the endoplasmic reticulum.* Plant Cell, 2002. **14**(6): p. 1311-27.

263. Gu, A.Z., et al., *Functionally relevant microorganisms to enhanced biological phosphorus removal performance at full-scale wastewater treatment plants in the United States.* Water Environment Research, 2008. **80**(8): p. 688-98.

264. He, S., A.Z. Gu, and K.D. McMahon, *Progress toward understanding the distribution of Accumulibacter among full-scale enhanced biological phosphorus removal systems.* Microbial Ecology, 2008. **55**(2): p. 229-36.

265. Rees, G.N., et al., *Differentiation of polyphosphate and poly-Î²-hydroxybutyrate granules in anAcinetobactersp. isolated from activated sludge.* FEMS Microbiology Letters, 1992. **94**(1-2): p. 171-173.

266. Serafim, L.S., et al., *Methods for detection and visualization of intracellular polymers stored by polyphosphate-accumulating microorganisms.* Journal of Microbiological Methods, 2002. **51**(1): p. 1-18.

267. Martinez, R.J., *On the nature of the granules of the genus spirillum.* Archiv für Mikrobiologie, 1963. **44**(4): p. 334-343.

268. Kulaev, I.S., V.M. Vagabov, and T.V. Kulakovskaya, *The biochemistry of inorganic polyphosphates*. John Wiley & Sons. 2004: John Wiley & Sons. 294.

269. Yagisawa, F., et al., *Identification of novel proteins in isolated polyphosphate vacuoles in the primitive red alga Cyanidioschyzon merolae.* The Plant Journal, 2009. **60**(5): p. 882-93.

270. Keck, K. and H. Stich, *The widespread occurrence of polyphosphate in lower plants.* Annals of Botany, 1957. **21**(4): p. 611-619.

271. ERS, T., *Polyphosphate containing particles of blue-green algae.* Cytologia, 1963. **28**(1): p. 76-80.

272. Chilvers, G., M. Ling-Lee, and A. Ashford, *Polyphosphate granules in the fungi of two lichens.* New Phytologist, 1978. **81**(3): p. 571-574.

273. Kapuscinski, J., *Interactions of nucleic acids with fluorescent dyes: spectral properties of condensed complexes.* Journal of Histochemistry & Cytochemistry, 1990. **38**(9): p. 1323-9.

274. Kolozsvari, B., F. Parisi, and A. Saiardi, *Inositol phosphates induce DAPI fluorescence shift.* Biochemical Journal, 2014. **460**(3): p. 377-85.

275. Martin, P. and B.A. Van Mooy, *Fluorometric quantification of polyphosphate in environmental plankton samples: extraction protocols, matrix effects, and nucleic acid interference.* Applied and Environmental Microbiology, 2013. **79**(1): p. 273-81.

276. Martin, P. and B.A. Van Mooy, *Correction for martin and van mooy, fluorometric quantification of polyphosphate in environmental plankton samples: extraction protocols, matrix effects, and nucleic acid interference.* Applied and Environmental Microbiology, 2015. **81**(1): p. 461.

277. Gomes, F.M., et al., *New insights into the in situ microscopic visualization and quantification of inorganic polyphosphate stores by 4',6-diamidino-2-phenylindole (DAPI)-staining.* European Journal of Histochemistry, 2013. **57**(4): p. e34.

278. Aschar-Sobbi, R., et al., *High sensitivity, quantitative measurements of polyphosphate using a new DAPI-based approach.* Journal of Fluorescence, 2008. **18**(5): p. 859-66.

279. Ruiz, F.A., et al., *The polyphosphate bodies of Chlamydomonas reinhardtii possess a proton-pumping pyrophosphatase and are similar to acidocalcisomes.* Journal of Biological Chemistry, 2001. **276**(49): p. 46196-203.

280. Tijssen, J.P.F., H.W. Beekes, and J. Van Steveninck, *Localization of polyphosphates in Saccharomyces fragilis, as revealed by 4',6-diamidino-2-phenylindole fluorescence.* Biochimica et Biophysica Acta (BBA) - Molecular Cell Research, 1982. **721**(4): p. 394-398.

281. Angelova, P.R., et al., *In situ investigation of mammalian inorganic polyphosphate localization using novel selective fluorescent probes JC-D7 and JC-D8.* ACS Chemical Biology, 2014. **9**(9): p. 2101-2110.

282. Zhu, J., et al., *Two bifunctional inositol pyrophosphate kinases/phosphatases control plant phosphate homeostasis.* Elife, 2019. **8**: p. e43582.

283. Saito, K., et al., *Direct labeling of polyphosphate at the ultrastructural level in Saccharomyces cerevisiae by using the affinity of the polyphosphate binding domain of Escherichia coli exopolyphosphatase.* Applied and Environmental Microbiology, 2005. **71**(10): p. 5692-701.

284. Jimenez-Nuñez, M.D., et al., *Myeloma cells contain high levels of inorganic polyphosphate which is associated with nucleolar transcription.* Haematologica, 2012. **97**(8): p. 1264.

285. Moreno-Sanchez, D., et al., *Polyphosphate is a novel pro-inflammatory regulator of mast cells and is located in acidocalcisomes.* Journal of Biological Chemistry, 2012. **287**(34): p. 28435-44.

286. Negreiros, R.S., et al., *Inorganic polyphosphate interacts with nucleolar and glycosomal proteins in trypanosomatids.* Molecular Microbiology, 2018. **110**(6): p. 973-994.

287. Lorenzo-Orts, L., et al., *Molecular characterization of CHAD domains as inorganic polyphosphate-binding modules.* Life Science Alliance, 2019. **2**(3).

288. Diaz, J., et al., *Marine polyphosphate: a key player in geologic phosphorus sequestration.* Science, 2008. **320**(5876): p. 652-5.

289. Khoshmanesh, A., P.L. Cook, and B.R. Wood, *Quantitative determination of polyphosphate in sediments using Attenuated Total Reflectance-Fourier Transform Infrared (ATR-FTIR) spectroscopy and partial least squares regression.* Analyst, 2012. **137**(16): p. 3704-9.

290. Chen, K.Y., *Study of polyphosphate metabolism in intact cells by 31-P nuclear magnetic resonance spectroscopy.* Progress in Molecular and Subcellular Biology, 1999. **23**: p. 253-73.

291. Beauvoit, B., et al., *Polyphosphates as a source of high energy phosphates in yeast mitochondria: A 31*

P NMR study. FEBS Letters, 1989. **252**(1-2): p. 17-21.

292. Castro, C.D., et al., *In situ 31P nuclear magnetic resonance for observation of polyphosphate and catabolite responses of chemostat-cultivated Saccharomyces cerevisiae after alkalinization.* Applied and Environmental Microbiology, 1995. **61**(12): p. 4448-53.

293. Ault-Riche, D., et al., *Novel assay reveals multiple pathways regulating stress-induced accumulations of inorganic polyphosphate in Escherichia coli.* Journal of Bacteriology, 1998. **180**(7): p. 1841-7.

294. Sweeney, B.M. and G.B. Bouck, *Crystal-like particles in luminous and non-luminous dinoflagellates*, in *Bioluminescence in Progress*, F.H. Johnson and Y. Haneda, Editors. 1966, Princeton University Press: Princeton, New York. p. 331-348.

295. Jantschke, A., et al., *Anhydrous β-guanine crystals in a marine dinoflagellate: Structure and suggested function.* Journal of Structural Biology, 2019. **207**(1): p. 12-20.

296. Taylor, D.L., *In situ studies on the cytochemistry and ultrastructure of a symbiotic marine dinoflagellate.* Journal of the Marine Biological Association of the United Kingdom, 2009. **48**(2): p. 349-366.

297. Kevin, M.J., et al., *Symbiodinium microadriaticum Freudenthal, a revised taxonomic description, ultrastructure.* Journal of Phycology, 1969. **5**(4): p. 341-50.

298. Strychar, K.B., P.W. Sammarco, and T.J. Piva, *Apoptotic and necrotic stages of Symbiodinium (Dinophyceae) cell death activity: bleaching of soft and scleractinian corals.* Phycologia, 2019. **43**(6): p. 768-777.

299. Krueger, T., et al., *Temperature and feeding induce tissue level changes in autotrophic and heterotrophic nutrient allocation in the coral symbiosis - A NanoSIMS study.* Scientific Reports, 2018. **8**(1): p. 12710.

300. Kopp, C., et al., *Highly dynamic cellular-level response of symbiotic coral to a sudden increase in environmental nitrogen.* mBio, 2013. **4**(3): p. e00052-13.

301. DeSa, R. and J.W. Hastings, *The characterization of scintillons. Bioluminescent particles from the marine dinoflagellate, Gonyaulax polyedra.* Journal of General Physiology, 1968. **51**(1): p. 105-22.

302. Waite, M. and G. Walker, *Guanine in Balanus balanoides (L.) and Balanus crenatus Bruguière.* Journal of Experimental Marine Biology and Ecology, 1984. **77**(1-2): p. 11-21.

303. Mojzeš, P., et al., *Guanine, a high-capacity and rapid-turnover nitrogen reserve in microalgal cells.* Proceedings of the National Academy of Sciences of the United States of America, 2020. **117**(51): p. 32722-32730.

304. Roush, A.H., *Crystallization of purines in the vacuole of Candida utilis.* Nature, 1961. **190**(4774): p. 449.

305. Soldo, A.T. and W. Van Wagtendonk, *Nitrogen metabolism in Paramecium aurelia.* The Journal of Protozoology, 1961. **8**(1): p. 41-55.

306. Soldo, A., G. Godoy, and F. Larin, *Purine-excretory nature of refractile bodies in the marine ciliate Parauronema acutum.* The Journal of Protozoology, 1978. **25**(3): p. 416-418.

307. Schmitter, R.E., *The fine structure of Gonyaulax polyedra, a bioluminescent marine dinoflagellate.* Journal of Cell Science, 1971. **9**(1): p. 147-73.

308. Lewis, J. and P. Burton, *A study of newly excysted cells of Gonyaulax-polyedra (Dinophyceae) by electron-microscopy.* British Phycological Journal, 1988. **23**(1): p. 49-60.

309. Clode, P.L., et al., *Uric acid deposits in symbiotic marine algae.* Plant Cell and Environment, 2009. **32**(2): p. 170-177.

310. Tuschel, D., *Why are the Raman spectra of crystalline and amorphous solids different?* 2017.

311. Van Zee, R.J. and A.U. Khan, *Striking deuterium effect in phosphorus chemiluminescence. Identification of the emitting species.* Journal of the American Chemical Society, 1974. **96**(21): p. 6805-6806.

312. Nitschke, J.R., *The two faces of phosphorus.* Nature Chemistry, 2011. **3**(1): p. 90.

313. Ashley, K., D. Cordell, and D. Mavinic, *A brief history of phosphorus: from the philosopher's stone to nutrient recovery and reuse.* Chemosphere, 2011. **84**(6): p. 737-46.

314. Krafft, F., *Phosphorus. From elemental light to chemical element.* Angewandte Chemie International Edition in English, 1969. **8**(9): p. 660-71.

315. Dorozhkin, S.V., *A history of calcium orthophosphates (CaPO4) and their biomedical applications.* Morphologie, 2017. **101**(334): p. 143-153.

316. von Liebig, J.F., *Die organische Chemie in ihrer Anwendung auf Agricultur und Physiologie*. 1840: F. Vieweg und Sohn.

317. White, J. and K. Reddy, *Influence of phosphorus loading on organic nitrogen mineralization of Everglades soils.* Soil Science Society of America Journal, 2000. **64**(4): p. 1525-1534.

318. Bennett, E.M., S.R. Carpenter, and N.F. Caraco, *Human impact on erodable phosphorus and eutrophication: a global perspective: increasing accumulation of phosphorus in soil threatens rivers, lakes, and coastal oceans with eutrophication.* Bioscience, 2001. **51**(3): p. 227-234.

319. Hinsinger, P., *Bioavailability of soil inorganic P in the rhizosphere as affected by root-induced chemical changes: A review*, in *Plant and Soil*. 2001, Kluwer Academic Publishers. p. 173-195.

320. Cembella, A.D., N.J. Antia, and P.J. Harrison, *The utilization of inorganic and organic phosphorous compounds as nutrients by eukaryotic microalgae: A multidisciplinary perspective: Part I.* CRC Critical Reviews in Microbiology, 1982. **10**(4): p. 317-391.

321. Otsuki, A. and R.G. Wetzel, *Coprecipitation of phosphate with carbonates in a marl lake.* Limnology and Oceanography, 1972. **17**(5): p. 763-767.

322. Sedlak, R.I., *Phosphorus and Nitrogen Removal from Municipal Wastewater*. CRC Press. 1991: CRC Press. 256.

323. Smith, E., C. Mayfield, and P. Wong, *Naturally occurring apatite as a source of orthophosphate for growth of bacteria and algae.* Microbial Ecology, 1977. **4**(2): p. 105-117.

324. Morse, G., et al., *Review: Phosphorus removal and recovery technologies.* The Science of the Total Environment, 1998. **212**(1): p. 69-81.

325. Weimberg, R. and W.L. Orton, *Synthesis and Breakdown of the Polyphosphate Fraction and Acid Phosphomonoesterase of Saccharomyces mellis and Their Locations in the Cell.* Journal of Bacteriology, 1965. **89**(3): p. 740-747.

326. Ricketts, T.R., *Inorganic pyrophosphatase in Prymnesium parvum Carter.* Archives of Biochemistry and Biophysics, 1965. **110**(1): p. 184-90.

327. Keefe, A.D. and S.L. Miller, *Are polyphosphates or phosphate esters prebiotic reagents?* Journal of Molecular Evolution, 1995. **41**(6): p. 693-702.

328. Kulaev, I.S., V. Vagabov, and T. Kulakovskaya, *The biochemistry of inorganic polyphosphates*. 2005.

329. Kulaev, I.S., *Biochemistry of inorganic polyphosphates.* Reviews of Physiology, Biochemistry and Pharmacology, 1975. **73**(Chapter 5): p. 131-58.

330. Schlegel, H.G., *General Microbiology*. Cambridge University Press. 1993: Cambridge University Press. 655.

331. Tyagi, R.D., et al., *Sustainable sludge management: production of value added products.* American Society of Civil Engineers, 2009: p. 352.

332. Harold, F.M., *Inorganic polyphosphates in biology: structure, metabolism, and function.* Bacteriological Reviews, 1966. **30**(4): p. 772-94.

333. Ogawa, N., et al., *Inorganic polyphosphate in Vibrio cholerae: genetic, biochemical, and physiologic features.* Journal of Bacteriology, 2000. **182**(23): p. 6687-93.

334. Manganelli, R., *Polyphosphate and stress response in mycobacteria.* Molecular Microbiology, 2007. **65**(2): p. 258-60.

335. Kornberg, A., N.N. Rao, and D. Ault-Riche, *Inorganic polyphosphate: a molecule of many functions.* Annual Review of Biochemistry, 1999. **68**: p. 89-125.

336. Kornberg, A., *Inorganic polyphosphate: toward making a forgotten polymer unforgettable.* Journal of Bacteriology, 1995. **177**(3): p. 491-6.

337. Zhu, J., et al., *A genetically validated approach for detecting inorganic polyphosphates in plants.* The Plant Journal, 2020. **102**(3): p. 507-516.

338. Miyachi, S. and H. Tamiya, *Distribution and turnover of phosphate compounds in growing Chlorella cells.* Plant and Cell Physiology, 1961. **2**(4): p. 405-414.

339. Tewari, K. and M. Singh, *Acid soluble and acid insoluble inorganic polyphosphates in Cuscuta reflexa.* Phytochemistry, 1964. **3**(2): p. 341-347.

340. Werner, T.P., *Quantification and localization of inorganic polyphosphate in fungi and algae*, in *Zurich ETH*. 2007.

341. Aksoy, M., W. Pootakham, and A.R. Grossman, *Critical function of a Chlamydomonas reinhardtii putative polyphosphate polymerase subunit during nutrient deprivation.* The Plant Cell, 2014. **26**(10): p. 4214-4229.

342. Jensen, T.E., et al., *Aspects of phosphate utilization by blue-green algae*. 1976. 122.

343. Grillo, J.F. and J. Gibson, *Regulation of phosphate accumulation in the unicellular cyanobacterium Synechococcus.* Journal of Bacteriology, 1979. **140**(2): p. 508-17.

344. Gomez-Garcia, M.R., M. Losada, and A. Serrano, *Concurrent transcriptional activation of ppa and ppx genes by phosphate deprivation in the cyanobacterium Synechocystis sp. strain PCC 6803.* Biochemical and Biophysical Research Communications, 2003. **302**(3): p. 601-9.

345. Goodenough, U., et al., *Acidocalcisomes: ultrastructure, biogenesis, and distribution in microbial eukaryotes.* Protist, 2019. **170**(3): p. 287-313.

346. Jensen, T. and W. Corpe, *Elemental composition of the polyphosphate bodies in microbial cells from a small lake.* Archiv für Hydrobiologie, 1993. **127**(4): p. 385-393.

347. Docampo, R., P. Ulrich, and S.N. Moreno, *Evolution of acidocalcisomes and their role in polyphosphate storage and osmoregulation in eukaryotic microbes.* Philosophical Transactions of the Royal Society B: Biological Sciences, 2010. **365**(1541): p. 775-784.

348. Tsednee, M., et al., *Manganese co-localizes with calcium and phosphorus in Chlamydomonas acidocalcisomes and is mobilized in manganese-deficient conditions.* Journal of Biological Chemistry, 2019. **294**(46): p. 17626-17641.

349. Martin, P., et al., *Accumulation and enhanced cycling of polyphosphate by Sargasso Sea plankton in response to low phosphorus.* Proceedings of the National Academy of Sciences of the United States of America, 2014. **111**(22): p. 8089-94.

350. Vercesi, A.E., S.N. Moreno, and R. Docampo, *Ca2+/H+ exchange in acidic vacuoles of Trypanosoma brucei.* Biochemical Journal, 1994. **304 (Pt 1)**: p. 227-33.

351. Pestov, N.A., T.V. Kulakovskaya, and I.S. Kulaev, *Inorganic polyphosphate in mitochondria of Saccharomyces cerevisiae at phosphate limitation and phosphate excess.* Fems Yeast Research, 2004. **4**(6): p. 643-648.

352. Abramov, A.Y., et al., *Targeted polyphosphatase expression alters mitochondrial metabolism and inhibits calcium-dependent cell death.* Proceedings of the National Academy of Sciences of the United States of America, 2007. **104**(46): p. 18091-6.

353. Docampo, R., et al., *Acidocalcisomes - conserved from bacteria to man.* Nature Reviews Microbiology, 2005. **3**(3): p. 251-61.

354. Miranda, K., et al., *Acidocalcisomes in Apicomplexan parasites.* Experimental Parasitology, 2008. **118**(1): p. 2-9.

355. Docampo, R., *The origin and evolution of the acidocalcisome and its interactions with other organelles.* Molecular and Biochemical Parasitology, 2016. **209**(1-2): p. 3-9.

356. Docampo, R. and G. Huang, *Acidocalcisomes of eukaryotes.* Curr Opin Cell Biol, 2016. **41**: p. 66-72.

357. Werner, T.P., N. Amrhein, and F.M. Freimoser, *Inorganic polyphosphate occurs in the cell wall of Chlamydomonas reinhardtii and accumulates during cytokinesis.* BMC Plant Biology, 2007. **7**: p. 51.

358. Van Mooy, B.A., et al., *Phytoplankton in the ocean use non-phosphorus lipids in response to phosphorus scarcity.* Nature, 2009. **458**(7234): p. 69-72.

359. Murata, K., et al., *Ultrastructure of compacted DNA in cyanobacteria by high-voltage cryo-electron tomography.* Scientific Reports, 2016. **6**: p. 34934.

360. Binder, B.J. and S.W. Chisholm, *Relationship between DNA cycle and growth rate in Synechococcus sp. strain PCC 6301.* Journal of Bacteriology, 1990. **172**(5): p. 2313-9.

361. Binder, B.J. and S.W. Chisholm, *Cell cycle regulation in marine Synechococcus sp. strains.* Applied and Environmental Microbiology, 1995. **61**(2): p. 708-17.

362. Mori, T., B. Binder, and C.H. Johnson, *Circadian gating of cell division in cyanobacteria growing with average doubling times of less than 24 hours.*

Proceedings of the National Academy of Sciences of the United States of America, 1996. **93**(19): p. 10183-8.

363. Watanabe, S., et al., *Light-dependent and asynchronous replication of cyanobacterial multi-copy chromosomes.* Molecular Microbiology, 2012. **83**(4): p. 856-65.

364. Ohbayashi, R., et al., *DNA replication depends on photosynthetic electron transport in cyanobacteria.* FEMS Microbiology Letters, 2013. **344**(2): p. 138-44.

365. Seki, Y., K. Nitta, and Y. Kaneko, *Observation of polyphosphate bodies and DNA during the cell division cycle of Synechococcus elongatus PCC 7942.* Plant Biology, 2014. **16**(1): p. 258-63.

366. Orchard, E.D., et al., *Polyphosphate in Trichodesmium from the low-phosphorus Sargasso Sea.* Limnology and Oceanography, 2010. **55**(5): p. 2161-2169.

367. Diaz, J.M., et al., *Polyphosphate dynamics at S tation ALOHA, N orth P acific subtropical gyre.* Limnology And Oceanography, 2016. **61**(1): p. 227-239.

368. Dijkstra, N., et al., *Phosphorus dynamics in and below the redoxcline in the Black Sea and implications for phosphorus burial.* Geochimica et Cosmochimica Acta, 2018. **222**: p. 685-703.

369. Martin, P., et al., *Particulate polyphosphate and alkaline phosphatase activity across a latitudinal transect in the tropical Indian Ocean.* Limnology and Oceanography, 2018. **63**(3): p. 1395-1406.

370. Bental, M., et al., *Metabolic studies with NMR spectroscopy of the alga Dunaliella salina trapped within agarose beads.* European Journal of Biochemistry, 1990. **188**(1): p. 111-6.

371. Leitão, J.M., et al., *Osmotic-stress-induced synthesis and degradation of inorganic polyphosphates in the alga Phaeodactylumtricornutum.* Marine Ecology Progress Series, 1995. **121**: p. 279-288.

372. van Groenestijn, J.W., et al., *Polyphosphate-degrading enzymes in Acinetobacter spp. and activated sludge.* Applied and Environmental Microbiology, 1989. **55**(1): p. 219-23.

373. Rao, N.N. and A. Kornberg, *Inorganic polyphosphate regulates responses of Escherichia coli to nutritional stringencies, environmental stresses and survival in the stationary phase.* Progress in Molecular and Subcellular Biology, 1999. **23**: p. 183-95.

374. Andreeva, N., et al., *Cytoplasmic inorganic polyphosphate participates in the heavy metal tolerance of Cryptococcus humicola.* Folia Microbiologica, 2014. **59**(5): p. 381-9.

375. Barcyte, D., et al., *The arctic cylindrocystis (Zygnematophyceae, Streptophyta) green algae are genetically and morphologically diverse and exhibit effective accumulation of polyphosphate.* Journal of Phycology, 2020. **56**(1): p. 217-232.

376. Reusch, R.N., *Transmembrane ion transport by polyphosphate/poly-(R)-3-hydroxybutyrate complexes.* Biochemistry (Mosc), 2000. **65**(3): p. 280-95.

377. Reusch, R.N., *Polyphosphate/poly-(R)-3-hydroxybutyrate) ion channels in cell membranes.* Progress in Molecular and Subcellular Biology, 1999. **23**: p. 151-82.

378. Gray, M.J., et al., *Polyphosphate is a primordial chaperone.* Molecular Cell, 2014. **53**(5): p. 689-99.

379. Xie, L. and U. Jakob, *Inorganic polyphosphate, a multifunctional polyanionic protein scaffold.* Journal of Biological Chemistry, 2019. **294**(6): p. 2180-2190.

380. Azevedo, C., T. Livermore, and A. Saiardi, *Protein polyphosphorylation of lysine residues by inorganic polyphosphate.* Molecular Cell, 2015. **58**(1): p. 71-82.

381. Chiu, C.H. and U. Paszkowski, *Mechanisms and impact of symbiotic phosphate acquisition.* Cold Spring Harbor Perspectives In Biology, 2019. **11**(6): p. a034603.

382. Penen, F., et al., *Pools of cadmium in Chlamydomonas reinhardtii revealed by chemical imaging and XAS spectroscopy.* Metallomics, 2017. **9**(7): p. 910-923.

383. Roewe, J., et al., *Bacterial polyphosphates interfere with the innate host defense to infection.* Nature Communications, 2020. **11**(1): p. 4035.

384. Brown, M.R.W. and A. Kornberg, *Inorganic polyphosphate in the origin and survival of species*, in *Proceedings Of The National Academy Of Sciences Of The United States Of America*. 2004. p. 16085-16087.

385. Brown, M.R. and A. Kornberg, *The long and short of it - polyphosphate, PPK and bacterial survival.* Trends in Biochemical Sciences, 2008. **33**(6): p. 284-90.

386. Hooley, P., M.P. Whitehead, and M.R. Brown, *Eukaryote polyphosphate kinases: is the 'Kornberg' complex ubiquitous?* Trends in Biochemical Sciences, 2008. **33**(12): p. 577-82.

387. Hothorn, M., et al., *Catalytic core of a membrane-associated eukaryotic polyphosphate polymerase.* Science, 2009. **324**(5926): p. 513-6.

388. Akiyama, M., E. Crooke, and A. Kornberg, *An exopolyphosphatase of Escherichia coli. The enzyme and its ppx gene in a polyphosphate operon.* Journal of Biological Chemistry, 1993. **268**(1): p. 633-9.

389. Rodrigues, C.O., et al., *An acidocalcisomal exopolyphosphatase from Leishmania major with high affinity for short chain polyphosphate.* Journal of Biological Chemistry, 2002. **277**(52): p. 50899-906.

390. Fang, J., et al., *Overexpression of a Zn2+-sensitive soluble exopolyphosphatase from Trypanosoma cruzi depletes polyphosphate and affects osmoregulation.* Journal of Biological Chemistry, 2007. **282**(44): p. 32501-10.

391. Lichko, L.P., T.V. Kulakovskaya, and I.S. Kulaev, *Properties of partially purified endopolyphosphatase of the yeast Saccharomyces cerevisiae.* Biochemistry (Mosc), 2010. **75**(11): p. 1404-7.

392. Karl, D.M., *Nutrient dynamics in the deep blue sea.* Trends in Microbiology, 2002. **10**(9): p. 410-8.

393. Karl, D.M., *Microbially mediated transformations of phosphorus in the sea: new views of an old cycle.* Annual Review of Marine Science, 2014. **6**: p. 279-337.

394. Dyhrman, S.T. and B. Palenik, *Phosphate stress in cultures and field populations of the dinoflagellate Prorucentrum minimum detected by a single-cell alkaline phosphatase assay.* Applied And Environmental Microbiology, 1999. **65**(7): p. 3205-3212.

395. Riegman, R., et al., *Nutrient uptake and alkaline phosphatase (ec 3:1:3:1) activity ofemiliania huxleyi(PRYMNESIOPHYCEAE) during growth under n and p limitation in continuous cultures.* Journal of Phycology, 2001. **36**(1): p. 87-96.

396. Hoppe, H.-G., *Phosphatase activity in the sea.* Hydrobiologia, 2003. **493**(1/3): p. 187-200.

397. Dyhrman, S.T. and K.C. Ruttenberg, *Presence and regulation of alkaline phosphatase activity in eukaryotic phytoplankton from the coastal ocean: Implications for dissolved organic phosphorus remineralization.* Limnology and Oceanography, 2006. **51**(3): p. 1381-1390.

398. Bar-Yosef, Y., et al., *Enslavement in the water body by toxic Aphanizomenon ovalisporum, inducing alkaline phosphatase in phytoplanktons.* Current Biology, 2010. **20**(17): p. 1557-61.

399. Harke, M.J., et al., *Molecular response of the bloom-forming cyanobacterium, Microcystis aeruginosa, to phosphorus limitation.* Microbial Ecology, 2012. **63**(1): p. 188-98.

400. Reistetter, E.N., et al., *Effects of phosphorus starvation versus limitation on the marine cyanobacterium Prochlorococcus MED4 II: gene expression.* Environmental Microbiology, 2013. **15**(7): p. 2129-43.

401. Munoz-Martin, M.A., et al., *Monitoring bioavailable phosphorus in lotic systems: a polyphasic approach based on cyanobacteria.* Science of the Total Environment, 2014. **475**: p. 158-68.

402. Wan, L., et al., *Phosphorus strategy in bloom-forming cyanobacteria (Dolichospermum and Microcystis) and its role in their succession.* Harmful Algae, 2019. **84**: p. 46-55.

403. Björkman, K.M. and D.M. Karl, *Bioavailability of dissolved organic phosphorus in the euphotic zone at Station ALOHA, North Pacific Subtropical Gyre.* Limnology and Oceanography, 2003. **48**(3): p. 1049-1057.

404. Moseley, J. and A.R. Grossman, *Phosphate metabolism and responses to phosphorus deficiency*, in *The Chlamydomonas Sourcebook*. 2009, Elsevier. p. 189-215.

405. Harold, F.M., *Accumulation of Inorganic Polyphosphate in Aerobacter Aerogenes. I. Relationship to Growth and Nucleic Acid Synthesis.* Journal of Bacteriology, 1963. **86**(2): p. 216-21.

406. Harold, F.M., *Enzymic and genetic control of polyphosphate accumulation in aerobacter aerogenes.* Journal of General Microbiology, 1964. **35**(1): p. 81-90.

407. Voelz, H., U. Voelz, and R.O. Ortigoza, *The "polyphosphate overplus" phenomenon in Myxococcus xanthus and its influence on the architecture of the cell.* Archives of Microbiology, 1966. **53**(4): p. 371-88.

408. Aitchison, P.A. and V.S. Butt, *The relation between the synthesis of inorganic polyphosphate and phosphate uptake byChlorella vulgaris.* Journal of Experimental Botany, 1973. **24**(3): p. 497-510.

409. Karl, D., et al., *Dinitrogen fixation in the world's oceans.* Biogeochemistry, 2002. **57**(1): p. 47-98.

410. Hupfer, M., S. Gloess, and H.P. Grossart, *Polyphosphate-accumulating microorganisms in aquatic sediments.* Aquatic Microbial Ecology, 2007. **47**(3): p. 299-311.

411. Falkner, G. and R. Falkner, *The complex regulation of the phosphate uptake system of cyanobacteria*, in *Bioenergetic Processes of Cyanobacteria*. 2011, Springer. p. 109-130.

412. Voronkov, A. and M. Sinetova, *Polyphosphate accumulation dynamics in a population of Synechocystis sp. PCC 6803 cells under phosphate overplus.* Protoplasma, 2019. **256**(4): p. 1153-1164.

413. Chopin, T., H. Lehmal, and K. Halcrow, *Polyphosphates in the red macroalga Chondrus crispus (Rhodophyceae).* New Phytologist, 1997. **135**(4): p. 587-594.

414. Sicko-Goad, L. and D. Lazinsky, *Quantitative ultrastructural changes associated with lead-coupled luxury phosphate uptake and polyphosphate utilization.* Archives of Environmental Contamination and Toxicology, 1986. **15**(6): p. 617-627.

415. Siderius, M., et al., *Chlamydomonas eugametos (Chlorophyta) stores phosphate in polyphosphate bodies together with calcium1.* Journal of Phycology, 1996. **32**(3): p. 402-409.

416. Droop, M.R., *Some thoughts on nutrient limitation in algae.* Journal of Phycology, 1973. **9**(3): p. 264-272.

417. Falkner, R. and G. Falkner, *Distinct Adaptivity During Phosphate Uptake by the CyanobacteriumAnabaena variabilisReflects Information Processing About Preceding Phosphate Supply.* Journal of Trace And Microprobe Techniques, 2003. **21**(2): p. 363-375.

418. McMahon, K.D. and E.K. Read, *Microbial contributions to phosphorus cycling in eutrophic lakes and wastewater.* Annual Review of Microbiology, 2013. **67**: p. 199-219.

419. Dyhrman, S.T., et al., *The transcriptome and proteome of the diatom Thalassiosira pseudonana reveal a diverse phosphorus stress response.* Plos One, 2012. **7**(3): p. e33768.

420. Aksoy, M., et al., *Tiered regulation of sulfur deprivation responses in Chlamydomonas reinhardtii and identification of an associated regulatory factor.* Plant Physiology, 2013. **162**(1): p. 195-211.

421. Ota, S., et al., *Deciphering the relationship among phosphate dynamics, electron-dense body and lipid accumulation in the green alga Parachlorella kessleri.* Scientific Reports, 2016. **6**: p. 25731.

422. Samadani, M. and D. Dewez, *Cadmium accumulation and toxicity affect the extracytoplasmic polyphosphate level in Chlamydomonas reinhardtii.* Ecotoxicology and Environmental Safety, 2018. **166**: p. 200-206.

423. Samadani, M. and D. Dewez, *Effect of mercury on the polyphosphate level of alga Chlamydomonas reinhardtii.* Environmental Pollution, 2018. **240**: p. 506-513.

424. Samadani, M., J. El-Khoury, and D. Dewez, *Tolerance capacity of Chlamydomonas VHLR mutants for the toxicity of mercury.* Water, Air, & Soil Pollution, 2020. **231**(4).

425. Lawry, N.H. and T.E. Jensen, *Condensed phosphate deposition, sulfur amino acid use, and unidirectional transsulfuration in Synechococcus leopoliensis.* Archives of Microbiology, 1986. **144**(4): p. 317-323.

426. Lawry, N.H. and T.E. Jensen, *Deposition of condensed phosphate as an effect of varying sulfur deficiency in the cyanobacterium Synechococcus sp.(Anacystis nidulans).* Archives of Microbiology, 1979. **120**(1): p. 1-7.

427. Hong-Hermesdorf, A., et al., *Subcellular metal imaging identifies dynamic sites of Cu accumulation in Chlamydomonas.* Nature Chemical Biology, 2014. **10**(12): p. 1034-42.

428. Kuesel, A., et al., *P-31 in-vivo NMR investigation on the function of polyphosphates as phosphate-and energysource during the regreening of the green alga Chlorella fusca.* Archives of Microbiology, 1989. **152**(2): p. 167-171.

429. Chu, F.F., et al., *Phosphorus plays an important role in enhancing biodiesel productivity of Chlorella vulgaris under nitrogen deficiency.* Bioresource Technology, 2013. **134**: p. 341-6.

430. Chu, F.F., et al., *Polyphosphate during the Regreening of Chlorella vulgaris under Nitrogen Deficiency.* International Journal of Molecular Sciences, 2015. **16**(10): p. 23355-68.

431. Pick, U., et al., *Polyphosphate-hydrolysis--a protective mechanism against alkaline stress?* FEBS Letters, 1990. **274**(1-2): p. 15-8.

432. Field, C.B., et al., *Primary production of the biosphere: integrating terrestrial and oceanic components.* Science, 1998. **281**(5374): p. 237-40.

433. Cleveland, C.C., et al., *Relationships among net primary productivity, nutrients and climate in tropical rain forest: a pan-tropical analysis.* Ecology Letters, 2011. **14**(9): p. 939-947.

434. Harvey, H., *Nitrogen and phosphorus required for the growth of phytoplankton.* Journal of the Marine Biological Association of the United Kingdom, 1940. **24**(1): p. 115-123.

435. Browning, T.J., et al., *Iron limitation of microbial phosphorus acquisition in the tropical North Atlantic.* Nature Communications, 2017. **8**(1): p. 15465.

436. Schmollinger, S., et al., *Nitrogen-sparing mechanisms in Chlamydomonas affect the transcriptome, the proteome, and photosynthetic metabolism.* Plant Cell, 2014. **26**(4): p. 1410-1435.

437. Egeland, E.S., *Carotenoids*, in *The Physiology of Microalgae*, M.A. Borowitzka, J. Beardall, and J.A. Raven, Editors. 2016, Springer International Publishing: Cham. p. 507-563.

438. Turpin, D.H., *Effects of inorganic N availability on algal photosynthesis and carbon metabolism.* Journal of Phycology, 1991. **27**(1): p. 14-20.

439. Berges, J.A., et al., *Differential effects of nitrogen limitation on photosynthetic efficiency of photosystems I and II in microalgae.* Plant Physiology, 1996. **110**(2): p. 689-696.

440. Anderson, D.M., P.M. Glibert, and J.M. Burkholder, *Harmful algal blooms and eutrophication: nutrient sources, composition, and consequences.* Estuaries, 2002. **25**(4): p. 704-726.

441. Antia, N., P. Harrison, and L. Oliveira, *The role of dissolved organic nitrogen in phytoplankton nutrition, cell biology and ecology.* Phycologia, 1991. **30**(1): p. 1-89.

442. Ludwig, C., *The availability of different forms of nitrogen to a green alga.* American Journal of Botany, 1938. **25**(6): p. 448-458.

443. Berman, T. and S. Chava, *Algal growth on organic compounds as nitrogen sources.* Journal of Plankton Research, 1999. **21**(8).

444. Raven, J.A. and M. Giordano, *Combined nitrogen*, in *The physiology of microalgae*, M.A. Borowitzka, J. Beardall, and J.A. Raven, Editors. 2016, Springer. p. 143-154.

445. Carpenter, E.J., C.C. Remsen, and S.W. Watson, *Utilization of urea by some marine phytoplankters.* Limnology and Oceanography, 1972. **17**(2): p. 265-269.

446. Neilson, A.H. and T. Larsson, *The utilization of organic nitrogen for growth of algae: physiological aspects.* Physiologia Plantarum, 1980. **48**(4): p. 542-553.

447. Cain, B.J., *Nitrogen utilization in 38 freshwater chlamydomonad algae.* Canadian Journal of Botany, 1965. **43**(11): p. 1367-1378.

448. Pettersen, R. and G. Knutsen, *Uptake of guanine by synchronized Chlorella fusca.* Archives of Microbiology, 1974. **96**(1): p. 233-246.

449. Antia, N.J. and V. Chorney, *Nature of nitrogen compounds supporting phototrophic growth of marine cryptomonad Hemiselmis virescens.* The Journal of Protozoology, 1968. **15**(1): p. 198-201.

450. Antia, N.J., et al., *Comparative evaluation of certain organic and inorganic sources of nitrogen for phototrophic growth of marine microalgae.* Journal of the Marine Biological Association of the United Kingdom, 1975. **55**(3): p. 519-539.

451. Shah, N. and P.J. Syrett, *Uptake of guanine by the diatom, Phaeodactylum-tricornutum.* Journal of Phycology, 1982. **18**(4): p. 579-587.

452. Lisa, T., et al., *Utilization of adenine and guanine as nitrogen sources by Chlamydomonas reinhardtii cells.* Plant, Cell & Environment, 1995. **18**(5): p. 583-588.

453. Gooday, G., *A physiological comparison of the symbiotic alga Platymonas convolutae and its free-living relatives.* Journal of the Marine Biological Association of the United Kingdom, 1970. **50**(1): p. 199-208.

454. Shah, N. and P. Syrett, *The uptake of guanine and hypoxanthine by marine microalgae.* Journal of the Marine Biological Association of the United Kingdom, 1984. **64**(3): p. 545-556.

455. Shah, N. and P. Syrett, *Enzymes of purine metabolism in the diatom, Phaeodactylum tricornutum.* Journal of the Marine Biological Association of the United Kingdom, 1984. **64**(3): p. 557-562.

456. Syrett, P., et al., *Effects of nitrogen deprivation on rates of uptake of nitrogenous compounds by the diatom, Phaeodactylum tricornutum Bohlin.* New Phytologist, 1986. **102**(1): p. 39-44.

457. Roush, A.H., L.M. Questiaux, and A.J. Domnas, *The active transport and metabolism of purines in the yeast, Candida utilis.* Journal of Cellular Physiology, 1959. **54**(3): p. 275-86.

458. Jaworski, A., J.S. Kwiatkowski, and B. Lesyng, *Why isoguanine and isocytosine are not the components of the genetic code.* International Journal of Quantum Chemistry, 1985. **28**(S12): p. 209-216.

459. Roush, A.H. and T.R. Shieh, *Diffusion, active transport and metabolism of purines in the yeast Torulopsis candida.* Biochimica et Biophysica Acta, 1962. **61**(2): p. 255-64.

460. Svihla, G., J.L. Dainko, and F. Schlenk, *Ultraviolet microscopy of purine compounds in the yeast vacuole.* Journal of Bacteriology, 1963. **85**(2): p. 399-409.

461. Pettersen, R., *Control by ammonium of intercompartmental guanine transport in Chlorella.* Zeitschrift für Pflanzenphysiologie, 1975. **76**(3): p. 213-223.

462. Gold, K. and K.S. Pokorny, *Effects of carbon, nitrogen, and allopurinol on the abundance of participate inclusions in a marine dinoflagellate12.* Journal of Phycology, 1973. **9**(2): p. 225-229.

463. Douglas, A., *Uric acid utilization in Platymonas convolutae and symbiotic Convoluta roscoffensis.* Journal of the Marine Biological Association of the United Kingdom, 1983. **63**(2): p. 435-447.

464. Bode, V.C., R. Desa, and J.W. Hastings, *Daily rhythm of luciferin activity in Gonyaulax polyedra.* Science, 1963. **141**(3584): p. 913-5.

465. Schmitter, R.E., et al., *Dinoflagellate bioluminescence: a comparative study of invitro components.* Journal of Cellular Physiology, 1976. **87**(1): p. 123-34.

466. Desa, R., J.W. Hastings, and A.E. Vatter, *Luminescent "Crystalline" Particles: An Organized Subcellular Bioluminescent System.* Science, 1963. **141**(3587): p. 1269-70.

467. Fogel, M., R.E. Schmitter, and J.W. Hastings, *On the physical identity of scintillons: bioluminescent particles in Gonyaulax polyedra.* Journal of Cell Science, 1972. **11**(1): p. 305-17.

468. Antia, N. and V. Chorney, *Nature of the nitrogen compounds supporting phototrophic growth of the marine cryptomonad Hemiselmis virescens.* The Journal of Protozoology, 1968. **15**(1): p. 198-201.

469. Antia, N.J. and A.F. Landymore, *Physiological and ecological significance of the chemical instability of uric acid and related purines in sea water and marine algal culture medium.* Journal of the Fisheries Board of Canada, 1974. **31**(8): p. 1327-1335.

470. Jantschke, A., et al., *Biomineralization pathways in calcifying dinoflagellates: Uptake, storage in MgCaP-rich bodies and formation of the shell.* Acta Biomaterialia, 2020. **102**: p. 427-439.

471. Gur, D., et al., *Light manipulation by guanine crystals in organisms: biogenic scatterers, mirrors, multilayer reflectors and photonic crystals.* Advanced Functional Materials, 2017. **27**(6): p. 1603514.

472. Spector, D.L., *Dinoflagellates*. 2012: Academic Press.

473. Pokorny, K.S. and K. Gold, *Two morphological types of particulate inclusions in marine dinoflagellates.* Journal of Phycology, 1973. **9**(2): p. 218-224.

474. Palmer, B.A., et al., *The image-forming mirror in the eye of the scallop.* Science, 2017. **358**(6367): p. 1172-1175.

475. Hirsch, A., et al., *Biologically Controlled Morphology and Twinning in Guanine Crystals.* Angewandte Chemie International Edition in English, 2017. **56**(32): p. 9420-9424.

476. Miyashita, Y., M. Iwasaka, and H. Endo, *Chlorophyll fluorescence control in microalgae by biogenic guanine crystals.* Journal of Applied Physics, 2015. **117**(17): p. 17E130.

477. Iwasaka, M., *Effects of static magnetic fields on light scattering in red chromatophore of goldfish scale.* Journal of Applied Physics, 2010. **107**(9): p. 09B314.

478. Iwasaka, M., Y. Mizukawa, and Y. Miyashita, *Rapid magnetic wiper featuring biogenic guanine particles: Magnetic non-contact switching of opto-fluidic mirrors featuring biogenic guanine crystals.* Applied Physics Letters, 2014. **104**(2): p. 024108.

479. Iwasaka, M. and Y. Mizukawa, *Effect of intense magnetic fields on the convection of biogenic guanine crystals in aqueous solution.* Journal of Applied Physics, 2015. **117**(17): p. 17E127.

480. Jasinski, S.M., *Phosphate Rock.* 1999: p. 1-14.

481. Abelson, P.H., *A potential phosphate crisis.* Science, 1999. **283**(5410): p. 2015.

482. Chen, M. and T.E. Graedel, *A half-century of global phosphorus flows, stocks, production, consumption, recycling, and environmental impacts.* Global Environmental Change, 2016. **36**: p. 139-152.

483. Kirkham, M., *Agricultural use of phosphorus in sewage sludge.* Advances in Agronomy, 1982. **35**: p. 129-163.

484. Ajmal, P.Y., et al., *External gamma radiation levels and natural radioactivity in soil around a phosphate fertilizer plant at Mumbai.* Journal of Radioanalytical and Nuclear Chemistry, 2014. **300**(1): p. 23-27.

485. Sattari, S.Z., et al., *Residual soil phosphorus as the missing piece in the global phosphorus crisis puzzle.* Proceedings of the National Academy of Sciences, 2012. **109**(16): p. 6348-6353.

486. Innes, R., *Economics of agricultural residuals and overfertilization: Chemical fertilizer use, livestock waste, manure management, and environmental impacts.* Encyclopedia of energy, natural resource, and environmental economics, 2013: p. 2-3.

487. Gburek, W.J., et al., *Phosphorus management at the watershed scale: A modification of the phosphorus index.* Journal of Environmental Quality, 2000. **29**(1): p. 130-144.

488. Schoumans, O.F., et al., *Phosphorus management in Europe in a changing world.* Ambio, 2015. **44**(2): p. 180-192.

489. Butler, H.J., et al., *Using Raman spectroscopy to characterize biological materials.* Nature Protocols, 2016. **11**(4): p. 664-687.

490. Conley, D.J., et al., *Controlling eutrophication: nitrogen and phosphorus*. 2009, American Association for the Advancement of Science.

491. Tilman, D., S.S. Kilham, and P. Kilham, *Phytoplankton community ecology: the role of limiting nutrients.* Annual Review of Ecology and Systematics, 1982. **13**(1): p. 349-372.

492. Forchhammer, K. and R. Schwarz, *Nitrogen chlorosis in unicellular cyanobacteria - a developmental program for surviving nitrogen deprivation.* Environmental Microbiology, 2019. **21**(4): p. 1173-1184.

493. Watzer, B. and K. Forchhammer, *Cyanophycin synthesis optimizes nitrogen utilization in the unicellular cyanobacterium Synechocystis sp strain PCC 6803.* Applied and Environmental Microbiology, 2018. **84**(20): p. 18.

494. Yonamine, Y., et al., *Spatiotemporal monitoring of intracellular metabolic dynamics by resonance Raman microscopy with isotope labeling.* RSC Advances, 2020. **10**(28): p. 16679-16686.

495. Zhang, D., et al., *Drop coating deposition Raman spectroscopy of fluorescein isothiocyanate labeled protein.* Applied Spectroscopy, 2010. **64**(10): p. 1078-85.

496. Puppels, G., et al., *Laser irradiation and Raman spectroscopy of single living cells and chromosomes: sample degradation occurs with 514.5 nm but not with 660 nm laser light.* Experimental Cell Research, 1991. **195**(2): p. 361-367.

497. Zięba-Palus, J. and A. Michalska, *Photobleaching as a useful technique in reducing of fluorescence in Raman spectra of blue automobile paint samples.* Vibrational Spectroscopy, 2014. **74**: p. 6-12.

498. Pelletier, M. and R. Altkorn, *Efficient elimination of fluorescence background from Raman spectra collected in a liquid core optical fiber.* Applied Spectroscopy, 2000. **54**(12): p. 1837-1841.

499. Onogi, C. and H.-o. Hamaguchi, *Photobleaching of the ˂ Raman spectroscopic signature of life˃ and mitochondrial activity in Rho− budding yeast cells.* The Journal of Physical Chemistry B, 2009. **113**(31): p. 10942-10945.

500. Golcuk, K., et al., *Is photobleaching necessary for Raman imaging of bone tissue using a green laser?* Biochimica et Biophysica Acta (BBA)-Biomembranes, 2006. **1758**(7): p. 868-873.

501. Darvin, M., N. Brandt, and J. Lademann, *Photobleaching as a method of increasing the accuracy in measuring carotenoid concentration in human skin by Raman spectroscopy.* Optics and Spectroscopy, 2010. **109**(2): p. 205-210.

502. Schleusener, J., J. Lademann, and M.E. Darvin, *Depth-dependent autofluorescence photobleaching using 325, 473, 633, and 785 nm of porcine ear skin ex vivo.* Journal of Biomedical Optics, 2017. **22**(9): p. 091503.

503. Weng, J., et al., *Raman enhancement and photo-bleaching of organic dyes in the presence of chemical vapor deposition-grown graphene.* Nanomaterials 2017. **7**(10): p. 337.

504. Diaspro, A., et al., *Photobleaching*, in *Handbook of Biological Confocal Microscopy*. 2006, Springer. p. 690-702.

505. Dittrich, P. and P. Schwille, *Photobleaching and stabilization of fluorophores used for single-molecule analysis. with one-and two-photon excitation.* Applied Physics B, 2001. **73**(8): p. 829-837.

506. Lingvay, M., et al., *Photobleaching of Chlorophyll in Light-Harvesting Complex II Increases in Lipid Environment.* Frontiers in Plant Science, 2020. **11**(849).

507. Wang, Y., et al., *Metabolomic basis of laboratory evolution of butanol tolerance in photosynthetic Synechocystis sp. PCC 6803.* Microbial Cell Factories, 2014. **13**(1): p. 1-12.

508. LaPanse, A.J., A. Krishnan, and M.C. Posewitz, *Adaptive Laboratory Evolution for algal strain improvement: methodologies and applications.* Algal Research, 2020: p. 102122.

509. Hirota, R., et al., *Bacterial phosphate metabolism and its application to phosphorus recovery and industrial bioprocesses.* Journal of Bioscience and Bioengineering, 2010. **109**(5): p. 423-32.

510. Powell, N., *Biological phosphorus removal by microalgae in waste stabilisation ponds : a thesis presented in partial fulfilment of the requirements for the degree of*

Doctor of Philosophy in Environmental Engineering at Massey University, Palmerston North, New Zealand. 2009.

511. Ye, Y., J. Gan, and B. Hu, *Screening of phosphorus-accumulating fungi and their potential for phosphorus removal from waste streams.* Biotechnology and Applied Biochemistry, 2015. **177**(5): p. 1127-36.

512. Roy-Bolduc, A. and M. Hijri, *The use of mycorrhizae to enhance phosphorus uptake: a way out the phosphorus crisis.* Journal of Biopesticides, 2011. **2**(104): p. 1-5.

513. Patching, S.G., *Recent developments in nucleobase cation symporter-1 (NCS1) family transport proteins from bacteria, archaea, fungi and plants.* Journal of Biosciences, 2018. **43**(4): p. 797-815.

514. Keilin, J., *The biological significance of uric acid and guanine excretion.* Biological Reviews, 1959. **34**(3): p. 265-294.

515. Johnston, C. and J. Eales, *Influence of temperature and photoperiod on guanine and hypoxanthine levels in skin and scales of Atlantic salmon (Salmo salar) during parr–smolt transformation.* Journal of the Fisheries Board of Canada, 1968. **25**(9): p. 1901-1909.

516. Bagnara, J.T., *Pigment cells*, in *Biology of the Integument*. 1986, Springer. p. 136-149.

517. Maeda, M. and N. Taga, *Occurrence and distribution of deoxyribonucleic acid-hydrolyzing bacteria in sea water.* Journal of Experimental Marine Biology and Ecology, 1974. **14**(2): p. 157-169.

518. Shaw, G., *Purines*, in *Comprehensive Heterocyclic Chemistry*, A.R. Katritzky and C.W. Rees, Editors. 1984, Pergamon: Oxford. p. 499-605.

519. Yalkowsky, S.H., Y. He, and P. Jain, *Handbook of Aqueous Solubility Data*. Second ed. 2010, New York, U.S.A.: CRC Press.

520. Vogels, G.D. and C. Van der Drift, *Degradation of purines and pyrimidines by microorganisms.* Journal of Bacteriology, 1976. **40**(2): p. 403-68.

521. Gur, D., et al., *Guanine crystallization in aqueous solutions enables control over crystal size and polymorphism.* Crystal Growth & Design, 2016. **16**(9): p. 4975-4980.

522. Hirsch, A., et al., ≤ *Guanigma*≤ *: The revised structure of biogenic anhydrous guanine.* Chemistry of Materials, 2015. **27**(24): p. 8289-8297.

523. Albert, A. and D. Brown, *Purine studies. Part I. Stability to acid and alkali. solubility. Ionization. comparison with pteridines.* Journal of the Chemical Society (Resumed), 1954: p. 2060-2071.

524. Glynn, P., *Coral reef bleaching: ecological perspectives.* Coral Reefs, 1993. **12**(1): p. 1-17.

525. Hoegh-Guldberg, O., *Climate change, coral bleaching and the future of the world's coral reefs.* Marine and Freshwater Research, 1999. **50**(8): p. 839-866.

526. De'ath, G., et al., *The 27-year decline of coral cover on the Great Barrier Reef and its causes.* Proceedings of the National Academy of Sciences of the United States of America, 2012. **109**(44): p. 17995-17999.

527. Rosset, S., et al., *Phosphate deficiency promotes coral bleaching and is reflected by the ultrastructure of symbiotic dinoflagellates.* Marine Pollution Bulletin, 2017. **118**(1-2): p. 180-187.

528. Tanaka, Y., et al., *Effects of nitrate and phosphate availability on the tissues and carbonate skeleton of scleractinian corals.* Marine Ecology Progress Series, 2017. **570**: p. 101-112.

Chapter VI. Appendix

VI. A. Supplementary Information for Photobleaching

Photochemistry and Photobiology

Supplementary material for

Photobleaching of algal cells for rapid chemical mapping by Raman microscopy

Lu Gao*[1,2,3], Peter Mojzeš[1,2], Ladislav Nedbal[1]

1. Institute of Bio- and Geosciences/Plant Sciences (IBG-2), Forschungszentrum Jülich, Wilhelm-Johnen-Straße, D-52428 Jülich, Germany, [2]. Institute of Physics, Faculty of Mathematics and Physics, Charles University, Ke Karlovu 5, CZ-12116 Prague 2, Czech Republic, [3]. Faculty of Mathematics and Natural Sciences, Heinrich Heine University, Universitätsstraße 1, D-40225 Düsseldorf, Germany

*Corresponding author e-mail: lugao100@uni-duesseldorf.de (Lu Gao)

SUPPLEMENTARY MATERIAL for

Photobleaching of algal cells for rapid chemical mapping by Raman microscopy

Lu Gao*[1,2,3], Peter Mojzeš[1,2], Ladislav Nedbal[1]

[1]. Institute of Bio- and Geosciences/Plant Sciences (IBG-2), Forschungszentrum Jülich, Wilhelm-Johnen-Straße, D-52428 Jülich, Germany, [2]. Institute of Physics, Faculty of Mathematics and Physics, Charles University, Ke Karlovu 5, CZ-12116 Prague 2, Czech Republic, [3]. Faculty of Mathematics and Natural Sciences, Heinrich Heine University, Universitätsstraße 1, D-40225 Düsseldorf, Germany

*Corresponding author e-mail: lugao100@uni-duesseldorf.de (Lu Gao)

This file includes:

Supplementary text
Figure S1 and S2
Tables S1 and S2
SI References

SUPPLEMENTARY TEXT

Sample preparation: The samples for all Raman measurements were prepared by the same method (1). Usually, 0.5 mL algal suspension was centrifuged for 2500xg, 30 s, and discarded its supernatant to condense the cultures. The equal volume (µL) of the pellet and 2% w/v low-melting agarose (Sigma Aldrich, US) were mixed to immobilize the cells. 3 µL mixture was usually placed on a quartz slide sealing with a quartz coverslip by Covergrip sealant (Biotium, US). All chemicals used for the preparation of mediums, photo-inhibitors, and -sensitizers were purchased from Sigma-Aldrich (St. Louis, MO, USA).

Raman microscopy: The photobleaching kinetics were measured by the Raman microscope WITec alpha 300 RSA (WITec, Ulm, Germany) with the oil-immersion objective UPlanFLN 100x, NA 1.30 (Olympus, Tokyo, Japan). The samples were irradiated with mainly 532nm laser (Compass Sapphire, Coherent, USA), which delivered maximum power ca. 52 mW and 28mW in-focus. We also applied a 785nm laser (single-mode laser StarBright785S AB, Sweden) with maximum power 310mW and 90mW in-focus. The power was measured by an inner power meter (Thorlabs, Newton, New Jersey). The spectrographs and CCD detectors are UHTS 300S, 600 gr/mm and Newton EMCCD (DU970N BVF-353), 1600 x 200 pxs, 16 mm x 16 mm, -95°C for blue-green visible range and UHTS 400S, 300 gr/mm and iDUS (DU401A-BR-DD-352), 1024 x 128 pxs, 26 mm x 26 mm, -95°C for red-near IR range (WITec, Ulm, Germany), respectively.

The multiple laser mapping was studied by an inverted Raman microscope LabRam Evolution (Horiba Scientific, Longjumeau, France) with 532 nm laser excitation (10 mW excitation power at the focal plane) and using the water-immersion objective Plan Apo VC 60×, NA 1.20 (Nikon, Minato, Japan). The spectrograph was equipped with a 150 gr/mm grating providing a spectral resolution of 9 cm^{-1}. Raman mapping was conducted with 500 nm steps in both directions, and with two accumulations, each of 0.3 s integration time at each voxel. Every time after changing the wavelengths, the system was re-calibrated.

Photobleaching, data treatments and analysis: A low-power wide-area photobleaching of each sample and the subsequent Raman measurements were performed as described in (1) also as shown in Figure 1. Under the microscopy, the cell was focused at first and then defocused for +30 µm. The acquisition time for each spectrum was 0.1s × 600 steps. Repeat the measurements at least 4 times replicates. Control was measured at the beginning of every series to ensure the feasibility of comparisons. The measurement time lengths in each live algal cell usually were not less than 30 seconds but it kept as fast as possible to ensure the proper data analysis, to measure as many cells in a certain time, and avoid artifacts from cell movement.

After background subtractions, the photobleaching spectra with time has to plateau at intensity approximately to 0; otherwise approximately to the instrumental noises. The average plateau is 667.0 ± 4.2 rel. for green laser CCD, Newton EMCCD (DU970N BVF-353).

Photobleaching: The mass production of ROS might enhance photobleaching to destruct the photosensitive excited fluorescent compounds, especially the potential of singlet oxygen (2-4). By that, the highly reactive singlet state attacks the donating species to cleavage the bond. Thus, ROS could oxidize fluorescent chlorophyll to non-fluorescent pheophytin and also eliminate carotenoids to achieve photobleaching. However, singlet oxygen sensitizers as pigments, such as bengal rose, hypericin or merocyanine 54, are not suitable for accelerating photobleaching due to inducing extra autofluorescence background. This inconvenience may also apply for hydroxyl and superoxide radicals' generators. Table SI1 lists the name and concentration of chemicals in this study for Figure 4. Usually, 20-min reaction time was allowed that chemicals can permeate cell and organelle membranes.

<Table S1>

Chemical fixation: Fixation by glutaraldehyde and formalin is usually considered to maintain cellular integrity (5). Photobleaching in 1% glutaraldehyde- and 4% formalin-fixed cells was studied to provide the opportunities to decouple algal sampling with Raman measurement. The retained photosynthetic abilities (6) might explain photobleaching occurring in both yielded cells (Fig.4). Unlike photobleaching in glutaraldehyde-fixed cells, photobleaching in formalin-fixed cells is as effective as in living cells (Figure 4). Formalin fixation can be used to limit autofluorescence for fluorescence microscopy (7, 8) while glutaraldehyde-based fixation increases the level of autofluorescence (7, 9). Moreover, after photobleaching, Raman mapping was conducted to the guanine-rich cells after fixations. Formalin-fixed cells can be

characterized by Raman mapping that reveals the intracellular components, including guanine crystals and carotenoids (Figure 5). The quality of the Raman map is comparable to that obtained with fresh cells before formalin fixation. Further, the same guanine-rich algal cells were heat-induced for 30-min before fixation to inactivate Photosystem II. Ineffective photobleaching occurred for both pre-heat-induced glutaraldehyde- and formalin-fixed cells. Formalin-fixed cells were performance as bad as the cell before fixation. No valid signal can be measured in glutaraldehyde-fixed cells. The performance was recorded in Table S2.

Formalin fixation provides a practical solution, especially for rapid dynamic changes in algae or situations, which cannot do Raman measurements *in situ*. Interestingly, formalin was observed to induce the fluorescence background within ca. 1-hour after fixation. It does not invalidate formalin's applicability because fixation might take several hours to complete (10). Particularly, phosphate-buffered formalin was not considered in case of any interaction by adding phosphate to algae during the long period of fixation. Alcoholic formalin, formol acetic alcohol, and formaldehyde-glutaraldehyde mixtures were also not suitable because their performances were approximately as bad as glutaraldehyde.

<Table S2>

SUPPLEMENTARY FIGURES AND TABLES

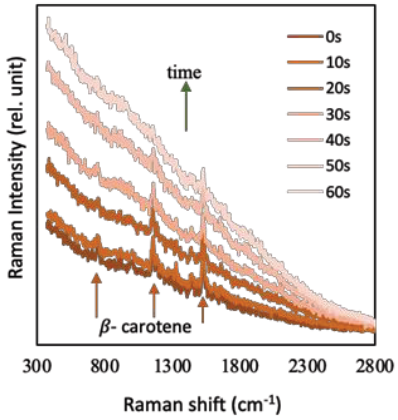

Figure S1. Time-evolution of Raman spectra of freshly harvested *C. vulgaris* C1 cell during the photobleaching by a defocused 785 nm laser beam. A gradual decrease of the carotenoid Raman signal accompanied by an increase of the fluorescence background of photoproducts was observed.

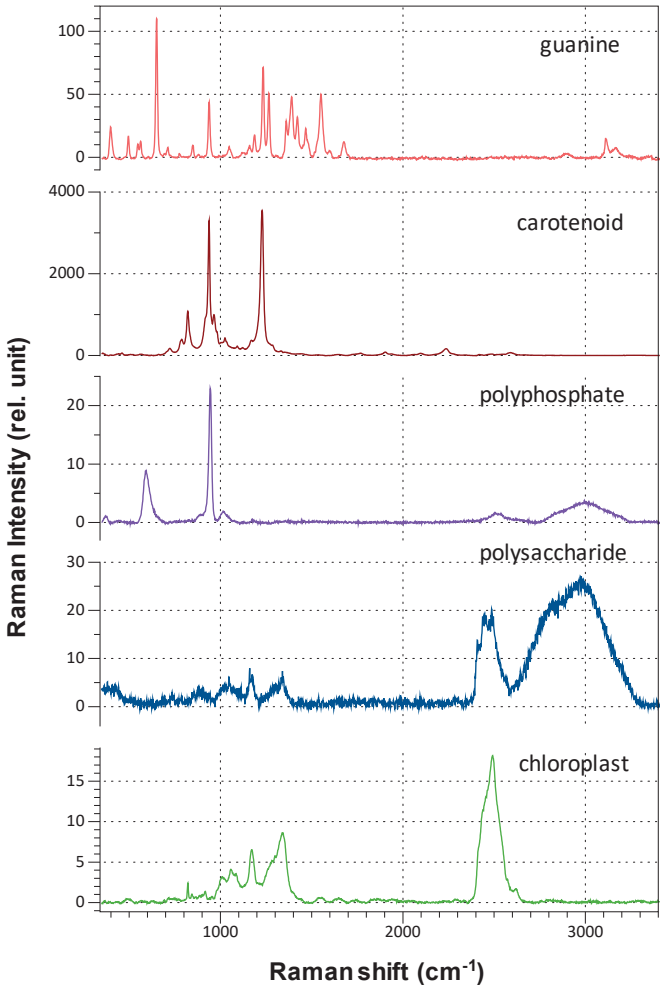

Figure S2. Raman spectra of guanine crystal, carotenoid, polyphosphate, polysaccharide, and chloroplast.

Table S1. The information of chemicals in this study.

Name and concentration	Sources
10uM 3-(3,4-dichlorophenyl)-1,1-dimethylurea	S8409-3KU, SIGMA
few grains sodium dithionite	CAT85,617-7, ALDRICH
56mM glucose/100nM glucose oxidase/1.5mM catalase	NA
glucose	G8270-1KG, SIGMA
glucose oxidase	G7141-10KU, SIGMA
1.5mM catalase	C1345-1G, SIGMA
20ug/mL superoxide dismutase	S8409-309-3KU, SIGMA
1mM methyl viologen	856177-250MG, SIGMA
2.50% or 0.05% hydrogen peroxide	#607-094-00-8, PENTA
1% glutaraldehyde	G5882-50ML, SIGMA
4% Formalin	F8775-500ML, SIGMA
1% glutaraldehyde + 0.05% hydrogen peroxide	NA
2mg/mL rose bengal	MKCC4630, ALDRICH

	Photobleaching	***Raman mapping***
guanine-rich (positive control) in situ	fast (ca. within 20 s), completely pale cells	carbohydrates, carotenoids, guanine-rich
glutaraldehyde fixation in situ	slow (ca. 5-min), Chl left	carbohydrates, little or no guanine
formalin fixation in situ	fast (ca. within 20 s), Chl might be left	carbohydrates, carotenoids, guanine-rich
heat treatment for the positive control (negative control)	slow (ca. ≥ 10-min)	ca. only carbon backbone (C-H) to reveal cell structures
glutaraldehyde fixation for 60 °C heat-induced cells	slow (ca. ≥ 10-min)	no available signal
formalin fixation for heat-induced cells	slow (ca. ≥ 10-min)	ca. only carbon backbone (C-H) to reveal cell structures

Table S2. The summary of photobleaching and following Raman mapping in heat-induced and then chemically fixed cells.

REFERENCE

1. Š. Moudříková, P. Mojzeš, V. Zachleder, C. Pfaff, D. Behrendt, and L. Nedbal, *Raman and fluorescence microscopy sensing energy-transducing and energy-storing structures in microalgae.* Algal Research, 2016. **16**: p. 224-232.

2. K. McCluskey, E. Shaw, D.A. Lafontaine, and J.C. Penedo, *Single-molecule fluorescence of nucleic acids*, in *Fluorescence Spectroscopy and Microscopy*. 2014, Springer. p. 759-791.

3. A. Andreeva and M. Velitchkova, *Resonance Raman studies of carotenoid molecules within photosystem I particles.* Biotechnology & Biotechnological Equipment, 2009. **23**(sup1): p. 488-492.

4. M.V.S. Abarova, D. Lazarova, K. Stoitchkova, D. Stanoeva, and A. Andreeva, *Protective effect of histidine against pigment photobleaching in Photosystem I particles.* Journal of Optoelectronics and Advanced Materials, 2009. **11**(9): p. 1230-1233.

5. C. Hawes and B. Satiat-Jeunemaitre, *Plant cell biology: a practical approach*. 2001: Oxford University Press.

6. U.W. Hallier and R.B. Park, *Photosynthetic Light Reactions in Chemically Fixed Anacystis nidulans, Chlorella pyrenoidosa, and Porphyridium cruentum.* Plant Physiology, 1969. **44**(4): p. 535-9.

7. T.J. Staughton, C.J. McGillicuddy, and P.D. Weinberg, *Techniques for reducing the interfering effects of autofluorescence in fluorescence microscopy: improved detection of sulphorhodamine B-labelled albumin in arterial tissue.* Journal of Microscopy, 2001. **201**(Pt 1): p. 70-6.

8. Y. Sun, P. Ip, and A. Chakrabartty, *Simple Elimination of Background Fluorescence in Formalin-Fixed Human Brain Tissue for Immunofluorescence Microscopy.* Journal of Visualized Experiments, 2017(127): p. e56188.

9. K. Lee, S. Choi, C. Yang, H.C. Wu, and J. Yu, *Autofluorescence generation and elimination: a lesson from glutaraldehyde.* Chemical Communications, 2013. **49**(29): p. 3028-30.

10. J.A. Kiernan, *Formaldehyde, formalin, paraformaldehyde and glutaraldehyde: what they are and what they do.* Microscopy Today, 2000. **1**(5): p. 8-12.

PNAS
www.pnas.org

Supplementary material for

Guanine, a high-capacity and rapid-turnover nitrogen reserve in microalgal cells

PNAS
www.pnas.org

Supplementary Information for

Guanine, a high-capacity and rapid-turnover nitrogen reserve in microalgal cells

Peter Mojzeš[1,2], Lu Gao[2,3], Tatiana Ismagulova[4], Jana Pilátová[5], Šárka Moudříková[1], Olga Gorelova[4], Alexei Solovchenko[4,6], Ladislav Nedbal[2*], Anya Salih[7]

Corresponding author: Ladislav Nedbal
Email: l.nedbal@fz-juelich.de

This PDF file includes:

Other supplementary materials for this manuscript include the following:

I. Supplementary Information Text

I.1. Localization of guanine, lipids, chloroplasts, and starch by Raman microscopy (Fig. 1 in the main text). The images in Fig. S1 are complementary to those in Fig. 1 in the main text and show Raman maps of individual cell components in separate panels (D-O). The separate maps in Fig. S1 provide a more detailed information than the overlays in Fig. 1C–E (here repeated in Fig. S1 A-C). The method to obtain these maps is described in detail in SI II.1.C

I.2. Kinetics of guanine accumulation and maximum storage capacity (Figs. 2 in the main text). The mean amount of guanine accumulated per cell can be calculated from the drop in the guanine concentration in the supernatant (Fig. 2) and by normalization to cell density. We assumed that during the short uptake periods of our experimental treatments, the guanine was neither used for growth nor transformed into other chemical forms. This assumption was supported by the guanine accumulation analysis shown in Fig. 1.
Fig. S2 shows data used to calculate the guanine storage capacity of *A. carterae.* The most diluted experimental algal suspension (triangles in Figs. 2 and S2) took up only a fraction of the available guanine and by dividing this amount by the number of cells present, the resultant estimated maximal storage capacity of *A. carterae* cells was 143 ± 37 (SD) pg (guanine)·cell^{-1}.

I.3. Raman spectra of various purines and stable-isotope-labelled guanines (Figs. 4 and 5 in the main text). *Identification.* The chemical nature of the crystalline inclusions within cells was determined by comparing their Raman spectra with Raman spectra of reference samples (SI II.1.C.). Raman spectra of several purines, including crystalline guanine and uric acid, are shown in Fig. S4. Fig. S5 presents a comparison with various forms of uric acid. Raman spectra of calcite, calcium oxalate monohydrate, and calcium oxalate dihydrate that were earlier suspected to be present in algal inclusions are shown in Fig. S6.
Deuterium-labelling. Deuterated crystalline d_1-guanine, d_4-guanine, and d_5-guanine were used as reference samples. The materials and preparation are described in SI II.2.A. Raman spectra of these isotopically-labeled deuterium-guanine forms can be easily distinguished due to their distinct spectral fingerprints (Fig. S7).
^{15}N-labelling. To distinguish the N-source of guanine biosynthesized *de novo* from the compounds constituting N-sources in the media commonly used for microalgal cultivation (*i.e.*, nitrate, ammonium, urea), and to eliminate any doubt about the origin of the endogenous guanine, isotopically labeled ^{15}N-compounds were used as the alternative N-sources. Consequently, ^{15}N-guanine newly biosynthesized from specific exogenous ^{15}N-sources was easily distinguished from the preexisting ^{14}N-guanine or from ^{14}N-guanine recycled from degraded cellular components. Spectral differences between Raman spectra of crystalline ^{14}N- and ^{15}N-guanine are highlighted in Fig. S8.

I.4. In situ chemical identification of inclusions in diverse algal species (Tab.1 in the main text). Diverse algal species listed in the table below together with their origin were tested in cultivation media and under conditions recommended for their cultivation by the source collections (Table S1) as further specified in SI II.3.

Species	Origin.	Code
Symbiodiniaceae	Isolates. *Symbiodiniaceae* cells were isolated from tissues of various cnidarian species (*Aiptasia* sp., *Euphyllia paraancora*, *Rhodactis indosinensis*, *Sinularia asterolobata*, *Zoanthus* sp.) purchased from the local marine aquarium shops. Regardless of their origin, all *Symbiodiniaceae* cells contained crystalline guanine unless their host was exposed to long-term (at least 3 months) nitrogen deficiency.	
Amphidinium carterae	**MCNA** - National Center for Marine Algae and Microbiota, Bigelow, USA	CCMP1314
Chromera velia	**MCNA** - National Center for Marine Algae and Microbiota, Bigelow, USA	CCMP2878
Microchloropsis gaditana	**NIES** - National Institute for Environmental Studies, Tsukuba, Japan	NIES-2587

Vacuoliviride crystalliferum	**NIES** - National Institute for Environmental Studies, Tsukuba, Japan	NIES-2860
Vischeria sp.	**CAUP** - Culture Collection of Algae of Charles University, Prague, Czech Republic	Q202
Trachydiscus minutus	**CCALA** - Culture Collection of Autotrophic Organisms of the Institute of Botany of the Czech Academy of Science, Třeboň, Czech Republic	838
Synura petersenii	**CAUP** - Culture Collection of Algae of Charles University, Prague, Czech Republic	Q13
Lobosphaera incisa	**CAUP** - Culture Collection of Algae of Charles University, Prague, Czech Republic	H4301
Desmodesmus quadricauda	**CCALA** - Culture Collection of Autotrophic Organisms of the Institute of Botany of the Czech Academy of Science, Třeboň, Czech Republic	463
Chlamydomonas reinhardtii	**CRC** - Chlamydomonas Resource Center, University of Minnesota, St. Paul, USA	CC-1690
Dunaliella acidophila	**CAUP** - Culture Collection of Algae of Charles University, Prague, Czech Republic	G301
Haematococcus pluvialis	**CAUP** - Culture Collection of Algae of Charles University, Prague, Czech Republic	G1002
Klebsormidium flaccidum	**NIES** - National Institute for Environmental Studies, Tsukuba, Japan	NIES-2285

I.5 Detection of guanine in symbiotic dinoflagellates in intact corals and in extracted algae (Fig. 7 in the main text). Following the enrichment of the artificial seawater (prepared from Reef Crystals sea salt, Aquarium Systems, Sarrebourg, France) in aquaria by 0.3 mM ^{15}N-$NaNO_3$ as a sole source of N, the newly synthesized ^{15}N-guanine crystals re-appeared within 24 hours inside endosymbionts of *Euphylia paraancora* as was documented by the respective Raman spectra (SI II.1.C.) that precisely distinguished between ^{14}N- and ^{15}N-guanine (Fig. 6C, Fig. S14C). To the best of our knowledge, this is the first *in situ* identification of crystalline guanine within the intact symbiotic zooxanthellae directly in tissues of several anthozoan species.
Symbiodiniaceae within cnidarians obtained from a commercial marine store and maintained under optimal nutrient conditions contained a considerable amount of guanine crystals (Fig. 7A, Fig. S14). When whole organisms (*e.g,*, *Euphyllia paraancora*) were subjected for four months to N-starvation under N-depleted conditions (combined nitrate, nitrite and ammonium concentration < 1 μM) with only autotrophic feeding, their symbiotic algae lost all guanine reserves, while the coral polyps showed a pronounced reduction in size and became pale (*i.e.*, bleached). N limitation is known to cause an increased accumulation of lipid bodies and floridean starch granules (1, 2), as well as the reduction of chloroplast volume in symbiotic dinoflagellates (Fig. 6B, Fig. S14B).
We also explored the presence of guanine in symbiotic dinoflagellates of *Acropora millepora*, a common coral species from the Great Barrier Reef (Australia), in colonies freshly collected from the reef (Heron Island, GBR) and in their explants, prepared from colony fragments, maintained in small closed-system seawater aquaria. Symbionts were analyzed either *in situ,* in the host tissue, or as extracted cells cultivated in natural seawater (Fig. 7 D-F). The crystalline guanine inclusions were identified in both types of samples characterized by confocal Raman microscopy and correlated with the highly reflective properties of guanine visualized by confocal reflection microscopy (Figs. S15, and S16). Similar to observations of the free-living *A. carterae* and to symbiotic dinoflagellates from the store aquarium kept corals, the crystals of guanine were observed in very large quantities inside the guanine-fed *Symbiodiniaceae* of *A. millepora*, were almost absent in the N-starved samples and were present in low to moderate amounts in the extracted symbionts of corals freshly collected from the reef (Fig. S15).

I.6 Confocal fluorescence and reflection imaging. Confocal fluorescence microscopy is far more widely available in biological laboratories than Raman microscopy. Confocal imaging is fast, with high-throughput, and confocal reflection images can be acquired along with the confocal fluorescent ones. Since Raman microscopy enables the precise *in situ* identification of the

chemical nature of crystalline inclusions, we first tested the validity of (SI II.1.C) of the confocal reflection microscopy to image and quantify crystalline inclusions by corresponding measurement of the same samples by Raman imaging. By being more reflective/light scattering than other cell components, we showed that crystalline inclusions such as guanine can be easily visualized in reflection mode using a confocal fluorescence microscope. Thus, the inclusions in *Symbiodiniaceae* cells were first identified by Raman microscopy as guanine crystals and immediately after, cells from the same algal extracts were imaged by the confocal fluorescence microscope Leica TCS SP8 (Leica Microsystems, Germany) in reflection mode. Guanine accumulations were seen as crystal-like, highly light-scattering inclusions. All other organelles, e.g., the nucleus, the pyrenoid, the lipid droplets, the chloroplasts, and the accumulation bodies did not produce a reflection signal (Figs. S15 and S16).
Importantly, the reflection imaging technique enabled the visualization of crystalline deposits much faster than by Raman microscopy, however, this technique could not differentiate between crystalline guanine and other light scattering crystalline inclusions, *e.g.*, calcite, calcium oxalate or uric acid. A combination of both techniques would therefore be desirable for rapid, high-throughput studies.

II. Supplementary Information: Materials and Methods

All chemicals were used for the preparation of media, the stable-isotope labeled ^{15}N-$NaNO_3$, ^{15}N-KNO_3, urea-$^{15}N_2$, ND_4OD, and DCl, as well as the crystalline nucleobases (adenine, guanine, xanthine, hypoxanthine and uric acid) were purchased from Sigma-Aldrich (St. Louis, MO, USA), unless other supplier was specified.

II.1. Uptake kinetics of dissolved guanine and intracellular guanine inclusions of A. carterae (Figs. 1- 3 in the main text).

II.1.A. Cultivation of A. carterae

The marine dinoflagellate *Amphidinium carterae* was obtained from the National Center for Marine Algae and Microbiota (NCMAS, CCMP1314), Bigelow, USA. First, 1 L culture was grown in the closed photobioreactor FMT150 (PSI, Drasov, Czech Republic) in a full f/2 medium (composition shown below in SI II.1.Aa). The suspension was sparged by 0.2 $L \cdot min^{-1}$ filtered ambient air passed through a humidifier. The cultivation regime was 12 h light / 12 h dark illumination. The irradiance was 40 µmol (photons)$\cdot m^{-2} \cdot s^{-1}$ generated by blue- and red-light emitting diodes. The temperature of the suspension was kept constant at 20 °C. Minor losses of medium volume due to evaporation were replenished with distilled water. The culture growth was monitored spectrophotometrically and checked by cell counting.
N-starvation. A stationary culture grown with nitrate was harvested by centrifugation (2000 ×g, 3 min), washed by and suspended in N-deficient f/2 medium (composition in II.1.Aa.) and filtered through sintered glass filter (P100, Schott-Duran, Germany) to remove clumps of cells.
The culture remained largely synchronous and was N-starved for approximately one week. The suspension was split into equal 20 mL batches, transferred to 100 mL flasks (Schott-Duran), and placed on an orbital shaker in the growth chamber 350H (Sanyo, Osaka, Japan) at T= 20°C, illumination 40 µmol (photons) m^{-2} s^{-1}. The cells were maintained in this N-free environment for additional five days to degrade all remaining guanine crystals. The absence of crystalline guanine was checked by Raman microscopy (SI II.1.C.) and by polarization microscopy (II.1.D.).

II.1.Aa. ASW f/2 medium with and without N-source

The f/2 medium was prepared from artificial seawater (ASW) according to (3) and its N-deficient variant contained: 400 mM NaCl, 10 mM KCl, 9 mM $CaCl_2 \cdot 2H_2O$, 20 mM $MgCl_2 \cdot 6H_2O$, 20 mM $MgSO_4 \cdot 7H_2O$ and 1.85 mM KBr, 3.62×10^{-5} M $NaH_2PO_4 \cdot H_2O$, 1.06×10^{-4} M $Na_2SiO_3 \cdot 9H_2O$, 1.17×10^{-5} M $FeCl_3 \cdot 6H_2O$, 1.17×10^{-5} M $Na_2EDTA \cdot 2H_2O$, 3.93×10^{-8} M $CuSO_4 \cdot 5H_2O$, 2.60×10^{-8} M $Na_2MoO_4 \cdot 2H_2O$, 7.65×10^{-8} M $ZnSO_4 \cdot 7H_2O$, 4.20×10^{-8} M $CoCl_2 \cdot 6H_2O$ and 9.10×10^{-7} M $MnCl_2 \cdot 4H_2O$. The final concentrations of vitamins added into the autoclaved ASW f/2 from the stock solution were 2.96×10^{-7} M thiamine HCl (vitamin B1), 2.05×10^{-9} M biotin (vitamin H) and 3.69×10^{-10} M cyanocobalamin (vitamin B12).

The full ASW f/2 medium used for cultures grown on nitrate as a sole source of N was prepared from the N-deficient f/2 by adding 0.882 mM $NaNO_3$. The media were stored in amber glass bottles at 20 °C and used for no more than 30 days after preparation.

II.1.Ab. Medium with saturated guanine as a sole N-source
The saturated solution (~35 μM, (4)) of neutral guanine without visible solid particles was obtained by dissolving a slightly excessive amount of solid guanine in N-deficient f/2 at 60°C (stirred for 30 min) that was cooled to 20°C and filtered through a 0.22 μm Millipore membrane filter (Merck, Kenilworth, NJ, USA). The f/2 medium saturated with dissolved guanine was stored in amber glass bottles at 20 °C and used for no more than 5 days after preparation.
II.1.Ac. Feeding N-starved A. carterae by ground fish scales
The f/2 medium enriched by fish scales was prepared by leaching 100 mg of ground dry fish scales (rainbow trout, Atlantic salmon) in 100 mL of the N-deficient f/2 medium (SI II.1.Aa.) at 25°C for 24 hours. The remaining large pieces of fish scales were removed in the form of precipitate.

II.1.B. Determination of soluble guanine by UV-absorption spectrophotometer
The dissolved guanine concentration in f/2 medium was determined spectrophotometrically using the absorption spectrophotometer Specord 250 (Analytik Jena, Jena, Germany) and its published extinction coefficient value (5). Standard spectroscopic quartz cuvettes (Hellma Analytics, Jena, Germany) with optical lengths of 10, 50 and 100 mm were used depending on the measured concentrations. Spectra between 210 – 400 nm were recorded to avoid artifacts that can occur with single wavelength measurements. For each measurement, aliquots of 5, 10, or 20 mL were centrifuged (14000 ×g, 1 min) and the supernatant was filtered through the 0.22 μm Millipore membrane filter (Merck, Kenilworth, NJ, USA) to remove suspended nanoparticles. We used N-deficient f/2 medium as a blank reference.

II.1.C. Confocal Raman and confocal fluorescence - reflection microscopies
Sample preparation. The specimens for all Raman measurements were prepared and treated according to the methodology described in detail elsewhere (6-8). The algal cells were harvested by centrifugation (2000 ×g, 10 – 30 s) of 1 – 2 mL of cell culture and excess medium was discarded. Each cell pellet and a small amount of remaining medium were mixed with an approximately equal volume of 2% w/v solution of low-gelling agarose (T = 30 – 40°C) in the respective medium. The agarose solution was used to prevent movement of cells during measurements and was prepared using the low melting/gelling agarose (melting T = 65°C, gelling T=28°C) purchased from Carl Roth (Karlsruhe, Germany). Several microliters of the suspension were spread as a thin layer between a quartz slide and a quartz coverslip; wet edges were dried with blotting paper and sealed with a CoverGrip sealant (Biotium, Fremont, CA, USA).
To remove the autofluorescence of chlorophyll that obscured the Raman spectra, a wide-area low-power photobleaching of the entire cell by a defocused 532 nm laser beam was applied prior to the mapping, as described previously (6). The mean guanine content per cell was quantified by Raman microscopy by measuring 5 – 12 randomly selected cells for each time point.
For confocal analysis the symbiotic algae were extracted from *Zoanthus* sp and *A. millepora* by excising and abrading tissues with a brush into filtered seawater (FSW). They were first cleaned of debris by passing through a fine nylon mesh and were further cleaned by repeated centrifugation and resuspension of the pelleted algae in FSW. A drop of microalgal suspension (*A. carterae, Zoanthus sp, A. millepora)* was placed on a glass slide under a glass coverslip for confocal analysis and for each, several slides were analysed with a total of 28-34 cells analysed from each culture or organism, and per treatment for *A. millepora*.
Raman microscopy. The quantitative dynamic studies of guanine biosynthesis and uptake by N-starved *A. carterae* were carried out using an inverted Raman microscope LabRam Evolution (Horiba Scientific, Longjumeau, France) with 532 nm laser excitation (10 mW power at the focal plane) and using the water-immersion objective Plan Apo VC 60×, NA 1.20 (Nikon, Minato, Japan). The spectrograph was equipped with a 150 gr/mm grating providing spectral resolution of 9 cm^{-1}. Raman mapping was conducted with 500 nm steps in both directions, and with two accumulations, each of 0.3 s integration time at each voxel. The apparatus was controlled by a

LabSpec 6 software (Horiba Scientific, Longjumeau, France). Further details of the apparatus were described elsewhere (6). After the format conversion, spectra were treated and analyzed by a home-made GNU Octave software (9) as described previously (8).
All other Raman measurements were conducted using an upright Raman microscope WITec alpha 300 RSA (WITec, Ulm, Germany) with a 532 nm laser excitation (20 mW power at the focal plane), an oil-immersion objective UPlanFLN 100×, NA 1.30 (Olympus, Shinjuku, Japan) and the spectrograph providing spectral resolution of 6 cm^{-1}. Scanning step in *x*- and *y*-direction was 200 nm, with an integration time of 0.1 s per voxel. Further details on the apparatus can be found in (8).
The acquired Raman spectra were treated, and the Raman chemical maps constructed by multivariate decomposition of the baseline-corrected spectra into the spectra of pure chemical components by using WITec Project Plus 5.1 software (WITec, Ulm, Germany). No differences that could affect data interpretation were observed between the results obtained with Horiba and with WITec Raman microscopes.
Confocal microscopy. For each analysis, we used Leica TCS SP5 or Leica TCS SP8 (Leica Microsystems, Heidelberg, Germany) inverted microscopes. Fluorescence imaging was by 63x water immersion objective (Plan-Apo, 1.2 NA) at excitation by Argon laser 488nm line and capturing the emission bands at 500 – 560 nm for organelles as the accumulation body and at 670-700nm for chlorophyll in two photomultiplier tubes (PMTs). Reflection from guanine was simultaneously imaged by excitation at 488nm, with the third PMT detection range centered on the laser line at 485-489nm to capture scattered wavelengths from crystals. Images were taken at approximately mid-depth into each cell at 512x512 pixel resolution.

II.1.D. Polarization microscopy
To acquire images and videos in polarized light, a polarizing accessory of the upright Raman microscope WITec alpha 300 RSA (WITec, Ulm, Germany) was used. The videos visualizing the fast formation of crystalline guanine within *A. carterae* cells were taken by WITec Project Plus 5.1 software (WITec, Ulm, Germany).
The N-starved *A. carterae* cells were immobilized between a glass slide and a glass coverslip by low-melting agarose (SI II.1.C) of approximately 100 □m thickness, without sealing the coverslip edges. Several drops of guanine-enriched f/2 medium (II.1.Ab.) were placed at the coverslip edges and the microalgae located near the edges were monitored through the crossed polarizes. As the dissolved guanine diffused towards the nearby algae, its uptake was confirmed by a considerable amount of crystalline guanine appearing inside them. The rapid accumulation was visualized by the strong light depolarization by newly formed crystals as early as within 14 minutes after the guanine solution was added (Movie S1).

II.1.E. Ultrastructural transmission electron microscopy (TEM)
The microalgae for TEM were fixed in 2% v/v glutaraldehyde solution in culture medium at room temperature for 0.5 h and then post-fixed for 4 h in 1% (w/v) OsO_4 in the 0.1 M sodium cacodylate buffer. The samples, after dehydration through graded ethanol series including anhydrous ethanol saturated with uranyl acetate, were embedded in araldite. Ultrathin sections were made with an LKB-8800 (LKB, Sweden) ultratome, mounted to the formvar-coated TEM grids, stained with lead citrate according to Reynolds (10) and examined under JEM-1011 (JEOL, Tokyo, Japan) microscope.

II.1.F. Energy-dispersive X-ray spectroscopy (EDX)
The samples for nanoscale elemental analysis in analytical TEM using EDX were fixed, dehydrated and embedded in araldite as described above, excepting the staining with uranyl acetate and lead citrate. Semi-thin sections were examined under JEM-2100 (JEOL, Japan) microscope equipped with a LaB_6 gun at the accelerating voltage 200 kV. Point EDX spectra were recorded using JEOL bright-field scanning TEM (STEM) module and X-Max X-ray detector system (Oxford Instruments, UK). The energy range of recorded spectra was 0–10 keV with a resolution of 10 eV per channel. At least ten cells per specimen were analyzed. Spectra were processed with INKA software (Oxford Instruments, UK) and presented in a range 0.1-4 keV.

II.2. Combining isotopic-labelling with Raman microscopy (Fig.4 and 5 in the main text).

II.2.A. Deuterated guanine for uptake solid guanine experiments (Fig. 4 in the main text).

Heavy water (D_2O, 99.9%) used in the experiments was purchased from Silantes (München, Germany). Deuterated d_1-guanine (8)D, d_4-guanine (1,2,2,9)D and d_5-guanine (1,2,2,8,9)D were prepared from crystalline guanine (Sigma-Aldrich) according to the procedure described in (11). The isotopic purity of d_1-, d_4-, and d_5-guanine was checked by Raman microscopy (SI II.1.C.) and compared with the corresponding spectra reported in (11).

The base media and studied organisms were the same as described above in relation to Figs. 1-3. The methodological approach is described in the main text, and in further detail in SI. II.1.A for cultivation and SI II.1.C. for Raman measurements.

II.2.B. ^{15}N-sources for cell growths and guanine dynamics (Fig. 5 in the main text).

For *de novo* biosynthesis experiments, various ^{15}N-labeled compounds constituting N-sources in the media commonly used for microalgae cultivation were tested. The stable-isotope labeled ^{15}N-$NaNO_3$, ^{15}N-KNO_3 and urea-$^{15}N_2$ were purchased from Sigma-Aldrich (St. Louis, MO, USA). The ^{15}N-NH_4Cl was acquired from Silantes (München, Germany). The stable-isotope fully-labeled crystalline ^{15}N-guanine was prepared from commercially available guanosine-$^{15}N_5$ 5′-monophosphate, sodium salt, (Sigma-Aldrich) by acid hydrolysis of the N-glycosidic bond (12) and subsequent neutralization by NaOH. The precipitated neutral $^{15}N_5$-guanine (^{15}N-guanine) was washed by deionized water and dried. The isotopic purity was checked by Raman microscopy (SI II.1.C.) and compared with the corresponding spectrum reported in (11). The spectral differences between ^{15}N- and ^{14}N-guanine are shown in Fig. S8. The frequency downshifts by 5 – 20 cm^{-1} caused by the heavier ^{15}N atoms largely exceeded the experimental error (< ±1 cm^{-1}) and enabled a straightforward and an unambiguous identification of the respective species.

The media and the organisms used for the biosynthesis and uptake experiments were as described above in relation to Figs. 1-3. The 20 mL batches (in triplicate) of the N-starved *A. carterae* cells (II.1.A.) were supplemented with various ^{15}N-sources.

To provide the same amounts of N atoms regardless of the N-source, we added either ^{15}N-nitrate to the final concentration of 0.882 mM corresponding to the full f/2 medium (54.69 $mg \cdot L^{-1}$), or 0.882 mM ^{15}N-ammonium (15.91 $mg \cdot L^{-1}$), or 0.441mM ^{15}N-urea (26.48 $mg \cdot L^{-1}$) or 0.1764 mM ^{15}N-guanine as the sole N sources. Nitrate, ammonium and urea were added in the form of 1000-fold concentrated solution. Guanine was added as a solid powder (0.53 mg per 20 mL cell suspension) because of its limited solubility.

The cell density and average cell size were measured in triplicate by the Coulter counter Multisizer 3 (Beckman Coulter, Brea, CA, USA) with a 100 µm aperture or by using Bürker counting chamber (n=9).

The mean guanine content per cell was quantified by Raman microscopy measuring 5–12 randomly selected cells for each time point.

In other methodological aspects, our approach is further described in detail in the main text, in SI II.1.A for cultivation and SI II.1.C. for Raman measurements.

II.3. Source and maintenance of free-living microalgae (Tab. 1 in the main text).

The free-living marine algal species were cultivated in a full ASW f/2 medium prepared from N-deficient f/2 (SI II.1.Aa.) enriched by 8.82×10^{-4} M $NaNO_3$ as a sole source of N (3).

The freshwater microalgae were cultivated in the Bold's Basal Medium (BBM) (13), ½SŠ medium (14), BG-11 medium (15) or media recommended by the supplier of the algal strain. None of the media used for basic screening was enriched with guanine or other purines.

II.4. Source and maintenance of symbiotic microalgae (Fig. 7 in the main text).

II.4.A. Symbiodiniaceae from aquaria-kept anthozoans (Fig. 7 A–C in the main text).

Various cnidarian species, *e.g.*, anemone *Aiptasia* sp., corallimorpharian *Rhodactis indosinensis*, scleractinian coral *Euphyllia paraancora*, leather coral *Sinularia asterolobata*, and *Zoanthus* sp. were obtained from a marine aquarium store.

They were maintained in small experimental aquaria (8 L, closed circulation of filtered water, 25 °C, 12h/12h light/dark cycle, 100 $\mu mol(photons) \cdot m^{-2} \cdot s^{-1}$ illumination by white- and blue-light emitting diodes) under controlled nutrient conditions in the artificial marine water prepared from

the Reef Crystals sea salt (Aquarium Systems, Sarrebourg, France) according to the manufacturer's instructions and supplemented with trace elements by a weekly dosage of commercially available solutions Coral Colours (Red Sea, Eilat, Israel).
Commercially available colorimetric Profi Test kits (Salifert, the Netherlands) were used to test and maintain the pH, carbonate hardness/alkalinity, concentrations of nitrate, nitrite, ammonia, and phosphate according to the manufacturer's instructions. The resultant color changes were quantified by the absorption spectrophotometer Specord 250 (Analytik Jena, Germany) and *via* calibration based on the concentration series of the respective compounds.
The chemical nature of the crystalline inclusions of anthozoan endosymbionts were first analysed immediately after acquisition, and subsequently, at regular intervals, by excising a small piece of soft tissue, positioning it between glass microscope slide and coverslip, and immediately analyzing by Raman microscopy (SI II.1.C.).

II.4.B. Symbiodiniaceae from reef collected coral Acropora millepora (Fig. 7 D–F *in the main text).*
Replicate explants from four *A. millepora* colonies were starved in N-depleted artificial seawater in experimental aquaria for 4 weeks. Dinoflagellate symbionts were extracted by repeated centrifugation and filtering, cultured in nutrient depleted media for additional 4 days, analyzed by confocal reflection microscopy and compared to cells one day later following the addition of crystalline guanine to the artificial seawater and to symbionts extracted from three *A. millepora* that were used for analysis immediately after reef collection and transportation to the laboratory.

III. Supplementary Information: Results

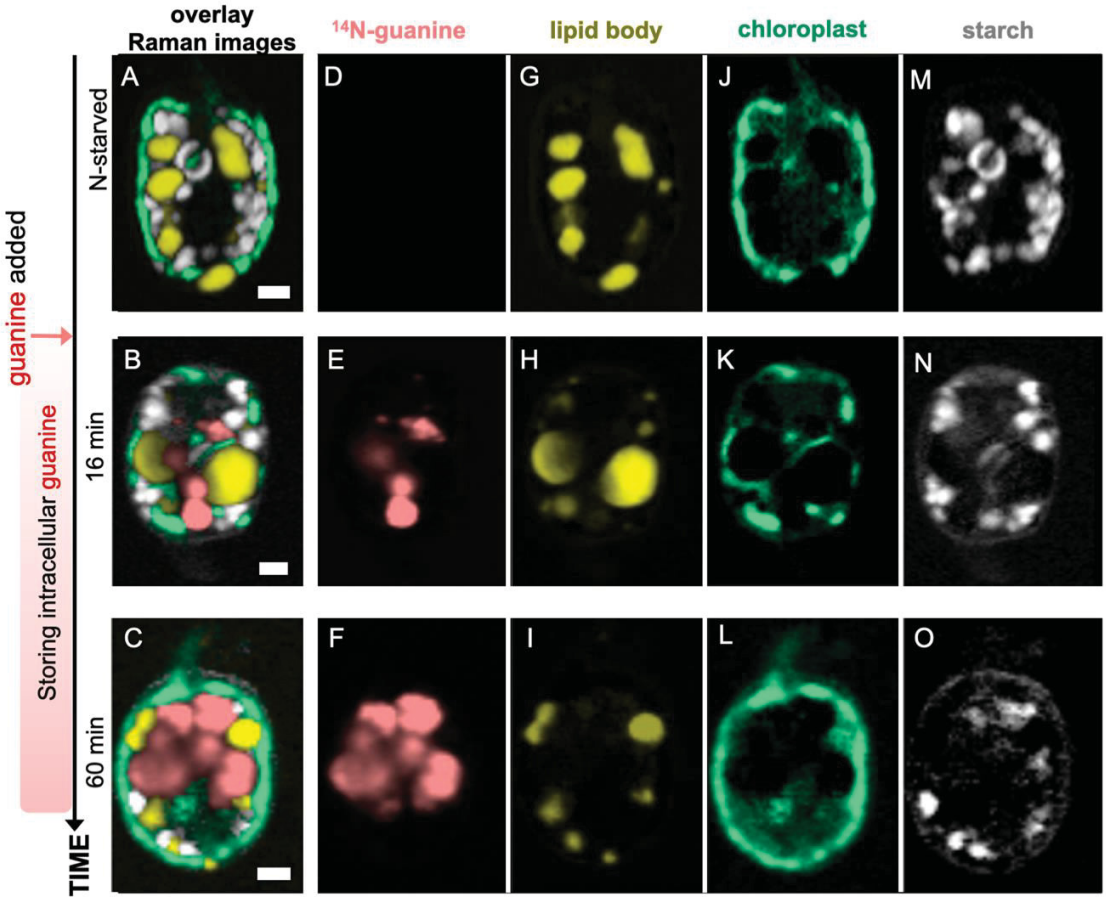

Fig. S1 (complementing Figs. 1C–E). Rapid uptake of guanine by N-starved *A. carterae* led to accumulation of intracellular guanine inclusions. The combined Raman maps (A–C) represent typical cells after two weeks of N-starvation (first row) and cells during progressive guanine accumulation (second and third rows). Intracellular distribution of crystalline guanine (D–F), neutral lipids (G–I), chloroplasts (J–L) and floridean starch (M–O) are shown in separate panels for clarity. The corresponding Raman spectra are shown in Fig. 1B. Scale bar: 2 µm.

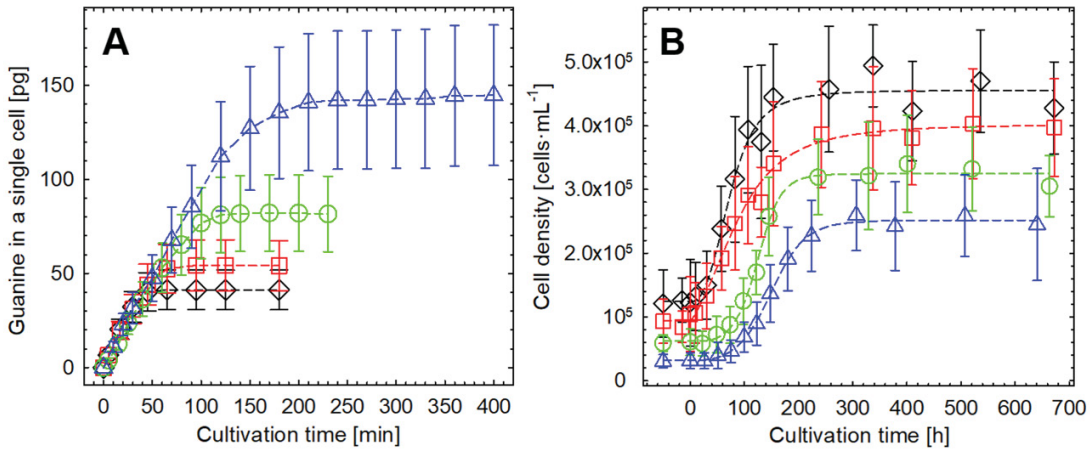

Fig. S2 (complementing Fig. 2). Rapid uptake of guanine by N-starved *A. carterae* and subsequent growth of the culture at the expense of accumulated stocks. (A) Accumulation of guanine reserves inside cells estimated from the uptake kinetics shown in Fig. 2. The cell densities were (12.2 ± 3.1*) × 10^4 cells·mL^{-1} (◇), (9.3 ± 2.3) × 10^4 cells·mL^{-1} (□), (6.1 ± 1.5) × 10^4 cells·mL^{-1} (◯), and (3.1 ± 0.8) × 10^4 cells·mL^{-1} (△). The cells of the most diluted culture (△) did not take all of the dissolved guanine from the medium, thus indicating that their maximum storage capacity was 143 ± 37 pg of crystalline guanine.
(B) Growth of cell cultures influenced by guanine reserves generated by the rapid uptake shown in **A**. Cultures were cultivated under identical conditions until they reached a new stationary phase. Their growth was monitored by cell counting (Bürker counting chamber; 2 replicates, 18 readouts). From the initial cell densities (12.2 ± 3.1) × 10^4 cells·mL^{-1} (◇), (9.3 ± 2.3) × 10^4 cells·mL^{-1} (□), (6.1 ± 1.5) × 10^4 cells·mL^{-1} (◯), and (3.1 ± 0.8) × 10^4 cells·mL^{-1} (△), the final cell densities increased by 3.7 ± 1.1, 4.2 ± 1.4, 5.3 ± 1.7 and 8.1 ± 3.1 times, respectively. The growths were fitted to five-parameter logistic function (RSQR ≥ 0.985).
*a number that follows the ± sign is a standard deviation (SD) in this work.

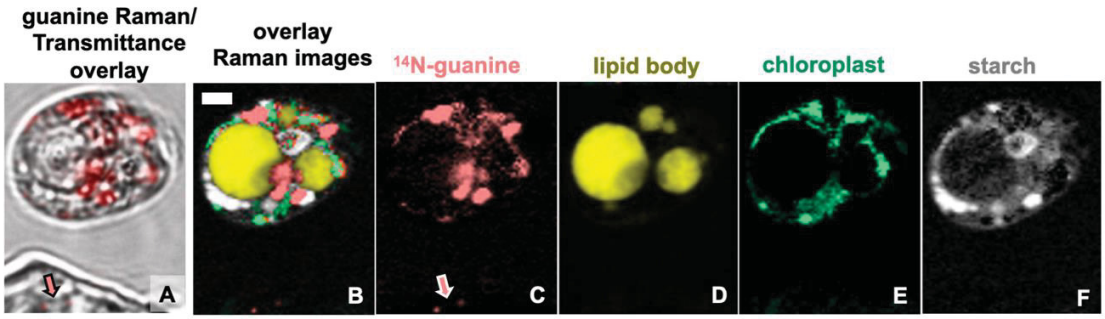

Fig. S3. N-starved *A. carterae* fed by ground fish scales. Bright field image (A) overlaid by guanine Raman map which is shown separately in panel C. Multicomponent Raman chemical map (B). Individual Raman maps of crystalline guanine (C), neutral lipids (D), chloroplasts (E) and floridean starch (F).
Outside the cell, a piece of fish scale containing a small amount of guanine is indicated by the pink arrows in (A) and (C). The cell was mapped 60 min after leachate from the fish scales was added. Raman mapping was conducted in dozens of replicates; a representative cell is shown. Scale bar: 2 μm.
The f/2 medium enriched with leachate from fish scales was prepared by maintaining 100 mg of ground dry fish scales (rainbow trout, Atlantic salmon) in 100 mL of the N-deficient f/2 medium at 25°C for 24 hours. The N-starved cells were transferred to the leachate cleaned free of coarse pieces of sediments. The presence of guanine was confirmed by Raman microscopy of 5 or more of randomly selected cells.

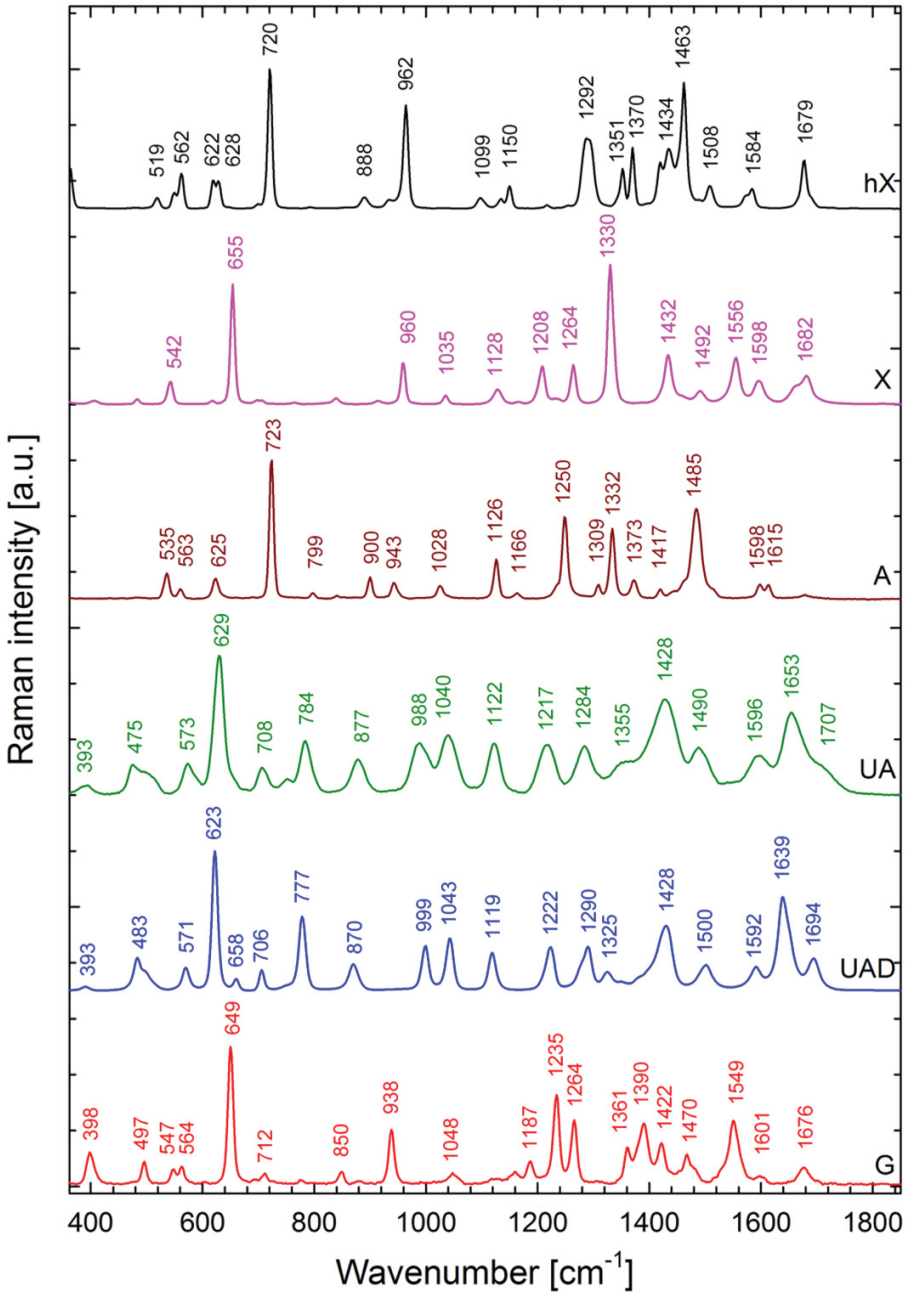

Fig. S4. Comparison of Raman spectra of crystalline anhydrous guanine (G) and crystalline forms structurally related purine bases (adenine – A; xanthine – X; hypoxanthine – hX; uric acid – UA, UAD). The spectrum UA shows uric acid detected in microalgae (*e.g.*, *Klebsormidium flaccidum*) and UAD shows the most similar spectrum of a single crystal of uric acid dihydrate for a specific crystal orientation. Uric acid present in some microalgae species could not be easily identified by means of the reference spectrum of polycrystalline anhydrous uric acid (see Fig. S5 for details). For the sake of clarity, only the range of characteristic vibrations (360 – 1850 cm^{-1}) is shown.

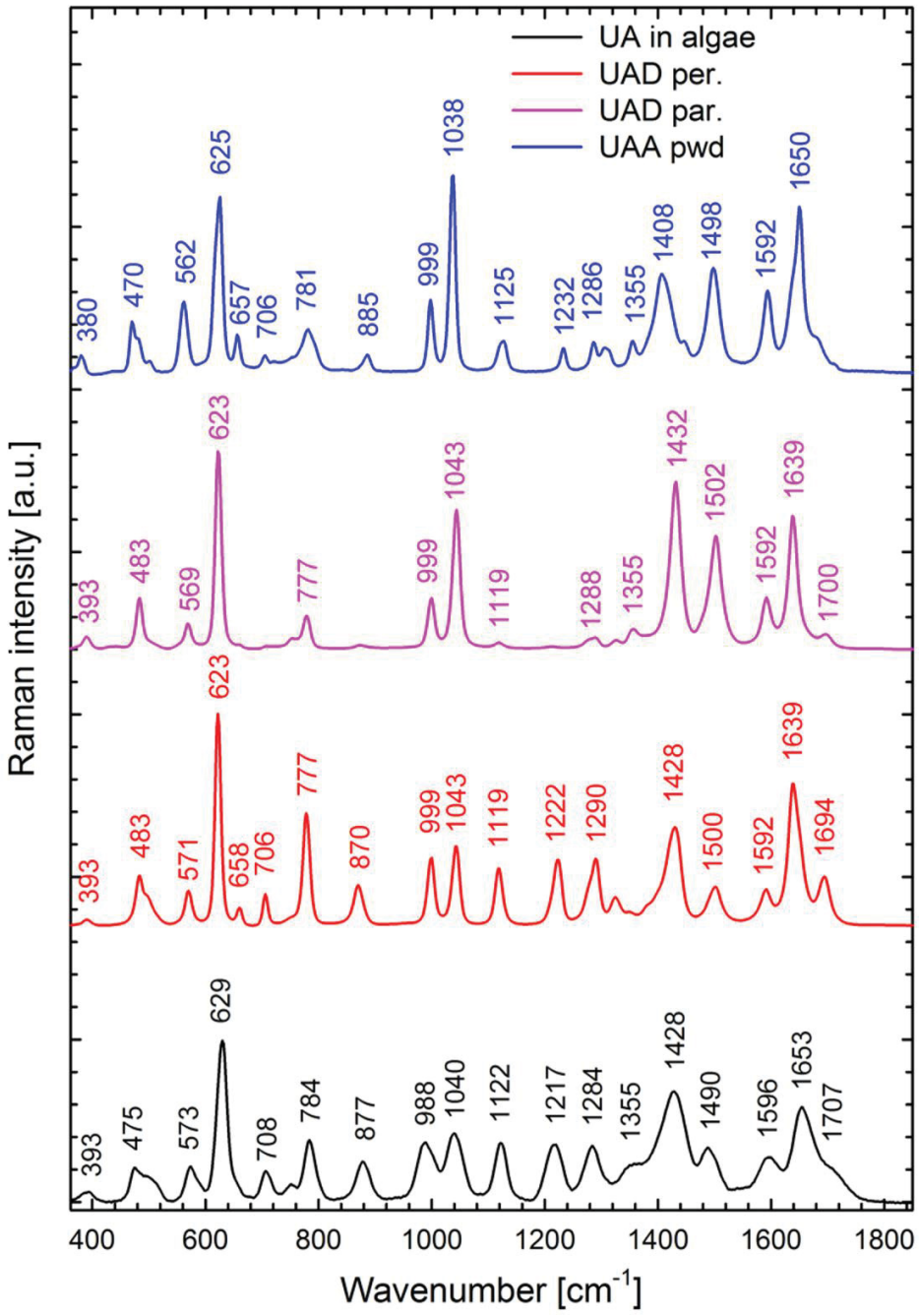

Fig. S5. Comparison of Raman spectra of different crystalline forms of uric acid. Uric acid was commercially available as an anhydrous polycrystalline powder (UAA pwd, blue line) from which it can be recrystallized under specific conditions to anhydrous or dihydrate single crystals (16). Unlike the polycrystalline UAA powder, the relative intensities of the Raman bands of single crystals were sensitive to the orientation of their flat plate faces with respect to the electric vector of the excitation beam, as was evidenced by the spectra of dihydrate uric acid single crystal oriented parallelly (UAD par, magenta line) and perpendicularly (UAD per, red line). Raman spectra of uric acid detected in microalgae (UA in algae, black line) were most similar to the

spectrum of UAD per., nevertheless, Raman bands were broader, indicating a less strict crystal packing of the molecules.

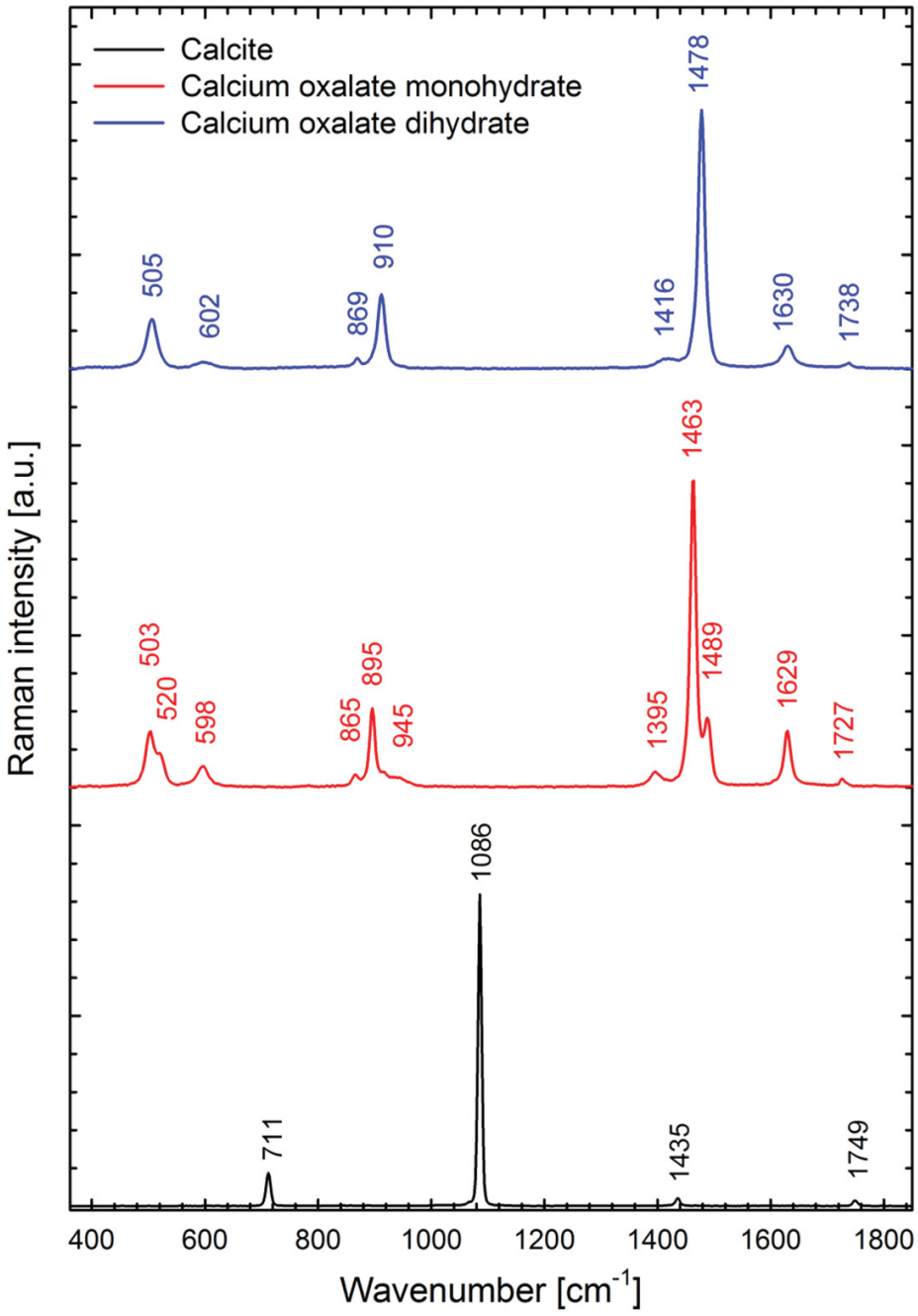

Fig. S6. Raman spectra of calcite, calcium oxalate monohydrate, and calcium oxalate dihydrate.

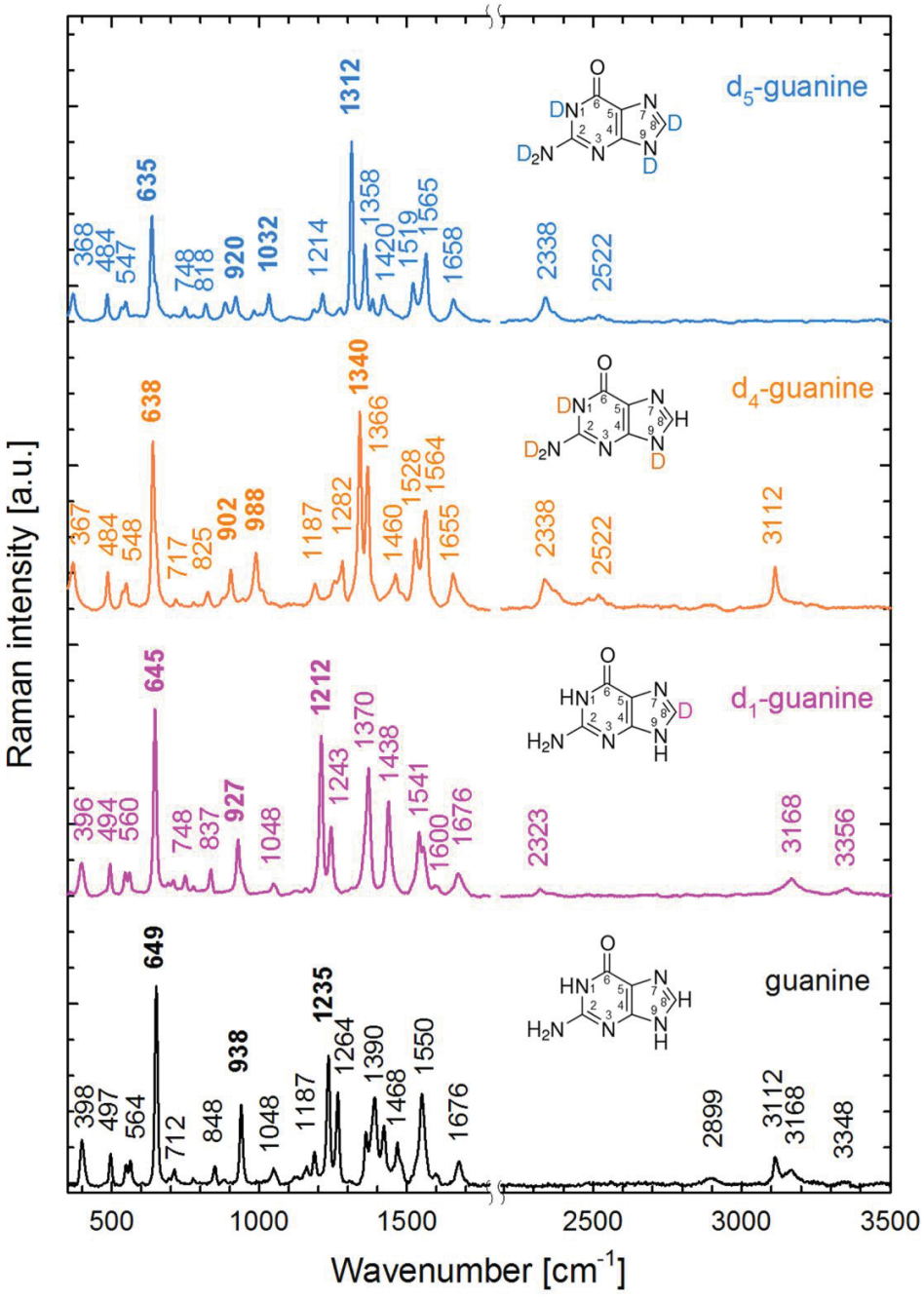

Fig. S7 (complementing Fig. 4). Raman spectra of normal guanine and its deuterium-labeled derivatives.

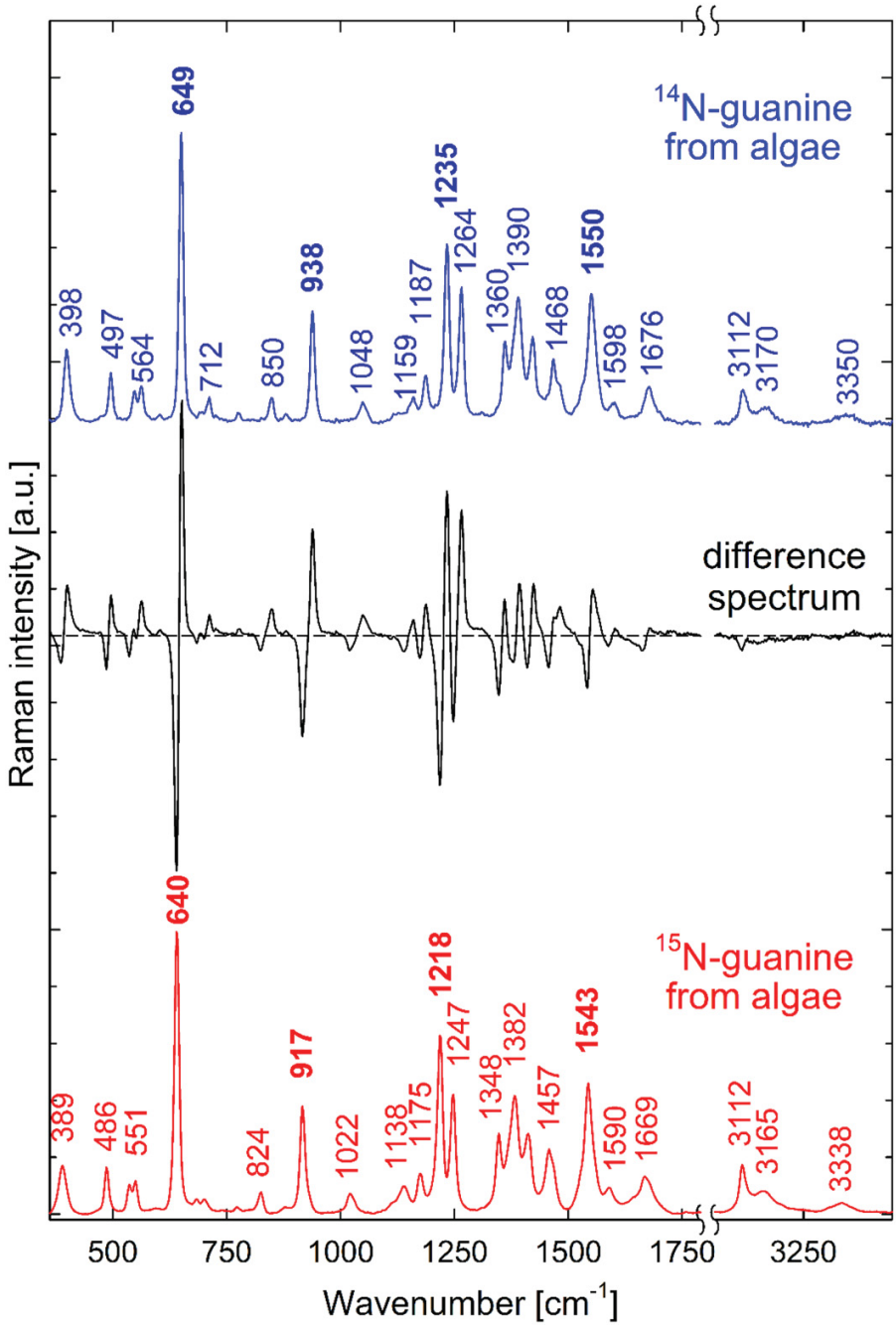

Fig. S8 (complementing Fig. 7). Direct comparison of Raman spectra of crystalline ^{14}N- and ^{15N}-guanine. To highlight the specific isotopic frequency shifts between both isotopic guanine species, the difference spectrum is shown for clarity. The differences in wavenumbers of individual bands of the ^{14}N- and ^{15}N-guanine were found sufficiently large for a reliable discrimination by Raman spectroscopy. In fact, the shifts were as large as 5–20 cm^{-1}, while the spectral resolution of our Raman spectrometer was better than ± 1 cm^{-1}.

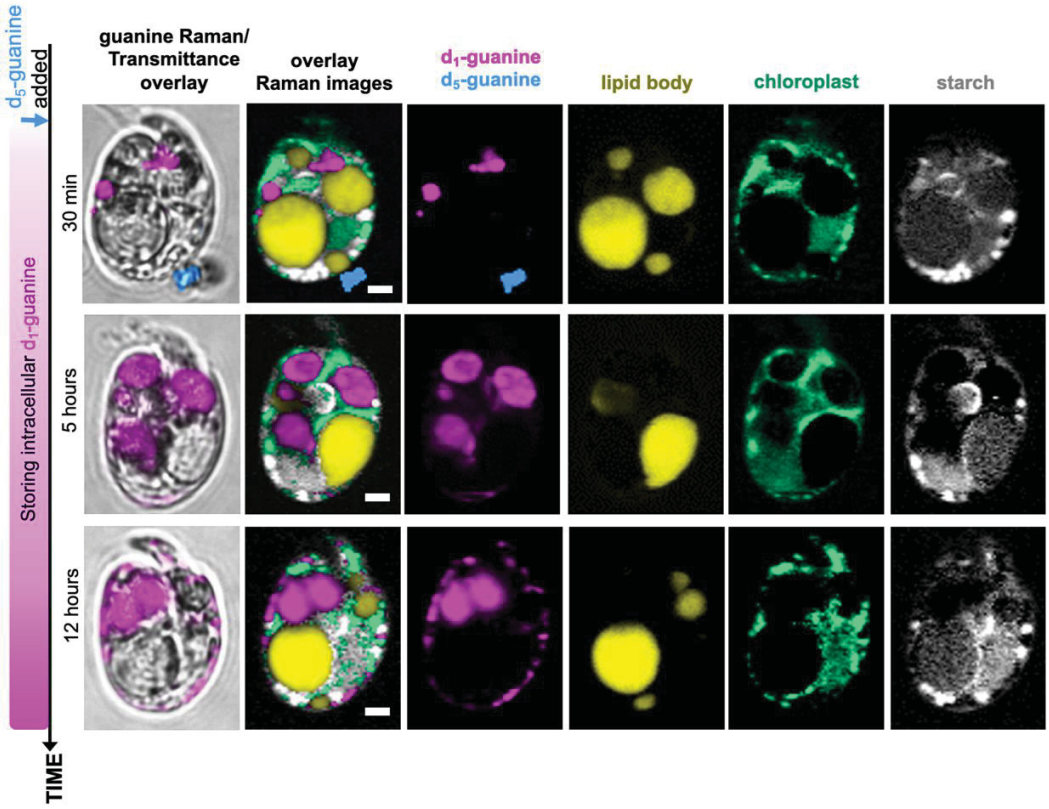

Fig. S9 (complementing Fig. 4). Uptake of guanine includes the exchange of deuterium for hydrogen atoms. Bright field images overlaid by guanine Raman maps (A, B, C), multicomponent Raman maps (D, E, F) and Raman maps of the most important components (G–R) of the N-starved *A. carterae* after the addition of solid crystalline d_5-guanine into N-depleted medium. Images collected 30 min, 5 hours and 12 hours after d_5-guanine addition. Raman maps of d_5- and d_1-guanine (G–I) are represented in blue and magenta, respectively, both in the corresponding Raman spectrum (Fig. S7) and in the images. Other colors: yellow – neutral lipids, green – chloroplasts, gray – floridean starch. Scale bars (D–F): 2 μm.

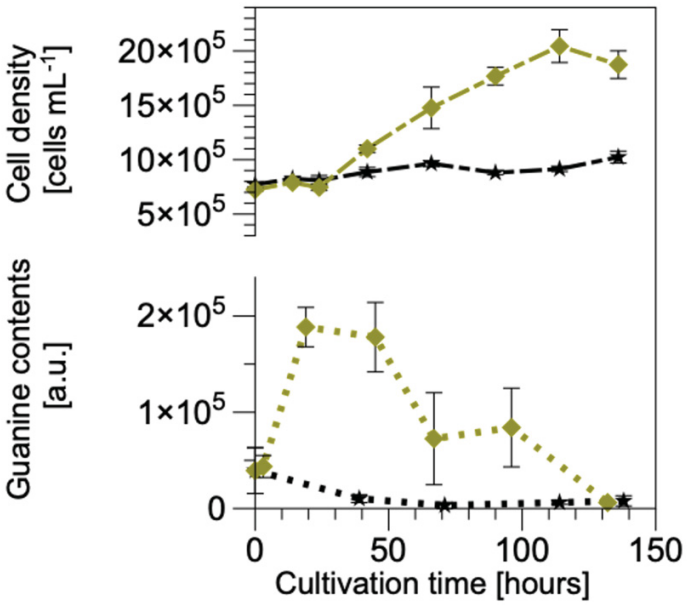

Fig. S10 (complementing Fig. 5). Nitrogen in ^{15}N-guanine inclusions originated directly from the supplied ^{15}N-labelled urea. *A. carterae* cell density stagnated in the control samples without N-feeding (black line, upper graph) and resumed growth after the addition of ^{15}N-labelled urea at concentration of 0.882 mM (N) (yellow line, upper graph). The corresponding intracellular crystalline guanine contents per cell are shown in the bottom graph representing Raman measurements of 5–12 cells.

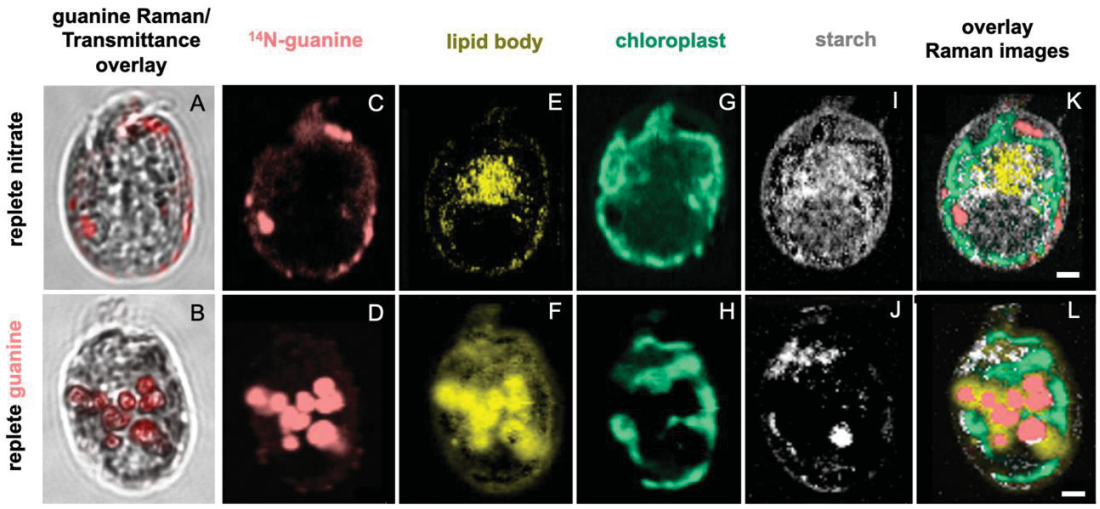

Fig. S11 (complementing Fig. 6). Localization of guanine inclusions in *A. carterae* fed by nitrate (top row) or guanine (bottom row) after 24 hours. Bright field images overlaid by guanine Raman maps (A, B). Separate Raman maps of guanine (C, D), neutral lipids (E, F), chloroplast (G, H), and floridean starch (I, J). Combined multicomponent Raman chemical map (K, L). Scale bar: 2 μm.

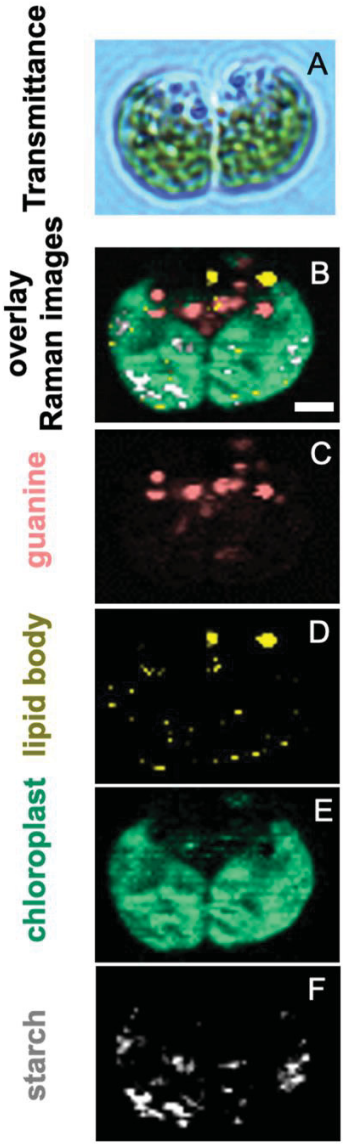

Fig. S12. Crystalline guanine inclusions in the dividing *Chlamydomonas reinhardtii*. Bright field image (A), multicomponent Raman chemical map (B), separate Raman map of guanine (C), neutral lipids (D), chloroplasts (E), and starch (F). Scale bar: 2 μm.

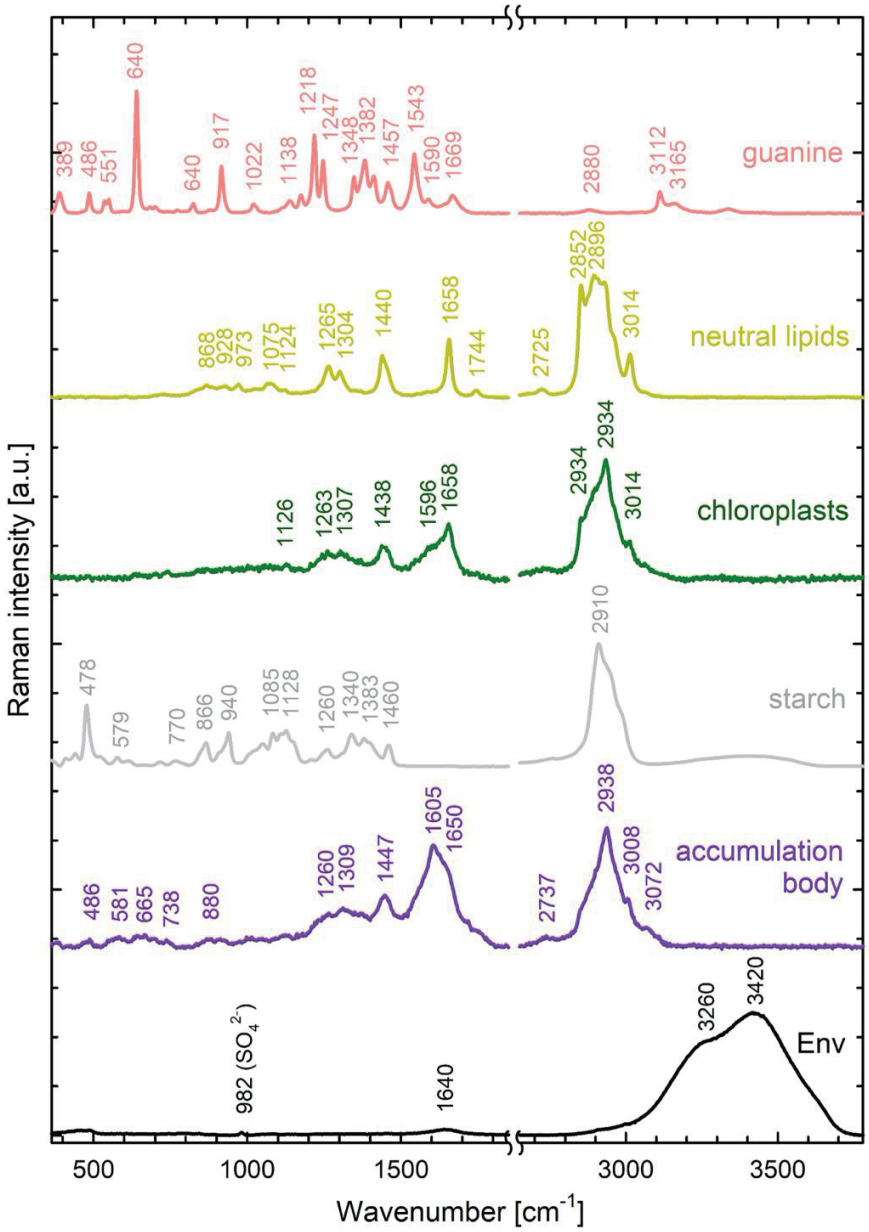

Fig. S13 (complementing Fig. 7). Raman spectra of pure components identified in *Symbiodiniaceae* cells re-fed with ^{15}N-NaNO$_3$. The full–range Raman spectra of crystalline ^{15}N-guanine, neutral lipids, chloroplasts, floridean starch, accumulation body, and seawater surrounding the cell were used for multivariate decomposition of Raman maps of *Symbiodiniaceae* cells and construction of chemical maps shown in Fig. 7.

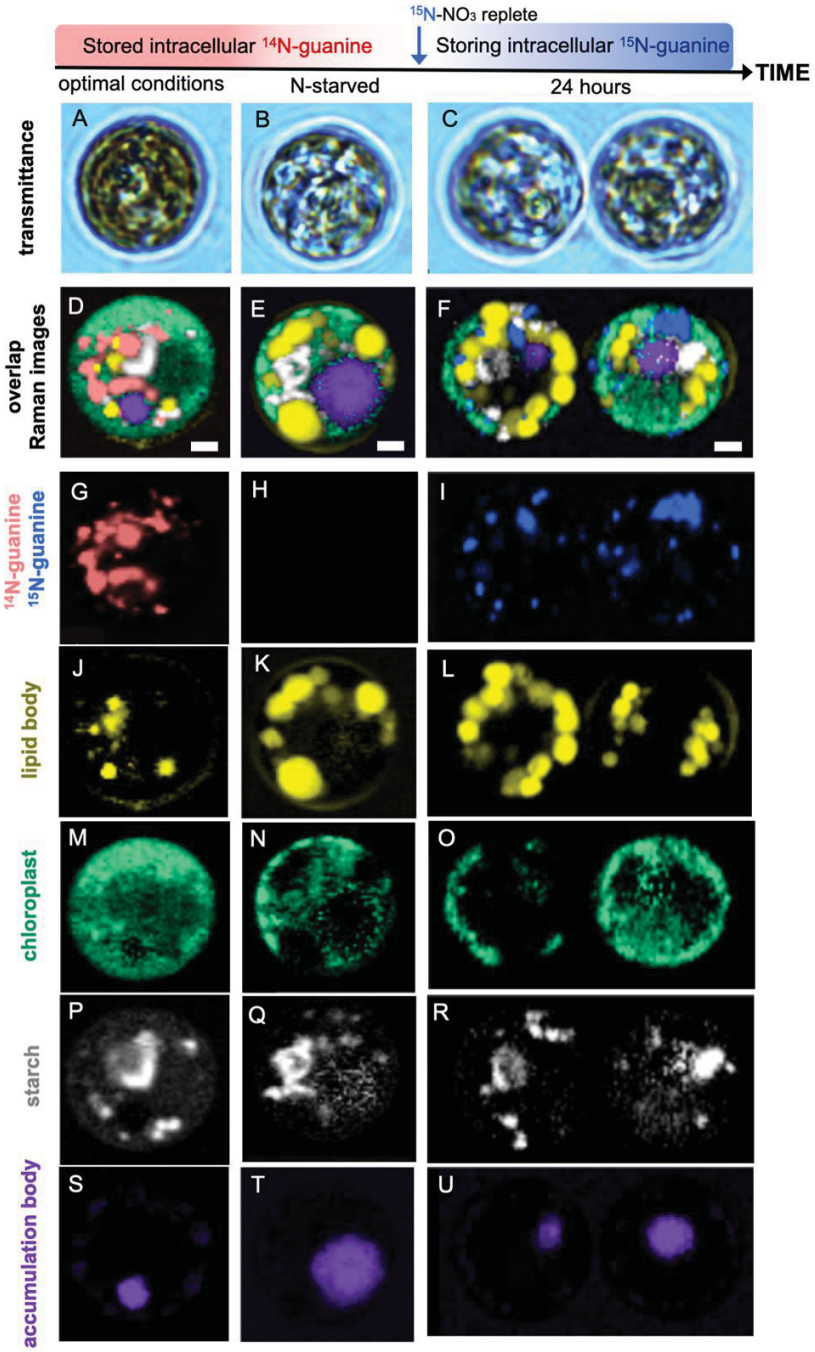

Fig. S14 (complementing Fig. 7). Raman chemical maps of *Symbiodiniaceae* cells extracted from the tissue of the coral *Euphylia paraancora.* *Algae* from corals cultivated under optimal nutrient conditions in an aquarium shop contained guanine crystals (D, G). After four-month cultivation of the entire holobiont in N-depleted seawater, they lost their guanine reserves (E, H). When corals were transferred into seawater enriched by 0.3 mM ^{15}N-$NaNO_3$, newly synthesized ^{15}N-guanine crystals appeared within 24 h (F, I) in algae as documented by the highly specific Raman spectra clearly distinguishing between ^{14}N- and ^{15}N-guanine (Fig. S8). Raman mapping was replicated (n=12 or more cells) and conducted on three holobiont replicates; representative cells are shown. Scale bar: 2 µm.

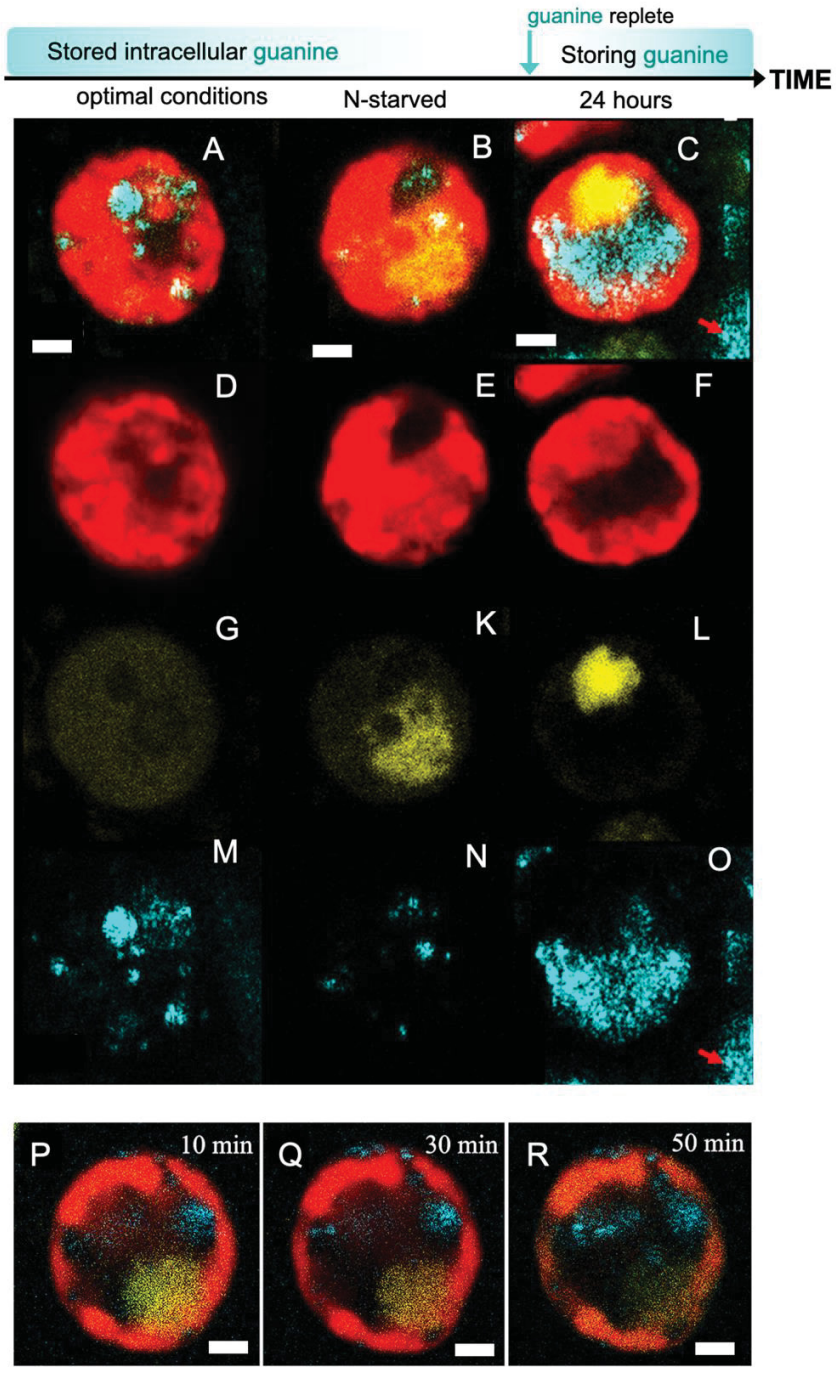

Fig. S15 (complementing Fig. 7). Confocal fluorescence and reflectance images of *Symbiodiniaceae* cells extracted from the coral *A. millepora*. Combined images (A–C), chlorophyll fluorescence 670 – 700 nm (D–F), fluorescence at 500 – 560 nm assigned predominantly to accumulation body (G–L), and 488 nm reflection of guanine microcrystals (M–O) of cells extracted from freshly reef collected corals (left column), from N-depleted corals (middle column) and from the N-depleted symbionts 24 h after the supplementation by guanine powder (right column). Combined images (P–R) illustrate the time evolution of the uptake showing the same cell 10 min (P), 30 min (Q) and 50 min (R) after the addition of guanine. Gradual bleaching

of the fluorescence is visible due to laser scanning. Red arrow in images C and O indicate undissolved crystalline guanine outside the cell. Scale bar: 2 μm.

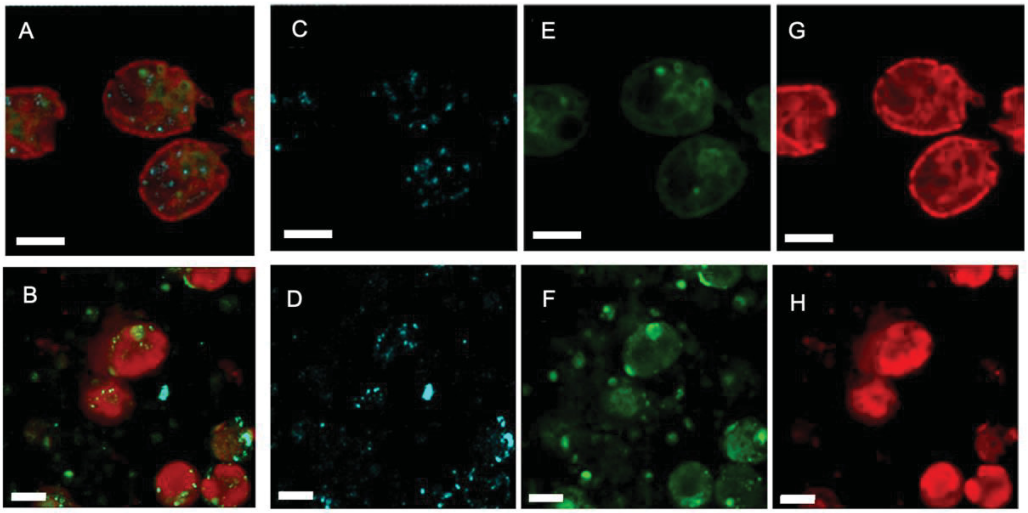

Fig. S16. (complementing Fig. 7D-F and Fig. S15). Confocal images of *A. carterae* and *Symbiodiniaceae* cells after N feeding. Confocal images of free-living *A. carterae* cells (A, C, E, G) and *Symbiodiniaceae* cells (B, D, F, H) extracted from reef *Zoanthus* sp. and fed with guanine powder highlighting the crystalline inclusions in a reflection mode of 488 nm laser line (C, D); fluorescence emission at 500 – 560 nm from accumulation bodies and other organelles (E, F); fluorescence emissions of chlorophyll from chloroplasts 670 – 700 nm (G, H); and overlaid combined image (A, B). The presence of crystalline guanine within cells from the same batch was confirmed by Raman microscopy. Scale bar: 5 µm.

Movie S1 (separate file, complementing Fig. 1) shows a sequence captured in real time by polarization microscopy. The cover figure shows bright field (A, C) and polarization images (B, D) of an N-starved *A. carterae* cell before (A, B) and 14 minutes after feeding with dissolved guanine (C, D). The video will start upon clicking the cover figure.

SI References

1. S. Rosset, C. D'Angelo, J. Wiedenmann, Ultrastructural Biomarkers in Symbiotic Algae Reflect the Availability of Dissolved Inorganic Nutrients and Particulate Food to the Reef Coral Holobiont. *Frontiers in Marine Science* **2**, 103 (2015).
2. S. Rosset, J. Wiedenmann, A. J. Reed, C. D'Angelo, Phosphate deficiency promotes coral bleaching and is reflected by the ultrastructure of symbiotic dinoflagellates. *Marine Pollution Bulletin* **118**, 180-187 (2017).
3. R. R. L. Guillard (1975) Culture of phytoplankton for feeding marine invertebrates. in *Culture of Marine Invertebrate Animals*, eds W. L. Smith, M. H. Chanley (Plenum Press, New York, USA), pp 26-60.
4. S. H. Yalkowsky, Y. He, P. Jain, *Handbook of Aqueous Solubility Data* (CRC Press, New York, U.S.A., ed. Second, 2010).
5. D. B. Dunn, R. H. Hall, "Purines, Pyrimidines, Nucleosides, and Nucleotides: Physical Constants and Spectral Properties" in Handbook of Biochemistry and Molecular Biology. (CRC Press, 2018), 10.1201/b21846-50 chap. Purines, Pyrimidines, Nucleosides, and Nucleotides: Physical Constants and Spectral Properties.
6. Š. Moudříková *et al.*, Raman and fluorescence microscopy sensing energy-transducing and energy-storing structures in microalgae. *Algal Research* **16**, 224-232 (2016).
7. Š. Moudříková, L. Nedbal, A. Solovchenko, P. Mojzeš, Raman microscopy shows that nitrogen-rich cellular inclusions in microalgae are microcrystalline guanine. *Algal Research* **23**, 216-222 (2017).
8. Š. Moudříková *et al.*, Quantification of polyphosphate in microalgae by Raman microscopy and by a reference enzymatic assay. *Analytical Chemistry* **89**, 12006-12013 (2017).
9. J. W. Eaton, D. Bateman, S. Hauberg, R. Wehbring (2015) GNU Octave version 4.0.0 manual: a high-level interactive language for numerical computations. (CreateSpace Independent Publishing Platform).
10. E. S. Reynolds, The use of lead citrate at high pH as an electron-opaque stain in electron microscopy. *Journal of Cell Biology* **17**, 208-212 (1963).
11. J. M. Delabar, M. Majoube, Infrared and Raman-spectroscopic study of N-15 and D-substituted guanines. *Spectrochimica Acta Part a-Molecular and Biomolecular Spectroscopy* **34**, 129-140 (1978).
12. H. Ishikawa, Hydrolysis of nucleotides by acid. *The Journal of Biochemistry* **22**, 385-395 (1935).
13. H. W. Bischoff, H. C. Bold, *Some soil algae from Enchanted Rock and related algal species*, Phycological studies (University of Texas Publication, Austin, Texas, 1963), vol. IV.
14. V. Zachleder, I. Šetlík, Effect of irradiance on the course of RNA-synthesis in the cell cycle of *Scenedesmus quadricauda*. *Biol Plantarum* **24**, 341-353 (1982).
15. R. Rippka, J. Deruelles, J. B. Waterbury, M. Herdman, R. Y. Stanier, Generic assignments, strain histories and properties of pure cultures of cyanobacteria. *Journal of General Microbiology* **111**, 1-61 (1979).
16. F. Liu, D. E. Hooks, N. Li, N. A. Mara, J. A. Swift, Mechanical properties of anhydrous and hydrated uric acid crystals. *Chem. Mat.* **30**, 3798-3805 (2018).

HardwareX
Volume 8, October 2020, e00143

Bottom-illuminated orbital shaker for microalgae cultivation

Jakub Nedbal [a], Lu Gao [b, c], Klaus Suhling [a]

[a] Department of Physics, King's College London, Strand, London WC2R 2LS, UK
[b] Institute of Bio- and Geosciences/Plant Sciences (IBG-2), Forschungszentrum Jülich, Wilhelm-Johnen-Straße, D-52428 Jülich, Germany
[c] Faculty of Mathematics and Natural Sciences, Heinrich Heine University, Universität Straße 1, D-40225 Düsseldorf, Germany

Received 1 May 2020, Revised 24 July 2020, Accepted 7 September 2020, Available online 16 September 2020.

HardwareX 8 (2020) e00143

Contents lists available at ScienceDirect

HardwareX

journal homepage: www.elsevier.com/locate/ohx

Bottom-illuminated orbital shaker for microalgae cultivation

Jakub Nedbal [a,*], Lu Gao [b,c], Klaus Suhling [a]

[a] Department of Physics, King's College London, Strand, London WC2R 2LS, UK
[b] Institute of Bio- and Geosciences/Plant Sciences (IBG-2), Forschungszentrum Jülich, Wilhelm-Johnen-Straße, D-52428 Jülich, Germany
[c] Faculty of Mathematics and Natural Sciences, Heinrich Heine University, Universität Straße 1, D-40225 Düsseldorf, Germany

ARTICLE INFO

Article history:
Received 01 May 2020
Received in revised form 24 July 2020
Accepted 7 September 2020

Keywords:
Orbital shaker
Shaking incubator
Growth chamber
Cultivation
Microalgae
Algae
Cyanobacteria
Cell culture
Desmodesmus quadricauda
Chlorella vulgaris
3D printing
Open source hardware
Open hardware
Open source
Free and open source
FOSS
Free
Education
Teaching
Electronics

ABSTRACT

A bottom-illuminated orbital shaker designed for the cultivation of microalgae suspensions is described in this open-source hardware report. The instrument agitates and illuminates microalgae suspensions grown inside flasks. It was optimized for low production cost, simplicity, low power consumption, design flexibility, consistent, and controllable growth light intensity.

The illuminated orbital shaker is especially well suited for low-resource research laboratories and education. It is an alternative to commercial instruments for microalgae cultivation. It improves on typical do-it-yourself microalgae growth systems by offering consistent and well characterized illumination light intensity. The illuminated growth area is 20 cm × 15 cm, which is suitable for three T75 tissue culture flasks or six 100 ml Erlenmeyer flasks. The photosynthetic photon flux density, is variable in eight steps ($26 - 800\ \mu mol \cdot m^{-2} \cdot s^{-1}$) and programmable in a 24-h light/dark cycle. The agitation speed is variable (0 – 210 RPM). The overall material cost is around £300, including an entry-level orbital shaker. The build takes two days, requiring electronics and mechanical assembly capabilities. The instrument build is documented in a set of open-source protocols, design files, and source code. The design can be readily modified, scaled, and adapted for other orbital shakers and specific experimental requirements.

The instrument function was validated by growing fresh-water microalgae *Desmodesmus quadricauda* and *Chlorella vulgaris*. The cultivation protocols, microalgae growth curves, and doubling times are included in this report.

Specifications table:

Hardware name	Bottom-Illuminated Orbital Shaker for Microalgae Cultures
Subject area	Biological Sciences (Algae, Photosynthesis, and Environmental Research)
Hardware type	Biological sample handling and preparation
Open source license	Creative Commons Attribution 4.0 International (CC BY 4.0)
Cost of hardware	€300
Source file repository	http://osf.io/wfp7x/

* Corresponding author.
E-mail address: jakub.nedbal@kcl.ac.uk (J. Nedbal).

https://doi.org/10.1016/j.ohx.2020.e00143
2468-0672/

1. Hardware in context

Microalgae, like plants, use photosynthesis as the primary energy source for their metabolic needs [1]. In laboratory conditions, microalgae are grown using dedicated instruments in growth media, which provide the nutrients and water [2,3]. These instruments vary in size between microfluidic [4,5] and industrial scale implementations [3,6]. Their purpose is to agitate and illuminate the cultures. Agitation is done by shaking, stirring or gas sparging to ensure microalgae mixing, nutrient, and gas exchange. The illumination typically covers the photosynthetically active spectral range 400 nm–700 nm (white), which excites a range of endogenous fluorophores required for full metabolic activity. Their illumination intensity is variable and programmable for daily (diurnal) light/dark cycle.

The instrument described in this report is an orbital shaker with a bottom-mounted light source for growing 10 s – 100 s ml of microalgae suspensions in flasks (Fig. 1A). The instrument offers consistent and controllable illumination with low power consumption at a fraction of the cost of a commercial instrument. Laboratory microalgae cultivation is typically done in photobioreactors, illuminated cabinets or on shakers. Closed system photobioreactors (Fig. 1B) offer controlled cultivation conditions for high biomass production [7,8]. Illuminated cabinets with controlled environment (temperature, humidity, gas composition) are used to grow microalgae inside flasks on orbital shakers (Fig. 1C). In the simplest case, this specialized cabinet is replaced by a common top-mounted lamp illuminating the microalgae culture grown at room temperature on an orbital shaker (Fig. 1D).

Closed system bioreactors (Fig. 1B) and temperature-controlled illuminated growth cabinets (Fig. 1C) are designed to offer regulated and versatile conditions for microalgae cultivation [2,3]. However, these specialized machines are expensive (£1000s – £10000s), can have large power (> kW) and space requirements, and operating costs. Yet, these commercial systems are not always essential and do-it-yourself (DIY) solutions to microalgae cultivation are therefore common [9–12,8]. However, the technical and design details of DIY cultivation systems are seldom published and open source hardware (OSHW) publications on microalgae cultivation remain rare. An OSHW photobioreactor design, build instructions, and application protocols were published recently in a peer-reviewed article [8]. 'NinjaPBR' is another photobioreactor for microalgae cultivation with its design files, assembly instructions, and control software made available on Github [13]. 'Bioreactor' is a device for the cultivation of bacteria, currently under development, released on GitHub [14]. It lacks a light source required for phototrophic cultivation of microalgae, but it lends itself to this modification. A suitable light source with programmable power, spectrum, and period is described in [15]. Another exemplary OSHW device is an automated turbidostat, which monitors and maintains optimal microalgae culture density to maximize photobioreactor production yield [16,17].

According to Büchs, over 90% of all culture experiments in biotechnology are performed in shaking bioreactors [18]. Similarly, in laboratory cultivation of microalgae, orbital shakers are widely used. Typically, flasks with microalgae are placed on top of an orbital shaker (Fig. 1D) with a light source illuminating the culture from the top [9,10]. This solution is cheap and simple to implement. However, it cannot ensure consistent and predictable illumination of the microalgae suspensions inside the flasks. The flask lids may cast shadows, screening off the light, and the lamp illumination may not be homogeneous across the area of the shaker. Bottom-illuminated orbital shaker systems for microalgae cultivation offer more consistent illumination [11,12], but are not widely used. This manuscript describes an open hardware design for a bottom-

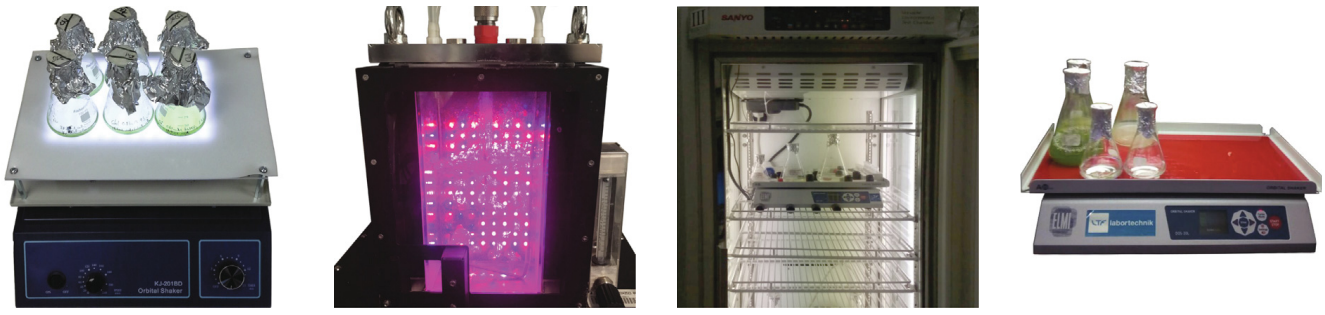

(A) Illuminated Orbital Shaker

(+) $, light control multiple samples low power

(−) no T & gas control

(B) Closed System Bioreactor

(+) light/T/gas control large culture volume

(−) $$$, high power single culture

(C) Culture Cabinet

(+) light/T/gas control multiple samples

(−) $$$, high power space requirement heterogeneous light

(D) DIY Shaker

(+) $, multiple samples moderate power

(−) no T & gas control heterogeneous light

Fig. 1. Different cultivation systems for microalgae and a summary of their strengths and weaknesses. A) Illuminated orbital shaker described in this manuscript. B) Closed system bioreactor for high biomass volume; C) Culture cabinet for large number of different cultures; D) Low-cost DIY shaker under top-mounted lights. T stands for temperature, $ for low cost, and $$$ for high cost.

illuminated orbital shaker for the cultivation of microalgae (Fig. 1A). It was optimized for production cost simplicity, low power consumption, design flexibility, and consistent and controllable growth light intensity to create reproducible experimental conditions.

2. Hardware description

This work describes an illuminated orbital shaker built around a commercial orbital shaker. A custom light-emitting diode (LED) [19,20] array illuminator and an electronic LED controller are placed on top of the shaking platform. An elevated transparent platform made of clear acrylic is fixed over the LED illuminator. The microalgae cultures are placed on top of this elevated platform, being illuminated from the bottom by the LEDs, and agitated by the rotational motion of the orbital shaker.

The LED illuminator is a light source with a rectangular area of 20 cm $\times$ 15 cm, positioned only 15 mm below the microalgae culture. The close proximity of the light source and its positioning below the culture flasks is highly beneficial. The illumination of the culture is consistent over time, regardless of the type of culture flask used, and requires comparably low power consumption ($\leq$ 29 W) to achieve irradiance sufficiently high for majority of microalgae cultivation requirements. The light/dark cycle is set by programming a 24-h socket timer, which regularly turns the light on and off. The irradiance at the bottom interface of the microalgae culture is reproducibly adjustable in eight steps, using a custom electronics controller described in Section 5. The brightness of the light can be regulated by manual switches or an external microcontroller. Excess heat generated by the LEDs is removed by a fan-cooled aluminium heatsink. The cooling ensures that the temperature at the top of the illuminated shaker platform does not increase more than 1 °C above the ambient temperature even at the highest light output.

The bottom-illuminated orbital shaker function was validated by successful cultivation of freshwater microalgae, described in Section 7.2. However, its design is more versatile and should support wider range of applications than described in this report:

- Different species of freshwater and seawater suspension microalgae and cyanobacteria can be cultivated in the appropriate growth medium [9,21,10].
- Thermophilic or psychrotrophic microalgae and cyanobacteria can be cultivated with the orbital shaker placed inside a temperature-controlled space [22–24].
- Seed cultures can be cultivated for inoculation into high-volume bioreactors [9].
- The design can be modified for different orbital shaker models and types. A readily available shaker can be substituted for the model described here. The design can be modified to feature larger illuminator and orbital shaker to support larger culture volumes.
- The peak brightness of the illuminator can be changed by altering the spacing of the LED strips[1].
- The spectral properties of the light source can be modified to suit different experimental regimes [25]. The white LED strips, described here, can be swapped for multi-color LED strips [15]. Multiple copies of the described LED controller can be built to independently control the output of the three colors of the multicolor LED strip, and thus vary the spectral properties and timing of the light source.
- The illumination light intensity and cycle can be controlled using a microcontroller or a computer for advanced growing protocols. The described LED controller is prepared for such external control. It has 0.30 V – 1.25 V analog input regulating the LED current between 25% and 100%. Arduino DUE, Zero or the MKR-family feature in-built digital-to-analog converters for direct voltage control of LED illuminator brightness.
- Pulse width modulation (PWM) can be used to control the brightness with most microcontrollers or microcomputers, including all members of the Arduino and Raspberry Pi families using the same external input of the LED controller.
- The light/dark cycle can be upgraded to longer and more complex illumination patterns by a straightforward replacement of the basic 24-h plug-in timer with a more advanced weekly programmable plug-in timer.
- The orbital shaker can be used in education. It could be an educational engineering project focusing on the instrument development, and a tool for learning about population biology and photosynthesis [26].

3. Design files

Design files are provided for readers to use them directly or modify them according to their specific needs. The design files and the associated assembly steps can be grouped into four areas:

- LED controller electronics.
- 3D printed case for the LED controller electronics.

[1] Any changes to the total length of the LED strip must be accompanied by verifying that the maximum current delivered by the LED controller does not exceed the maximum current rating for the given length of the LED strip. Replace LED driver DC1 (Supplementary Fig. S1) with LDU2430S700, LDU2430S600 or LDU2430S500 for maximum LED current of 700 mA, 600 mA or 500 mA, respectively. With longer LED strips, offering higher maximum current rating, wire them into two or more parallel sections, each powered by its own LED controller.

Table 1
List of design files used in the build of the illuminated orbital shaker for microalgae cultivation.

Design filename	File type	Open source license	Location of the file
LEDcontroller.zip	KiCAD project	CC BY-SA 4.0	osf.io/b4wph
LEDcontroller_PCB.zip	Gerber PCB files	CC BY-SA 4.0	osf.io/vejbw
LEDcontroller_Case.zip	3D CAD files	CC BY-SA 4.0	osf.io/dsmk7
Acrylic_Sheet.dxf	Laser cutter file	CC BY-SA 4.0	osf.io/qwh6t

- Cooled LED illuminator.
- Transparent orbital shaker platform.

The electronic circuit and the printed circuit board (PCB) have been designed in KiCAD electronic design automation suite. The 3D and 2D computer aided design (CAD) models of the electronics circuit case and the transparent orbital shaker platform were designed in Onshape CAD software system.

3.1. Design files summary

The design files are listed in Table 1 and are briefly described in the list below. Their use in the build of the illuminated orbital shaker in explained later in Section 5 and the accompanying protocols.

- `LEDcontroller.zip` The archive contains KiCAD project source files with the electronics schematics, printed circuit board (PCB), bill-of-materials list, and PCB production files. The latest version is available at rebrand.ly/etuuxu. The schematics of the LED controller is in Supplementary Fig. S1.
- `LEDcontroller_PCB.zip` Gerber files for LED controller PCB production are in this archive. The latest version is available at rebrand.ly/xhsc9i.
- `LEDcontroller_Case.zip` STL files for 3D printing the parts of the custom LED controller case are in this archive. The Onshape 3D CAD project with the 3D models of the electronics and the case is available at rebrand.ly/hvjd1o.
- `Acrylic_Sheet.dxf` This DXF file is for the use with laser cutters to produce the secondary transparent orbital shaker platform from clear acrylic. The Onshape 3D CAD project with the latest DXF file, technical drawing and 3D model of the shaker platform is available at rebrand.ly/9nqpar.

4. Bill of materials

The materials, required to build the bottom-illuminated orbital shaker for microalgae cultivation, include an orbital shaker, mechanical fasteners and fixings, clear acrylic sheet, electrical, and electronics components. A number of workshop tools and stationaries are used in the process of building the illuminated orbital shaker. Both the components and tools are organized in a spreadsheet at osf.io/tqhy9 and are also listed in Supplementary Tables S3 to S7.

The spreadsheet is divided into five tabs named:

- **Electronics Parts:** Electronics components are soldered to the PCB to complete the LED controller circuit. Their total cost is £38
- **Laboratory Parts:** The orbital shaker forms the basis of this project. A commonly available low cost orbital shaker (£95) is described in this manuscript. However, other makes and models can be substituted – including used ones.
- **Fixings:** Widely available screws, nuts, washers, and standoffs are required. The total cost is £9.
- **LED Illuminator Parts:** Electrical and electromechanical components required to build the LED illuminator include self-adhesive LED strips, heatsink, cooling fans, cables, power supply, 24-h socket time switch, and a clear acrylic sheet. The total cost is £155.
- **Tools:** A number of commonly available workshop tools and office stationaries are required during the assembly of the orbital shaker. The total cost of brand new tools used in the assembly would be £436, excluding the 3D printer. The tools are organized into five categories:
  - **Workshop Tools:** Common mechanical workshop tools, thread tap set, tap wrench, and a digital multimeter.
  - **Stationaries:** Multipurpose glue, scissors, fine-tip marker pen, and a ruler.
  - **Soldering equipment:** Soldering station with solder and flux, electrical tape, and PCB-cleaning supplies (isopropyl alcohol, tub, and brush).
  - **3D Printing:** Fused deposition modeling 3D printer with consumables or a commercial 3D printing service.
  - **Cutting and Drilling Tools:** Either a drill, drill bit, hacksaw, and a sandpaper, or a laser cutter capable of cutting acrylic sheets.

The electronics circuit PCB manufacture can be outsourced. The total cost of the manufacture, including shipping, is £10. The instructions for ordering the custom PCB are in the following Section 5.

The total cost of the bill of materials, including surplus electronics parts and fixings, is approximately £300. This price includes a basic shaker for ≈ £100.

5. Build instructions

Building the bottom-illuminated orbital shaker for microalgae cultivation requires electronics and mechanical assembly skills. The build is thoroughly documented in a series of protocols listed below. The protocols are published online using **protocols.io** platform under CC BY 4.0 license. The links to the protocols and their brief summaries are in Table 2. Their more detailed description follows.

- **Protocol 1: Illuminated Orbital Shaker for Microalgae Culture (osf.io/hd2c6)** [27] This is a high-level protocol summarizing the steps in building the illuminated orbital shaker. It starts with procuring parts and tools and finishes with the final assembly. Links to the sub-protocols, explaining each step in detail, are provided.
- **Protocol 2: Procuring Parts for Algal Shaker (osf.io/jy7gc)** [28] Number of tools, equipment and parts are required to build the illuminated orbital shaker. Detailed bills of electronics and mechanical materials are provided. The process of ordering the printed circuit board for the LED controller is also detailed here.
- **Protocol 3: Assembling LED Controller Electronics (osf.io/bftxm)** [29] The LED controller is an electronics circuit, which regulates the illuminator power by varying LED current and drives the cooling fans, which prevent overheating of the LEDs and microalgae cultures. The function of the LED controller electronics circuit, step-by-step assembly, and testing instruction are detailed in this protocol. A 3D render of the assembled electronics circuit is shown in Fig. 2A.
- **Protocol 4: 3D Printing Case for LED Controller (osf.io/7ycnr)** [30] The design files to produce a custom housing for the LED controller electronics by 3D printing are introduced. The process of the assembly of the LED controller is explained in this protocol. A 3D render of the assembled LED controller inside the case is shown in Fig. 2B.
- **Protocol 5: Assembling Cooled LED Illuminator (osf.io/hywec)** [31] The cooled LED illuminator consists of a heatsink holding the illuminating LED strips, cooling fans, and the LED controller. Instructions for the mechanical and electrical assembly of the cooled LED illuminator are provided in this protocol. The initial testing of the LED controller circuit is also outlined here. A photograph of the assembled LED illuminator is shown in Fig. 2D.
- **Protocol 6: Cutting and Drilling Clear Acrylic Sheet (osf.io/69f8t)** [32] A clear acrylic sheet is used as a secondary transparent shaking platform holding the microalgae culture flasks. Two sets of instructions are provided in this protocol: One for the manual cutting of the clear acrylic sheet using workshop tools; the second for automatic cutting using a laser cutter. A 3D render of the cut and drilled acrylic sheet is in Fig. 2C.
- **Protocol 7: Assembling Algal Shaker (osf.io/ewc87)** [33] Once all components of the illuminated orbital shaker are built, the final instrument is assembled by mounting the parts to the orbital shaker platform and connecting them electrically. These last assembly steps are detailed in this protocol. A photograph of the assembled illuminated orbital shaker is shown in Fig. 2E.
- **Protocol 8: Measuring PPFD on Algal Shaker (osf.io/va54p)** [34] The light output is characterized by measuring the photosynthetic photon flux density (PPFD), as described in this protocol. Experimental details are in Section 7.1.

The above protocols explain in detail the steps required to build and test the illuminated orbital shaker.

Table 2
List of protocols with instructions on building and calibrating the illuminated orbital shaker platform. All protocols are licensed under CC BY 4.0 license. The URL links to the protocols in this table lead to their static snapshots current at the time of this publication. The bibliographic citations point to entries on **protocols.io**, which may be updated with new versions in the future.

Designator	Protocol	Summary	Protocol URL
Protocol 1	Illuminated Orbital Shaker for Microalgae Culture	High level summary of build instructions	osf.io/hd2c6 [27]
Protocol 2	Procuring Parts for Algal Shaker	List of components and tools; PCB order instructions	osf.io/jy7gc [28]
Protocol 3	Assembling LED Controller Electronics	Description of the electronics circuit and its assembly steps	osf.io/bftxm [29]
Protocol 4	3D Printing Case for LED Controller	3D printing of a case for electronics; instructions for LED controller assembly	osf.io/7ycnr [30]
Protocol 5	Assembling Cooled LED Illuminator	Electromechanical assembly instructions for illuminator	osf.io/hywec [31]
Protocol 6	Cutting and Drilling Clear Acrylic Sheet	Transparent orbital shaker platform build instructions	osf.io/69f8t [32]
Protocol 7	Assembling Algal Shaker	Final assembly and testing steps	osf.io/ewc87 [33]
Protocol 8	Measuring PPFD on Algal Shaker	Light output calibration protocol	osf.io/va54p [34]

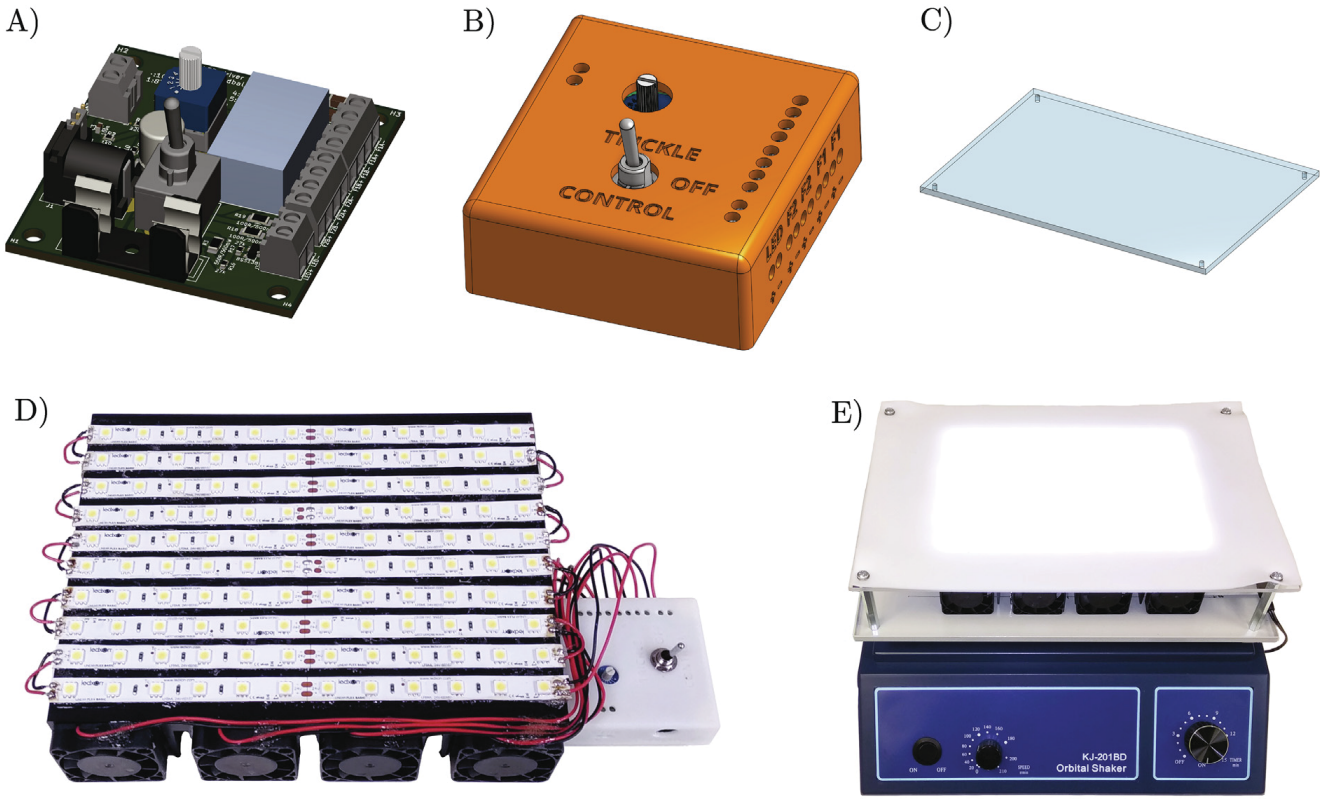

Fig. 2. Progress of building the illuminated orbital shaker. A) LED controller electronics circuit; B) 3D printed case for LED controller; C) Clear acrylic sheet for transparent shaker platform; D) LED illuminator; E) Assembled illuminated orbital shaker.

6. Operation instructions

The illuminated orbital shaker offers three variable parameters: (1) platform shaking frequency, (2) growth light intensity, and (3) daily ratio of light and dark periods. These parameters can be operated independently. Their meaning and use is explained in the rest of this section.

The platform shaking frequency is set on the orbital shaker as described in its instruction manual. Usually, this would be done by turning a knob with a scale calibrated in revolutions per minute (RPM). The orbital shaker described in this manuscript supports frequencies between 0 and 210 RPM. The shaking speed needs to be high enough to keep the cell culture suspended and well mixed. Frequency higher than required unnecessarily increases the power consumption, heat generation, noise, and the risk of fall of flasks from the shaking platform. The validation experiments in this paper had the orbital shaker operating at 100 RPM.

The growth light intensity is controlled through the LED controller. There are two modes of operation: the trickle current and variable current modes, selected by a toggle switch. In the trickle current mode, a current of 26 mA is flowing through the LEDs, which creates photosynthetic photon flux density (PPFD) of $\approx 26\ \mu mol \cdot m^{-2} \cdot s^{-1}$ inside a glass Erlenmeyer flask containing deionized water (Fig. 3). The trickle current setting is used for maintaining slow growing cultures of cells or for microalgae species requiring low light conditions. The variable current mode allows adjusting the LED current between 240 mA and 1 A and PPFD between 220 and 800 $\mu mol \cdot m^{-2} \cdot s^{-1}$. In the variable current mode, the LED current, and thus PPFD, are adjusted in seven steps by the rotary switch on the LED controller (Fig. 3). The LED current is set by the resistors in the LED controller circuit and will remain the same irrespective of the implementation of the illuminated orbital shaker. The PPFD will depend on the geometry of the orbital shaker platform, the material of the anti-slip mat holding the culture flasks, spacing of the LED strips, and the type of the LED strips. It can therefore vary significantly in different implementations of the illuminated orbital shaker and will have to be calibrated individually.

The operation of the illuminated orbital shaker requires several safety considerations. The main risks are associated with the mains electricity, fire, and bright light. Ensure that the mains electrical leads are away from the orbital shaker to prevent the orbital platform from cutting through the insulation material of the cables. Make sure that mains socket connections are away from the orbital shaker. This will minimize the risk of fire or electrocution in case any flask containing the liquid culture falls from the orbital and spills its content. Ensure the orbital shaker is placed in a tidy space, away from splashing water. Allow enough space for sufficient airflow to prevent overheating and increased risk of fire. Regularly check that the electrical cables and connections are sound and reliable. Check that the heatsink is not becoming clogged with dust, impeding good airflow. Fix unreliable or failing wiring and brush any dust off the heatsink whenever problems are identified.

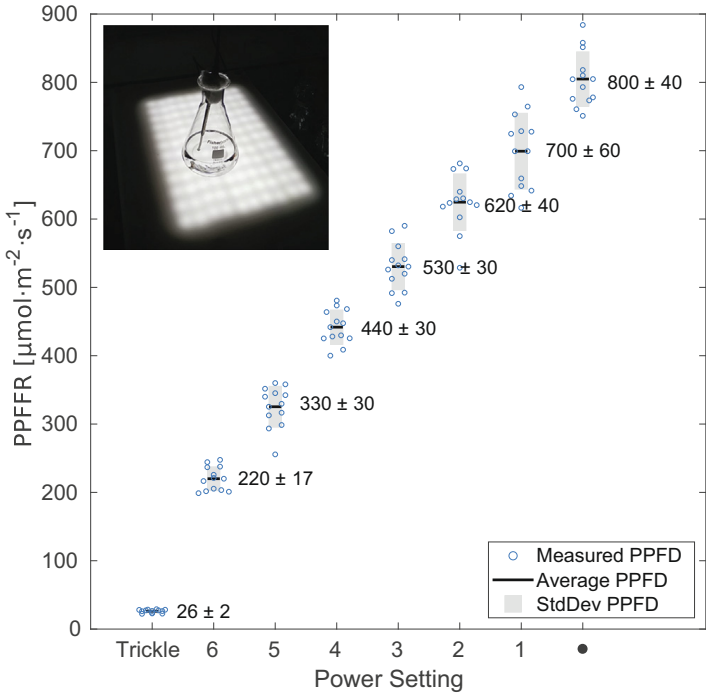

Fig. 3. Calibration graph of photosynthetic photon flux density (PPFD) in water in relation to eight different LED current settings. For each setting, PPFD measurement was repeated in twelve different randomly selected positions on the illuminated platform. (inset) The light sensor was fixed vertically in deionized water inside 100 ml glass Erlenmeyer flask, to mimic the light conditions experienced by the microalgae culture. The graph shows the twelve measurements (○) for each LED current setting, their average values (—), and standard deviations (▯).

The orbital shaker must not move during operation even at the highest speed setting. In case of any movement, change its placement or place a sticky mat underneath to minimize the risk of falling. The illuminated orbital shaker is a source of bright light. Avoid staring at the illuminator. Use protective glasses if eye irritation occurs or if it is required by local regulations. Further safety instruction are listed in Supplementary Section S2.

7. Validation and characterization

The illuminated orbital shaker has been characterized and validated by measuring produced photosynthetic photon flux density (PPFD) and successful growth of microalgae cell cultures. PPFD has been measured using a calibrated light detector at randomly selected positions on the surface of the illuminated shaking platform and submerged in water inside glass Erlenmeyer flasks. Cell counting was done regularly to assess the increase in the density of the culture. The validation by microalgae growth was performed with two commonly used species of freshwater microalgae, *D. quadricauda* and *C. vulgaris*. The microalgae cultures were grown in different media at two different LED current settings and regularly evaluated by counting the cell density. The average cell doubling time was estimated for each species and growth condition. The experiments verified that the illuminated orbital shaker can be used for reliable cultivation of microalgae (Section 7.2 and Supplementary Section S1).

7.1. Photosynthetic photon flux density

This section discusses the calibration measurements of the light source in the illuminated orbital shaker. The light source is an array of white LEDs. The spectral density of a white LED is a compound of blue LED emission and green–red phosphorescence [19]. The white LED spectrum spans most of the photosynthetically active radiation (PAR) spectral range (400 nm – 700 nm) [35], meaning it can efficiently drive photosynthesis. The photosynthetic quantum yield in microalgae is a complex function of the wavelength. The combined complexity of the LED emission spectrum and the photosynthetic quantum yield spectral dependence requires specialized techniques for quantifying light sources for their ability to drive photosynthesis. Photosynthetic photon flux density (PPFD) is a measure of the number of photons, with the wavelength between 400 nm and 700 nm, crossing a unit area per unit of time [35]. PPFD is measured using a quantum sensor, which is a spectrally corrected light sensor with constant spectral sensitivity in the PAR region and a zero response outside. PPFD is typically expressed in $\mu mol(photons) \cdot m^{-2} \cdot s^{-1}$.

A spherical micro quantum sensor (US-SQS, Waltz) was used in conjunction with a light meter (LI-250A, Li-COR). PPFD was measured in air, on the surface of the illuminated orbital shaker platform, and submerged in deionized water inside a glass Erlenmeyer flask, normally used for microalgae cultivation. The LED controller setting was switched between all eight

supported LED current settings. The measurement was taken at twelve different randomly chosen positions to sample the PPFD across the illuminated orbital shaker platform area. The average value and the standard deviation were calculated for each medium and LED current setting (Table S2). The dependence of PPFD on the LED controller setting, measured in water, is plotted in Fig. 3 and, measured in air, is in Supplementary Fig. S2. The measurements show the expected increase in PPFD with the growing LED current as the power settings were changed. For each power setting, the twelve measurements are spread around their average value. The spread is due to the spatial inhomogeneity of the illumination, with local maxima right above the LEDs and minima in between the LEDs. This variation should have negligible effect on the microalgae cultures. The cell suspensions are being continuously mixed and therefore individual cells experience the same average PPFD over time. PPFD was slightly lower in water than air, which is consistent with the absorption and reflection losses introduced by the extra layers of glass and water (Supplementary Table S2). The PPFD can be set between 26 and 800 $\mu mol \cdot m^{-2} \cdot s^{-1}$ (in water), which covers a broad range of radiant fluxes comparable to a wide range of natural daylight conditions. The protocol, detailing the experimental execution of the PPFD measurements and the data analysis steps, is at osf.io/va54p [34]. The raw measurement data, Matlab code for their analysis, and the resulting figures are available at osf.io/zamnf and in a GitHub repository at rebrand.ly/fmkm7hv.

7.2. Microalgae cultivation

This section discusses microalgae cultivation using the bottom-illuminated orbital shaker. The objectives were to demonstrate the successful and consistent growth of microalgae at different PPFDs, to test microalgae growth in different media, and to find optimal cultivation conditions for future experiments. Two commonly used freshwater species, *Chlorella vulgaris* (#256, CCALA, Třeboň, Czech Republic) and *Desmodesmus quadricauda* (#463, CCALA), were cultivated. The experiments are described in further detail in Supplementary Section S1, introducing the experimental steps, protocols (Supplementary Table S1), and data analysis. This section reports on the results of an experiment, in which microalgae were grown at two different LED illuminator settings (PPFD of 26 and 220 $\mu mol \cdot m^{-2} \cdot s^{-1}$) and in different growth media. Self-prepared medium 1/2SŠ [36] and a commercial Bold's basal medium [37,38] (BBM) (B5282, Merck, Gillingham, UK) were used. The 1/2SŠ medium was supplemented with 0.83 mm $NaHCO_3$, as an additional source of carbon. The BBM medium was used both with 10 mm $NaHCO_3$ and without any $NaHCO_3$. Two light settings of 26 and 220 $\mu mol \cdot m^{-2} \cdot s^{-1}$ were used. Cultures were seeded into fresh medium at the starting density of $2 \times 10^5\ ml^{-1}$ for *D. quadricauda* and $1 \times 10^6\ ml^{-1}$ for *C. vulgaris*. The cell densities were regularly obtained by counting using a Neubauer hemocytometer until saturation was reached (Supplementary Section S1.2).

7.2.1. Cell growth rate results

The cell density time evolution data for *D. quadricauda* are in Fig. 4A and of *C. vulgaris* in Fig. 4B. The graphs show the repeats of cell density counts for each day and experimental condition in the form of univariate scatter clouds ($\times, \bigcirc, \nabla, \triangle$). The average values of the cell densities are plotted as horizontal lines (▬). The linear regression of the quasi-linear part of the plot for each condition are marked by the dotted lines (···). The quasi-linear parts of the growth data were automatically identified and their linear regressions were calculated by a Matlab script (osf.io/52348 and on GitHub at rebrand.ly/t4zwgz1). The resulting doubling times during the exponential growth phase for each species and cultivation condition are listed in Table 3. The data show that doubling times shorten, and thus the growth rates become faster, for both species with brighter light (higher PPFD). The doubling times for *C. vulgaris* were similar in all three media (1/2SŠ, BBM, and BBM with $NaHCO_3$). *D. quadricauda* grown in the 1/2SŠ medium had shorter doubling time and faster growth compared to when grown in the BBM medium[2].

The increase of the cell density over time did not follow perfect exponential model (linear increase on the semi-logarithmic plot) in these cultures. This had two reasons. Towards the saturation of the culture density, the growth naturally slowed down due to less light reaching the optically dense culture and the gradual exhaustion of nutrients. The second phenomenon was the daily fluctuation away from the ideal exponential growth model. We speculate, that the fluctuations were caused by a combination of hemocytometer loading errors and cell cycle oscillations in the synchronized cultures. After a period of stress[3], the cultures did not exhibit steady exponential growth. Instead, the culture density increased considerably the first day after inoculation into fresh growth medium. This was followed by a day of subdued growth. These oscillations of faster and slower growth gradually evened out over the course of a week under stress-free conditions. Despite the cultures being conditioned for a week before the start of the experiments, the dilution to the initial inoculation density may have contributed to the observed daily fluctuations away from the ideal exponential growth model.

8. Capabilities of the illuminated orbital shaker

- Growth area: 20 cm × 15 cm

[2] *D. quadricauda* was not cultured in BBM with $NaHCO_3$ during these experiments, as large proportion of coenobia were malformed or had non-canonical cell number, when grown in this medium (data not shown).

[3] Growth to saturation, large step change in the illumination light PPFD, more than 10-fold dilution with fresh medium.

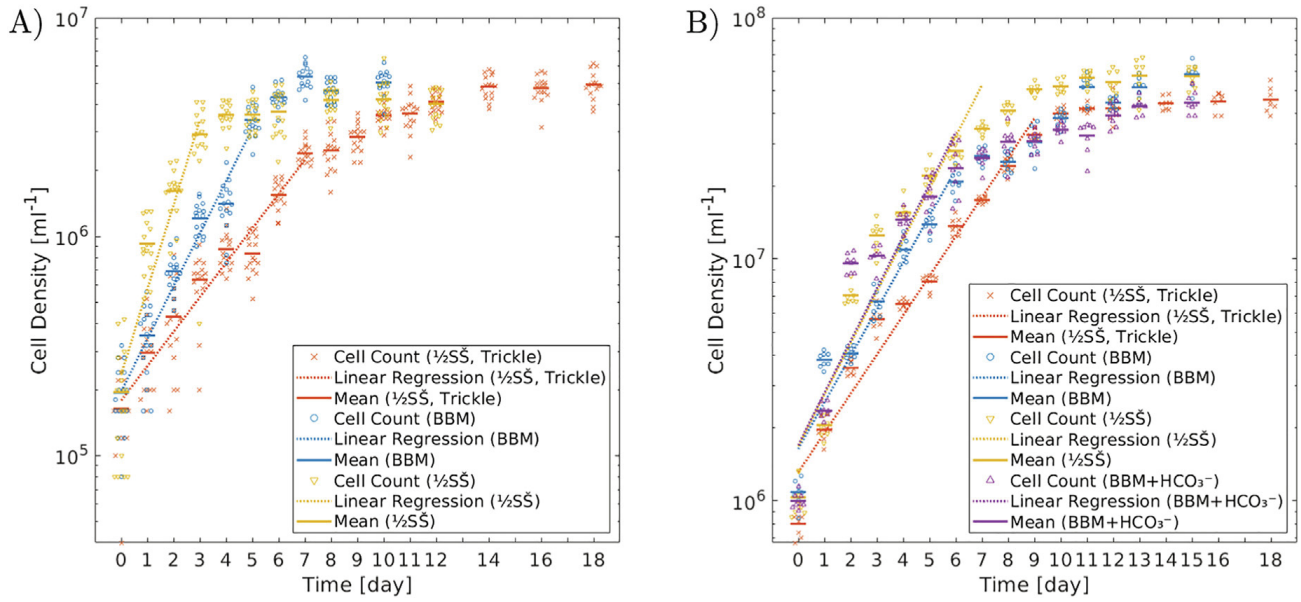

Fig. 4. Growth data of (A) *D. quadricauda* and (B) *C. vulgaris* on semi-logarithmic plots. Cells were grown in (orange) 1/2SŠ medium at the trickle current setting (26 µmol · m^{-2} · s^{-1}), (blue) 1/2SŠ at switch position 6 (220 µmol · m^{-2} · s^{-1}), (yellow) BBM at switch position 6, and (purple) BBM with $NaHCO_3$ at switch position 6. The average values of the cell density for each day and condition are marked by the colored horizontal bars (▬). The cell density counted in each segment of the hemocytometer is plotted as a univariate scatter plot surrounding the average value (×, ◯, ▽, △). The linear regression of the quasi-linear part of the growth curve is marked by the colored dotted lines (···).

Table 3
List of doubling periods for *D. quadricauda* and *C. vulgaris* grown at PPFD of 26 µmol · m^{-2} · s^{-1} and 220 µmol · m^{-2} · s^{-1} in 1/2SŠ with 0.83 mm $NaHCO_3$, BBM, and BBM with 10 mm $NaHCO_3$. The listed doubling time values are the slopes of the linear regressions through the quasi-linear part of the logarithm of the cell culture density growth data. The stated uncertainties are the errors of the linear regression slope.

Species	PPFD [**µmol · m^{-2} · s^{-1}**]	Growth Medium	Doubling Time [**hours**]
D. quadricauda	26 (trickle current)	1/2SŠ + 0.83 mm $NaHCO_3$	46 ± 3
D. quadricauda	220 (switch position 6)	1/2SŠ + 0.83 mm $NaHCO_3$	19 ± 3
D. quadricauda	220	BBM	30 ± 2
C. vulgaris	26	1/2SŠ + 0.83 mM $NaHCO_3$	44 ± 2
C. vulgaris	220	1/2SŠ + 0.83 mM $NaHCO_3$	34 ± 2
C. vulgaris	220	BBM	37 ± 2
C. vulgaris	220	BBM + 10 mM $NaHCO_3$	33 ± 3

- 100 ml Erlenmeyer flask capacity: 6
- T75 plastic tissue culture flask capacity: 2
- T25 plastic tissue culture flask capacity: 8
- Light source PPFD: 26 – 800 µmol · m^{-2} · s^{-1} (in eight steps, see Supplementary Table S2)
- Light source peak power consumption: 29 W (excluding the shaker)
- Shaking speed: 0 – 210 RPM

9. Conclusions and discussion

Protocols for building, testing, and using the bottom-illuminated orbital shaker for microalgae culture are presented. The protocols are accompanied by design files, which are editable using free-of-charge software. To encourage third-party customization for different purposes or experimental requirements, the design files, protocols, and code are released under minimally restrictive licenses[4].

The illuminated orbital shaker light output was calibrated by measuring the photosynthetic photon flux density (PPFD). Its function for the intended purpose was verified by culturing *C. vulgaris* and *D. quadricauda*. The manuscript is accompanied by a set of protocols detailing the process of microalgae cultivation (Supplementary Section S1 and Table S1). The protocols

[4] The restrictions on the CC BY and BSD licenses require crediting the authors in any future use. The CC BY-SA license additionally mandates sharing any derivatives under a similar license.

introduce the growth media, the cultivation process, and the assessment of culture growth. The raw data from counting cell density and the Matlab code for their analysis are also openly shared.

The bottom-illuminated orbital shaker for microalgae culture was found perfectly suitable for our research on photosynthesis. Any suitably equipped workshop should be able to reproduce it within days, once all components are purchased, at a cost of around £300. All adopters are encouraged to openly share their applications, implementations, and changes to the illuminated orbital shaker. The remaining discussion covers possible improvements and modifications.

The design is flexible and well suited to alteration. A different orbital shaker can be used instead of the one described in this manuscript. The illuminated growth area and the maximum PPFD can be modified for specific needs. This requires scaling to a different-sized heatsink and/or changing the spacing and length of the LED strips. The light source color could be varied by choosing triple-color LED strips with three copies of the LED controller regulating each color separately. Longer than 24-h light cycles can be achieved by using a weekly, rather than daily programmable timer. Alternatively, flexible control of timing and brightness can be done by driving the LED controller input from a microcontroller, as described below.

To support advanced and programmable growth protocols, the LED controller features an external control input. This allows the control of the growth light brightness by a microcontroller or microcomputer (e.g. Arduino or Raspberry Pi). The external input accepts either an analog voltage (0.30 V – 1.25 V), or a pulse-width modulation (PWM) with the amplitude of 1.25 V. The rotary switch can be conveniently used to match the maximum input voltage of the LED controller (1.25 V) to different microcontroller output voltages[5] (e.g. 3.3 V or 5 V).

The illuminated orbital shaker could be placed inside a growth cabinet to allow temperature, humidity, and/or CO_2 control for experiments or species requiring particular environmental conditions. 'OpenTCC' is an OSHW temperature-controlled cabinet that could be built to house the illuminated orbital shaker and maintain the flasks with microalgae cultures at a set temperature [39]. 'Polar Bear', a temperature- and humidity-controlled environmental chamber, is described in [40]. For microalgae cultivation, the humidity control could be left out of the 'Polar Bear' for simplicity. A well described guide to repurposing a refrigerator into a temperature-controlled environmental chamber is described on the commercial 'BrewPi' project website [41]. The design instructions and source code for the 'BrewPi' are open source. The company offers components for sale, which could simplify and speed up its the customization for microalgae cultivation. A large scale temperature-controlled walk-in space made from inexpensive parts is described in [42]. This could accommodate many illuminated orbital shakers for mass batch cultivation.

There are a number of OSHW solutions for CO_2 control. A temperature- and CO_2-controlled tissue culture cabinet, described by Pelling et al. [43], could be repurposed to house the illuminated orbital shaker. The described system lacks cooling capability, which limits its application without further redesign. A related company was started with the promise to sell a refined low-cost open source incubator based on the design by Pelling et al. It currently provides open source Arduino code for CO_2 and temperature control on GitHub [44]. Another implementation of a temperature- and CO_2-controlled incubator with design files and source code is described in a thesis by Al-Sayagh [45]. This device is too small to house the illuminated orbital shaker, but its low-cost closed-loop CO_2 regulator can be potentially adapted for use with a larger cabinet and gas cylinder. A small temperature- and CO_2-controlled incubator is described as a part of a live-cell imaging system in [46]. The manuscript discusses the regulation in detail, however the design files and source code are not open source and are available upon request only. A different implementation uses a decommissioned neonatal infant incubator [47]. Finally, a temperature- and CO_2-controlled cabinet, using chemically generated CO_2 rather than compressed gas, is described in an entry to the IGEM 2019 competition [48]. To the best of our knowledge, there is no existing OSHW cooled and CO_2-controlled cabinet, which would be ideal for housing the illuminated orbital shaker.

The calibration between the LED controller setting and the PPFD at the surface of the LED illuminator was measured using a commercial PAR meter. This, or a similar device, may not be universally available, requiring an alternative solution for its accurate calibration. PARduino is an OSHW data logger combining a commercial quantum PAR sensor with an Arduino [49]. Kuhlgert et al. published an advanced portable OSHW plant phenotyping station, which incorporates a PAR sensor [50]. They used a low-cost 4-channel spectrally-resolved photodiode array instead of a quantum sensor and derived a transformation to convert its output voltages into PPFD. They verified the accuracy of their PAR sensor under different experimental conditions using a calibrated quantum sensor. Kutschera and Lamb simplified their design to build a stand-alone PAR meter based on an Arduino and the same photodiode array [51]. There are many other non-scientific PAR detector projects created by aquarium enthusiasts and hydroponic growers available online. Among them, one suggests using a particular low-cost lux meter as an approximate PAR meter after this was calibrated against a proprietary quantum sensor with different types of light sources [52]. PAR meters that do not rely on calibrated quantum sensors may offer a suitable low-cost alternative to proprietary solutions. However, their calibration, reproducibility, and accuracy need to be evaluated, given the specific experimental requirements and lighting conditions.

Human and animal rights

Not applicable.

[5] Switch position 5 allows connecting the LED controller to a 3.3 V microcontroller and position 6 to a 5 V microcontroller.

Declaration of Competing Interest

The authors declare that they have no known competing financial interests or personal relationships that could have appeared to influence the work reported in this paper.

Acknowledgements

We would like to acknowledge the funding from Biotechnology and Biological Sciences Research Council (UK), Grant/Award Number: BB/R004803/1. We would like to thank the following people. Ladislav Nedbal of Forschungszentrum Jülich, Germany advised us on setting up the cultures and critically read the manuscript. Ben Blackburn of King's College London operated the 3D printer to produce the LED controller case. Giorgio Perin and Patrick Jones of Imperial College London, United Kingdom lent us their quantum light sensor and light meter for the PPFD calibration measurements of the illuminated orbital shaker.

Appendix A. Supplementary data

Supplementary data associated with this article can be found, in the online version, at https://doi.org/10.1016/j.ohx.2020.e00143.

References

[1] J. Masojídek, G. Torzillo, and M. Koblížek. Photosynthesis in Microalgae. In: A. Richmond and Q. Hu (Eds.), Handbook of Microalgal Culture. John Wiley & Sons, 2013. Chap. 2, 21–36. https://doi.org/10.1002/9781118567166.ch2.
[2] A. Guedes, F. Malcata, Bioreactors for microalgae: a review of designs, features and applications, in: P.G. Antolli, Z. Liu (Eds.), Bioreactors: Design, Properties and Applications, Nova Science Publishers, 2012, pp. 1–52.
[3] O. Pulz, Photobioreactors: production systems for phototrophic microorganisms, Appl. Microbiol. Biotechnol. 57 (2001) 287–293. https://doi.org/10.1007/s002530100702.
[4] H.S. Kim, T.L. Weiss, H.R. Thapa, T.P. Devarenne, A. Han, A micro uidic photobioreactor array demonstrating high-throughput screening for microalgal oil production, Lab Chip 14 (2014) 1415–1425. https://doi.org/10.1039/C3LC51396C.
[5] C. Westerwalbesloh, C. Brehl, S. Weber, C. Probst, J. Widzgowski, A. Grünberger, C. Pfaff, L. Nedbal, D. Kohlheyer, A microfluidic photobioreactor for simultaneous observation and cultivation of single microalgal cells or cell aggregates, PLoS One 14 (4) (2019) 1–13. https://doi.org/10.1371/journal.pone.0216093.
[6] M.A. Borowitzka. Commercial Production of Microalgae: Ponds, Tanks, Tubes and Fermenters, J. Biotechnol. 70 (1) (1999). Biotechnological Aspects of Marine Sponges, 313–321. https://doi.org/10.1016/S0168-1656(99)00083-8.
[7] A.P. Carvalho, L.A. Meireles, F.X. Malcata, Microalgal reactors: a review of enclosed system designs and performances, Biotechnol. Prog. 22 (6) (2006) 1490–1506. https://doi.org/10.1021/bp060065r.
[8] Q. Wang, H. Peng, B.T. Higgins, Cultivation of green microalgae in bubble column photobioreactors and an assay for neutral lipids, JOVE 143 (2019) e59106. https://doi.org/10.3791/59106.
[9] L. Rodolfi, G. Chini Zittelli, N. Bassi, G. Padovani, N. Biondi, G. Bonini, M.R. Tredici, Microalgae for oil: strain selection, induction of lipid synthesis and outdoor mass cultivation in a low-cost photobioreactor, Biotechnol. Bioeng. 102 (1) (2009) 100–112. https://doi.org/10.1002/bit.22033.
[10] O. Savchenko, J. Xing, X. Yang, Q. Gu, M. Shaheen, M. Huang, X. Yu, R. Burrell, P. Patra, J. Chen, Algal cell response to PulsedWaved stimulation and its application to increase algal lipid production, Sci. Rep. 7 (2017) 42003. https://doi.org/10.1038/srep42003.
[11] E.O. Ojo, H. Auta, F. Baganz, G.J. Lye, Engineering characterisation of a shaken, single-use photobioreactor for early stage microalgae cultivation using Chlorella sorokini- ana, Bioresour. Technol. 173 (2014) 367–375. https://doi.org/10.1016/j.biortech.2014.09.060.
[12] E.O. Ojo, H. Auta, F. Baganz, G.J. Lye, Design and parallelisation of a miniature photobioreactor platform for microalgal culture evaluation and optimisation, Biochem. Eng. J. 103 (2015) 93–102. https://doi.org/10.1016/j.bej.2015.07.006.
[13] R. Lehmann, NinjaPBR – The Photobioreactor for Cyanobacteria and Microalgae. https://github.com/roblehmann/NinjaPBR, 2015 (accessed 06/26/2020).
[14] J. Sanabria et al. Open Source Bioreactor. https://github.com/hackuarium/bioreactor/, 2020 (accessed 06/26/2020)
[15] A. Wishkerman, E. Wishkerman, Application note: a novel low-cost open-source LED system for microalgae cultivation, Comput. Electron. Agric. 132 (2017) 56–62. https://doi.org/10.1016/j.compag.2016.11.015.
[16] B.T. Nguyen, B.E. Rittmann, Low-cost optical sensor to automatically monitor and control biomass concentration in microalgal cultivation, Algal. Res. 32 (2018) 101–106. https://doi.org/10.1016/j.algal.2018.03.013.
[17] B.T. Nguyen, B.E. Rittmann, A simple turbidity monitor and control system for microalgae. https://www.instructables.com/id/A-Simple-Turbidity-Monitorand-Control-System-for-/, 2018 (accessed 06/26/2020).
[18] J. Büchs, Introduction to Advantages and Problems of Shaken Cultures, Biochem. Eng. J. 7(2) (2001). Special Issue: Shaking Bioreactors, 91–98. https://doi.org/10.1016/S1369-703X(00)00106-6.
[19] J. Cho, J.H. Park, J.K. Kim, E.F. Schubert, White light-emitting diodes: history, progress, and future, Laser Photonics Rev. 11 (2) (2017) 1600147. https://doi.org/10.1002/lpor.201600147.
[20] The Nobel Prize in Physics 2014. https://www.nobelprize.org/prizes/physics/2014/prize-announcement/, 2014 (accessed 04/17/2020).
[21] S.E. Loftus, Z.I. Johnson, Reused cultivation water accumulates dissolved organic carbon and uniquely influences different marine microalgae, Front. Bioeng. Biotech. 7 (2019) 101. https://doi.org/10.3389/fbioe.2019.00101.
[22] E.J. Kim, S. Kim, H.-G. Choi, and S.J. Han. Co-Production of Biodiesel and Bioethanol using Psychrophilic Microalga Chlamydomonas sp. KNM0029C Isolated from Arctic Sea Ice, Biotechnol Biofuels 13(1) (2020) 20. https://doi.org/10.1186/s13068-020-1660-z.
[23] M. Morita, Y. Watanabe, H. Saiki, High Photosynthetic Productivity of Green Microalga Chlorella sorokiniana, Appl Biochem Biotechnol 87 (2000) 203–218. https://doi.org/10.1385/ABAB:87:3:203.
[24] E. Ono, J. Cuello, Carbon dioxide mitigation using thermophilic cyanobacteria, Biosyst. Eng. 96 (2007) 129–134. https://doi.org/10.1016/j.biosystemseng.2006.09.010.
[25] P. Schulze, L. Barreira, H. Pereira, J. Perales, J. Varela, Light emitting diodes (LEDs) applied to microalgal production, Trends Biotechnol. 32 (2014) 422–430. https://doi.org/10.1016/j.tibtech.2014.06.001.
[26] N. Forget, C. Belzile, P. Rioux, C. Nozais, Teaching the microbial growth curve concept using microalgal cultures and flow cytometry, J. Biol. Educ. 44 (4) (2010) 185–189. https://doi.org/10.1080/00219266.2010.9656220.
[27] J. Nedbal, Illuminated Orbital Shaker for Microalgae Culture, protocols.io (2020). https://doi.org/10.17504/protocols.io.bdubi6sn.

[28] J. Nedbal, Procuring Parts for Algal Shaker, protocols.io (2020). https://doi.org/10.17504/protocols.io.bdtwi6pe.
[29] J. Nedbal, Assembling LED Controller Electronics, protocols.io (2020). https://doi.org/10.17504/protocols.io.bdiai4ae.
[30] J. Nedbal, 3D Printing Ccase for LED Controller, protocols.io (2020). https://doi.org/10.17504/protocols.io.bdici4aw.
[31] J. Nedbal, Assembling Cooled LED Illuminator, protocols.io (2020). https://doi.org/10.17504/protocols.io.bcrniv5e.
[32] J. Nedbal. Cutting and Drilling Clear Acrylic Sheet, protocols.io (2020). https://doi.org/10.17504/protocols.io.bcueiwte.
[33] J. Nedbal, Assembling Algal Shaker, protocols.io (2020). https://doi.org/10.17504/protocols.io.bdcdi2s6.
[34] J. Nedbal. Measuring PPFD on Algal Shaker, protocols.io (2020). https://doi.org/10.17504/protocols.io.bdyxi7xn.
[35] K.J. McCree, Photosynthetically Active Radiation. In: O.L. Lange, P.S. Nobel, C.B. Osmond, H. Ziegler (Eds.), Physiological Plant Ecology I: Responses to the Physical Environment. Berlin, Heidelberg: Springer, Berlin Heidelberg, 1981, 41–55. https://doi.org/10.1007/978-3-642-68090-83.
[36] V. Zachleder, I. Šetlík, Effect of irradiance on the course of RNA synthesis in the cell cycle of Scenedesmus quadricauda, Biol. Plant 24 (5) (1982) 341–353. https://doi.org/10.1007/BF02909100.
[37] H.C. Bold, The morphology of chlamydomonas chlamydogama, sp. nov, Bull. Torrey Bot. Club 76 (2) (1949) 101–108. https://doi.org/10.2307/2482218.
[38] H.W. Bischoff, H.C. Bold, Phycological Studies. IV: Some Soil Algae From Enchanted Rock and Related Algal Species, 93, University of Texas, 1963.
[39] C. Sánchez, P. Dessí, M. Duffy, P.N.L. Lens, OpenTCC: an open source low-cost temperature-control chamber, HardwareX 7 (2020) e00099. https://doi.org/10.1016/j.ohx.2020.e00099.
[40] J.M. Pearce, Open-Source Lab: How to Build Your Own Hardware and Reduce Research Costs, Elsevier Science, 2013.
[41] E. Jacobs, BrewPi: A Modern Brewery Controller. https://www.brewpi.com/, 2020 (accessed 06/30/2020).
[42] E. Martinez, S.J. Agosta, Budget-limited thermal biology: design, construction and performance of a large, walk-in style temperature-controlled chamber, J. Therm. Biol. 58 (2016) 29–34. https://doi.org/10.1016/j.jtherbio.2016.03.009.
[43] A. Pelling, DIY CO2 Incubator Bioreactor for Mammalian Cell Culture. https://www.pellinglab.net/post/diy-diy-co2-incubator-bioreactor-for-mammalian-cell-culture, 2014 (accessed 06/30/2020).
[44] Incuvers Inc., Model 1 Tri-Gas Incubator. https://github.com/Incuvers-Inc/Model-1, 2019 (accessed 06/30/2020).
[45] A Highly Adaptive and Cost Effective Second Generation Incubator (SGI) towards Educational, Research and Clinical Processes (MSc thesis), University of Nebraska Lincoln, Biological Systems Engineering, 2014.
[46] M.P. Walzik, V. Vollmar, T. Lachnit, H. Dietz, S. Haug, H. Bachmann, M. Fath, D. Aschenbrenner, S. Abolpour Mofrad, O. Friedrich, D.F. Gilbert, A portable low-cost long-term live-cell imaging platform for biomedical research and education, Biosens. Bioelectron. 64 (2015) 639–649. https://10.1016/j.bios.2014.09.061.
[47] M. Brinn, S.F. Al-Sarawi, T. Lu, B.J.C. Freeman, J. Kumaratilake, and M.A. Henneberg. A Portable Live Cell Culture and Imaging System with Optional Umbilical Bioreactor Using a Modified Infant Incubator, Preprints (2017), 2017010137. https://doi.org/10.20944/preprints201701.0137.v1.
[48] Team Amazonas Brazil. CO2 Incubator: IGEM 2019 Competition Entry. https://2019.igem.org/Team:Amazonas-Brazil/Hardware, 2019 (accessed 06/30/2020).
[49] H.R. Barnard, M.C. Findley, J. Csavina, PARduino: a simple and inexpensive device for logging photosynthetically active radiation, Tree Physiol. 34 (6) (2014) 640–645. https://10.1093/treephys/tpu044.
[50] S. Kuhlgert, G. Austic, R. Zegarac, I. Osei-Bonsu, D. Hoh, M.I. Chilvers, M.G. Roth, K. Bi, D. TerAvest, P. Weebadde, D.M. Kramer, MultispeQ Beta: a tool for large-scale plant phenotyping connected to the open PhotosynQ network, R. Soc. Open Sci. 3 (10) (2016) 160592. https://10.1098/rsos.160592.
[51] A. Kutschera, J. Lamb, Light meter for measuring photosynthetically active radiation, Am. J. Plant Sci. 9 (12) (2018) 2420–2428. https://doi.org/10.4236/ajps.2018.912175.
[52] S. Torpey. PAR Meter Hack 30. https://www.youtube.com/watch?v=YiVVAePNtXo, 2020 (accessed 06/30/2020).